Vol. 155, December 1, 1983
Complete in one issue

ISSN 0003-2670

ANALYTICA CHIMICA ACTA

International journal devoted to all branches of analytical chemistry

ELSEVIER

ANALYTICA CHIMICA ACTA

International journal devoted to all branches of analytical chemistry
Revue internationale consacrée à tous les domaines de la chimie analytique
Internationale Zeitschrift für alle Gebiete der analytischen Chemie

PUBLICATION SCHEDULE FOR 1983

	J	F	M	A	M	J	J	A	S	O	N	D
Analytica Chimica Acta	145	146	147	148	149	150/1 150/2	151/1	151/2	152	153	154	155

Scope. *Analytica Chimica Acta* publishes original papers, short communications, and reviews dealing with eve aspect of modern chemical analysis, both fundamental and applied.

Submission of Papers. Manuscripts (three copies) should be submitted as designated below for rapid and efficie handling:

Papers from the Americas to: Professor Harry L. Pardue, Department of Chemistry, Purdue University, West Lafayet IN 47907, U.S.A.

Papers from all other countries to: Dr. A. M. G. Macdonald, Department of Chemistry, The University, P.O. Box 36 Birmingham B15 2TT, England. Papers dealing particularly with computer techniques to: Professor J. T. Cle Universität Bern, Pharmazeutisches Institut, Baltzerstrasse 5, CH-3012 Bern, Switzerland.

Submission of an article is understood to imply that the article is original and unpublished and is not being consider for publication elsewhere. Upon acceptance of an article by the journal, authors will be asked to transfer the copyrig of the article to the publisher. This transfer will ensure the widest dissemination of information.

Information for Authors. Papers in English, French and German are published. There are no page charg Manuscripts should conform in layout and style to the papers published in this Volume. Authors should cons Vol. 132, p. 239 for detailed information. Reprints of this information are available from the Editors or from: Elsevi Editorial Services Ltd., Mayfield House, 256 Banbury Road, Oxford OX2 7DH (Great Britain).

Reprints. Fifty reprints will be supplied free of charge. Additional reprints (minimum 100) can be ordered. An ord form containing price quotations will be sent to the authors together with the proofs of their article.

Advertisements. Advertisement rates are available from the publisher.

Subscriptions. Subscriptions should be sent to: Elsevier Science Publishers B.V., Journals Department, P.O. B 211, 1000 AE Amsterdam, The Netherlands. Tel: 5803 911, Telex: 18582.

Publication. *Analytica Chimica Acta* appears in 11 volumes in 1983. The subscription for 1983 (Vols. 145–155) Dfl. 1980.00 plus Dfl. 220.00 (p.p.h.) (total approx. U.S. $880.00). All earlier volumes (Vols. 1–144) except Vols. and 28 are available at Dfl. 200.00 (U.S. $80.00), plus Dfl. 15.00 (U.S. $6.00) p.p.h., per volume.

Our p.p.h. (postage, packing and handling) charge includes surface delivery of all issues, except to subscribers in t U.S.A., Canada and India who receive all issues by air delivery (S.A.L. — Surface Air Lifted) at no extra cost. For t rest of the world, airmail and S.A.L. charges are available upon request.

Claims for issues not received should be made within three months of publication of the issues. If not they cannot honoured free of charge.

For further information, or a free sample copy of this or any other Elsevier Science Publishers journal, readers in t U.S.A. and Canada can contact the following address: Elsevier Science Publishing Co., Inc., Journal Informati Center, 52 Vanderbilt Avenue, New York, NY 10017, U.S.A., Tel: (212) 867-9040.

ANALYTICA CHIMICA ACTA
VOL. 155 (1983)

ANALYTICA CHIMICA ACTA

International journal devoted to all branches of analytical chemistry

ELSEVIER Amsterdam–Oxford–New York–Tokyo

0003-2670/83/$03.00

Printed in The Netherlands

Analytica Chimica Acta, 155 (1983) 1–9
Elsevier Science Publishers B.V., Amsterdam — Printed in The Netherlands

BIPOLAR PULSE CONDUCTOMETRIC MONITORING OF ION-SELECTIVE ELECTRODES
Part 4. Interferences from Electroactive Species in Measurements with the Calcium Electrode

CHARLES R. POWLEY[a] and TIMOTHY A. NIEMAN*
School of Chemical Sciences, University of Illinois, Urbana, IL 61801 (U.S.A.)
(Received 14th June 1983)

SUMMARY

The effects of electroactive interferences on bipolar pulse conductance measurements with calcium electrodes are evaluated. Stainless steel and platinum rods are evaluated as counter electrodes in the presence of oxidizing agents, reducing agents, and electroactive couples. Some of these species, such as Cu^{2+}, Ag^{+}, and the I_3^-/I^- couple, can poise a metal counter electrode at a characteristic electrochemical potential. The presence of electroactive species yields the same errors in conductometric measurements as they would in potentiometric measurements when stainless steel or platinum electrodes were used as reference electrodes. These interferences are not observed in conductometric monitoring, if a Ag/AgCl electrode is used as the counter electrode. Voltage pulses of long-duration (10 ms) in bipolar pulse conductometric monitoring of the calcium electrode yielded errors in current measurements because of faradaic reactions. Such faradaic errors were especially noticeable when Ag^{+}, Cu^{2+}, or ascorbic acid was present. Plots of measured current vs. applied voltage pulse amplitude were nonlinear, and showed increasingly larger errors at the higher applied pulse amplitudes. The studies show that voltage pulses of short duration must be used in conductometric monitoring of ion-selective electrodes if electroactive species are present in solution.

The evaluation of interferences in potentiometric measurements with ion-selective electrodes (i.s.e.'s) caused by the presence of electroactive species has not received much attention in the literature. Several studies have focused on the oxidation of components of the Ag/AgCl, Ag/AgBr, Ag/Ag_2S, and Ag_2S/CdS electrodes [1—4]. It was postulated that reversible or irreversible oxidation of Ag and S^{2-} could occur in the presence of oxidizing agents such as iron(III), permanganate, cerium(IV) and dichromate. Other studies have shown that dissolved oxygen can also affect electrode potentials. Oxygen was shown to oxidize copper in the copper i.s.e., thereby increasing the Cu^{2+} concentration in solution [5]. A related study showed that oxygen can diffuse through the membrane of calcium coated-wire electrodes and form a half-cell at the metal/membrane interface [6].

[a]Present address: Department of Chemistry, University of Georgia, Athens, GA 30602, U.S.A.

0003-2670/83/$03.00

Bipolar pulse conductometric monitoring [7, 8] of i.s.e.'s has been shown [9—11] to be an alternative to the standard potentiometric method. An important advantage of conductometric monitoring is that a simple metal contact to solution can be used instead of a reference electrode. However, it is well known that the presence of electroactive species in solution can change the potential of a polarizable electrode [12]. Therefore, the aim of the present study is to determine what effects electroactive species can have on bipolar pulse conductance measurements with i.s.e.'s. Interferences from electroactive species are evaluated in cells containing polarizable (platinum and stainless steel) and nonpolarizable (Ag/AgCl) counter electrodes. The bipolar conductance method involves the passage of a significant amount of current through the cell, compared to the potentiometric method. Therefore, we determined the pulse duration and amplitude conditions under which a faradaic reaction could occur in the bipolar conductance monitoring of i.s.e.'s, if there are electroactive species in solution.

EXPERIMENTAL

Equipment and reagents

Conductance instrument. The bipolar pulse conductance technique has been described [7, 8], as has the application of bipolar pulse conductometric monitoring to i.s.e. measurements [9—11]. The instrument used in this work [9, 13] operates in the voltage pulse mode.

Electrodes. The calcium electrodes used in this work were of the coated-wire type developed by Freiser and Cattrall [14] and the specific construction has been described [10]. The ratio of ion-exchanger to poly(vinyl chloride) was 70/30. The polarizable counter electrodes studied were platinum and stainless steel wires, each 2.5 cm long and 0.7 mm in diameter. They were both mounted parallel to the membranes of the calcium electrode with a spacing of about 5 mm between electrodes. A single-junction Ag/AgCl electrode (Corning Model 476029) was also used as a counter electrode.

Reagents. Many electroactive species are soluble only in strongly acidic solutions, which cannot be used in conjunction with the calcium electrode. It was desired to use species that were stable in neutral, unbuffered solution. Therefore, the triiodide/iodide couple (1 mM each) was chosen, and the solution was generated by combination of 1 mM I_2 and 2 mM NaI. The Fe^{2+}/Fe^{3+} couple (1 mM) was also studied, but had to be prepared fresh each day, as both iron(II) and iron(III) slowly precipitate from neutral solution as hydroxides. The ascorbic acid solution (10 mM) was also prepared fresh each day. All solutions were prepared using deionized-distilled water and reagent-grade chemicals.

Measurement techniques

Conductance measurements. Current measurements were made using a computer-controlled bipolar pulse conductance instrument [15]. For each

set of experimental conditions studied, a current-voltage (i/V) curve was obtained [10]. The pulse amplitude, as measured from the foot of the pulse (instrumental ground) to its plateau, ranged from 0.0 to 5.0 V. At each pulse amplitude, 256 individual current measurements were taken. For each set of experimental conditions, a i/V curve was taken for a cell containing the calcium electrode and each of the three counter electrodes to be studied (Pt, stainless steel, and Ag/AgCl). All solutions were stirred magnetically during measurements.

Potentiometric measurements. Potentiometric measurements were made with a Corning Model 130 pH meter operating in the millivolt mode. The Ag/AgCl electrode was used as the reference electrode. All solutions were stirred magnetically during measurements.

RESULTS AND DISCUSSION

Investigation of shifting of electrode potentials

The most likely type of electrochemical interference one could encounter in bipolar pulse conductance monitoring of i.s.e.'s would be a shift in the electrochemical potential of the polarizable counter electrode, caused by the presence of electroactive species in solution. This possibility was first investigated with potentiometric measurements, then with i/V curve construction in the conductometric method.

Potentiometric measurements. Table 1 is a summary of potentiometric measurements made with the calcium electrode and three different "reference" electrodes, the Ag/AgCl electrode being the only true reference electrode. The values tabulated are the differences in measurements between a

TABLE 1

Potentiometric measurements with different counter electrodes
(All values are the difference between the potential measured for the indicated solution and that measured for a 1 mM Ca^{2+} solution)

Species	Conc. (mM)	Potential difference (mV)		
		Stainless steel	Pt	Ag/AgCl
Ca^{2+}	0.1	−50	−30	−30
Ca^{2+}	10	+60	+60	+30
Ascorbic acid	10[a]	0	+20	0
Fe^{3+}/Fe^{2+}	0.5 each[a]	0	−100	+50
Cu^{2+}	10[a]	−150	0	+10
I_3^-/I^-	5 each[a]	−360	−760	−240
Ag^+	10[a]	−690	−520	0
$Fe(CN)_6^{3-}/Fe(CN)_6^{4-}$	5 each[a]	−150	−290	0

[a]Also contained 1 mM Ca^{2+}.

1 mM Ca^{2+} solution and a solution of the electroactive species containing 1 mM Ca^{2+}. Most of the potentials measured with the stainless steel and platinum electrodes drifted substantially (20—40 mV), with the platinum electrode showing more drift in most cases. The potential of the steel electrode is affected most by the triiodide/iodide and hexacyanoferrate(II)/(III), and by Ag^+ and Cu^{2+}. Silver(I) and copper(II) probably react with the steel electrode, because the reactions $Fe + Cu^{2+} \rightleftharpoons Fe^{2+} + Cu$ ($E = +0.777$ V vs. NHE) and $Fe + 2Ag^+ \rightleftharpoons Fe^{2+} + 2Ag$ ($E = +1.239$ V vs. NHE) are favorable [16]. It is interesting to note that the iron couple does not affect the potential of the steel electrode, which suggests that the electrode reaches a potential on its own that involves redox processes of iron.

The platinum electrode does not stabilize to any great extent and drifts in the absence of electroactive agents. The three redox couples did stabilize it, and the individual species all produced some effect, except for copper(II). A passivating layer of platinum oxide probably accounts for any small extent of self-stabilization, and may not have been affected by a weak oxidizing agent such as copper(II).

The potential of the Ag/AgCl electrode can be assumed to be unaffected by the electroactive species in solution, because the half-cell of the electrode is well poised, and shielded from the test solution by a ceramic junction. Therefore, the deviations shown in Table 1 must be due to an interaction with the calcium i.s.e. The change caused by copper(II) is reasonable (considering selectivity) as is the effect of the iron couple. The change caused by the I_3^-/I^- couple was unexpected. Apparently, triiodide can enter the membrane, and was observed to discolor it. Also, the conductometric measurements discussed in the next section indicate penetration of the membrane by an ionic species when triiodide was present in solution.

Conductometric measurements. It was shown previously with the calcium and fluoride electrodes that a series of current measurements at increasing pulse heights yielded a plot of current vs. voltage which was a straight line. The slope of the line was equal to conductance of the cell (R_x^{-1}) and the intercept was a measure of the short-circuited electrode potential. This line was defined as a current-voltage curve [10].

Current-voltage curves were obtained for the solutions and calcium electrode/counter electrode combinations that were evaluated above with potentiometric monitoring. A pulse width of 100 μs was used, and all of the i/V curves were linear. However, the presence of electroactive species did affect the intercept in most cases, and sometimes the slope. Table 2 is a summary of the changes in the intercept of the i/V curve for the various electroactive species/counter electrode combinations. Once again, the differences in measurements for 1 mM Ca^{2+} and 1 mM Ca^{2+} solution containing the electroactive species are tabulated. The identities of the species that cause changes and the directions of change in the intercepts are reasonably consistent with the potentiometric values reported in Table 1. There is a fair degree of correlation (correlation coefficient = 0.94) in the magnitudes of

TABLE 2

Conductometric measurements with different counter electrodes
(All values are the difference between the i/V curve intercept obtained for the indicated solution and that obtained for a 1 mM Ca^{2+} solution)

Species (mM)	Conc. (mM)	Current difference (nA)		
		Stainless steel	Pt	Ag/AgCl
Ca^{2+}	0.1	−34	−7	−12
Ca^{2+}	10	+24	+19	+12
Ascorbic acid	10[a]	0	+18	0
Fe^{3+}/Fe^{2+}	0.5 each[a]	0	−32	+17
Cu^{2+}	10[a]	−62	−7	+1
I_3^-/I^-	5 each[a]	−41	−190	−49
Ag^+	10[a]	−110	−88	0
$Fe(CN)_6^{3-}/Fe(CN)_6^{4-}$	5 each[a]	−29	−37	0

[a] Also contained 1 mM Ca^{2+}.

the conductometric and potentiometric errors. The potentiometric measurements with stainless steel and platinum counter electrodes were subject to errors caused by drift, so the agreement between potentiometric and conductometric measurements is not expected to be very good.

Copper(II) had a significant effect on the stainless steel electrode. It was observed earlier [10] that Cu^{2+} had a negative selectivity coefficient when the bipolar pulse conductance method was used to monitor the calcium electrode, whereas the other cations yielded the expected positive coefficients. The negative shift of the counter electrode potential caused by copper(II) probably accounts for the negative selectivity coefficient. A small effect of Cu^{2+} at the Pt counter electrode was noted conductometrically, and was probably obscured by drift in the potentiometric measurements.

The i/V curve slope, (cell resistance)$^{-1}$, is increased in the presence of triiodide; this indicates that the cell resistance is decreased by the presence of more charge carriers in solution, and possibly also by penetration of the membrane by ionic species. The resistance decreased significantly upon continued exposure of the i.s.e. to triiodide solution, accompanied by a corresponding decrease in the value of the intercept; these observations indicate some change in membrane composition.

The large drift obtained in potentiometric measurements with the stainless steel and platinum electrodes as reference electrodes was not obtained in conductometric measurements. The bipolar pulse conductance method entails passage of a significant amount of current through the cell, and a small percentage of this current may induce interfacial faradaic reactions, thereby setting up a stabilizing half-cell at the counter electrode. Any effects from faradaic reactions were not noticed when 100-μs pulses were used, but could still have been present to an extent that was insignificant with respect

to the ohmic and capacitive charging currents that were measured. One would expect measurement errors from faradaic reactions to become significant as longer pulse durations are used, and these errors are characterized in the next section.

Investigation of errors from faradaic reactions

Previous treatments of possible errors in bipolar pulse conductance measurements [7, 8, 17] have not considered errors from faradaic reactions. However, it is relatively easy to predict qualitatively in what situations a faradaic reaction could occur and what effect it would have on a conductometric measurement. A faradaic reaction would be expected whenever the double-layer capacitances of the two electrodes are charged to a large enough extent to give the cell sufficient e.m.f. to drive an electrolytic reaction. Double-layer capacitances receive increasing amounts of charge as pulse duration and/or pulse amplitude are increased.

The theory of voltage pulse measurements in bipolar conductance has been discussed [7, 8]. It has been shown that the first voltage pulse places a certain charge on the double-layer capacitances. The second pulse, which is equal in magnitude but opposite in sign to the first pulse, removes this charge and leaves a small residual voltage on the double layer. This residual voltage is due to the simultaneous decay and removal of the charge placed on the cell capacitances during the first pulse, and accounts for the main source of error in bipolar pulse conductance measurements. The current, which is measured at the end of the second pulse, decreases as this residual voltage increases:

$$i_m = [e_2 - (e_c)_2] / R_x \tag{1}$$

where i_m is the measured current, e_2 is the magnitude of the second voltage pulse, $(e_c)_2$ is the residual voltage, and R_x is the cell resistance. The absolute error in the measurement of ohmic currents is therefore $-(e_c)_2/R_x$. This error term increases with increasing pulse height and especially with increasing pulse duration [7, 8].

A faradaic reaction is most likely to occur at the end of the first voltage pulse, because that is the point during the cycle at which the double layer is charged to the greatest extent. Any charge which is lost by some reaction during the first pulse obviously cannot be removed from the double layer during the second pulse. Therefore, the second pulse will overcompensate for the first pulse to a greater extent than it does in the absence of faradaic reactions. If a faradaic reaction can be initiated as i/V data are collected, it will result in a negative error in measured current, and this error will be most predominant at the higher pulse heights. Longer pulse durations would be expected to allow more charging of the double-layer capacitances and could subsequently initiate a faradaic reaction.

The i/V curves collected at 100-μs pulse widths for this work did not show any apparent deviations from linearity. If a faradaic reaction did occur at the

higher pulse heights, its effects were negligible. However, the predicted deviations from linearity did occur when 10-ms pulses were used. Figure 1 shows a set of i/V plots obtained for a solution containing 10 mM ascorbic acid and 1 mM Ca^{2+}. There is a slight bend in the plot obtained for 10-ms pulse duration. The plots for 0.1, 1, and 100 ms are all linear. Presumably, a faradaic reaction was initiated around the midpoint of the 10-ms curve, and was in effect for all the points in the 100-ms curve.

A slight deviation from linearity in the i/V curves was noticed for all of the solutions studied if 10-ms voltage pulses were used to generate the current. For example, Fig. 2 shows i/V plots obtained for a solution containing 1 mM Ca^{2+}. Both Ag/AgCl and stainless steel electrodes gave plots with a slight negative deviation from linearity. A platinum counter electrode also showed the same effect. This nonlinearity may be due to a faradaic reaction involving some constituents of the cell such as dissolved oxygen, or to nonlinearities in the double-layer capacitances. However, the deviation from linearity increases significantly when the stainless steel counter electrode is

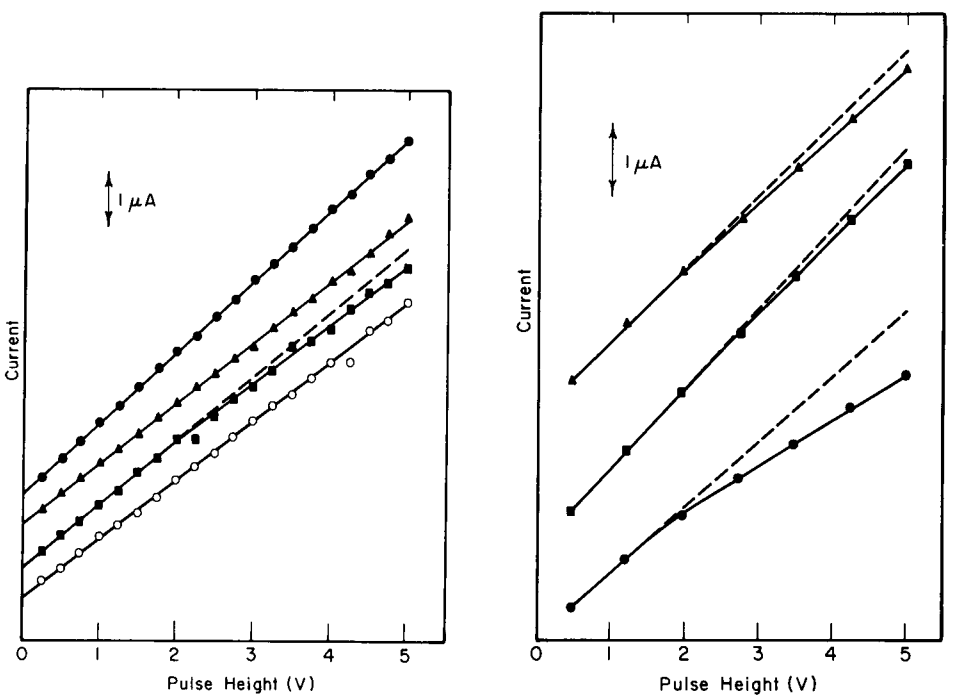

Fig. 1. Current-voltage curves for solutions containing 10 mM ascorbic acid and 1 mM Ca^{2+}. A platinum counter electrode was used. Pulse duration: (•) 0.1 ms; (▲) 1 ms; (■) 10 ms; (○) 100 ms.

Fig. 2. Current-voltage curves using 10-ms pulse durations: (▲) Ag/AgCl counter electrode in 1 mM Ca^{2+}; (■) stainless steel counter electrode in 1 mM Ca^{2+}; (•) stainless steel counter electrode in 1 mM Ca^{2+}, 10 mM Cu^{2+}.

used and copper(II) is added to the solution. The same effect was observed for the platinum electrode, but not for the Ag/AgCl electrode.

Large deviations from linearity such as that caused by copper(II) were observed for silver(I) and ascorbic acid. The counter electrode was pulsed negative, then positive, in the bipolar conductance measurements reported here. Therefore, if a faradaic reaction could occur during the first pulse, it would most likely be a reduction. Copper(II) and silver(I) are very easily reduced, and might be expected to yield a faradaic reaction error. Interestingly enough, ascorbic acid, which is easily oxidized, also gives a negative error, possibly because of removal of charge from the double layer by a faradaic oxidation during the second pulse.

It is obvious that if a reduction occurs at the counter electrode, a corresponding oxidation must be taking place within the i.s.e., and vice versa. The site for a faradaic reaction within a coated-wire electrode would naturally be the interface between the copper wire and the PVC membrane. The most likely oxidation is the oxidation of copper to copper(II), while the most likely reduction would be the reduction of oxygen that had diffused in from solution [6]. An electrolytic reaction was probably prevented in our previous work [10] because short pulse durations (0.1 ms) were used and because there was no appreciable concentration of an electroactive species at the counter electrode. However, it was shown that the performance of the membrane deteriorated rapidly if long (100—1000 ms) pulse durations were used, and it was postulated that a faradaic reaction could be taking place. The results from the present work suggest that faradaic reactions can occur to a greater extent at long pulse durations when electroactive species are present in solution. Therefore, the use of short duration voltage pulses in bipolar conductance measurements with i.s.e.'s is even more essential if electroactive species are present in solution.

Conclusion

The results from this work indicate that a real reference electrode must be used in bipolar conductance monitoring of i.s.e.'s if electroactive species that can polarize an inert counter electrode are present in solution. Otherwise, the electrochemical potential of the counter electrode could shift significantly, and would yield large errors in the i/V plot intercept. Faradaic reactions can occur at long (10 ms) pulse durations, and a nonlinear i/V plot is obtained. Long pulse durations should be avoided, as errors in measurements can result, along with deterioration of the electrode membrane.

We thank L. R. Faulkner for helpful ideas and discussion. One of us (C. R. P.) gratefully acknowledges an American Chemical Society, Division of Analytical Chemistry Fellowship sponsored by FACSS. This research was supported in part by the National Science Foundation (CHE-81-08816).

REFERENCES

1 C. Harzdorf, Anal. Chim. Acta, 136 (1982) 61.
2 J. W. Bixler, R. Nee and S. P. Perone, Anal. Chim. Acta, 99 (1978) 225.
3 F. G. K. Baucke, Fresenius Z. Anal. Chem., 282 (1976) 105.
4 S. Sakura and R. Virtanen, Bull. Chem. Soc. Jpn., 54 (1981) 1360.
5 D. Midgley, Anal. Chim. Acta, 87 (1976) 7.
6 A. Hulanicki and M. Trojanowicz, Anal. Chim. Acta, 87 (1976) 411.
7 D. E. Johnson and C. G. Enke, Anal. Chem., 42 (1970) 329.
8 K. J. Caserta, F. J. Holler, S. R. Crouch and C. G. Enke, Anal. Chem., 50 (1978) 1534.
9 C. R. Powley, R. F. Geiger, Jr. and T. A. Nieman, Anal. Chem., 52 (1980) 705.
10 C. R. Powley and T. A. Nieman, Anal. Chim. Acta, 139 (1982) 61; 139 (1982) 83.
11 C. R. Powley and T. A. Nieman, Anal. Chim. Acta, 152 (1983) 173.
12 A. J. Bard and L. R. Faulkner, Electrochemical Methods, Wiley, New York, 1980, Ch. 1, 2.
13 R. F. Geiger, Jr., Ph.D. Thesis, University of Illinois, 1983.
14 R. W. Cattrall and H. Freiser, Anal. Chem., 43 (1971) 1905.
15 C. R. Powley, Ph.D. Thesis, University of Illinois, 1982.
16 D. G. Peters, J. M. Hayes and G. M. Hieftje, Chemical Separations and Measurements, W. B. Saunders, New York, 1974, pp. A17—20.
17 P. H. Daum and D. F. Nelson, Anal. Chem., 45 (1973) 463.

Analytica Chimica Acta, 155 (1983) 11—20
Elsevier Science Publishers B.V., Amsterdam — Printed in The Netherlands

POLYMER-MEMBRANE pH ELECTRODES AS INTERNAL ELEMENTS FOR POTENTIOMETRIC GAS-SENSING SYSTEMS

W. N. OPDYCKE, S. J. PARKS and M. E. MEYERHOFF*
Department of Chemistry, University of Michigan, Ann Arbor, MI 48109 (U.S.A.)
(Received 2nd June 1983)

SUMMARY

The use of polymer-membrane pH electrodes as internal sensing elements for the fabrication of inexpensive ammonia and carbon dioxide gas sensing systems is reported. The pH-responsive polymer membranes are prepared by incorporating tridodecylamine as the neutral carrier in plasticized poly(vinyl chloride) membranes. Both static and continuous-flow gas-sensing arrangements are described. For miniature static gas sensors, the internal polymer pH electrode can be made with or without an internal reference solution. In the latter case, the polymeric membrane is coated directly onto a graphite substrate. The polymer pH electrode can also be prepared in tubular form and used in conjunction with a gas dialysis chamber for automated continuous-flow determinations of carbon dioxide and ammonia. Slopes, response times, and reproducibility of these new gas-sensing systems are evaluated using optimized internal electrolytes, flow rates, and gas-permeable membrane materials. When appropriate reagents and materials are used, the static sensors exhibit slopes in the range 48—62 mV/decade with potentials reproducible to less than ±1.5 mV at gas concentrations greater than 10^{-3} M.

The use of potentiometric gas sensors for the direct measurement of dissolved gases (NH_3, CO_2, NO_2, etc.) or as final detectors for indirect bioanalytical methods involving enzymes and microbial cells has grown rapidly in recent years [1—3]. Commercial gas sensors commonly utilized in such applications have glass pH electrodes as internal elements [3]. Although these sensors often exhibit theoretically predicted response properties and Nernstian behavior [4], the commercial devices are rather large (tip diameter 12—15 mm) and expensive. Moreover, efforts to miniaturize these probes have been hampered by the fragile nature of the glass electrode and the flat bottom geometry required for functional static gas sensor designs.

In view of the limitations imposed by the use of glass electrodes, several workers have prepared gas sensors with alternative internal pH-responsive transducers. Mascini and Cremisini [5] reported the use of thermo-molded antimony-type pH electrodes as inner elements while workers at General Electric have patented the concept of using electrodes based on palladium or iridium oxide for the fabrication of miniature CO_2 sensors [6]. Unfortunately, metal/metal oxide pH transducers may be subject to interferences from the redox environment of the sample (e.g., oxygen content) and this could limit their utility in the design of stable gas sensing systems.

0003-2670/83/$03.00

Over the past few years, our research efforts have focused on replacing the traditional glass-membrane electrodes in gas sensors with polymer-membrane ion-selective electrodes [7—11]. Thus far, polymer membranes responsive to ammonium and carbonate ions have been utilized, along with appropriate internal buffer reagents, to prepare small, inexpensive, and rugged gas sensors for NH_3 and CO_2 [7—9]. The polymer-membrane electrodes have also been fabricated in a novel tubular form and used in conjunction with a gas dialysis chamber and flowing internal electrolyte to develop attractive automated continuous-flow gas sensing arrangements [11, 12].

Recently, Schulthess et al. [13] introduced a new pH-responsive polymer membrane electrode based on the incorporation of tridodecylamine in a poly(vinyl chloride) (PVC) matrix. Although the use of this polymer pH membrane has already been suggested for the fabrication of inexpensive gas sensors [8], it is the purpose of this paper thoroughly to evaluate and document this approach. Miniature static as well as automated CO_2 gas-sensing arrangements are described and evaluated. The feasibility of utilizing polymer-coated graphite pH electrodes within the miniature static probes is also examined. It will be shown that when constructed with appropriate internal electrolytes, gas-permeable membranes, etc., the resulting gas-sensing devices have response properties that compare favorably with the costly commercial glass pH electrode-based probes.

EXPERIMENTAL

Apparatus and materials

All potentiometric measurements were made using a Corning model 12, a Fisher Accumet model 620, or an Altex SelectIon 2000 pH/mV meter, and were recorded on either a Heath/Schlumberger model SR-204 or a Houston Instruments Omniscribe strip-chart recorder. Potentials for the polymer-membrane pH electrodes were evaluated against a saturated calomel reference electrode (SCE).

A schematic diagram for the automated CO_2-sensing system is shown in Fig. 1. The ammonia system was essentially the same, except that the segmented stream required debubbling prior to passage through the dialysis chamber. The dialysis block and mixing coils were heated to 30°C for CO_2 determinations. Two dialysis chambers were used for these studies, one with a channel/volume ratio of 1:1, and the other with a volume ratio of 1:4. These chambers were fitted with a polytetrafluoroethylene (PTFE) membrane (W. L. Gore Inc.) for the NH_3-sensing system and a silicone polycarbonate membrane (General Electric) for the CO_2-sensing system.

Reagents

All chemicals used were of reagent grade. Standard solutions and buffers were prepared with distilled, deionized water.

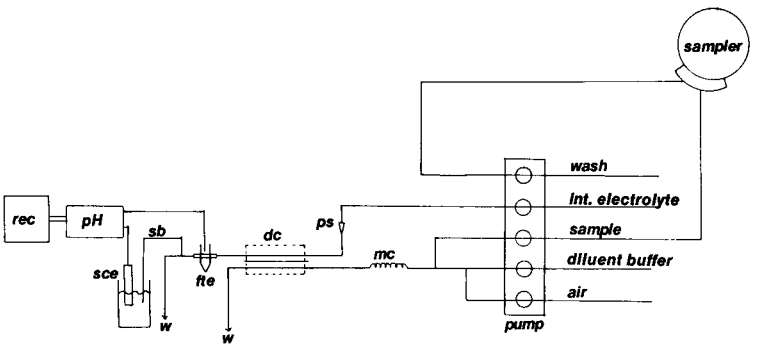

Fig. 1. Schematic diagram of automated carbon dioxide assay system: (rec) recorder; (pH) pH-mV meter; (SCE) saturated calomel reference electrode; (sb) salt bridge; (fte) flow-through electrode; (w) waste; (dc) dialysis chamber; (ps) pulse suppressor; (mc) 7-turn mixing coil.

The pH-sensitive polymer membrane consisted of tridodecylamine, sodium tetraphenylborate (Eastman Kodak), poly(vinyl chloride) (chromatographic grade; Polysciences), and dibutyl sebacate (Sigma Chemical Co.).

In the automated system for carbon dioxide, the flowing internal electrolyte was a 0.001 M $NaHCO_3$ solution prepared in 0.01 M NaCl. The diluent stream was 0.1 M citrate buffer (pH 4.45). Various concentrations of sodium hydrogencarbonate were prepared as standards for calibration purposes. The internal reference solution for the tubular electrode was 0.5 M citrate buffer (pH 4.45) containing 0.1 M NaCl.

For the automated ammonia-sensing system, the flowing internal electrolyte was 0.001 M NH_4Cl. The diluent was 0.001 M NaOH. Several concentrations of ammonium chloride were prepared as standards for calibration purposes. The internal reference solution for the polymer pH electrode was 0.01 M NH_4Cl.

Preparation of polymer pH electrodes and gas sensors

Polymer pH electrodes were of two types, those with and those without internal reference solutions. Preparation of the polymer pH membrane and its incorporation into pH electrodes with internal reference solutions were described previously [8]. A schematic diagram of a pH electrode without the internal reference solution and the corresponding static gas sensor is shown in Fig. 2. This electrode consists of a 0.5-mm diameter graphite rod (Pentel Hi-Polymer mechanical pencil lead) encased in a stainless steel syringe needle for strength and to provide electrical contact. This assembly is encased in heat-shrink tubing to provide insulation. The tip of the graphite rod is left exposed and is fitted with a piece of PVC tubing to provide a suitable surface for bonding the membrane. The pH-sensitive membrane is applied dropwise (as a solution in tetrahydrofuran) to the tip. The gas sensors were constructed from pipet tips as described earlier [7]. The gas-

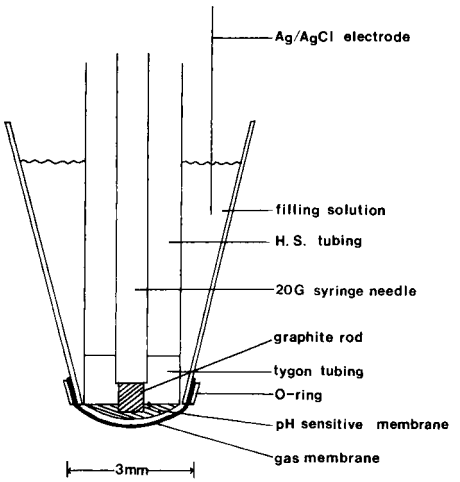

Fig. 2. Schematic diagram of static gas-sensing system utilizing a coated-graphite pH electrode.

permeable membrane used was microporous PTFE (0.2-μm pore; W. L. Gore and Assoc.). The tubular flow-through pH electrodes were prepared as described previously for ammonium and carbonate systems [9, 11].

These electrodes and corresponding gas sensors were evaluated for potentiometric response and analytical utility under the specific conditions described below.

Calibration curves for pH electrodes and static sensors

Potentiometric response for the polymer-based pH electrodes was obtained in a solution which was 0.05 M each in sodium acetate, tris-[hydroxymethyl]-aminomethane hydrochloride, and *N*-[2-acetamido]-2-aminomethanesulfonic acid. Microliter volumes of sodium hydroxide or hydrochloric acid were added to this solution and the actual pH was monitored after each addition with a calibrated glass pH electrode (Fisher 13-639-90). The potential of the polymer-membrane electrode (vs. SCE) was plotted vs. the measured pH value. Results for the static CO_2 gas sensors were obtained from additions of sodium hydrogencarbonate to a 0.1 M citrate buffer (pH 4.5) while data for the ammonia sensors were obtained from additions of ammonium chloride to 0.1 M NaOH. Measurements were usually made at room temperature.

RESULTS AND DISCUSSION

Static pH electrodes

Conventional polymer-based pH electrodes are those that have internal reference solutions. Their performance has been described [4, 13] and the response characteristics of our electrodes are essentially the same. There is,

however, a possible problem when attempts are made to use conventional polymer pH electrodes (i.e., ones with internal reference solutions) in gas-sensing configurations. Analyte gas dissolved in the thin electrolyte film of the sensor may diffuse through the PVC ion-selective membrane and change the pH of the internal reference solution. This would result in errant or drifting response. Indeed, this behavior has been exploited to produce a hydrogen carbonate ion-selective electrode [14], which in reality functions as an inverted gas sensor. Thus, in order to produce useful gas sensors, the internal reference solution of the pH electrode must be buffered. Four buffers were evaluated to establish which would best maintain a constant pH in the internal reference solution. The buffers investigated were 0.1 M and 1 M phosphate—HCl, pH 7.0, and 0.1 M and 1 M citrate—HCl, pH 4.2. For this study, an Orion 95-02 gas-sensor body was used with a pH-sensitive polymer membrane as the gas-permeable membrane and the various buffers as the internal filling solutions. The pH of the thin buffer film was monitored with the internal glass pH electrode as the analyte gas (NH_3 or CO_2) concentration was increased. Although all of the buffers worked well, the 1 M citrate buffer yielded best results, holding the pH change to just 0.03 units even for gas concentrations as high as 10^{-2} M. Because it was found later that the 0.5 M and 0.25 M citrate buffers worked nearly as well, these were used for all subsequent experiments to prevent large osmotic effects.

Coated-substrate pH electrodes were also evaluated. Both graphite rods and platinum wires were used as substrates. For most experiments, graphite electrodes were used because it was easier to make them with the proper flat-bottom geometry desirable for good gas-sensor design and response. A calibration curve for the coated graphite pH electrode is shown in Fig. 3. The electrode responds logarithmically (typical slopes of 59—64 mV/10-fold change in H^+ activity) to changes in hydrogen ion activity between pH 4 and 10. Response was observed as low as pH 2 and as high as pH 12. Response times to reach equilibrium potentials were typically 15—20 s per unit pH change. Equilibrium was assumed when the potential drift was less than 0.4 mV min^{-1}. Depending on the electrode, the reproducibility of potentials on consecutive calibrations can be as good as ±1 mV or as poor as ±4 mV. Day-to-day reproducibility with regard to absolute potential values was found to be poor, although the slopes remained relatively constant. One possible explanation for this has to do with the nature of the inner reference potential of the coated substrate electrodes. This inner potential system is usually described as a metal/metal oxide half-cell with the necessary oxygen coming from diffusion of oxygen and water through the polymer membrane [15]. Changes in the oxygen concentration of the surrounding electrolyte will change the oxygen concentration in the membrane and perhaps alter the metal-oxide layer on the inner conductor. This will produce drifting or unstable potentials. Keeping the membrane hydrated apparently slows this process and helps to improve the reproducibility somewhat. In general, it was found that the coated-graphite pH electrodes were more stable than the coated-wire types.

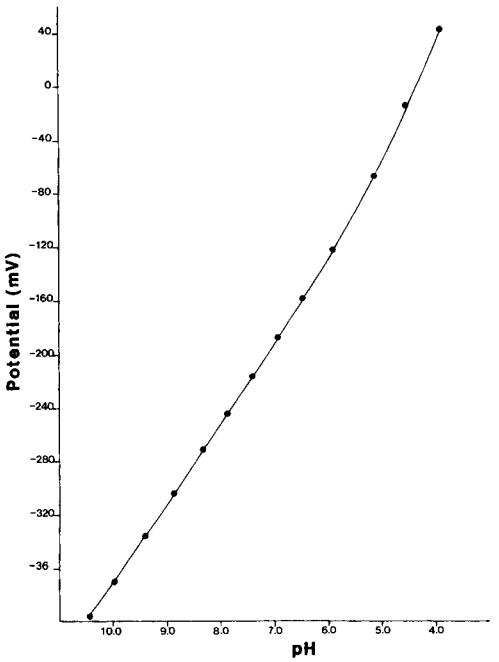

Fig. 3. Typical calibration curve for the coated-graphite pH electrode.

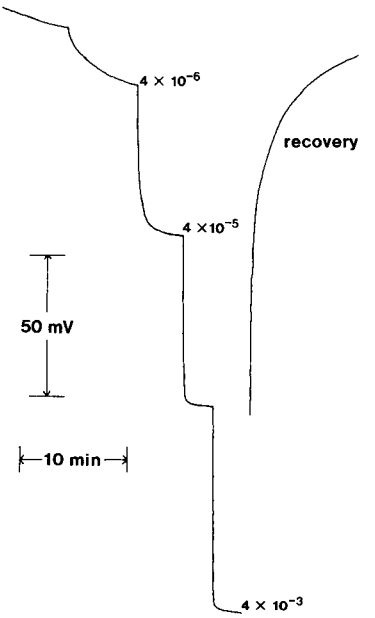

Fig. 4. Typical chart recording showing response and recovery times for the static ammonia sensor. Molar concentrations are given on the curves.

Static gas sensors

Gas sensors were constructed from both conventional polymer pH electrodes and coated-graphite electrodes. Both types of sensors displayed similar response properties. To avoid repetition, the response characteristics of the conventional polymer pH electrode-based sensors will be discussed in detail and only significant differences between the two will be mentioned.

An important parameter controlling gas-sensor response is the composition of the internal filling solution. The components of this solution and their concentrations determine the detection limits, slope, and time response of the sensor [4]. In order to obtain optimal response with the ammonia sensor, four internal filling solutions were evaluated. Two were commercial solutions (Orion 95-10-02 and HNU 10-10-01) and two were laboratory preparations (0.01 M NH_4Cl in 0.1 M NaCl and 0.1 M NH_4Cl). The laboratory preparations performed better than the commercial ones, giving slopes that were typically 57—60 mV/decade. The 0.1 M NH_4Cl solution gave the best dynamic measurement range, but the solution which was 0.01 M NH_4Cl in 0.1 M NaCl yielded lower detection limits and faster response times. The results described below were obtained using the latter solution.

The static ammonia gas sensor was evaluated for time response, linear response range, slope, and reproducibility. Figure 4 shows a typical recording

for the NH_3 sensor response as ammonium chloride was added to a 0.1 M NaOH solution. The time response was slow at low concentrations (5—10 min) but improved rapidly with increasing gas concentration. It can also be seen that the recovery time of the sensor, when placed into a fresh solution of sodium hydroxide without ammonia, was similar to that of commercial ammonia sensors (i.e., 20 min). A typical calibration curve for the ammonia gas sensor is shown in Fig. 5. Near-Nernstian response (59—62 mV/decade) was observed from 2×10^{-5} M to 4×10^{-2} M ammonia. The detection limit was estimated to be of the order of $1—2 \times 10^{-6}$ M. With regard to reproducibility, seven consecutive calibrations on a given day, yielded a slope of 61.2 ± 0.8 mV over a range from 4×10^{-5} M to 4×10^{-2} M ammonia. However, variations in the absolute potentials at equal analyte concentrations were somewhat greater, ranging from ±2.5 mV at a concentration of 4×10^{-5} M to ±1.6 mV at 4×10^{-3} M. Day-to-day reproducibility of absolute potentials was poor, because of evaporation of the internal filling solution. For best results, the internal filling solution should be renewed daily, and as with any membrane electrode system, the sensor should be calibrated before and after measurements of unknowns.

The CO_2 gas sensor was evaluated in a similar fashion. Again, four filling solutions were studied: HNU ISE 10-22-02, Orion 95-02-02, 0.01 M $NaHCO_3$ in 0.1 M NaCl, and 0.01 M $NaHCO_3$ in 0.25 M NaCl. The last solution was evaluated in an attempt to establish whether matching the osmolarity of the internal filling solution with that of the sample solution would reduce e.m.f. drift caused by diffusion of water vapor. Drift was reduced, but the performance of both of the laboratory-prepared solutions was inferior to that obtained with the commercial solutions. Operation with the commercial

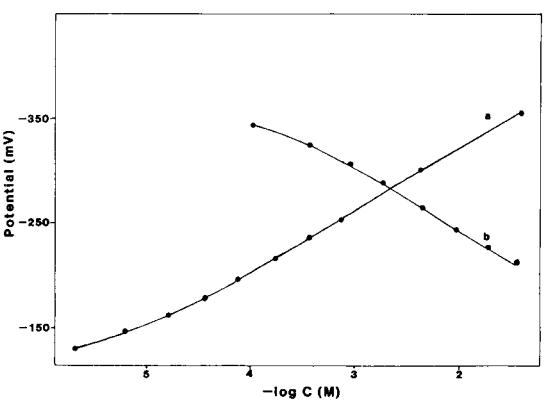

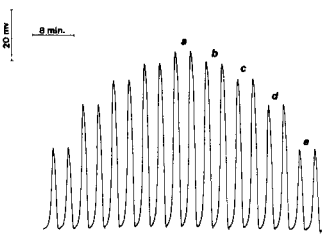

Fig. 5. Typical calibration curve for the static sensors based on an internal polymer membrane pH electrode: (a) ammonia; (b) carbon dioxide.

Fig. 6. Typical strip-chart recording obtained for automated CO_2 system. Concentrations refer to $NaHCO_3$ standards placed into the sampler: (a) 1×10^{-3} M; (b) 8×10^{-4} M; (c) 6×10^{-4} M; (d) 4×10^{-4} M; (e) 2×10^{-4} M.

solutions yielded larger linear response ranges and improved slopes. The HNU internal filling solution was used for all subsequent experiments.

Another important parameter of the CO_2 gas sensor is the selection of the gas-permeable membrane. Silicone rubber membranes are often used in commercial CO_2 sensors rather than PTFE membranes. However, in the particular sensor configuration evaluated in this work, difficulties in attaching the silicone rubber membranes severely limited their usefulness; such membranes did not fit the shape of the sensor well and tended to leak. Thus, the PTFE membrane was used exclusively in the fabrication of the static gas sensors.

Response times for the static CO_2 sensor ranged from 7 min at concentrations of 10^{-4}—10^{-3} M to less than 1 min at concentrations greater than 10^{-3} M. Figure 5 shows a typical calibration curve for the polymer pH electrode-based CO_2 sensor. Response is logarithmic (slopes of 48—53 mV/decade) from 2×10^{-4} M to 4×10^{-2} M CO_2. Reproducibility is generally the same as for the ammonia gas sensor (±2.5 mV at low gas concentrations, ±1.5 mV for concentrations greater than 10^{-3} M).

In general, the static sensors prepared with the polymer membrane pH electrodes possess response properties quite similar to those of conventional glass pH electrode-based probes. The one major difference is the larger variation in absolute potentials from day to day. However, provided that appropriate calibration procedures are used, the new devices appear to perform adequately.

Automated systems

The automated NH_3- and CO_2-sensing systems described here utilize the same chemical detection principles as the static sensors described above. The configurations used to adapt the static sensors to the automated mode are variations of those described previously [11] based on a tubular ammonium ion-sensitive polymer membrane electrode as the detector. These variations along with response characteristics for each system are presented below.

Of the two systems constructed, the CO_2 sensing system was the more extensively studied. In developing this system, the aim was to optimize the operating parameters to permit low-level CO_2 measurements with good sample throughput. The continuous flow manifold shown in Fig. 1 differs in several ways from that described earlier [11]. A major change in the apparatus involved utilizing the sample stream without removing the air segmentation. A microporous teflon membrane was used in the gas dialysis chamber for the ammonia system [11]. Air can pass through that membrane resulting in large open circuit noise in the detection stream. Therefore, for the CO_2 system, a homogeneous silicone polycarbonate membrane was used, through which air bubbles do not permeate. The advantage of using an air-segmented sample stream is that it allows for more of the sample CO_2 to be detected. This is because any CO_2 formed in the sample slug will equilibrate with the adjacent air bubbles. Removal of these air bubbles results in

a substantial loss of the total CO_2 sample. Using this arrangement, the signal resulting from low CO_2 concentrations was greatly increased.

As Durst [16] has suggested, the sensitivity of the system can be enhanced by increasing the flow rate of the sample stream relative to the recipient stream. To this end, a flow rate ratio of 2:1 was used. This results in a concentration effect of the sample in the recipient electrolyte stream because this stream is flowing much more slowly than the sample stream. In an effort to improve further the sensitivity of the system, a special dialysis chamber was prepared with the recipient stream being 1/4 the volume of the sample stream. If the system was allowed to reach equilibrium using this chamber, with solutions of equal pH in both streams, the concentration of sample in the recipient stream would be 80% of that originally present in the sample stream relative to only 50% for the usual channel ratio of 1:1. Therefore, although equilibrium is never actually achieved and the two streams do not actually have the same pH value, in practice, using the 1:4 chamber enables the recipient stream to contain a higher concentration of sample and thus results in a larger signal.

The concentration of the electrolyte in the recipient stream also plays an important role in the sensitivity of the system. Bailey and Riley [17] reported that the concentration of the electrolyte should be ten times higher than the lowest sample concentration to be quantified. This is because low levels of CO_2 cannot produce a large enough pH change to be detected when the electrolyte is too concentrated. Several concentrations of electrolytes were examined and 10^{-3} M $NaHCO_3$ was found to be the best for samples containing between 10^{-4} M and 10^{-3} M CO_2. Figure 6 shows a typical strip-chart recording for the CO_2 detector based on the tubular polymer membrane pH electrode, operating at 20 samples per hour. It can be seen that the automated system displays excellent precision with peak potentials generally reproducible to ±1 mV. Resulting calibration graphs typically had slopes of 53—58 mV/decade with a logarithmic range from 2×10^{-4} to 10^{-3} M CO_2. For determinations of carbon dioxide at levels above 10^{-3} M, higher concentrations of sodium hydrogencarbonate in the recipient stream are recommended.

The ammonia-sensing system was constructed similarly to that described earlier [11] except that the ammonium ion-selective membrane used in the tubular electrode was replaced with a pH-sensitive one. Good results were obtained with this system, but it was not as sensitive as the one utilizing the ammonium ion-selective electrode. That system had lower detection limits because it utilized a "buffer trap" effect (i.e., the recipient stream is buffered to an appropriate pH so that NH_3 is converted to NH_4^+, thus preventing any loss of analyte by diffusion). Obviously this could not be done in gas-sensing systems based on pH detection. Although measuring pH changes does not provide a system optimized for the determination of low levels of ammonia, it does offer a convenient method of determining higher concentrations over a larger concentration range.

In summary, several designs for static and automated ammonia and carbon dioxide gas sensors based on polymer pH-sensitive membrane electrodes have been evaluated. In view of their low cost, simple design, and ease of miniaturization, these gas sensors offer an attractive alternative to gas-sensing devices based on conventional glass pH electrodes.

The authors acknowledge the support of the National Institute of Health (Grant GM 2882-01). In addition, S. J. Parks acknowledges support from the Environmental Protection Agency (Grant EPA-R-80806301).

REFERENCES

1 M. E. Meyerhoff and Y. M. Fraticelli, Anal. Chem., 54 (1982) 27R.
2 G. A. Rechnitz, Science, 214 (1981) 287.
3 M. Riley, in A. K. Covington (Ed.), Ion-Selective Electrode Methodology, Vol. II, CRC Press, Boca Raton, 1979, Ch. 1.
4 M. Mascini and C. Cremisini, Anal. Chim. Acta, 97 (1978) 237.
5 M. Mascini and C. Cremisini, Anal. Chim. Acta, 92 (1978) 277.
6 R. A. Macur, O. H. LeBlanc and W. T. Grubb, U.S. Pat. No. 3,905, 889, September 16, 1975.
7 M. E. Meyerhoff, Anal. Chem., 52 (1980) 1532.
8 M. E. Meyerhoff, Y. M. Fraticelli, J. A. Greenberg, J. Rosen, S. J. Parks and W. N. Opdycke, Clin. Chem., 28 (1982) 1973.
9 J. A. Greenberg and M. E. Meyerhoff, Anal. Chim. Acta, 141 (1982) 57.
10 M. E. Meyerhoff and R. H. Robins, Anal. Chem., 52 (1980) 2383.
11 Y. M. Fraticelli and M. E. Meyerhoff, Anal. Chem., 53 (1981) 992.
12 Y. M. Fraticelli and M. E. Meyerhoff, Anal. Chem., 55 (1983) 359.
13 W. Schulthess, Y. Shijo, H. V. Pham, E. Pretsch, D. Ammann and W. Simon, Anal. Chim. Acta, 131 (1981) 111.
14 R. J. J. Funck, W. E. Morf, P. Schultess, D. Ammann and W. Simon, Anal. Chem., 54 (1982) 423.
15 J. G. Schindler, G. Stork, H. J. Struh, W. Schmid and K. D. Karaschinski, Fresenius Z. Anal. Chem., 295 (1979) 248.
16 R. A. Durst, Anal. Lett., 10 (1977) 961.
17 P. L. Bailey, M. Riley, Analyst (London), 100 (1975) 1948.

Analytica Chimica Acta, 155 (1983) 21—27
Elsevier Science Publishers B.V., Amsterdam — Printed in The Netherlands

EFFECT OF POLISHING THE FLUORIDE-SELECTIVE ELECTRODE ON THE RESPONSE TIME AND SENSITIVITY IN FLOW SYSTEMS

W. J. VAN OORT* and E. J. J. M. VAN EERD

Department of Analytical Pharmacy, Subfaculty of Pharmacy, State University of Utrecht, Catharijnesingel 60, 3511 GH Utrecht (The Netherlands)

(Received 28th April 1983)

SUMMARY

The lanthanum fluoride electrode is not very successful for monitoring fluoride in flow streams, e.g., from chromatographic processes, because of its slow response rate. Much faster responses are possible when mixtures of methanol and TISAB-II solutions containing 10^{-6} M fluoride are used as the carrier stream and when the electrode surface is polished with very fine wet alumina powder. The flow cell was constructed in such a way that the diffusion film thickness was minimal. Flow streams injected centrally and perpendicular to the electrode surface and very thin flows along the surface proved to be the best hydrodynamic configuration. With this set-up, response times of 2—6 s could be achieved in detecting concentration changes between 10^{-3} and 10^{-6} M fluoride.

Ion-selective electrodes are frequently used in detection systems in flow streams. These measuring devices combine sensitivity and selectivity with simplicity but, unlike detection systems involving ultraviolet and fluorescence spectrophotometry, they show a time-dependent response to concentration changes in the measuring solutions. Particularly in flow-injection systems, in high-performance liquid chromatography (h.p.l.c.) of compounds with short retention times and in ion chromatography, the time scales of concentration changes and of the response times of ion-selective electrodes are of the same order of magnitude. Furthermore, the response times of ion-selective electrodes depend on the concentration level and the direction of concentration changes. According to Stulík and Pacáková [1], ion-selective electrodes are rarely used in h.p.l.c. detection systems because of these properties. The time-dependent behaviour of ion-selective electrodes has frequently been investigated for batch analysis and flow systems. The main methods make use of activity-step perturbation [2—6] and non-equilibrium potentiometric conditions [7]. A thorough review has been published by Lindner et al. [8].

The fluoride ion-selective electrode provides one of the most selective determinations of fluoride, if it is used between pH 3 and 8 with a special ionic-strength adjustment buffer (TISAB) [9]. A serious drawback of this electrode is its relatively slow response at low concentrations, which are

0003-2670/83/$03.00

often the most important in flow-injection analysis and chromatography. For instance, in fast-flow injection experiments, Mertens et al. [5] found that response times of 2—17 s were needed to reach 90% of the equilibrium potential for a concentration jump from 10^{-5} to 10^{-4} M fluoride and of 2—22 s in the reverse direction. They found 117 and 273 s, respectively, for similar concentration jumps in continuous flow systems when lower but more practical actual flow rates were used. Recently, Lindner et al. [2] explained the flow-rate dependence in terms of a theory based on the finding that below a critical activity, the electrode response is determined principally by processes slower than film diffusion.

Very little attention has been paid to the quality and the age of the electrode surface as parameters influencing dynamic behaviour. Lindner et al. [10] reported an increased response on polishing precipitate-based ion-selective electrodes. Dencks and Neeb [11] obtained reproducible and short response times by polishing their chloride ion-selective electrode with 1-μm diamond paste followed by appropriate conditioning. Landry et al. [12] rinsed their fluoride ion-selective electrode with a solution of beryllium sulphate in order to reduce the response time, but they still obtained peaks after about 3 min at flow rates of 2 ml min^{-1}. The results obtained in the present work led to the conclusion that polishing the electrode surface is one of the best ways of improving its dynamic and Nernstian behaviour. Other important parameters like the polarity and the composition of the flow solution and the geometry of the detector cell in a flow-injection system are also discussed.

EXPERIMENTAL

Reagents and equipment

Fluoride solutions ranging from 10^{-1} to 10^{-6} M fluoride were prepared from reagent-grade sodium fluoride (Merck; p.a.) and TISAB-II solutions (Orion Research, Cambridge, MA). Methanol (Merck; p.a.) was used as received. Aluminium oxide powder (Metrohm; EA 1086) was applied with a cotton cloth as polishing base.

An Orion 94-09 fluoride electrode and an Ag/AgCl reference electrode (Ingold 373-90) were used in conjunction with a Knick pH meter type 70 and a Knick Titrier Zusatz. The signals were recorded on a Knick BD8 recorder. The flow streams were produced by an LKB double-headed multiperspex peristaltic pump (model 2115). Between the pump and the 4-way valve, a pulse-suppressor manifold 116-0452-01 (Technicon) was mounted to decrease pulse fluctuations in the flow stream.

Flow cell

The stainless steel flow cell was home-made (Fig. 1) and was specially constructed for use as a chromatographic detector. The flow stream entered perpendicularly to the electrode surface, via the nozzle (0.10 mm i.d.). The

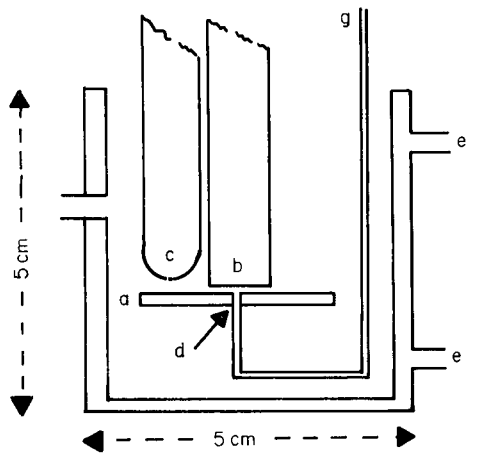

Fig. 1. Flow cell: (a) nozzle plate; (b) LaF_3 electrode; (c) Ag/AgCl reference electrode; (d) nozzle; (e) inlet/outlet for thermostated vessel; (f) outlet to waste; (g) input from chromatographic column.

distance between the nozzle plate and the electrode was about 0.20 mm. At smaller distances the response times were longer because of back-mixing. Both electrodes were carefully fixed, to minimize noise. Because of the small dimensions of the nozzle, the actual linear flow rates were high when chromatographic flow rates of 0.5—1.5 ml min^{-1} were used. In the flow system outlined above, continuous flow measurements were done at a flow rate of 0.75 ml min^{-1}. By turning the 4-way valve, it was possible to alter the concentration of the measuring solution stepwise, the lag time being negligible in relation to the response time of the electrode.

RESULTS AND DISCUSSION

Batch-wise calibration curves in water and water/methanol mixtures

To investigate the influence of polishing on the Nernstian behaviour and the detection limit of the electrode in batch-wise experiments (immersion method), sodium fluoride solutions were prepared in TISAB-II solutions (to control pH and mask interfering ions). Figure 2 shows the calibration curves in aqueous solutions and in mixtures of water and methanol. Methanol was selected because the fluoride electrode was intended for use as a detector in h.p.l.c. systems. Potentials were considered as established when the deviation from the final equilibrium potential was less than 0.5 mV. There was no significant difference in the dynamic behaviour when the electrode surface was dried with a tissue and rinsed with a blank TISAB-II solution. There was a marked difference, however, when the electrode surface was pretreated by polishing with very fine alumina, as in the procedure widely used for polishing glassy carbon electrodes in amperometric detectors. The slopes of the calibration curves were almost equal: 58 mV per decade in buffer and 57 mV per decade in buffer/methanol mixtures, in the range 10^{-1}—10^{-4} M fluoride.

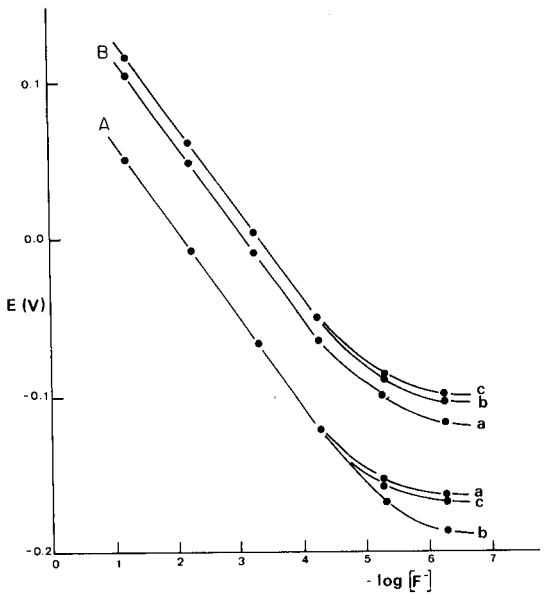

Fig. 2. Calibration curves for fluoride with the LaF_3 electrode in batch experiments: (A) in water/TISAB-II (1:1); (B) water/methanol/TISAB-II (1:2:1). Polishing of electrode: (a) polished with powdered Al_2O_3; (b) freshly polished with TISAB-II and a tissue; (c) none. TISAB-II was added to the test solutions in a 1:1 volume ratio.

When the pure aqueous solution was replaced by a solution containing 50% methanol, the whole calibration curve shifted by about 54 mV in the positive direction. The shape of the curve between 10^{-4} and 10^{-5} M fluoride was identical for both solutions. The detection limits in both media were equal. This is in agreement with the findings of Coetzee and Martin [6] who determined fluoride with the LaF_3 electrode in well-buffered, partly aqueous solutions, and of Kakabadse et al. [13] studied the effects of varying the methanol concentration of the fluoride-containing solution.

When the polished and untreated electrodes were used in batch-wise procedures in pure aqueous solutions, the polished electrodes showed lower detection limits. In solutions containing 50% methanol, polishing had only a negligible effect on the detection limit but the whole curve was shifted by 10 mV for the polished compared to the untreated electrode. Coetzee and Martin [6] discussed the potential mechanism of the lanthanum fluoride electrode in non-aqueous solutions. These authors followed the argument of Buffle et al. [14] that the controlling factor in the potential mechanism was not the solubility of the lanthanum fluoride crystal, but the absorption of fluoride ions to form a surface film on the electrode. After the electrode has been polished, the surface film would be expected to form again. In dilute fluoride solutions this film formation (or ageing) at the electrode/solution interface was found to take at least a day to reach equilibrium. After this

period no difference could be detected between the time-dependent behaviour of the treated and the untreated electrodes.

Response times and sensitivities in flow systems

Table 1 shows the results obtained for the response times of the electrode and the potential differences on changing the fluoride concentration stepwise, at different methanol concentrations. In these tests, the TISAB solution was added in a proportion of only 1:9 to the fluoride solution to prevent precipitation in the less polar solutions; the buffer capacity was still adequate. Figure 3 shows some typical chart outputs, which confirm that the response of the electrode obeys first-order kinetics, as proved earlier [8].

The time constant τ, as expressed in first-order kinetics $y(t) = A[1 - \exp(-t/\tau)]$, was chosen to characterize the dynamic behaviour, because of its domain-independent properties, e.g., its value is unchanged after Laplace transformation. As usually happens, responses are faster for an increase in the concentration than for a decrease in concentration. The response of a polished electrode in methanolic solutions is always faster than it is in pure aqueous solutions (Table 1). When the potential differences in these flow measurements are compared with the data from batch-wise tests, the difference is seen to be negligible for aqueous solutions but significant for solutions that are partly methanolic, especially in the lower concentration ranges; the difference leads to lower detection limits.

These observations can be explained only partly by film diffusion pro-

TABLE 1

Response times[a] of fluoride electrode for stepwise changes in fluoride concentration with and without methanol

Fluoride conc. change (M)	No methanol in mobile phase			50% Methanol			80% Methanol			95% Methanol		
	τ_1 (s)	τ_2 (s)	ΔE (mV)[b]	τ_1 (s)	τ_2 (s)	ΔE (mV)	τ_1 (s)	τ_2 (s)	ΔE (mV)	τ_1 (s)	τ_2 (s)	ΔE (mV)
$10^{-1} \rightarrow 10^{-2}$	14	14	57	14	6							
$10^{-2} \rightarrow 10^{-3}$	16	21	58	18	16	62						
$10^{-3} \rightarrow 10^{-4}$	9	20	52	19	13	59	19	3	57	22	12	60
$10^{-4} \rightarrow 10^{-5}$	31	20	33	16	9	50	10	10	54	14	9	53
$10^{-5} \rightarrow 10^{-6}$	15	14	14	18	13	38	7	3	36	31	22	33
$10^{-2} \rightarrow 10^{-1}$	8	12	57	6	3							
$10^{-3} \rightarrow 10^{-2}$	6	10	58	6	3	62						
$10^{-4} \rightarrow 10^{-3}$	8	13	51	9	6	59	10	2	57	7	3	60
$10^{-5} \rightarrow 10^{-4}$	9	7	33	9	6	50	4	3	54	11	6	53
$10^{-6} \rightarrow 10^{-5}$	9	12	14	12	9	38	7	6	36	15	6	33

[a] τ_1 is the time taken to reach 63% of the equilibrium reading for an unpolished electrode. τ_2 is the corresponding time for an electrode freshly polished with Al_2O_3 powder. [b] ΔE is the potential difference obtained for the stepwise concentration change.

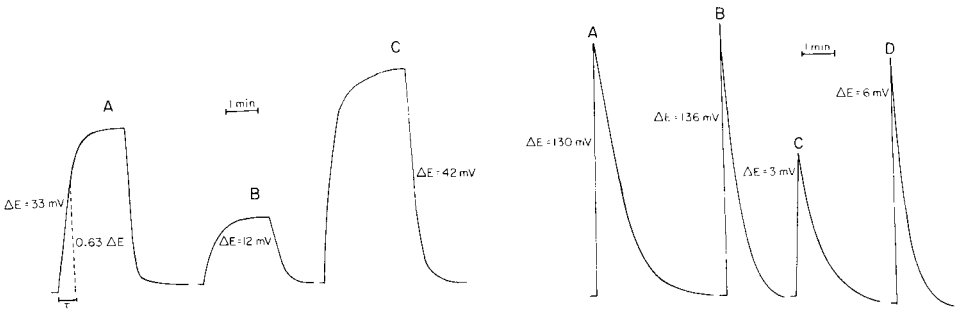

Fig. 3. Traces obtained for different fluoride concentration changes with a polished electrode at a flow rate of 0.75 ml min^{-1}. (The τ-time is about 63% of final potential value.) Concentration changes: A, from 10^{-4} to 10^{-5} M fluoride in aqueous solution; B, from 10^{-5} to 10^{-6} M fluoride in aqueous solution; C, from 10^{-5} to 10^{-6} M fluoride in 50% methanolic solution.

Fig. 4. Flow-injection measurements of 10-μl aliquots of NaF solutions at a flow rate of 0.75 ml min^{-1}: A, 10 μl of 10^{-1} M fluoride injected into a carrier stream composed of 50% methanol, 45% water and 5% TISAB solution, with a polished electrode; B, as under A, with 10^{-6} M fluoride added to the carrier stream; C, 10 μl of 10^{-5} M fluoride injected into the same carrier stream as B, with an unpolished electrode; D, as under C, with a polished electrode.

cesses. According to Lindner et al. [2], other processes (e.g., dissolution of the membrane) are also rate-controlling. The fact that the response times were almost independent of the flow rate below 10^{-4} M fluoride in the present work also indicated other processes than film diffusion. When the findings of Buffle et al. [4, 14] and Lindner et al. [2] are combined, it becomes clear that cleaning the fluoride electrode surface with wet, fine alumina powder removes the surface film and adsorbed (gel) layer. The new gel layer and diffusion film formed after contact with the sample solution will have different thicknesses in the batch and flow systems, especially when the jet stream is as strong as that obtained in the present detector cell. This thinner film, without memory effects, provides faster responses, especially in more apolar solutions. The optimal concentration used here was about 80% methanol. Kakabadse et al. [13] obtained an optimal value of about 85% for a pH glass electrode.

The enhanced sensitivity at low concentrations of fluoride in methanolic solutions (Table 1) can be explained by the changed diffusion rates of fluoride ions, by the changed percentage of solvation and by the partly dehydrated gel layer on the outer electrode surface. It can be concluded that faster response rates and lower detection limits can be obtained in solutions that are partly methanolic and in a flow system with appropriate cell geometry.

Optimum composition of flow stream

In addition to the percentage of methanol in the flow stream, another factor can be used to increase the response rate and to stabilize the baseline.

Addition of a small quantity of fluoride to the carrier solution leads to faster responses and baselines with less drift and noise [15]. An added concentration of 10^{-6} M fluoride proved adequate, as suggested by Cowell [15]; the improvement in the τ times is about 3-fold.

Figure 4 shows the difference in the response rate of injections of 10 μl of 10^{-1} M sodium fluoride into carrier streams with and without 10^{-6} M fluoride, and the difference in the response rate and peak height for a low concentration of fluoride with a polished and an unpolished electrode. In this experiment only one pump was used and the 4-way valve contained a 10-μl injection loop.

Conclusions

By a suitable combination of flow cell geometry, the composition of the carrier stream and preparation of the electrode surface, it is possible to achieve a remarkable acceleration of the response of the lanthanum fluoride electrode. By optimising the ratio of water to methanol in the carrier stream, the sensitivity can also be enhanced, so that fluoride-containing flow streams can be monitored rapidly and sensitively.

The authors thank Mr. W. Jonker and Mr. K. R. Kooistra for helping with part of the experiments. The discussions they had with Drs. J. den Hartigh and Drs. J. J. M. Holthuis were very valuable.

REFERENCES

1 K. Stulík and V. Pacáková, J. Electroanal. Chem., 129 (1981) 1.
2 E. Lindner, K. Tóth and E. Pungor, Anal. Chem., 54 (1982) 72.
3 A. Shatkay, Anal. Chem., 48 (1976) 1039.
4 J. Buffle, N. Parthasarathy and W. Haerdi, Anal. Chim. Acta, 93 (1977) 121.
5 J. Mertens, P. van den Winkel and D. L. Massart, Anal. Chem., 48 (1976) 272.
6 J. F. Coetzee and M. W. Martin, Anal. Chem., 52 (1980) 2412.
7 F. S. Stover, T. R. Bruinleve and R. P. Buck, Anal. Chim. Acta, 109 (1979) 259.
8 E. Lindner, K. Tóth and E. Pungor, Bunseki Kagaku, 30 (1981) S67.
9 J. Ross and M. Frant, Science, 154 (1966) 3756; Analytical Method Guide, 8th edn., Orion Research, Cambridge, MA, 1977, p. 29.
10 E. Lindner, K. Tóth, E. Pungor, W. E. Morf and W. Simon, Anal. Chem., 50 (1978) 1627.
11 A. Dencks and R. Neeb, Fresenius Z. Anal. Chem., 297 (1979) 121.
12 J.-Cl. Landry, F. Cupelin and C. Michal, Analyst, 106 (1981) 1275.
13 G. J. Kakabadse, H. A. Maleila, M. N. Khayat, G. Tassopoulos and A. Vahdati, Analyst, 103 (1978) 1046.
14 J. Buffle, N. Parthasarathy and W. Haerdi, Anal. Chim. Acta, 68 (1974) 253.
15 D. C. Cowell, Med. Lab., 35 (1978) 265.

Analytica Chimica Acta, 155 (1983) 29—36
Elsevier Science Publishers B.V., Amsterdam — Printed in The Netherlands

A COMBINATION OF INVERTASE REACTOR AND GLUCOSE OXIDASE ELECTRODE FOR THE SUCCESSIVE DETERMINATION OF GLUCOSE AND SUCROSE

F. SCHELLER* and CH. KARSTEN

Zentralinstitut für Molekularbiologie der AdW der DDR, DDR-1115 Berlin-Buch (German Democratic Republic)

(Received 7th June 1983)

SUMMARY

Glucose and sucrose are determined successively by modifying the cell of a glucose-measuring instrument (Glukometer GKM 01). The glucose content is measured kinetically; after attainment of the steady-state signal for glucose immobilized invertase is inserted into the measuring cell to hydrolyse the sucrose, and the glucose formed is then measured. The slope of the resulting current-time plot depends linearly on sucrose up to 7 mmol l^{-1}. The r.s.d. for glucose is 1.2% and for sucrose 3.8%; 10 samples per hour can be analyzed. The rate of the overall process is controlled by the rate of spontaneous mutarotation.

The feasibility of glucose measurement by enzyme electrodes has been widely established [1—4]. These sensors have been successfully proven for the determination of glucose both in clinical and food production laboratories [4—9]. Enzyme-sequence electrodes based on glucose oxidase have been developed for the determination of disaccharides, e.g., sucrose [10—14].

In many food production processes, the parallel measurement of glucose and sucrose is important for effective process control. Unlike the case with enzyme sensors based on disaccharidases [15], glucose in samples interferes in disaccharide measurement by enzyme-sequence electrodes. Therefore, mixtures of glucose and sucrose must be subjected to a more complex procedure [12, 16]. Because of the limited region of additivity for glucose and disaccharide signals, the simultaneous determination of both sugars by two differently loaded enzyme electrodes [5] is practicable only in a narrow concentration range. With samples of high glucose content, the sucrose concentration is determined by subtracting the original glucose value from the glucose concentration present after enzymatic [17] or acidic [18] hydrolysis of the sucrose. An earlier paper described the successive measurement of glucose and sucrose by inverting the sucrose in the measuring cell using soluble invertase [19].

This paper describes the successive determination of glucose and sucrose by a glucose oxidase-membrane electrode in combination with immobilized

0003-2670/83/$03.00

invertase. Immobilized invertase is inserted into the measuring cell after a steady-state readout has been obtained for glucose. The rate of glucose formation which is indicated by the glucose oxidase electrode is proportional to the sucrose content over a wide concentration range. This approach was tested for standard mixtures of glucose and sucrose and for different instant cocoa powders.

EXPERIMENTAL

Chemicals

The enzymes used were lyophilized commercial products: glucose oxidase from *Penicillium notatum* (46 U mg^{-1}; VEB Arzneimittelwerk, Dresden), mutarotase (5000 U mg^{-1}; Boehringer, Mannheim), and invertase (100 U mg^{-1}; Serva Biochemica, Heidelberg). The glucose oxidase was entrapped in gelatin as described elsewhere [20]. The enzyme layer comprised 1 mg of gelatin and 1 mg of glucose oxidase per cm^2. The thickness of the dry layer was about 20 μm. This layer was sandwiched between two dialysis membranes (Nephrophan; VEB Chemiekombinat, Bitterfeld), 17 μm thick. In order to examine the effectiveness of mutarotation, a glucose oxidase/mutarotase electrode was used in combination with immobilized invertase. The invertase (1.25 mg cm^{-2}) was immobilized in admixture with bovine albumin (0.2 mg cm^{-2}) by cross-linking with glutaraldehyde on a silk carrier [21].

For comparative studies, an invertase/glucose oxidase sequence electrode was tested. The biocatalytic phase of this sensor comprised 1 mg of glucose oxidase and 0.5 mg of invertase per cm^2 entrapped in gelatin. Additionally, glucose and sucrose were measured by an invertase/mutarotase/glucose oxidase sequence electrode.

A 0.1 M phosphate buffer, pH 7.0, was used as the background solution. Stock solutions of glucose and sucrose were prepared by dissolving the water-free sugars separately in 0.1 M phosphate buffer, pH 7.0. The glucose standard was allowed to attain mutarotation equilibrium. The sucrose and glucose content of instant cocoa was directly measured in suspensions of 100 mg of powder in 10 ml of 0.1 M phosphate buffer, pH 7.0.

Apparatus and procedure

The glucose oxidase-sandwich membrane was attached to the tip of a modified oxygen electrode (VEB Metra, Radebeul); the diameter of the platinum indicator electrode was 0.5 mm. The indicator electrode was polarized at a constant potential of −600 mV vs. Ag/AgCl (0.1 M KCl) using a glucose measuring device (Glukometer GKM 01; AdW der DDR) thus indicating the oxygen consumption. The prepared electrode was placed into the thermostated measuring cell (25 ± 0.1°C) of the Glukometer containing 2 ml of the stirred background solution. After a constant baseline had been attained 50 μl of the sample was added. The current-time curve or its first derivative were recorded on a y-t recorder. A piece (0.5 × 2 cm) of the

invertase-bearing silk was installed on a rack mounted under the lid of the measuring cell (Fig. 1). For sucrose measurement, this immobilized invertase was immersed in the measuring solution.

RESULTS AND DISCUSSION

Invertase/glucose oxidase sequence electrode

With the glucose oxidase electrode (which was to be used in combination with the sucrose inversion by immobilized invertase), the kinetic signal for glucose depends linearly on concentration up to 2.8 mM, corresponding to 110 mM in the sample [5]. As expected, this electrode does not respond to sucrose, giving evidence of the absence of a disaccharidase inside the membrane. The invertase/glucose oxidase sequence electrode, however, is sensitive to both glucose and sucrose. A linear response to sucrose was obtained for 0.5—20 mmol l^{-1} (Fig. 2). The ratio of sensitivities for glucose and sucrose expressed by the stationary currents is almost 16. A ratio of about 10 was found by Cordonnier et al. [11] in experiments with an invertase/glucose oxidase electrode.

The sucrose sensitivity was not improved by increasing the invertase content inside the enzyme layer. This behaviour indicates that the inversion is not the limiting step in the overall reaction of sucrose measurement. Detailed studies of the reaction-transport coupling in the β-D-glucose measurement using the invertase/glucose oxidase electrode indicated that this

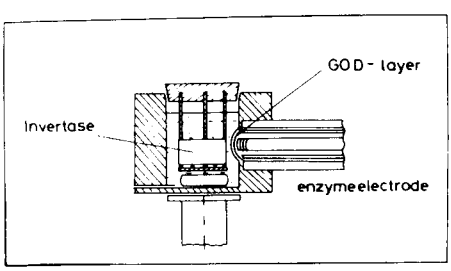

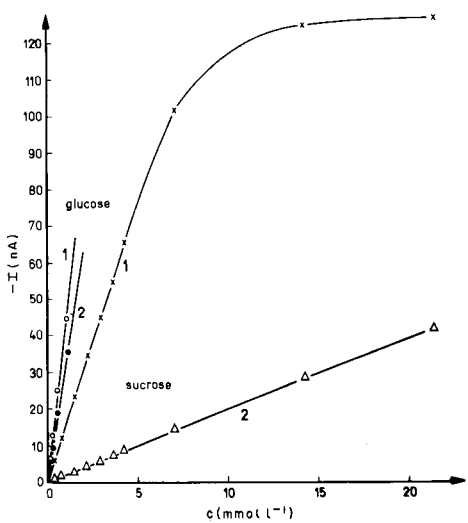

Fig. 1. Arrangement of the immobilized invertase in the measuring cell with the glucose oxidase (GOD) electrode.

Fig. 2. Current-concentration dependences for glucose (○, ●) and sucrose (×, △): (1) invertase/mutarotase/glucose oxidase electrode; (2) invertase/glucose oxidase electrode.

process is controlled by the internal glucose diffusion [22]. Therefore the glucose oxidase-catalyzed step also does not control the overall process of sucrose measurement. The co-immobilization of mutarotase (100 U cm^{-2}) in the glucose oxidase/invertase layer improves the sensitivity by a factor of about 8 (Fig. 2). This suggests that the low rate of spontaneous mutarotation in the neutral pH region is essentially responsible for the low sucrose sensitivity of the bienzyme electrode. The increase of the diffusional resistance for sucrose caused by the higher molecular weight, however, might maximally reduce the sensitivity by 50% as compared with glucose [23].

Combination of invertase reactor and glucose oxidase electrode

For glucose measurement, the immobilized invertase is not immersed in the solution. After addition of the sample, the β-D-glucose content causes a change in current of the glucose oxidase-covered oxygen electrode (curve 1, Fig. 3). In the differential mode, this change of the current-time curve is reflected by the glucose dependent maximum (curve 2, Fig. 3). The current reaches the steady-state value corresponding to the "zero-read out" in the dI/dt curve 30 s after addition of the sample. At this time the immobilized invertase is completely inserted into the stirred solution. The invertase catalyzes the splitting of sucrose into D-fructose and α-D-glucose. The α-D-glucose formed is not a substrate for the glucose oxidase (GOD). Thus the intermediate conversion of the α-D-glucose to β-D-glucose is necessary for the final electrochemical detection

$$\text{D-fructosyl-α-D-glucose (sucrose)} \xrightarrow{\text{Invertase}} \text{D-fructose} + \text{α-D-glucose}$$

$$\text{α-D-glucose} \xrightarrow{\text{Mutarotation}} \text{β-D-glucose}$$

$$\text{β-D-glucose} + O_2 \xrightarrow{\text{GOD}} \text{D-gluconolactone} + H_2O_2$$

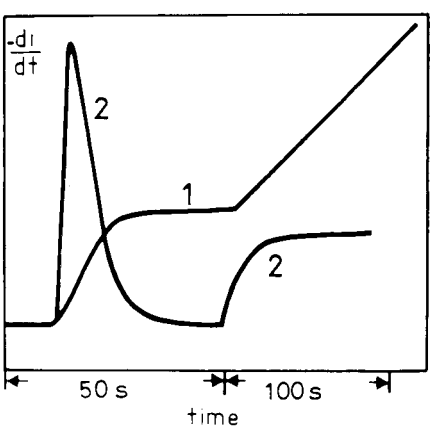

Fig. 3. Response curves for successive indication of glucose and sucrose: (1) I-t curve; (2) dI/dt curve.

The first step proceeds inside the measuring solution whilst the spontaneous conversion of α-glucose might also occur in the glucose oxidase layer. The degree of sucrose conversion is relatively low, as is indicated by the almost constant rate of glucose formation which is reflected by the constant value of the dI/dt curve (Fig. 3).

With pure sucrose solutions, the current-time plot after insertion of the immobilized invertase was linear up to 7 mmol l^{-1} sucrose in the measuring cell when the glucose oxidase electrode was used (Fig. 4). The sensitivity for sucrose was increased by a factor of 2.5 by combining the invertase with the glucose oxidase/mutarotase sensor. The linear measuring range then extended only up to ca. 5 mmol l^{-1} sucrose. The sucrose signal was obtained about 3 min after insertion of the immobilized invertase. The total time for successive glucose and sucrose determination including rinsing the cell and attainment of the baseline was 5—6 min.

The relatively low sensitivity for sucrose of the glucose oxidase electrode in combination with invertase might be explained both by the kinetic control of the formation of β-D-glucose and the external diffusion of the glucose from the invertase layer to the glucose oxidase electrode. Both the invertase-catalyzed reaction and the spontaneous mutarotation delay the overall process. This is underlined by the linear increase of the overall rate that was found when the amount of invertase was increased, from 2.5 nA min^{-1} at 125 U to 13 nA min^{-1} at 500 U, for 2.5 mmol sucrose l^{-1}.

The role of mutarotation is illustrated by the following experiments. After elimination of the immobilized invertase from the sucrose-containing solution, the current increase continues. This effect is not caused by leaching

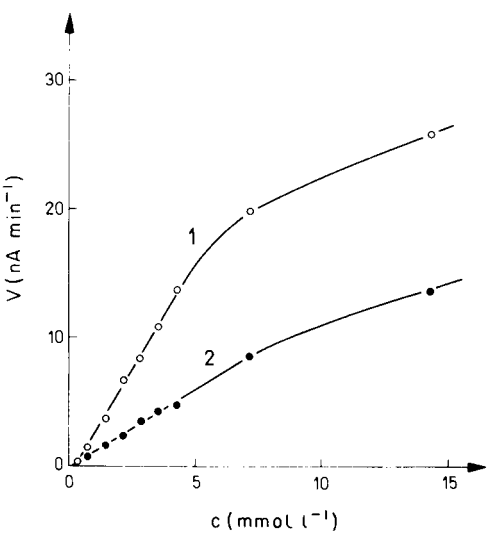

Fig. 4. Calibration graphs for sucrose obtained with immobilized invertase: (1) glucose oxidase/ mutarotase electrode; (2) glucose oxidase electrode.

of invertase; after the immobilized invertase had been soaked for 10 min in the sucrose-free background solution, the addition of sucrose did not result in a comparable current increase. When the glucose oxidase/mutarotase sensor was used, the glucose signal reached a constant value immediately after elimination of the immobilized invertase. The optimum pH for kinetic glucose measurement was found to be pH 7.0 while the optimal pH for sucrose indication was 6.6 (Fig. 5). On increasing the temperature of the measuring system by 10 K the sucrose signal doubled. The same temperature dependence for sucrose was found when the glucose oxidase/mutarotase sensor was used. The activation energy determined from the Arrhenius plot was 58.5 kJ mol^{-1} in the interval between 20 and 35°C. For the glucose signal, an activation energy of 30—33 kJ mol^{-1} was obtained [22] both with a glucose oxidase and the glucose oxidase/mutarotase sensor. The value of the activation energy for sucrose suggests that the overall process is controlled by the invertase-catalyzed reaction.

Successive glucose and sucrose measurements

For the measurement of mixtures containing both sugars, it is necessary that the two reactions do not affect each other. To ensure the absence of interferences, the calibration graphs for sucrose were obtained in the presence of different amounts of glucose. The sensitivity for sucrose was independent of the glucose content up to 0.6 mmol l^{-1} (Fig. 6). This concentration interval exceeds the maximum glucose content of the instant cocoa studied.

A high oxygen concentration inside the glucose oxidase layer, which must also be sufficient after reaching the maximum sucrose signal, is essential. Therefore, the higher sensitivity of the glucose oxidase/mutarotase sensor decreases the interference-free measuring range compared to that obtained with the glucose oxidase electrode. In order to exploit this larger interference-free region, the glucose oxidase electrode (without mutarotase) was used for the measurement of instant cocoa samples. The Glukometer was calibrated at 10.0% by using a standard solution of glucose mono-

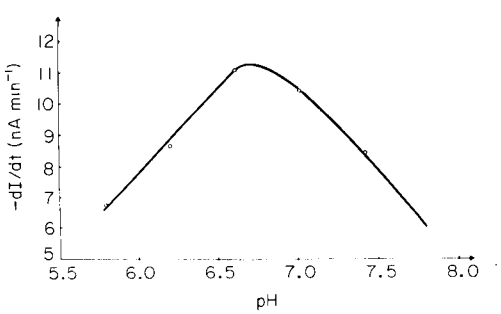

Fig. 5. pH dependence of the sucrose signal (2.5 mmol sucrose l^{-1}).

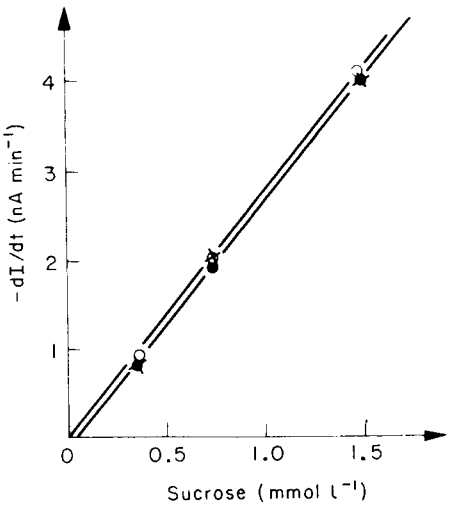

Fig. 6. Calibration graphs for sucrose obtained with the glucose oxidase electrode, in the presence of glucose at: (×) 0.14; (•) 0.28; (○) 0.56 mmol l^{-1}.

TABLE 1

Successive glucose and sucrose determinations in instant cocoa samples

Sample	Component	Content (%)	
		Declared	Found[a]
Trinkfix	Glucose	10	9.8 ± 0.4
(Trumpf GmbH, Aachen)	Sucrose	68.5	69.0 ± 0.5
Tropengold	Glucose	20	20.1 ± 0.3
(Aldi, Mühlhausen/Ruhr)	Sucrose	58.5	59.0 ± 0.5

[a]Mean of 9 measurements.

hydrate (10 mg in 10 ml) thus obtaining a numerical read-out in percent glucose in each cocoa sample (Table 1). The high precision of the glucose measurement in Trinkfix samples is reflected by the coefficient of variation of 1.2% (9 results). The respective value for sucrose was 3.8%. The mean values determined by the successive glucose and sucrose measurement are within 0.5% of the declared concentration for both products analysed (Table 1). Between 10 and 12 instant cocoa samples per hour were analyzed in this way.

Conclusions

The successive measurement of glucose and sucrose was achieved by modifying the measuring cell of the commercial glucose analyzer, Glukometer GKM 01. The procedure developed combines the advantages of membrane

enzyme electrodes with those of sequential reactors, i.e., the short response time of glucose measurement, the simple set-up of the stirred measuring cell, and the subsequent interference-free sucrose determination.

The principle of successive determination of different constituents might be extended to other substrates by applying a simple hydrogen peroxide-sensing electrode in combination with different immobilized oxidases.

REFERENCES

1 L. C. Clark and C. Lyons, Ann. N.Y. Acad. Sci., 102 (1962) 29.
2 G. G. Guilbault and G. Lubrano, Anal. Chim. Acta, 64 (1973) 439.
3 D. Thevenot, R. Sternberg, P. Coulet, J. Laurent and D. Gautheron, Anal. Chem., 51 (1979) 96.
4 F. Scheller, D. Pfeiffer, M. Kühn, J. Hundertmark, A. Quade, M. Jächen, G. Lange, H. Holesch and H. Dittmer, Acta Biol. Med. Ger., 39 (1980) 671.
5 D. Pfeiffer, F. Scheller, M. Jänchen, K. Bertermann and H. Weise, Anal. Lett., 13B (1980) 1179.
6 K. Bertermann, P. Elze, F. Scheller, D. Pfeiffer and M. Jänchen, Anal. Lett., 15B (1982) 397.
7 J.-L. Romette, B. Froment and D. Thomas, Clin. Chim. Acta, 95 (1979) 249.
8 M. Koyama, D. Koezuka and Y. Sato, Toshiba Rev., 12 (1981) 1.
9 T. Tsuchida and K. Yoda, Enzyme Microb. Technol., 3 (1981) 326.
10 I. Satoh, I. Karube and S. Suzuki, Biotechnol. Bioeng., 18 (1976) 269.
11 M. Cordonnier, F. Lawny, D. Chapot and D. Thomas, FEBS Lett., 59 (1975) 263.
12 C. Bertrand, P. Coulet and D. Gautheron, Anal. Chim. Acta, 126 (1981) 23.
13 J. J. Kulys, Anal. Lett., 14B (1981) 377.
14 P. Coulet and C. Bertrand, Anal. Lett., 12B (1979) 581.
15 C. Mandelius, B. Danielsson, F. Winqvist, B. Mattiasson and K. Mosbach, Appl. Biochem. Biotechnol., 7 (1982) 141.
16 M. Keyes, F. Semersky and D. Gray, Enzyme Microb. Technol., 1 (1979) 91.
17 L. Trauberman, Food Eng., 47 (1974) 58.
18 J. J. Kulys, E. Raslis and S. Penkora, Appl. Biochem. Microbiol. USSR, 15 (1979) 282.
19 H. Weise, F. Scheller, G. Kreibich and D. Pfeiffer, Lebensm.-Ind., 28 (1981) 401.
20 F. Scheller, D. Pfeiffer, M. Jänchen et al., GDR Pat. No. GO1N/127 843, 1979.
21 F. Scheller, M. Jänchen, D. Pfeiffer, I. Seyer and K. Müller, Z. Med. Labor.-Diagn., 18 (1977) 312.
22 F. Scheller, D. Pfeiffer, Th. Schulmeister and D. Kirstein, Bioelectrochem. Bioeng., 11 (1983) in press.
23 H. Braselmann, J. Vacik, J. Kopecek and D. Kirstein, Eur. Polym. J., 16 (1980) 431.

Analytica Chimica Acta, 155 (1983) 37—46
Elsevier Science Publishers B.V., Amsterdam — Printed in The Netherlands

SOME CONSIDERATIONS ON THE DESIGN OF TENSAMMETRIC FLOW-THROUGH DETECTORS

H. G. DE JONG*, W. TH. KOK and P. BOS

Department of Analytical Chemistry, Free University, De Boelelaan 1083, 1081 HV Amsterdam (The Netherlands)

(Received 22nd June 1983)

SUMMARY

A theoretical description of the influence on the electrochemical double-layer capacity of mass transfer-controlled adsorption of an electroinactive compound at a mercury electrode in a continuous-flow system is given. Four different types of polarographic flow-through cells are considered: classical dropping mercury electrodes with the fluid flow parallel, opposite and perpendicular to the mercury flow, and a static mercury drop detector. The theoretical expressions are used to evaluate electrodynamic cell characteristics for optimization of the signal-to-noise ratio and linearity which are features of interest for the detector performance. The theory is illustrated by some experiments with a static mercury drop flow-through detector and lynestrenol as model compound.

Electroinactive analytes that adsorb at the surface of a dropping mercury electrode (DME) can be detected by means of tensammetry. In batch experiments, adsorption and desorption phenomena have been investigated extensively for a wide range of compounds [1, 2]. These phenomena are theoretically well described [1].

The first attempt to use a tensammetric detector in a chromatographic system was described by Kemula et al. [3]. Recently, such detectors have been used in more modern chromatographic systems [4], especially h.p.l.c. [5, 6]. Studies devoted to continuous-flow tensammetry are centred on measuring the depression of the double-layer capacity caused by adsorption of the analyte, by monitoring the double-layer capacity (or its inverse) or by monitoring the capacitive current. The last method can be done with commercially available a.c. polarographic equipment. In principle, the desorption waves can also be used for detection but the concentration-dependence of both the peak height and the peak potential [1] makes it troublesome to use the desorption waves in continuous-flow detection. For further development of continuous-flow electrosorption analysis, a theoretical description of adsorption at electrode surfaces in flow-through systems is an essential prerequisite. In this study, the double-layer capacity changes caused by mass transfer-controlled adsorption of an electroinactive compound are described. Four different types of polarographic flow-through detectors are considered. The derived expressions are used to describe the

0003-2670/83/$03.00

optimization of tensammetric detection. The signal-to-noise ratio (S/N) and linearity evaluated from electrodynamic cell characteristics are considered. Lynestrenol (19-nor-17α-pregn-4-en-20-yn-17-ol) is used as model compound for experimental verification of the theoretical expression for the tensammetric current in a continuous-flow detector with a static mercury drop electrode (SMDE) as working electrode.

THEORY

Adsorption

When an analyte is adsorbed quickly and strongly at an electrode, the analyte concentration near the electrode surface tends to zero. Because of the concentration gradient settled as described, mass transfer will control the adsorption process [1, 7]. Thus for the mass flux towards the electrode, use can be made of the existing theory for mass transfer-controlled faradaic processes.

The number of analyte molecules adsorbed after t seconds, $N(t)$, is given [1] by

$$N(t) = \int_0^t DA(\tau)\left(\frac{\partial c}{\partial r}\right)_{r=a(\tau)} d\tau \tag{1}$$

(Symbols are defined in Table 1.)

For a faradaic process, the limiting current would be given by the well-known expression

$$i_l(t) = nFDA(t)\left(\frac{\partial c}{\partial r}\right)_{r=a(t)} \tag{2}$$

Combination of Eqns. 1 and 2 yields

$$N(t) = \int_0^t [i_l(\tau)/nF]\, d\tau \tag{3}$$

where i_l is the limiting current which would be measured for a faradaic process.

For analytical purposes, double-layer capacity changes caused by adsorption are monitored. This change $\Delta C(t)$ is related to $N(t)$ by the relation $\Delta C(t) = \Delta C_N N(t)$, according to Jehring, who defined ΔC_N as the molar capacity depression [8]. Combining the last two equations yields

$$\Delta C(t) = \Delta C_N \int_0^t [i_l(\tau)/nF]\, d\tau \tag{4}$$

Expressions for the faradaic limiting current for the different cell geometries

TABLE 1

List of symbols

a	electrode radius (cm)	i_{AC}	alternating current (μA)
c	concentration (mol cm^{-3})	κ	conductivity of a solution [Ω^{-1} cm^{-1}]
C^*	bulk concentration (mol cm^{-3})	m	mercury mass flow (mg s^{-1})
C_A	double layer capacity per unit area (μF cm^{-2})	n	number of electrons per molecule reduced (or oxidized)
C_{dl}	double layer capacity (μF)	N	noise (A)
$C_{dl,0}$	double layer capacity in blank electrolyte (μF)	$N(t)$	number of adsorbed analyte molecules (mol)
ΔC_N	molar capacity depression (μF mol^{-1})	R	electrolyte resistance (Ω)
$\Delta C(t)$	time-dependent double layer capacity depression (μF)	r	radial distance from electrode center (spherical coordinate) (cm)
d	nozzle inner diameter (cm)	S	signal (A)
D	diffusion coefficient (cm^2 s^{-1})	t	time (s)
ΔE_{AC}	modulation amplitude (V)	t_d	drop time (s)
E_{dc}	detection potential (V)	τ	integration dummy variable (s)
δE	applied alternating voltage (V)	v	mean linear velocity (cm s^{-1})
F	Faraday constant (96487 C mol^{-1})	ω	modulation angular frequency (s^{-1})
f_v	volume flow rate (cm^3 s^{-1})		
i_l	limiting current (A)		
A	electrode surface area (cm^2)		

considered are available in the literature. Using Eqn. 4, the double-layer capacity depression can be calculated in a straightforward way.

In the case of parallel mercury and fluid flows, Kimla and Stráfelda [9] derived the equation for the limiting current

$$i_l = 0.0605\, nFC^*D^{2/3}(mt)^{4/9}v^{1/3}[1 + 1.86\, D^{1/3}(mt)^{-1/9}v^{-1/3} + 0.00332\, D^{-1/3}m^{4/9}t^{-5/9}v^{-2/3}] \quad (5)$$

From Eqn. 5, $C(t)$ is readily calculated

$$\Delta C(t) = 0.0419\, \Delta C_N C^* D^{2/3} v^{1/3} m^{4/9} t^{13/9}[1 + 2.02\, D^{1/3}v^{-1/3}(mt)^{-1/9} + 0.00540\, D^{-1/3}m^{4/9}t^{-5/9}v^{-2/3}] \quad (6)$$

For mercury and fluid flows moving in opposite directions, the limiting current was calculated by Stráfelda and Kimla [10]. After some substitutions and rearrangements [11], the expression is

$$i_l = 0.0154\, nFC^*D^{1/2}(mt)^{1/2}v^{1/2}[1 + 39.3\, D^{1/2}(mt)^{-1/6}v^{-1/2} - 2154\, D(mt)^{-1/3}v^{-1} + 0.0710\, m^{1/3}t^{-2/3}v^{-1}] \quad (7)$$

Then from Eqn. 5,

$$\Delta C(t) = 0.0103\, \Delta C_N C^* D^{1/2} v^{1/2} m^{1/2} t^{3/2}[1 + 44.2\, D^{1/2}v^{-1/2}(mt)^{-1/6} - 2769\, Dv^{-1}(mt)^{-1/3} + 0.1278\, v^{-1}m^{1/3}t^{-2/3}] \quad (8)$$

In the case of a fluid flow directed perpendicularly to the mercury flow, Okinaka and Kolthoff [12] derived an expression for the limiting current. After some rearrangements [11], one obtains

$$i_l = 0.0178\, nFC^*D\, v^{1/2}(mt)^{1/2}[1 + 13.8\, D^{1/2}(mt)^{-1/6}v^{-1/2} + 0.134\, m^{1/6}t^{-1/3}v^{-1/2}] \quad (9)$$

and from Eqn. 5

$$\Delta C(t) = 0.0119\, \Delta C_N C^* D^{1/2} v^{1/2} m^{1/2} t^{3/2}[1 + 15.5\, D^{1/2}(mt)^{-1/6}v^{-1/2} + 0.173\, v^{-1/2}m^{1/6}t^{-1/3}] \quad (10)$$

The last design to be considered is a detector based on a static mercury drop electrode. The case of laminar flow around a fluid sphere of constant radius was treated by Kimla [13]. The expression obtained by Kimla for the maximal diffusional flux towards the sphere (his Eqn. 24) can be rearranged to give the limiting current for a faradaic process:

$$i_l = 5.78\, nFC^*D^{1/2}v^{1/2}a^{3/2}(1+\gamma)^{-1/2}[1 + \{2.10(1+\gamma)^{1/2} + 1.78\,\gamma\,(1+\gamma)^{-1/2}\}(D/va)^{1/2} + 56.0\,(D/va)] \quad (11)$$

where γ is the ratio of viscosities of mercury and the electrolyte. For a mercury drop in diluted electrolytes, $\gamma = 1.5$ [10]. Substitution of this value in Eqn. 11 and application of Eqn. 4 yields

$$\Delta C(t) = 3.66\, \Delta C_N C^* D^{1/2} v^{1/2} a^{3/2} t[1 + 5.01(D/va)^{1/2} + 56.0\,(D/va)] \quad (12)$$

This expression does not hold for the time of area growth, i.e., the first 50—200 ms of drop life depending on the drop size. The parameter t should be interpreted strictly as the drop lifetime minus the period of area growth. In practice, the complete drop life may be taken if one allows a small systematic error.

Linearity

A series capacitor and resistor may be used as the electrodynamic model system for a tensammetric cell [14—16]. Representing the applied alternating voltage as $\delta E = \Delta E_{AC} \sin \omega t$, and the total double-layer capacity as C_{dl}, the monitored current is

$$i_{AC} = \Delta E_{AC}\, \omega\, C_{dl}[1 + (R\omega C_{dl})^2]^{-1/2} \sin(\omega t + \phi) \quad (13)$$

with $\phi = \arctan[(R\omega C_{dl})^{-1}]$. The monitored current is linearly dependent on the analyte concentration if it is linearly dependent on the double-layer capacity (Eqns. 6, 8, 10 and 12). When Eqn. 13 is expanded in a power series

$$i_{AC} = \Delta E_{AC}\omega C_{dl}\left[1 - \frac{1}{2}(R\omega C_{dl})^2 + \frac{3}{8}(R\omega C_{dl})^4 - \ldots\right]\sin(\omega t + \phi) \quad (14)$$

it is readily seen that the condition for satisfactory linearity is

$$1/2\ (R\omega C_{dl})^2 \leqslant 0.01 \tag{15}$$

In tensammetry, capacity depressions are monitored and the largest double-layer capacity is thus measured in the blank electrolyte. Therefore, C_{dl} in this expression must correspond to the double-layer capacity in the blank electrolyte ($C_{dl,0}$). This capacity and the electrolyte resistance can be related to the radius of the mercury drop [14, 16] by the equations $C_{dl,0} = 4\pi a^2 C_{A,0}$ and $R = [4\pi a\kappa]^{-1}$.

Substitution of these two equations into Eqn. 15 yields an actual design criterion:

$$a \leqslant 0.14\ \kappa/\omega C_{A,0} \tag{16}$$

When this requirement is met, the electrodynamic cell characteristics will not affect the linearity. With normally encountered values for κ (0.01 ohm^{-1} cm^{-1}) and C_A (10 μF cm^{-2}) the condition would be $a \leqslant 140/\omega$ cm. If high analyte concentrations are used, however, deviations from linearity can be observed because of saturation of the electrode surface, when Eqn. 4 is no longer valid. This gives rise to an upper concentration limit even when Eqn. 16 is fulfilled.

Signal-to-noise ratio

Recently, noise phenomena in amperometric detectors were investigated [17]. It was concluded that the noise was linearly dependent on the double-layer capacity and thus linearly dependent on the electrode area. In the present work, it was shown experimentally that this result is also applicable to tensammetric detectors. It is thus possible to describe the signal-to-noise ratio.

The tensammetric signal (S) and the noise (N) observed on the recorder can be written as (see Eqn. 13)

$$S = k_1 \Delta E_{AC} \omega \Delta C(t) \text{ and } N = k_2 \Delta E_{AC} \omega a^2 \tag{17}$$

Combining Eqns. 6, 8, 10 and 17 with the well known expression $a = 0.026\ (mt_d)^{1/3}$, the signal-to-noise ratio for DME detectors can be expressed as a function of the drop time and hydrodynamics. Assuming $D = 10^{-5}$ cm^2 s^{-1}, $v = 3$ cm s^{-1} and $m = 2$ mg s^{-1}, the signal-to-noise ratio is reduced to a function of drop time. This function is summarized in Table 2 for various types of detector. The function is scaled on the proportionality constants of Eqn. 17, the molar capacity depression and the bulk concentration of analyte. The expressions shown in Table 2 are displayed in Fig. 1 to yield the signal-to-noise characteristics for various DME detectors.

Figure 1 shows that a detector in which the fluid flow is directed perpendicularly to the mercury flow provides the best geometry for a tensammetric detector based on a DME. This conclusion is similar to that reached for polarographic detectors used in the reductive mode [18]. An interesting feature is the increase in the signal-to-noise ratio with drop time. The electrode radius is proportional to $t_d^{1/3}$. The demands of linearity establish an

TABLE 2

Scaled signal-to-noise-ratio as a function of the drop time

Detector type	$(S/N)_H$
Normal	$6.85\ t^{5/6}[1 + 0.0254\ t^{-1/6} + 0.727\ t^{-1/3}]$
Parallel	$2.83\ t^{7/9}[1 + 0.0279\ t^{-1/9} + 0.819\ t^{-1/3}]$
Opposite	$7.93\ t^{5/6}[1 + 0.0719\ t^{-1/6} + 0.00733\ t^{-1/3} + 0.0537\ t^{-2/3}]$

upper limit for the electrode radius, as can be seen from Eqn. 16. Thus the demands of linearity define the signal-to-noise limit. From this point of view, it is advisable to use readily conducting electrolytes and a low modulation frequency, which is clear from Eqn. 16. Of course, the drop time will also be limited by the demands for undistorted monitoring of the concentration profile, e.g., in h.p.l.c.

For a detector cell based on a SDME, the signal-to-noise ratio, calculated as for the DME detectors, can be written as

$$(S/N)_H = 1.60a^{-1/2}t[1 + 0.0915a^{-1/2} + 0.000187a^{-1}]$$

This result shows that the highest signal-to-noise ratio is obtained when the electrode radius is as small as possible and the drop time as long as possible.

EXPERIMENTAL

To verify the expressions obtained for the tensammetric peak height (Eqns. 13 and 17), a flow-injection system was adapted. The detector used was a PAR 310 polarographic flow-through detector. Synchronization

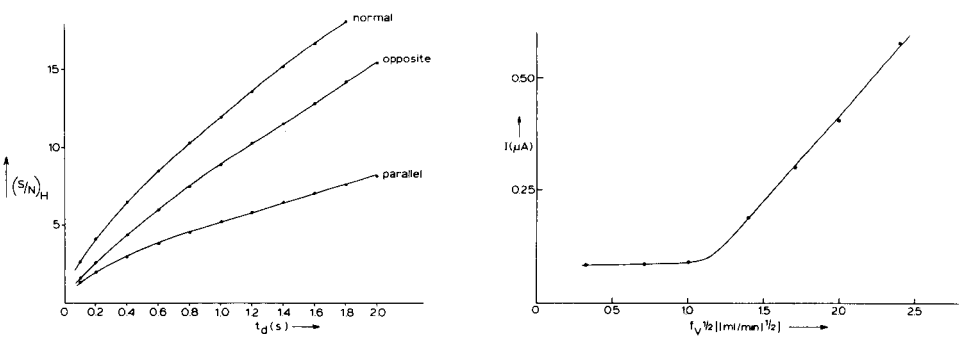

Fig. 1. Signal-to-noise ratio as function of the drop time.

Fig. 2. Tensammetric peak height as a function of the square root of the volume flow rate in f.i.a. Conditions: E_{dc} = −100 mV, $\omega/2\pi$ = 60 s^{-1}, ΔE_{AC} = 30 mV_{pp}; ϕ = 90°, a = 0.0736 cm (medium drop size), t_d = 1.0 s, 1-ml injections of 7 × 10^{-6} M lynestrenol. Electrolyte: 1/1 (v/v) methanol/water, 0.1 M KNO_3.

of drop time and electronics provides sampled-current measurements.

A Princeton Applied Research (PAR) model 174 polarograph and a PAR 129A lock-in amplifier (E.G. & G., Princeton Applied Research Co., Princeton, N.J.) both modified by our workshop for sampled a.c. operation, were used with the PAR 310 static mercury drop electrode. These devices were interconnected with a PAR 174/50 AC polarographic interface. A Peekel 053-A sine-wave oscillator (Peekel, Rotterdam) was used for generating the alternating voltage. The frequency of the alternating voltage was measured with a Hewlett-Packard HP-5300A measuring system. A Fluke 8000-A digital multimeter (John Fluke Mfg. Co., Washington) was used for checking the detection potential. The overall current was monitored on a Tektronix type 502 oscilloscope (Beverton, Oregon). The current was recorded on a Kipp and Zonen BD-8 multirange recorder. The applied potentials were measured vs. a Ag|AgCl| 1 M LiCl, methanol/water (1/1, v/v) reference electrode. In the flow-injection system, a Perkin-Elmer 601 pump and a Rheodyne 7120 injection valve were used.

All measurements were made in water/methanol (1/1, v/v) mixtures containing 0.1 M KNO_3. Water was demineralized and distilled. The stock solutions were deaerated by purging with nitrogen. Lynestrenol was supplied by Organon (Oss, The Netherlands). All other chemicals were analytical-reagent grade (Merck p.a. or Baker Analyzed). The samples were deaerated by purging with nitrogen for about 10 min.

RESULTS AND DISCUSSION

Flow dependence

For high fluid velocities, Eqn. 12 describing the SMDE in tensammetry can be reduced to

$$\Delta C(t) = 3.66\, \Delta C_n C^* D^{1/2} v^{1/2} a\, t \qquad (18)$$

The volume flow rate is related to the mean linear velocity by $f_V = \frac{1}{4}\pi d^2 v$. Equation 18 is valid if 5.01 $(D/va) \leqslant 0.01$. With $d = 0.03$ cm, $D = 10^{-5}$ cm^2 s^{-1} and $a = 0.0736$ cm (medium drop size), this leads to the demand: $f_V \geqslant 1.4$ ml min^{-1}. Equation 18 makes it relatively simple to verify the theoretical model used here. The dependence of tensammetric peak height on the volume flow rate was investigated in the range 0.1—6 ml min^{-1}. The detection potential was obtained from tensammograms recorded under non-flowing conditions. The results are shown in Fig. 2. It is clear that the theoretically predicted flow dependence is matched for $f_V \geqslant 1.6$ ml min^{-1}, which is in good agreement within the limit calculated above. For $f_V \leqslant 1.0$ ml min^{-1} the flow dependence disappears, a phenomenon which is also observed in experiments with flow-through polarographic detectors in the reductive mode [9, 12].

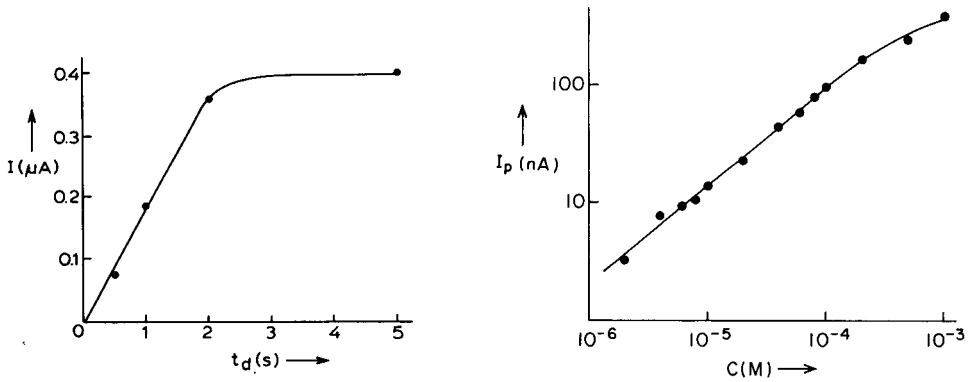

Fig. 3. Tensammetric peak height as a function of the drop time in f.i.a. Conditions: ΔE_{AC} = 10 mV_{pp}, f_V 3 ml min^{-1}. Other conditions as in Fig. 2.

Fig. 4. Tensammetric peak height as a function of the concentration of lynestrenol in h.p.l.c. Conditions: $\omega/2\pi$ = 20 Hz, ϕ = 85°, t_d = 3 s; detection potential, —200 mV vs. Ag/AgCl; large drop size (a = 0.0935 cm); time constant, 3 s; injection volume 100 μl. Eluent: water/methanol 30/70 (v/v) with 0.1 M KNO_3, f_V = 2 ml min^{-1}, k' (lynestrenol) = 3.2.

Dependence on drop time and concentration

In Fig. 3, the tensammetric peak height is shown as a function of the drop time. For $t_d < 2$ s, the peak height is linearly dependent on the drop time, as predicted theoretically (Eqn. 18). For $t_d > 2$ s, linearity is lost. In this region, the electrode surface probably becomes saturated with lynestrenol.

The phase angle of the background current was observed to be 82° (for conditions, see Fig. 4). From the equation ϕ = arctan $[(R\omega C_{dl})^{-1}]$ one calculates $R\omega C_{dl} \approx 0.01$, so that the requirements for linearity (Eqn. 15) are easily met. When small analyte concentrations are used, oxygen can affect the tensammetric signal at the actual detection potential. To avoid this problem a chromatographic system was set up for investigating the concentration/signal relationship. Lynestrenol was chromatographed in a reversed-phase system using a LiChrosorb RP-2 (10-μm) column and a flow rate of 2 ml min^{-1} (3/7 (v/v) water/methanol, 0.1 M KNO_3). In Fig. 4 is shown a logarithmic plot of the peak height/concentration relationship for lynestrenol. In the concentration range below 2×10^{-4} M, this relationship is linear (regression coefficient = 0.996). The loss of linearity for concentrations exceeding 2×10^{-4} M is probably due to saturation of the electrode surface with lynestrenol.

Dependence on modulation amplitude and frequency

The tensammetric peak height is listed as a function of the modulation amplitude in Table 3 and as function of the modulation frequency in Table 4. Both relationships were found to be linear, with regression coefficients of 0.998 and 0.997, respectively. This is in good agreement with Eqn. 13.

TABLE 3

Tensammetric peak height as a function of the modulation amplitude in f.i.a.[a]

ΔE_{AC} (mV_{pp})	I_p (nA)	ΔE_{AC} (mV)	I_p (nA)
10	127	50	585
20	253	60	708
30	400	70	828
40	439	80	910

[a]The typical error in I_p is 4% (3 consecutive injections). Conditions: $\omega/2\pi$ = 60 Hz, ϕ = 85°, detection potential −400 mV vs. Ag/AgCl; 100-µl injections of 7×10^{-5} M lynestrenol; t_d = 2 s; flow rate 1 ml min^{-1}; electrolyte 1/1 (v/v) methanol/water containing 0.1 M KNO_3; small drop size (a = 0.0605 cm).

TABLE 4

Tensammetric peak height as a function of the modulation frequency in f.i.a.[a]

f (Hz)	I_p (nA)	f (Hz)	I_p (nA)
10	51	60	309
20	101	70	381
30	163	80	441
40	201	90	496
50	267	100	577

[a]The typical error in I_p is 4% (3 consecutive injections). Conditions: ΔE = 30 mV_{pp}; otherwise as in Table 2.

Conclusion

The experimental work showed that the theory presented here for adsorption processes controlled by convective diffusional mass transport on a SMDE is relevant within the limitations discussed. Theoretical considerations on the construction of tensammetric flow-through detectors showed the existence of an optimal electrode radius or drop time, given the type of detector and experimental conditions. A detector cell in which the fluid flow is directed perpendicularly to the mercury flow is the optimal design for a tensammetric flow-through detector employing a DME as the working electrode.

W. H. Voogt is thanked for technical assistance.

REFERENCES

1 H. Jehring, Elektrosorptionsanalyse mit der Wechselstrompolarographie, Akademie-Verlag, Berlin 1974.
2 B. Breyer and H. H. Bauer, Alternating Current Polarography and Tensammetry, Interscience, New York, 1963.

3 W. Kemula, B. Behr, Z. Brokowska and J. Dojlido, Collect. Czech. Chem. Commun., 30 (1965) 4050.
4 J. Landelma and H. Poppe, J. Chromatogr. Sci., 14 (1976) 310.
5 W. Kemula and W. Kutner, J. Chromatogr., 204 (1981) 131.
6 H. G. de Jong, W. H. Voogt, P. Bos and R. W. Frei, J. Liq. Chromatogr., accepted.
7 P. Delahay and I. Trachtenberg, J. Am. Chem. Soc., 79 (1957) 2355.
8 H. Jehring, J. Electroanal. Chem., 20 (1969) 33.
9 A. Kimla and F. Stráfelda, Collect. Czech. Chem. Commun., 29 (1964) 2913.
10 F. Stráfelda and A. Kimla, Collect. Czech. Chem. Commun., 30 (1965) 3606.
11 H. B. Hanekemp and H. J. van Nieuwkerk, Anal. Chim. Acta, 121 (1980) 13.
12 Y. Okinaka and I. M. Kolthoff, J. Electroanal. Chem., 73 (1957) 3326.
13 A. Kimla, Collect. Czech. Chem. Commun., 30 (1965) 1416.
14 H. Jehring, J. Electroanal. Chem., 21 (1969) 77.
15 A. N. Frumkin and B. B. Damaskin, J. Electroanal. Chem., 3 (1962) 36.
16 R. D. Jee, J. Electroanal. Chem., 69 (1976) 109.
17 H. W. van Rooijen, Thesis, University of Amsterdam, 1981.
18 H. B. Hanekamp and H. G. de Jong, Anal. Chim. Acta, 135 (1982) 351.

Analytica Chimica Acta, 155 (1983) 47—56
Elsevier Science Publishers B.V., Amsterdam — Printed in The Netherlands

DETERMINATION OF HYDROGEN PEROXIDE FOR APPLICATION IN AEROBIC CELL SYSTEMS OXYGENATED VIA HYDROGEN PEROXIDE

HANS LUNDBÄCK and GILLIS JOHANSSON*

Department of Analytical Chemistry, University of Lund, P.O. Box 740, S-220 07 Lund (Sweden)

OLLE HOLST

Department of Applied Microbiology, University of Lund, P.O. Box 740, S-220 07 Lund (Sweden)

(Received 5th July 1983)

SUMMARY

An amperometeric method is described for the determination of hydrogen peroxide in reaction media used for production of dihydroxyacetone from glycerol by immobilized bacteria. The H_2O_2 was oxidized at +1.2 V vs. SCE at a glassy carbon flow-through electrode after dilution in a flow injection analysis system. Unexpected losses of H_2O_2 response in cell-free media necessitated a study of the cause. To validate the measurements two other methods for H_2O_2 determinations were used in parallel, a catalytic calorimetric method and an enzymatic flow injection method based on the use of immobilized peroxidase to produce a coloured product which was monitored spectrophotometrically. The three methods gave the same results. It was concluded that the responses of the methods were correct and that the loss of H_2O_2 is real and due to reactions with dihydroxyacetone or some of its decomposition products. A reverse reaction was also observed, i.e., the production of H_2O_2 from oxygen and decomposition products of dihydroxyacetone in an originally peroxide-free solution.

A suitable supply of oxygen is of the utmost importance for the productivity of aerobic cell systems, and the demands on the supply system become especially high in fermentors with high cell densities [1]. The solubility of oxygen in aqueous solutions is low compared to the normal substrate concentrations and the oxygen activity at the reaction site may be lowered still more by a slow mass transfer in the solution or within the cells. Enzymes such as catalase, present within the cell or in the cell membrane, can produce oxygen in situ through decomposition of hydrogen peroxide. Thus, addition of hydrogen peroxide to the medium is potentially a more efficient method of oxygenation than gas sparging. High concentrations of hydrogen peroxide may damage the cells, especially during the growth phase [2, 3], or may decrease the reaction rate by inhibition of enzymes. Increased productivity with hydrogen peroxide as the oxygen source has been demonstrated for both immobilized enzymes [4] and for resting immobilized cells [5].

0003-2670/83/$03.00

Gluconobacter oxydans immobilized in beads of calcium alginate can be used for the production of dihydroxyacetone from glycerol [5]. The immobilized cells are alive but do not multiply during production of dihydroxyacetone and they are therefore more tolerant towards hydrogen peroxide than cells in the growth phase. The system is thus well suited for a methodical study of oxygenation through additions of hydrogen peroxide. A proper control of the peroxide concentration is nevertheless essential for high productivity without undue cell damage or inhibition.

This work is concerned with the development of methods for monitoring the hydrogen peroxide in the reactor with an electrochemical method very similar to that which has been used in earlier work on hydrogen peroxide determinations in pickling baths [6]. Because of an unexpected time dependence, it was compared to two other methods, each based on a different principle, in order to achieve mutual validation and assessment.

EXPERIMENTAL

Amperometric flow injection analysis

A 5-μl sample was introduced into an unsegmented deaerated (vacuum) carrier stream of 0.2 M sodium acetate, pH 5.0, using a pneumatic injector. The sample was diluted 100 times in a dispersion coil and oxidized at a glassy carbon electrode, kept at +1.2 V vs. SCE by potentiostatic control. The electrode reaction is oxidation of hydrogen peroxide to oxygen and hydrogen ions, and the current is proportional to the concentration over a wide range. A new electrode is pretreated by keeping it at +1.2 V in a 10 mM peroxide solution until a stable value is obtained (some hours). After that, the electrode remains stable indefinitely if the potentiostat remains active. Further details of the method are available in an earlier paper [6].

Enzymatic spectrophotometric method

The flow injection system is outlined in Fig. 1.

A 25-μl sample was introduced into a stream consisting of deaerated 0.1 M sodium phosphate, pH 6.0, by means of a pneumatically activated loop injector (Cheminert SVA 8031). Hydrogen peroxide from the sample oxidizes the immobilized peroxidase in the enzyme reactor and the peroxidase is then reduced during an oxidative coupling of 4-aminoantipyrine to 2,4-dichlorophenolsulphonate (DCPS). The coloured product is monitored at 514 nm in a 10-μl flow cell (LKB model 2151). The flow rates were 0.70 and 0.35 ml min^{-1} in the buffer and reagent lines, respectively.

Horse-radish peroxidase (EC 1.11.1.7, Sigma Type VI, Cat. No. 6140) was azo-immobilized [7, 8] onto porous glass (CPG-10, pore diameter 33 nm, 120—200 mesh; Electro Nucleonics, Fairfield, NJ). The enzyme-treated glass was packed into a reactor consisting of teflon tubing (1.0 mm i.d., 28 mm long, volume 22 μl) connected to the detector with 0.3-mm i.d. teflon tubing. Mixing between reagent (10 mM DCPS, 1 mM 4-aminoantipyrine in

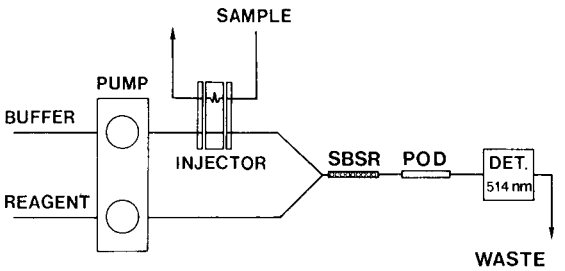

Fig. 1. Flow injection system for enzymatic determination of hydrogen peroxide. POD, peroxidase reactor; SBSR, single bead-string reactor.

0.1 M phosphate buffer, pH 6.0) and sample took place in a bead-string reactor [9] (i.d. 0.8 mm, length 100 mm, 0.5-mm diameter glass beads) which was inserted between the confluence point and the enzyme reactor. The samples were manually diluted 100 times before injection, to reduce the influence of substrate and products on the enzymatic reaction. The diluted samples were drawn into the sample loop by a separate peristaltic pump. The flow injection method was developed earlier at this laboratory for the determination of dissolved oxygen using other chromogens [10]. A thorough investigation of the oxidative coupling is under way.

Flow-through calorimetry

A 0.3-ml sample was introduced manually by a 4-way valve (Rheodyne) into a deaerated buffer stream consisting of 50 mM sodium succinate and 0.54 M glycerol, pH 5.0. Hydrogen peroxide from the sample was decomposed catalytically on platinized carbon (0.22 g) in a teflon reactor (i.d. 7 mm, length 18 mm) provided with a thermistor for temperature measurements [11]. A peristaltic pump (Bifok, FIA 08) was used to deliver the carrier solution (1 ml min^{-1}).

The reactor packing material was made by soaking granules of acid-washed carbon in hexachloroplatinic acid and drying it in an oven at 105°C for 1—2 h. The chloroplatinate was reduced at 300°C in a hydrogen stream until no acid fumes could be detected at the outlet. The amount of platinum was calculated to be 0.25 g g^{-1} of carbon. The calorimetric method has been described in detail elsewhere [12].

Chemicals

Hydrogen peroxide was obtained from Merck (Perhydrol, 30%). Stock solutions were standardized by titration with permanganate which in turn had been standardized against oxalate. A 5.54 M stock solution of dihydroxyacetone (98% pure; Merck) was prepared well in advance to ensure complete monomerization [13]. Methylglyoxal (grade II, 40% aqueous solution; Sigma) and DL-glyceraldehyde (>97%; Fluka), hexachloroplatinic(IV) acid (10%, p.a.; Merck), activated carbon (granules, 0.5—1.0 mm; KEBO AB,

Sweden) and 4-amino-1,2-dihydro-1,5-dimethyl-2-phenyl-3H-pyrazol-3-one (4-aminoantipyrine; BDH Chemicals) were used as received. DCPS was prepared as described by Barham and Trinder [14]. All other chemicals were from commercial sources and of p.a. quality.

RESULTS AND DISCUSSION

Amperometric method

The calibration graphs for hydrogen peroxide were strictly linear from 10^{-4} to 10^{-1} M. Electrochemical oxidation of glycerol, dihydroxyacetone or the buffer components takes place to some extent (see Table 1). The resulting currents were so small, however, that the interferences should be negligible in most cases (<6% for samples taken under the normal process conditions of 1—10 mM H_2O_2, 0—1.1 M dihydroxyacetone, 1.1—0 M glycerol, pH 5.0).

The effect of dihydroxyacetone on the electrochemical oxidation of hydrogen peroxide was investigated by cyclic voltammetry (Fig. 2). It can be seen that increasing amounts of dihydroxyacetone affect both the peak shape and the peak position. The actual concentration of dihydroxyacetone at the glassy carbon electrode will be at most 11 mM because of the dilution in the dispersion coil. Thus its effect on the response to hydrogen peroxide can be neglected. The same conclusion was found to hold for additions of glycerol.

Reactions of dihydroxyacetone

Dihydroxyacetone mutually isomerizes with DL-glyceraldehyde; both isomers can react in irreversible, acid-base catalyzed steps to form methylglyoxal, which in turn may react slowly to form, e.g., lactic acid [15, 16]. The isomerization is catalyzed by base, or possibly acid/base [17], and is

TABLE 1

Peak currents from the oxidation of sample components in the amperometric flow cell (The interference level is the H_2O_2 sample concentration which gives the same peak current as the compound)

Compound	Conc. (M)	Current (nA)	Interference level (mM H_2O_2)
Dihydroxyacetone	1.1	3.5	0.052
	0.5	1.8	0.027
	0.25	1.0	0.015
Succinate	0.05	0.32	0.004
Glycerol	1.1	0.49	0.007
	0.54	0.18	0.003
	0.27	0.13	0.002
Methylglyoxal	0.002	<0.05	<0.0007
Glyceraldehyde	0.011	0.43	0.004

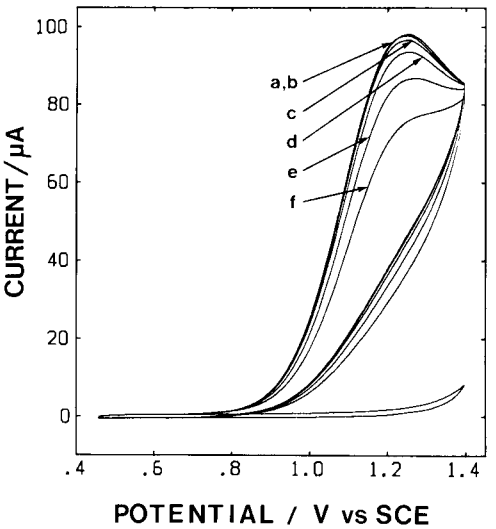

Fig. 2. Cyclic voltammograms of 5 mM H_2O_2 in (a) 0; (b) 0.011; (c) 0.039; (d) 0.093; (e) 0.22; (f) 0.47 M dihydroxyacetone. All solutions were 0.1 M in succinate, pH 5.0. The background current is shown as the bottom plot. Starting potential 0.50 V; sweep rate 50 mV s^{-1}.

quite rapid at higher pH. The formation of methylglyoxal is slow in water and in buffers like glutamate, succinate and pyrophosphate. Other ions, especially phytate and phosphate, act as powerful catalysts [18]. Methylglyoxal can be formed both from dihydroxyacetone and from glyceraldehyde although the latter reaction is slower. Some rate constants are available at 40°C [18] and at 50°C [15] but the data are not sufficient for a calculation of the rate of either formation of methylglyoxal or isomerization during measurement or production of dihydroxyacetone. It may be mentioned, however, that if Riddle and Lorenz's data [18] are applied to a solution containing 1.1 M dihydroxyacetone, 50 mM phosphate, pH 7.4 at 40°C, an initial production rate of methylglyoxal of 65×10^{-3} moles l^{-1} h^{-1} is predicted.

Dihydroxyacetone (1.1 M) was mixed with 10 mM hydrogen peroxide and the mixture was analyzed electrochemically at successive times (Fig. 3). The response decreases with time at first, then it levels out to form a plateau which decreases by 4% during the first hour. Standards run before and after showed that the electrode response remained constant. The initial decrease of response was very fast at pH 5 and 6, but slower in more acidic solutions. The initial decrease of response was also noted at pH 7 and 9, but no clear plateau could be seen. The overall loss of response was very fast at pH 7 with only 4% of the initial amount remaining after 90 min. About 20% remained after the same time in a solution which had a pH of 9. The response decreased with the same percentage and the same relative time course, independently of concentration in the range 1—10 mM hydrogen peroxide. Standard additions produced a step followed by a rapid 10—15% decrease

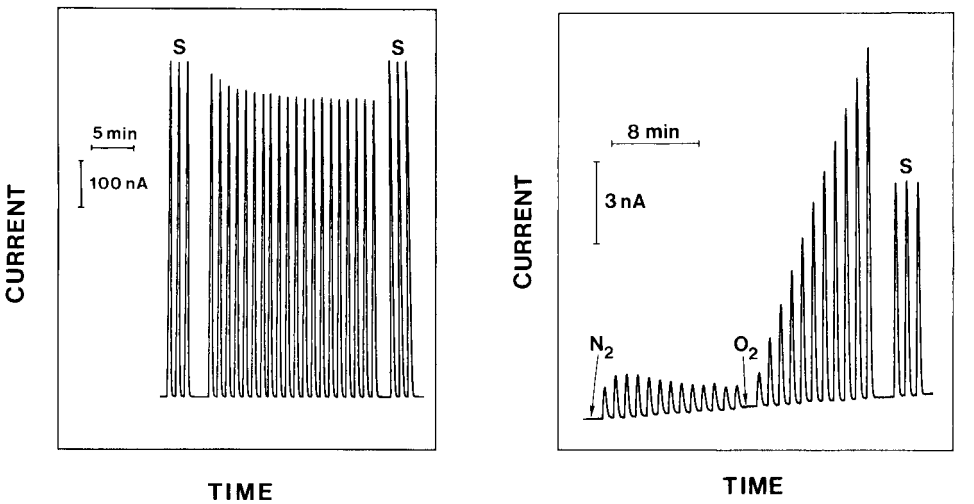

Fig. 3. The time-dependent decrease of the H_2O_2 signal in a solution containing 10 mM H_2O_2 and 1.1 M dihydroxyacetone in 50 mM phosphate buffer, pH 4.0. The S peaks are standards (10 mM H_2O_2) run before and after.

Fig. 4. The effect of oxygen on the peak signal (in 0.11 M dihydroxyacetone in a 0.1 M phosphate buffer, pH 7.0). S is a 0.1 mM H_2O_2 standard.

with the same relative shape as observed initially (pH $\leqslant$6.0).

The reported behaviour indicates that 10—15% of the hydrogen peroxide is consumed in a side reaction or bound as an adduct or complex which is electrochemically inactive. The possibility that other methods might respond in a different way to this fraction necessitated a comparative study as well as a study of the reactions between hydrogen peroxide and other compounds which are likely to be present in the medium.

About half of the hydrogen peroxide added to a 0.28 M glyceraldehyde solution (pH 4.0) had disappeared after 20 min. The decrease in response was almost exponential. The reaction is thus fairly fast but the formation of aldehyde through isomerization is slow in acidic solutions [15]. The total effect on the peroxide consumption in a dihydroxyacetone solution should therefore be small. There were no other significant reactions except between hydrogen peroxide and methylglyoxal.

Reactions of methylglyoxal

The data given by Riddle and Lorenz [18] show that no methylglyoxal should be produced in the reaction medium at pH 5.0 but that some should be produced in a phosphate buffer at pH 7.0 as mentioned above. Besides the methylglyoxal produced in this way some might be added with dihydroxyacetone as an impurity. It is therefore important to study the interaction between methylglyoxal and hydrogen peroxide.

Hydrogen peroxide was added to a 2.3 mM methylglyoxal solution and samples were analyzed by the electrochemical method at successive times. There was no initial rapid decrease in response such as that described above. There was, however, a slow continuous decrease in response which amounted to about 10% after 30 min at both pH 5 and 7 in a 10 mM peroxide solution. The decrease was slightly faster in a 1 mM peroxide solution. These observations show that it is unlikely that methylglyoxal is involved in the initial rapid decrease of response in the dihydroxyacetone solution.

Reactions of oxygen in dihydroxyacetone solutions

A fresh dihydroxyacetone solution, prepared from deaerated buffer, was bubbled with nitrogen and sampled into the flow injection system. Figure 4 shows that small peaks with time-dependent amplitudes were produced. Part of the response is due to a direct electrochemical oxidation of dihydroxyacetone and the rest to a reaction involving oxygen. Even during the nitrogen bubbling, some oxygen is present from contamination during preparation. When the nitrogen was replaced by oxygen, the analytical system showed successively increased responses. On returning to nitrogen bubbling, the peak heights decreased slowly with time. When the experiment was repeated with a 2.5 mM methylglyoxal solution no influence of oxygen could be seen.

The conclusion to be drawn is that hydrogen peroxide, or a compound with identical effect on the amperometric response, is formed in a reaction involving oxygen. The reaction seems to be reversible as evidenced by the decrease in peak heights during the nitrogen bubbling. It is known that methylglyoxal is produced from dihydroxyacetone via intermediates [17]. A possible explanation is therefore that one of the intermediates forms an adduct with oxygen, which hydrolyzes to hydrogen peroxide and pyruvate or lactate. The presence of small amounts of pyruvate was indeed demonstrated by its reaction with NADH and lactate dehydrogenase. The reaction rate with oxygen at a constant partial pressure and excess of dihydroxyacetone is expected to be constant in agreement with the observed linear increase of the peaks in Fig. 4. Table 2 gives the pH and medium dependence of the reaction, which was found to behave in the same way and to be catalyzed by the same ions as the reactions studied by Riddle and Lorenz [18]. In fact, the rates agreed with those extrapolated from the work of Riddle and Lorenz to within a factor of two. All this leads to the conclusion that hydrogen peroxide is produced spontaneously in the reaction medium if oxygen is present.

Comparison between the electrochemical, enzymatic and calorimetric methods

The amperometric method behaves almost ideally and can be used for almost interference-free determinations of hydrogen peroxide except for one possible deviation i.e., the time-dependent decrease of response in the pres-

TABLE 2

Effect of pH and anions on the production rate of H_2O_2 in a 56 mM dihydroxyacetone solution continuously sparged with oxygen

Medium[a]	pH	H_2O_2 formation (10^{-6} M min^{-1})
Water	—	0
Phosphate	2.0	0
Succinate	5.0	0
Phosphate	5.0	0
Pyrophosphate	6.0	0
Phosphate	6.0	1.5
Phosphate	7.0	7.8
Phosphate	8.0	20
Pyrophosphate	9.0	7.2

[a]0.1 M anion.

ence of dihydroxyacetone. It is therefore of interest to investigate whether the observed decrease in response reflects a real decrease in peroxide concentration or if it is an artefact of the method. Because both the enzymatic and the calorimetric methods were available in this laboratory and each measures hydrogen peroxide in a completely different way, it was decided to make measurements in parallel with the three methods.

Table 3 shows a comparison of the amperometric and calorimetric methods when they were used to follow the reaction in a solution containing dihydroxyacetone and hydrogen peroxide. It can be seen that the response decreases to the same degree with both methods. Table 4 gives a comparison of the amperometric and enzymatic methods when both were used to determine the peroxide in a series of solutions containing various amounts of dihydroxyacetone. Again, it can be seen that both methods record a decrease in the peroxide concentration as the dihydroxyacetone concentration increases. Similar results, with agreement between the responses of the two methods, were obtained at other pH values. Both dihydroxyacetone and glycerol produce transients in the spectrophotometer because of changes in the refractive index and this makes the evaluation somewhat more uncertain at low peroxide concentrations.

The enzymatic method was also used to check the mentioned production of peroxide in dihydroxyacetone solutions in the presence of oxygen. The results from the two methods parallelled each other very closely. The rates of peroxide production were found to be 7.8 and 8.1 μM peroxide min^{-1} with the enzymatic and amperometric methods, respectively. The rates relate to 50 mM dihydroxyacetone, 0.1 M phosphate buffer, pH 7.0. The agreement between the results obtained by the three methods supports the conclusion that each method measures the true hydrogen peroxide concentration even in ageing dihydroxyacetone solutions.

TABLE 3

Comparison of the amperometric and calorimetric methods used to follow the decrease of the H_2O_2 signal with time in a solution containing 10 mM H_2O_2 and 0.55 M dihydroxyacetone in 0.1 M sodium phosphate, pH 7.0

Time of reaction (min)	Relative peak signal (%)	
	Amperometric	Calorimetric
0	100	100
2.5	78	76
6.4	65	65
10.3	55	55

TABLE 4

Concentration of H_2O_2 after 4.0-h incubation as measured by the amperometric and enzymatic methods
(Measurements were made in parallel in solutions initially containing 10 mM H_2O_2 and various amounts of dihydroxyacetone (DHA) in a 0.1 M pyrophosphate buffer, pH 9.0)

DHA conc. (M)	Relative peak signal (%)	
	Amperometric	Enzymatic
0	100	100
0.11	86	89
0.55	40	42
1.1	19	20

If some of the hydrogen peroxide reacts to form organic peroxides, the methods must either be rather insensitive to such peroxides or respond to the same extent. The rate constants for the reaction between some peroxides and peroxidase for the formation of "Compound I" have been evaluated [19] and were found to decrease by one order of magnitude between hydrogen peroxide and methyl peroxide. The rate decreased by another factor of ten for butyl peroxide and still more for branched chain compounds. Peroxidase is known to be completely insensitive to dialkyl peroxides whereas acyl peroxides may react more quickly than hydrogen peroxide. Reactions between hydrogen peroxide and aldehydes are known to produce mono- and di-hydroxyalkyl peroxides. The dihydroxydialkyl peroxides are unstable and decompose rapidly in alkaline media [20].

Even if there is an excess of capacity in the peroxidase reactor of the enzymatic method, it will not be sufficient to give the same response towards organic peroxides with rate constants which are orders of magnitude less than that for hydrogen peroxide. The calorimetric reactor also has excess of capacity but it is insufficient for decomposition of organic peroxides with low reaction rates. Furthermore, there might be differences between the heat produced by decomposing hydrogen peroxide and organic peroxides.

In the amperometric method, the potential of the glassy carbon electrode was selected on the rising part of the oxidation curve in a potential-current diagram in order to reduce the background current [6]. The response will thus be very sensitive to small changes in the oxidation potential of the compounds. The method as designed is thus expected to give either quite different responses to hydrogen peroxide and organic peroxides or to give no response at all to the latter.

Peroxides which equilibrate fairly fast with hydrogen peroxide, and which could therefore be measured via hydrogen peroxide can also be excluded because of the different residence times in the reaction zones. The mean residence times were 40 ms, 1.6 s and 10 s for the amperometric, enzymatic and calorimetric methods, respectively. Unless the equilibration takes <40 ms, the methods should have given different results.

Taken together, these arguments show that it is very unlikely that the response is due to organic peroxides to any significant extent. The electrochemical method described here is therefore well suited for determination of hydrogen peroxide in the biotechnical process mentioned. It is fast and accurate and can easily be adapted to automated sampling. Work is now in progress to use it for computerized control of the hydrogen peroxide concentration in this process.

The authors thank Professor Bo Mattiasson and Mr. Bo Olsson for valuable discussions.

REFERENCES

1 S.-O. Enfors and B. Mattiasson, in B. Mattiasson (Ed.), Immobilized Cells and Organelles, Vol. II, CRC Press, Boca Raton, FL, 1983, Ch. 3.
2 M. Ibrahim and H. G. Schlegel, Biotechnol. Bioeng., 22 (1980) 1877.
3 J. A. Watson and J. Schubert, J. Gen. Microbiol., 57 (1969) 25.
4 F. Lawny, M. Cordonnier and D. Thomas, A.I.Ch.E. J., 21 (1975) 822.
5 O. Holst, S.-O. Enfors and B. Mattiasson, Eur. J. Appl. Microbiol. Biotechnol., 14 (1982) 64.
6 H. Lundbäck, Anal. Chim. Acta, 145 (1983) 189.
7 H. H. Weetal, in K. Mosbach (Ed.), Methods in Enzymology, Vol. 44, Academic Press, New York, 1976, p. 134.
8 B. Olsson and L. Ögren, Anal. Chim. Acta, 145 (1983) 87.
9 J. M. Reijn, W. E. van der Linden and H. Poppe, Anal. Chim. Acta, 126 (1981) 1.
10 B. Olsson, L. Ögren and G. Johansson, Anal. Chim. Acta, 145 (1983) 101.
11 O. Holst, B. Mattiasson, unpublished work.
12 B. Danielsson, B. Mattiasson and K. Mosbach, Appl. Biochem. Bioeng., 3 (1981) 97.
13 L. Davis, Bioorg. Chem., 2 (1973) 197.
14 D. Barham and P. Trinder, Analyst, 97 (1972) 142.
15 M. Fedoronko and J. Königstein, Collect. Czech. Chem. Commun., 34 (1969) 3881.
16 V. Prey, H. Berbalk and E. Steinbauer, Monatsh. Chem., 93 (1962) 237.
17 J. C. Speck, Jr., Adv. Carbohydr. Chem., 13 (1958) 63.
18 V. Riddle and F. W. Lorenz, J. Biol. Chem., 243 (1968) 2718.
19 K. G. Paul, P. I. Ohlsson and S. Wold, Acta Chem. Scand., Ser B, 33 (1979) 747.
20 B. L. Dunicz, D. D. Perrin and D. W. G. Style, Trans. Faraday Soc., 47 (1951) 1210.

Analytica Chimica Acta, 155 (1983) 57—65
Elsevier Science Publishers B.V., Amsterdam — Printed in The Netherlands

IMPROVED INFLECTION POINTS IN THE NON-AQUEOUS POTENTIOMETRIC TITRATION OF ACID FUNCTIONALITIES IN LIGNIN CHEMICALS BY USING INTERNAL STANDARDIZATION AND ION EXCHANGE

HARVEY POBINER*

Reed Lignin Inc., Princeton Research Center, P.O. Box 50, Princeton, NJ 08540 (U.S.A.)

(Received 1st April 1983)

SUMMARY

Potentiometric titration methods were developed for the acid functionalities in lignin chemicals. The inflection points for carboxylic acid and phenolic hydroxyl, which are normally diffuse and inexact for polymeric compounds such as the lignin chemicals, were significantly improved by the addition of an internal standard, *p*-hydroxybenzoic acid. This improved response is demonstrated by the addition and subtraction of titration curves of the mixture and the individual components. Because acid functionalities in lignosulfonates are present as the acid salts, the methods include such steps as acidification and a batch cation-exchange technique to liberate the free acids. Three nonaqueous titration methods developed for determining the two weak acids and the sulfonic acid in lignin chemicals are described.

Techniques were developed for the determination of the different acid functionalities in kraft lignin and in lignosulfonate samples. Through the application of these methods, the otherwise diffuse titration curves of lignin-type compounds were converted into useful ones with well-defined inflection points. These methods were needed to monitor changes in concentrations of these functionalities brought about by derivatization, oxidation and other treatments.

Titration curves of lignin chemicals often demonstrate ambiguous inflection points for the carboxylic acid and phenolic hydroxyl functionalities. It was found that the addition of an internal standard compound, *p*-hydroxybenzoic acid, markedly improves the instrumental response and facilitates resolution of the individual inflections in the titration curve. In this work, tetra-n-butylammonium hydroxide (TnBAH) is the titrant and *N,N'*-dimethylformamide (DMF) is the solvent. In practice, the theoretical titration volume for the internal standard is subtracted from the titrant consumed at each inflection, so that the carboxylic and phenolic hydroxyl acid groups in the lignin can be quantified.

*Address for correspondence: 29 Taylor Road, RD4, Princeton, NJ 08540, U.S.A.

0003-2670/83/$03.00

The titrations of lignosulfonates are more complex in that three acid functionalities, namely, sulfonic, carboxylic, and phenolic hydroxyl, should be quantified, and the first two are not present as free acids. One method, described herein, is based on acidification of the lignosulfonate with hydrochloric acid to liberate free acids, in the presence of the internal standard, followed by the nonaqueous titration. In this method, the inflections for hydrochloric acid and sulfonic acid are not cleanly differentiated, and only the two weak acids are determined. However, a cation-exchange batch technique can be used to convert the metallic salts in sodium and potassium lignosulfonates to the free sulfonic and carboxylic acids. The internal standard in the ion-exchange method is sodium benzoate, which is converted to benzoic acid, and serves to delineate the sulfonic and carboxylic acid inflections. In this ion-exchange method, it is necessary to correct for any titration of strong acids produced from the inorganic acid salts in the sample. Phenolic hydroxyl is not titratable in the aqueous solvent of the ion-exchange/titration method.

Results presented here indicate that the internal standard induces better inflections through arithmetic summation of responses, and possibly improves the overall electrode response of the mixture relative to that of the lignin alone.

The addition of internal standard compounds in a weak acid titration was demonstrated by Nakajima and Tanobe [1]; they added benzoic acid and phenol to solutions of bitumen in order to resolve inflections in a titration, and to group the titratable acids into categories of weak and very weak acids. More recently, Forss and Fremer [2] titrated sulfonic and phenolic hydroxyl groups in lignosulfonic acids dissolved in dimethylsulfoxide using a titrant of cetyltrimethylammonium hydroxide and an electrode system of a platinum reference and a prepolarized indicator electrode for each functionality.

An ion-exchange column was used by Griffin and Albaugh [3] to convert simple sodium sulfonates to titratable sulfonic acids. In applying their technique to solutions of lignosulfonates, it was found here that elution times were unduly long and a batch procedure was therefore preferred.

EXPERIMENTAL

Instrumentation and chemicals

An automatic titrator, such as the Mettler System 3-DV series, or equivalent equipment, is necessary. A glass indicating electrode and a calomel reference electrode are used; saturated KCl electrolyte in the calomel electrode must be replaced by 1 M tetra-n-butylammonium chloride (TnBACl) in water, which is available as polarographic grade material (Southwestern Analytical Chemicals, Austin, TX). The electrode is stored in the TnBACl solution when not in use. A nitrogen flow of 50—100 ml min^{-1} is maintained over the solution in the titration vessel.

The cation-exchange resin used was Dowex 50W-X8 (hydrogen form,

50—100 mesh; Bio-Rad Laboratories). Model compounds were obtained from Aldrich Chemicals.

To prepare 0.05 M TnBAH, transfer 100 g of tetra-n-butylammonium hydroxide, available as 25% (w/w) in methanol in 100-g quantities, into a 3-l glass-stoppered reagent bottle. Then add 2 l of anhydrous 2-propanol. Blanket with nitrogen, close the bottle, and mix thoroughly. Store under nitrogen in the refrigerator when not in use. The TnBAH is easily available (RSA Corp., Ardsley, New York, or Baker Chemicals). Standardize against 0.15 g of benzoic acid in DMF.

Procedures

Titration of weak acids in lignins. Weigh 0.35 g of lignin and 0.050 g of *p*-hydroxybenzoic acid in a titration vessel. Add 60 ml of DMF to dissolve the sample and the internal standard. If necessary, add 1 ml of distilled water to help dissolve the sample. Immerse the electrodes and titrate the magnetically-stirred solution with 0.05 M TnBAH under a nitrogen atmosphere. There will be two inflections, one for the carboxylic acid near −350 mV and one for the phenolic hydroxyl near −480 to −500 mV. These inflections can be resolved on the 500—200 mV full scale deflection ranges. A Metrohm end-point locator ruler was used to determine the inflections in all of these methods.

Titration of weak acids in lignosulfonates. Weigh 0.35 g of a lignosulfonate and 0.050 g of *p*-hydroxybenzoic acid into a 300-ml Fleaker beaker. Add 2 ml of distilled water. Pipet in 0.2 ml of concentrated, reagent-grade hydrochloric acid. Add 60 ml of DMF, cover with a Fleaker cap and stir magnetically for 5 min. Check for complete solubility and then titrate with 0.05 M TnBAH under nitrogen as described above. Run a blank containing 0.05 g of *p*-hydroxybenzoic acid, 2 ml of distilled water, 0.2 ml of hydrochloric acid, and 60 ml of DMF. There will be three inflections. The first inflection, near +200 to +100 mV, is due to excess of hydrochloric acid and strong acids generated from the sample; the next two inflections, as above, represent the titrations of carboxylic acid and phenolic hydroxyl, respectively.

Conditioning the ion-exchange resin. The Dowex 50W-X8 resin must be conditioned before use. To about 75 g of the resin, add 75 ml of 10% HCl, stir for 15 min, and filter under vacuum through Whatman No. 1 paper on a Büchner funnel. Wash with five 50-ml portions of distilled water. Continue the washing until the pH of the last washing agrees with that of the distilled water to within ±0.2 pH units.

Titration of sulfonic acid in lignosulfonate. Prepare a solution of 3.75 g of anhydrous, reagent-grade sodium benzoate in 250 ml of distilled water in a volumetric flask. Also, prepare a solution of 1 g of the lignosulfonate sample in 50 ml of distilled water in a volumetric flask. Into a 150-ml glass bottle containing 6 g of conditioned cation-exchange resin, pipet in 10 ml of the sodium benzoate solution and 30 ml of the sample solution. Into another bottle containing 6 g of the ion-exchange resin, pipet in only 10 ml of sodium

benzoate solution and 30 ml of distilled water. The latter solution serves as a check on reagents and technique. Cap the bottles and agitate the vessels for 15 min on a laboratory shaker, adjusting the motion so that the resin does not settle. Filter through Whatman No. 4 filter paper into a titration vessel. Wash the resin and the walls of the bottle with two 10-ml volumes each of hot distilled water and hot methanol, and five 10-ml volumes of warm acetone.

Place the washed filtrate aside until the washings of a second cycle become available. Remove the filter paper containing the 6 g of washed ion-exchange resin and place it back in the original bottle. Add about 3 g of additional conditioned resin and 30 ml of distilled water. Break up the filter paper with a glass rod, and repeat the mechanical agitation and the washing procedure with the three warm solvents, allowing the second group of washings to filter into the titration vessel containing the initial filtrate. Titrate with 0.05 M TnBAH as in the previous procedures. The initial inflection near +150 mV corresponds to the generated sulfonic acid component. The second inflection near −150 to −350 mV corresponds to carboxylic acid (generated from the internal standard and from RCOONa in the sample). The addition of the sodium benzoate serves to delineate the descending slope of the sulfonic acid inflection.

Calculate apparent percentages of SO_3H and sulfonic acid sulfur, uncorrected for any inorganic acids that are titrated. Then determine the non-sulfonate sulfur by gravimetry and subtract the value from the sulfonic acid sulfur to obtain the true percentage of sulfonic acid sulfur.

RESULTS AND DISCUSSION

Selection of internal standard

The internal standard was selected based on considerations of representative acid functionalities, resolution of inflection points, solubility, and acid strength. The pK_a of *p*-hydroxybenzoic acid for the phenol/phenoxide ionization is 9.32, compared with values for lignin of 10.6 determined here by a u.v. method [4] and of 10.9—11.0 by others [5]. Nakajima and Tanobe [1] observed that for 12 acids in a pK_a range of 2.2 to above 13, only two inflections resulted in mixtures with benzoic acid and phenol. They ascribed this phenomenon to a general narrowing of the differences in the half-neutralization potentials of the different acids in the nonaqueous solvent. The result was a general enhancement of acid strengths and a leveling of ionization differences, so that the acids were grouped into those titrating with benzoic acid and into those titrating with phenol. Evidence was obtained in the present work to suggest a leveling effect between lignin and the internal standard. It was found that other compounds with these weak acid functionalities, such as *p*-hydroxycinnamic acid and 3,5-dimethoxy-4-hydroxycinnamic acid, gave equivalent results in lignin titrations.

Inflection points

A typical non-aqueous titration curve of a kraft lignin in DMF is shown in Fig. 1A. Although there are slope changes in the titration curve, the inflections are ambiguous. Using conventional end-point locator techniques, one cannot obtain accurate inflections for the weak acid functionalities in the sample. Even the use of the first derivative mode does not delineate the individual end-points in the titration curve. Among the possible reasons for the loss of definition of the inflection points in a non-aqueous titration of a lignin sample are the inclusion of bound water in the polymer network and the low concentration of the acid functionalities in polymer chains. Upon addition of an internal standard, as in Fig. 1B, there is a marked improvement in resolution of inflection points. Analogous behavior is observed for the lignosulfonate titrations.

In general, most lignin titration curves obtained in the absence of the internal standard are unsatisfactory and the use of an internal standard is indicated. There are some titration curves that do show a suggestion of an inflection for each of the weak acids, and in those cases, a comparison can be made of results obtained with and without the internal standard. The comparison was run on 12 such samples. The agreements in the two methods, as indicated by correlation coefficients (0.999 for the carboxylic acid and 0.997 for the phenolic hydroxyl), suggested that the proper compound was selected for the internal standard.

The internal standard method was demonstrated on model compounds having one or more weak acid functionalities. The overall recovery data on eight compounds averaged 97.5% as shown in Table 1.

The method was put to a severe test by varying the weight ratio of lignin to internal standard from 1/1 to 18/1. Results showed a variation no greater than expected in normal replicate runs at the usual weight ratios of lignin to internal standard of 5/1 to 7/1. Inflection points were less pronounced in the case with an 18/1 weight ratio, but resolution was still improved relative to that with no internal standard.

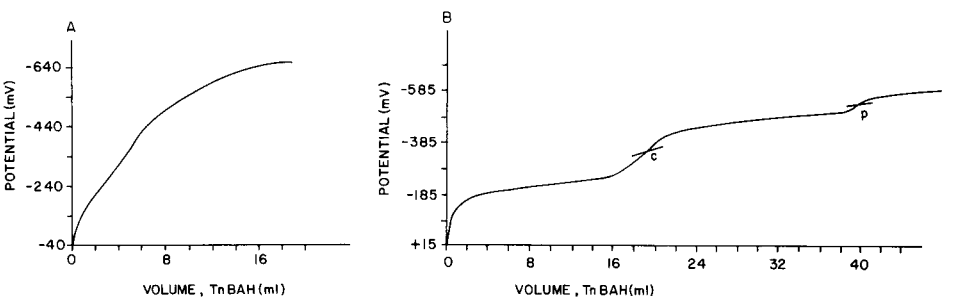

Fig. 1. Titrations in DMF with TnBAH (0.053 M): A, kraft lignin; B, kraft lignin in presence of *p*-hydroxybenzoic acid. Inflections: (c) RCOOH; (p) phenolic hydroxyl.

TABLE 1

Recovery of model compounds in the presence of *p*-hydroxybenzoic acid internal standard

Model compound	Recovery (%)	
	RCOOH inflection	Phenolic hydroxyl inflection
Benzoic acid	99.0	—
Sodium benzoate[a]	101.0	—
Benzoic acid + sodium benzoate[a]	98.3	—
Phenylacetic acid	99.9	—
Phenol	—	95.1
p-Hydroxyphenylacetic acid	100.1	97.6
p-Hydroxycinnamic acid	97.4	96.4
2,4-Dihydroxybenzoic acid	98.7	94.0
5-Sulfoisophthalic acid	98.6	—
	Av. 99.1	Av. 95.8
	Av. recov. 97.5	

[a]HCl added to liberate carboxylic acid.

Additive effect

Separate solutions of a hardwood kraft lignin and of *p*-hydroxybenzoic acid were prepared, as was a combined solution bearing the identical concentrations of the separate component solutions. Titration curves were obtained under identical conditions. A plot (Fig. 2A) obtained by adding volumes for the separate solutions at each point in the titration was similar to the titration curve for the mixture (Fig. 1B). End-points obtained from the two plots differed by less than 2%.

Similarly, a difference curve was obtained by subtracting the titrant volumes of the curves of *p*-hydroxybenzoic acid from the data of the experimental curve of the mixture of the kraft lignin with the internal standard. The difference curve is shown in Fig. 2B. The two indentations on the ascending slopes of each curve are attributed to the subtraction of the

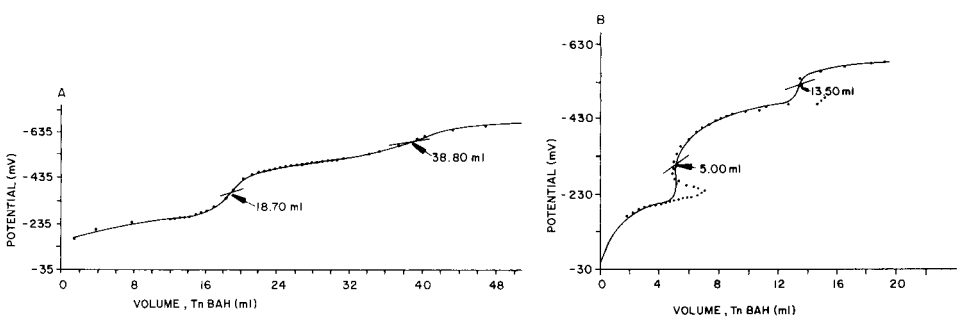

Fig. 2. Theoretical addition and difference titration curves obtained by manual plotting: A, addition curve of kraft lignin and *p*-hydroxybenzoic acid; B, difference curve obtained by subtraction of internal standard curve from mixture curve. TnBAH is 0.053 M.

significantly sharper slopes of the *p*-hydroxybenzoic acid curve from the mixture curve. Recoveries based on such curves ranged from 104 to 85%.

In an examination of the coincidence of end-point and equivalence points, least-squares intercepts obtained for fits of the volume of titrant consumed by increasing levels of a lignosulfonate sample vs. sample weight were 0.03 ml and 0.54 ml for the carboxylic acid and phenolic hydroxyl inflections, respectively. These data suggested reasonable agreement between end-points and equivalence points for the carboxylic acid titrations, and a possible deviation for the phenolic hydroxyl titrations.

Interferences of inorganic compounds. It was found that sodium hydroxide at concentrations up to 15% did not interfere with the weak acid titration because an excess of hydrochloric acid was usually added in the method. Sodium sulfate at levels greater than 5% could interfere. It is necessary to determine the non-sulfonic acid sulfur in order to monitor the possibility of interference. A silica gel purification was reported to remove sodium sulfate from petroleum sulfonates [6], and dialysis was used here to minimize inorganic impurities in lignosulfonates.

Ion-exchange method

The cation-exchange technique converts the sodium and potassium carboxylates and sulfonates of lignosulfonates to the free acids so that they can be readily titrated. Sodium benzoate, an internal standard, is converted to benzoic acid in the method and serves to delineate the inflections for RSO_3H and RCOOH. The value of this procedure is illustrated by Fig. 3. In Fig. 3A, the inflection for RSO_3H is not well resolved, and only a total acidity could be calculated. Upon introducing the sodium benzoate, the two inflections (Fig. 3B) were well resolved, and it was calculated that 1.75 meq RSO_3H/g and 2.63 meq RCOOH/g were present. The sum of the two (4.38 meq g^{-1}) is in reasonable agreement with the value of 4.47 meq g^{-1} from Fig. 3B.

In developing the batchwise cation-exchange method, it was found that one ion-exchange cycle and the use of solvents at room temperature provided recoveries of only 80—82% of sodium benzoate. This was increased to 99—100% recovery by the introduction of two cycles of ion-exchange and the use of hot solvents to wash any adsorbed sample from the resin. The

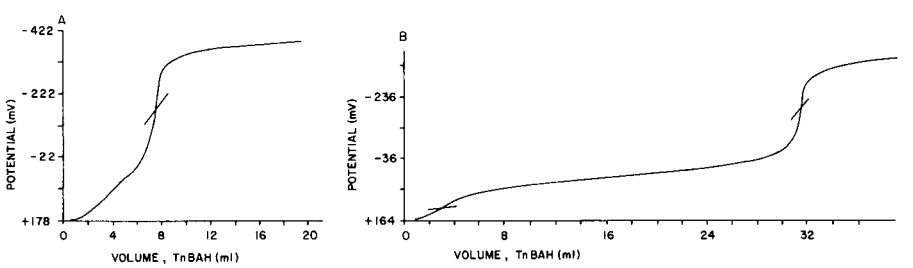

Fig. 3. Titrations of a lignosulfonate, after ion exchange, by TnBAH (0.041 M): A, in absence of sodium benzoate; B, in presence of sodium benzoate.

phenolic hydroxyl is not resolved in the ion-exchange method because it is too weakly acidic to be titrated in an aqueous acetonic medium.

Seven model compounds were taken through the ion-exchange/titration procedure. Recoveries ranged from 97 to 100% and the average recovery was 98.3%, as shown in Table 2.

Comparison of methods for RCOOH

In a series of sodium lignosulfonates and sodium lignites, there was good agreement between the carboxylic acid values obtained by the two titration methods. The least-squares equation for results obtained for eight samples processed by the two methods was $y = 1.04x - 0.02$ with a standard error of estimate of 0.09 meq g^{-1} and correlation coefficient $r = 0.991$. When calcium lignosulfonates were processed by the two methods, approximately half the carboxylic acid was obtained by the ion-exchange technique relative to the acidification technique. This may be due to the reduced solubility of the calcium salt under the conditions of the method and incomplete conversion to the acid form on the cation-exchange resin.

The standard deviation in a series of replicate runs of carboxylic acid at the 1.05 meq g^{-1} level in lignosulfonate was found to be 0.060 meq g^{-1}. For phenolic hydroxyl at the 0.94 meq g^{-1} level in the same series, the standard deviation was 0.036 meq g^{-1}. In the ion-exchange/titration method, the standard deviation for sulfonic acid at the 2.02 meq g^{-1} level was 0.04 meq g^{-1}, and for carboxylic acid at 1.19 meq g^{-1} the standard deviation was 0.025 meq g^{-1}.

The author thanks Reed Lignin Inc. for permission to publish this information, and Messrs. D. Briant and A. Allen for their extensive technical assistance. The initial work of Dr. J. Boudwin and Dr. J. Piechocki in the non-aqueous titrimetry of lignin is also acknowledged.

TABLE 2

Analyses of model compounds taken through the ion-exchange/titration procedure

Model compound	Recovery of free acid (%)	Model compound	Recovery of free acid (%)
Sodium benzoate	99.0	*p*-Toluene sodium sulfonate	99.6
Sodium salicylate	98.6	*p*-Toluene sulfonic acid monohydrate	98.8
5-Sulfoisophthalic acid, monosodium salt	96.5[a]	2,5-Dihydroxy-*p*-benzene disulfonic acid, Dipotassium salt	96.8
1-Dodecanesulfonic acid, Na salt	98.9		Av. 98.3

[a] At SO_3H Infl.; 100.0% at RCOOH Infl.

REFERENCES

1 T. Nakajima and C. Tanobe, J. Inst. Petroleum, 59 (1973) 32.
2 K. Forss and K. E. Fremer, Pap. Puu, 60 (1978) 121.
3 E. H. Griffin, Jr. and E. W. Albaugh, Anal. Chem., 38 (1966) 921.
4 A. Albert and E. P. Serjeant, The Determination of Ionization Constants, Chapman and Hall, London, 1971, Ch. 4.
5 G. B. Shtreis and V. M. Nikitin, Zh. Prikl. Khim., 40 (1967) 1814.
6 K. R. Voss, C. E. Bricker, M. J. Michnick, G. P. Willhite, Soc. Pet. Eng. J., 21 (1981) 771.

Analytica Chimica Acta, 155 (1983) 67—77
Elsevier Science Publishers B.V., Amsterdam — Printed in The Netherlands

PREDICTIVE COULOMETRY BASED ON FIRST-ORDER KINETIC LINEARIZATION

LOWELL M. SCHWARTZ*

Department of Chemistry, University of Massachusetts-Boston, Harbor Campus, Boston, MA 02125 (U.S.A.)

JACKSON E. HARRAR

Chemistry and Materials Science Department, Lawrence Livermore National Laboratory, University of California, Livermore, CA 94550 (U.S.A.)

(Received 10th May 1983)

SUMMARY

A general linearization method developed for the estimation of the parameters of kinetic processes obeying a first-order exponential decay is applied to the problem of predicting the end-point integral in controlled-potential coulometry. The method is capable of estimating and correcting for the continuous faradaic background current, and is also designed to tolerate transient perturbations such as those caused by uncompensated cell resistance or some types of kinetic complications in the electrochemical reaction. The technique was tested with data obtained from several different types of electrolyses and found to yield accurate results in 25—40% of the time required for a complete electrolysis.

As the technique of controlled-potential coulometry has been refined, several approaches have been developed for using the measurements obtained during an electrolysis to calculate the end-point value of the integral of the current, i.e., the quantity of electricity that would be consumed if the electrolysis were prolonged to completion. Such techniques offer the possibility of substantial savings in the time per determination, and in general their accuracy depends on the degree to which the analyte electrolysis current-time behavior conforms to that of a first-order exponential decay function. In addition to facilitating chemical analysis, these mathematical curve-fitting and estimation techniques can also reveal kinetic complications in the electrolysis and aid in the elucidation of electrochemical reaction mechanisms.

Several early approaches to predictive coulometry were reviewed in 1975 [1]. Probably the most noteworthy of these is the technique developed by Stephens et al. [1, 2], which can be used with an on-line laboratory computer while the electrolysis is in progress and which is capable of accurate (±0.2%) prediction in approximately a third of the normal electrolysis time. This algorithm is based on an equation of Meites [3] that relates the end-point integral to three values of accumulated charge measured during the electrolysis. In an analogous application, this algorithm has also been used to

0003-2670/83/$03.00

predict thermal equilibrium conditions in calorimetry [4]. More recently, Holland et al. [5], in a departure from basing the prediction on the current-time characteristics of the electrolysis, devised a method that combines measurements of accumulated charge with solution redox potentials. This method is applicable only to electrochemically reversible reactions. Brubaker et al. [6] proposed and briefly tested off-line a recursive, linear-least-squares estimation technique, but this method has not yet been thoroughly evaluated. Other procedures have been described for estimating the parameters of physical processes obeying exponential response functions [7, 8], but these have not been applied to predictive coulometry.

Two methods of parameter estimation in particular appear to be potentially superior to those used previously for predictive coulometry. One is the multiparameter nonlinear regression technique of Meites and coworkers [9—11], and the other is a first-order kinetic linearization technique developed by Schwartz [12]. Both algorithms incorporate rigorous statistical methods and criteria in their calculations, and both are capable of estimating the background electrolysis current as well as the quantity of analyte and electrolysis rate constant. Meites and coworkers [10, 11] have demonstrated the utility of their method for both the study of electrolytic reactions and off-line predictive coulometry; however, the methodology has not been tested in real time because compact computer hardware with sufficient speed has not been available. The linearization method [12] that is described here, while having the same features required for predictive coulometry, is less demanding of computer power. This paper presents the results of the application of the linearization technique to several typical electrolysis reactions and to computer-synthesized data featuring severe background current and uncompensated cell resistance. As a step toward real-time implementation, controlled-potential coulometric data obtained previously were processed to assess the performance of the method.

EXPERIMENTAL

Coulometric procedures examined

Table 1 lists and summarizes the characteristics of the controlled-potential coulometric determinations that were used to test the prediction algorithm. These are among a number of well established electrolysis reactions that are known to yield accurate ($\approx$0.1%) coulometric results when carried out to completion and when the results are subjected to appropriate blank or background-current corrections. In two of the electrolyses, the conditions were altered slightly from the normal procedure to illustrate the effect on the prediction. Thus uranium was reduced at a less negative potential than the usual —0.325 V vs. SCE because this tends to make the current-time characteristic of the electrolysis conform more closely to that of a simple first-order process [2]. Also, in Electrolysis 4, iron(II) was oxidized at a slower rate by stirring the solution less rapidly. Normally, the electrolytic oxidation and

TABLE 1

Electrolysis reactions used to evaluate the predictive coulometry technique

Electrolysis	Supporting electrolyte	Control potential (V vs. SCE)	Lit. ref.	Remarks
1. U(VI)→U(IV)	0.5 M H_2SO_4			Intermediate disproportionation;
	0.1 M sulfamic acid	−0.275	13	nonlinear log i vs. t; irreversible
2. Fe(II)→Fe(III)	0.5 M H_2SO_4	+0.62	14	Fast electrolysis
3. Fe(III)→Fe(II)	0.5 M H_2SO_4	+0.24	14	Reversal of previous reaction
4. Fe(II)→Fe(III)	0.5 M H_2SO_4	+0.24	14	Slower stirring speed to prolong electrolysis
5. Ti(IV)→Ti(III)	9 M H_2SO_4	−0.20	15	Inherently slow electrolysis
6. Cu(II)→Cu(Hg)	0.5 M H_2SO_4	−0.15	16	Fast electrolysis
7. Cu(Hg)→Cu(II)	0.5 M H_2SO_4	+0.15	16	Reversal of previous reaction

reduction of iron, as well as these reactions of copper, are fairly rapid. The reduction of titanium(IV) in strong sulfuric acid, in contrast, is an inherently slow process because of mass-transfer limitations and is an ideal application for predictive coulometry.

Apparatus and coulometric procedures

The electrolysis cells and coulometric instrumentation were as described previously [1, 17]. Solutions of titanium and copper were prepared from the high-purity metals; National Bureau of Standards U_3O_8 was used for the uranium solution; reagent-grade iron(II) ammonium sulfate was used to prepare the iron solution. The quantity of each test substance taken in each run was not carefully standardized; rather, the accuracy of the predictive coulometry algorithm was evaluated by comparing the predicted result with the value obtained in the complete electrolysis. On an absolute basis, the quantities taken were known to ±0.3%.

To provide data for off-line tests of the algorithm, values of the integrator output were recorded digitally at 1-s intervals for each complete electrolysis by means of a Tektronix Model 4051 Graphic System interfaced to a Hewlett-Packard Model 3455A 6-1/2-digit multimeter. Timing for the data acquisition was provided by a Tektronix Model 180A Time Mark generator. These data were then transferred to a CDC Cyber 175 computer for processing by the prediction routine. Analog traces of the logarithm of the electrolysis current vs. time were also obtained by means of an electronic noise filter and logarithmic converter system [1].

THEORY AND DATA PROCESSING

Figure 1 shows a typical current response of a controlled-potential coulometric run. This plot is the logarithm of the Cu(II) reduction described as Electrolysis 6 in Table 1. It can be seen that the log i vs. t plot is linear in the time segment from about 2 to 5 min, which corresponds to first-order be-

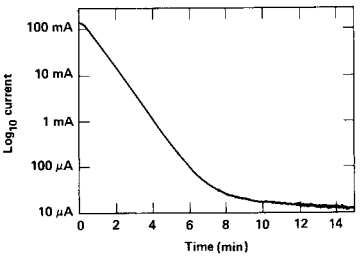

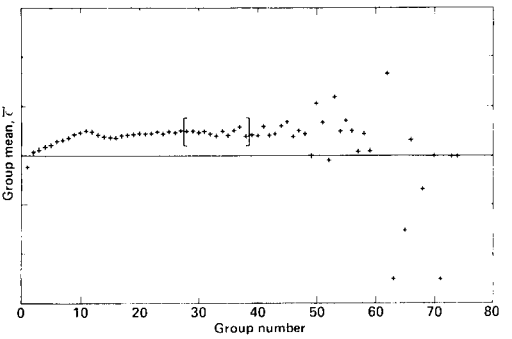

Fig. 1. Electrolysis current trace on log i vs. t coordinates for the Cu(II) reduction described in Table 1.

Fig. 2. Sequence of group mean $\bar{\epsilon}'$ values computed in search of ideal behavior for the Cu(II) reduction electrolysis shown in Fig. 1. The solid line is a horizontal reference and the brackets enclose groups spanning the initial 94 s of ideal behavior.

havior, and deviations from linearity occur both before and after this interval. Also there is a noise component which becomes more significant relative to the current magnitude as time increases. In the general case, the observed current may reflect a superposition of several mechanisms: exponentially decreasing current caused by electrolysis of analyte and impurity ions and by an initial charging effect, a continuous faradaic background current caused by electrolysis of the solvent, and an initial perturbation at high current levels caused by varying cell potential associated with uncompensated cell resistance. Certain cases where kinetic complications exist in the electrochemical reaction will also be considered. The proposed method is capable of predicting the end-point integral if a time segment exists during the run when all initial transients have become negligible but before the noise level in the integrated current signal masks the integral of the analyte current.

If it is assumed that the analyte current follows the Lingane equation [18], the observed noise-free total current after time t_i is given by

$$i(t) = I_0 \exp(-pt) + I_b \tag{1}$$

where I_b is the continuous faradaic background current, p is the rate constant for the analyte electrolysis, and I_0 is a constant. In this paper, current following Eqn. 1 is regarded as "ideal" behavior, and t_i denotes the earliest time during the electrolysis when the current is due solely to analyte and continuous faradaic background currents. In coulometry, the charge accumulated during the electrolysis is of primary interest and so the time integral of the current from the start of the ideal period is written as

$$q(t) = Q_2\{1 - \exp[-p(t - t_i)]\} + I_b(t - t_i) \qquad (\text{for } t \geqslant t_i) \tag{2}$$

At time t_i the total charge accumulated is

$$Q_i = Q_B + Q_1 + I_b t_i \quad (3)$$

where Q_B is the sum of charges arising from the impurity and charging currents, and Q_1 is the analyte charge accumulated by time t_i. When solid working electrodes are used, Q_B would also typically contain a contribution from the dissolution and formation of surface oxide films. The end-point integral Q_∞ is the charge accumulated at infinite time corresponding to complete electrolysis of the analyte and in terms of the parameters used here would be $Q_\infty = Q_1 + Q_2$.

The object is to find Q_∞ as quickly and as accurately as possible during the run. The general plan is to wait until the initial transients have decayed away and then to fit Eqn. 2 to instantaneous charge data by appropriate adjustment of the parameters Q_2, p, and I_b. The time t_i when this equation first becomes valid is not known beforehand and so the instantaneous charge data must be examined from the outset. Once t_i is found, the procedure uses subsequent data to find Q_2. A value of p is also calculated incidentally. In this calculation, one must trade off speed vs. precision. A rough value of Q_2 can be found quickly, but high precision requires more data and thus a longer run time. Once the ideal period has been identified, the charge Q_i corresponds to the time t_i and there only remains to subtract Q_B and $I_b t_i$ to obtain Q_1. Typically, Q_B cannot be found from a single electrolysis run of an analyte solution and so must be evaluated by a separate experiment, for example, by a blank run with supporting electrolyte alone, and subtracted manually. However, the continuous faradaic background current can be evaluated during the ideal period, and assuming that this has remained constant throughout, $I_b t_i$ can be calculated. In the present tests of the algorithm with actual data, the contribution of Q_B was neglected. For the electrolyses tested, the contribution of Q_B is small, and it is included in both the estimated and experimentally measured values of Q_∞.

For clarity of exposition, the procedure for calculation is subdivided into three parts: stage I involves finding t_i, the onset of the ideal period; stage II involves calculating Q_2 early in the ideal period; and stage III comprises calculating I_b. Data points of instantaneous charge accumulation $q(t)$ vs. elapsed time t must be recorded at equally-spaced time intervals and stored for later processing. This time spacing is typically 1 s but may have any convenient value.

Prior to the ideal period, the $i(t)$ behavior is not represented by Eqn. 1. This means that if the integrated version of Eqn. 1 is fitted to $q(t)$ vs. t data, the parameter p will not be a constant but will vary with time. To find the ideal period during stage I of the calculation, the equation to fit is

$$q(t) = Q[1 - \exp(-pt)] + I_b t \quad (4)$$

which is an exponential decay superimposed on the first-degree polynomial $Q + I_b t$. Several ways of extracting the parameter p from data which follow this type of equation have been demonstrated [12]. For this calculation, the method given by the earlier Eqn. 15 [12] was selected. This can be under-

stood as follows: starting at any time t_1 three data points are selected, separated by a fixed time lag τ so that $q(t_1 + 2\tau)$ and $q(t_1 + \tau)$ as well as $q(t_1)$ are obtained. Given the linear combination

$$\Lambda^{(1)} = q(t_1 + 2\tau) - 2q(t_1 + \tau) + q(t_1) \tag{5}$$

it can be shown that this equals $-Q(\epsilon - 1)^2 \exp(-pt_1)$ if Eqn. 4 is valid. Here $\epsilon = \exp(-p\tau)$. If, at time τ' after t_1, a second set of three points is selected (also separated by τ), this second set can be formed into the linear combination

$$\begin{aligned}\Lambda^{(2)} &= q(t_1 + \tau' + 2\tau) - 2q(t_1 + \tau' + \tau) + q(t_1 + \tau') \\ &= -Q(\epsilon - 1)^2 \exp(-pt_1) \exp(-p\tau')\end{aligned} \tag{6}$$

The ratio $\Lambda^{(1)}/\Lambda^{(2)}$ (denoted by ϵ') is thus $\exp(p\tau')$, and because τ' is a constant ϵ' will be a constant if p is a constant. To monitor the constancy of ϵ', several sequential sets of six data points are recorded and a sequence of ϵ' values is computed from these. If this sequence is found to vary with time in a nonrandom way, Eqn. 4 does not properly represent the current behavior and the ideal period has not yet commenced. However, the drift of ϵ' will disappear when all six points are taken from the ideal period. It can be observed that ϵ' values fluctuate randomly about a mean, because of the noise component. The procedure in stage I is thus to run statistical tests on the sequence of ϵ' values until an invariant mean is detected.

The statistical test chosen to monitor the drift of ϵ' is to gather sequential values into groups of, say, five and to compute the mean $\bar{\epsilon}'$ and standard deviation of each group. To test whether two groups have the same mean, the difference of the mean and the standard error estimate of that difference are calculated and then a t-test is applied for the null hypothesis that the difference of means is zero. Formulae used are those given by Davies and Goldsmith [19] for calculating the standard error estimate and the number of degrees of freedom appropriate for that estimate. If the means of groups 1 and 2 appear to be the same within this statistical criterion, then both groups are provisionally accepted into the ideal period and group 3 is t-tested against group 1. If groups 1 and 3 have equal means, 3 is accepted into the ideal period provisionally. Otherwise group 1 is rejected and group 2 is tested against group 3. The procedure continues until a continuous sequence of groups is found encompassing some preset length of time such that all $\bar{\epsilon}'$ values pass the t-test against one another. The time associated with the earliest data point of the earliest such group is taken as t_i, the onset of the ideal period. The preset length of time as well as the confidence level for the t-testing can be adjusted and are chosen judiciously considering the noise level in the data and the time scale of the electrolysis.

If the search procedure continues too long into the run, the signal $q(t)$ is essentially all due to continuous background current and noise. With little information in the signal from the analyte electrolysis, the calculated ϵ'

values fluctuate wildly. Therefore, it is prudent to abort the search when the standard error of a group exceeds a certain fraction, say, 20% of the group mean. Figure 2 shows the succession of mean $\bar{\epsilon}'$ values for groups of five for the Cu(II) electrolysis whose log i vs. t curve is given in Fig. 1.

In stage II, the parameter Q_2 is calculated by fitting Eqn. 2 to $q(t)$ data recorded after t_i. The procedure used here is a generalized Guggenheim method as described earlier (Eqn. 14 [12]). As in stage I, three points starting at t_1 relative to t_i and separated by τ are selected and formed into the linear combination Λ, according to Eqn. 5, which here equals $-Q_2\{\exp[-p(t_1 - t_i)]\}(\epsilon - 1)^2$. A series of these Λ are calculated starting at a series of later times so that Λ vs. t_1 data points are constructed. A plot of $\ln(-\Lambda)$ vs. t_1 is expected to yield a straight line with slope $(-p)$ and with intercept $\ln[Q_2(\epsilon - 1)^2]$. Knowledge of p from the slope leads to a value of $\epsilon = \exp(-p\tau)$ and then to a value of Q_2 from the intercept. The straight line is most properly evaluated by a weighted least-squares procedure because the ordinate values, $\ln(-\Lambda)$, cannot be equally precise even if the $q(t)$ raw data are equally precise. The weighting factors are taken inversely proportional to the variances of $\ln(-\Lambda)$. This is a rapidly-converging iterative process.

In stage III, it is assumed that the impurity charge Q_B is negligible, but that the continuous faradaic charge is not. The continuous faradaic component can be calculated once it becomes a significant part of the total current during the ideal period. The calculated analyte charge as expressed by the first term on the right-hand side of Eqn. 2 is subtracted from the recorded $q(t)$ data and this difference is expected to be $I_b(t - t_i)$. A weighted least-squares fit of these differences vs. t yields a line of slope I_b. The predicted value of Q_∞ is then calculated as

$$Q_\infty = Q_i - I_b t_i + Q_2 \tag{7}$$

FEASIBILITY STUDIES

This prediction procedure was evaluated by computer studies based on data from the seven electrolyses listed in Table 1. In each experimental run, an analog trace of log i vs. time was recorded along with a digital sequence of $q(t)$ data at 1-s time intervals with a precision of five significant figures. The seven complete $q(t)$ data sets were stored as separate files in the memory of the Cyber 175 computer and development work for the prediction algorithm was done with these files without regard to real-time computing speeds. The purpose of these studies was to verify that the algorithm could yield accurate assay predictions in times significantly less than those required for complete electrolysis. The procedure is designed to be used by an operator for routine assays of a solution containing a single electrolyzable analyte. The routine nature of the assay implies that the operator has a rough knowledge, say, within ±50%, of the first-order kinetic lifetime based on previous runs made under similar conditions. An electrolysis to 99.9% completion generally re-

quires a time period of $7T$, where $T(= 1/p)$ is the kinetic lifetime. This rough lifetime is used to set an appropriate interval for the time lag τ. The value of this parameter is not critical, but if the value is set too large, the prediction time is unnecessarily lengthened. If the value is set too small, the precision of the estimate of the end-point integral is reduced because of the round-off error in calculating differences in Λ.

Computational details are given as follows for the Cu(II) reduction, for which the analog trace is shown in Fig. 1. It can be seen from the linear segment at 2—5 min that the slope is approximately —0.59 min^{-1}, which is equivalent to a kinetic lifetime of about 44 s. The operator selects a rough lifetime T of 60 s based on previous experience, and using this setting, the algorithm sets $\tau = 0.33T$ or 20 s for stage I. Other parameter settings are the displacement $\tau' = 2$ s and starting times t_1 separated by 1 s. After a time 2τ s into the run, the first $\Lambda^{(1)}$ is computed from recorded points at 1, 21 and 41 s, and $\tau' = 2$ s later at 43 s, the first $\Lambda^{(2)}$ is computed from recorded points 3, 23 and 43 s. The ratio of the linear combinations is the first $\bar{\epsilon}'$. At the 47-s mark, five of these ϵ' values are gathered into a group; the mean $\bar{\epsilon}'$ and standard deviation of this group will be used in t-tests against future groups. Under the parameter settings in this run, these groups are completed at a rate of one per 5-s period; the sequence of group means is shown in Fig. 2. When the electrolysis current becomes ideal, the group means scatter about a horizontal line. Figure 2 shows a clear trend until after about 30 groups have passed. Then groups after about number 50 exhibit wild scatter, which reflects the fact that the analyte current has become small relative to the noise. The operator has two data-processing parameters to control the t-testing procedure which searches for the ideal behavior, as detected by a sequence of groups having statistically equal means. These are the length of time that this sequence of groups must span, and the confidence level of the t-test. These settings enable the operator to fine-tune the search to detect a small deviation from ideality which may be obscured within the noise scatter of the group means. In this case, the operator chose to search for a span of $1.5T = 90$ s of ideal behavior and selected a fairly stringent confidence level [19] for the t-tests. The algorithm detects a sequence of eleven groups, numbers 28 through 38 (bracketed in Fig. 2) beginning at time $t_i = 135$ s. The total accumulated charge Q_i to this time is scaled to 2.359 mg of copper(II) having been reduced to Cu(Hg).

In stage II, the Guggenheim procedure is applied within the first 94 s of the ideal period commencing at 135 s. A time lag of 31 s is used here. A weighted least-squares regression is done in the form of $\ln(-\Lambda)$ vs. $(t - t_i)$ where Λ is given by Eqn. 5 with t_1 replaced by $(t - t_i)$. The slope of this line is $-p = -(23.18 \pm 0.09) \times 10^{-3}$ s^{-1} which corresponds to a kinetic lifetime of 43.15 s. The intercept on the $\ln(-\Lambda)$ axis is $\ln[Q_2(1 - \epsilon)^2] = -3.381 \pm 0.001$ where $\epsilon = \exp(-p\tau)$. These uncertainties are standard error estimates of the least-squares parameters based on the residual scatter of data points from the line. The quality of the linear fit is reflected by the standard deviation of

the residuals of 1.1×10^{-4} compared to $|\ln(-\Lambda)|$ ordinate values ranging from 3.4 to 4.1, i.e., a scatter of about 0.003%. The algorithm combines the slope, intercept, their variances and covariance to calculate $Q_2 = 0.1294 \pm 0.0006$ mg.

In stage III, the $q(t)$ data already collected between $t_i = 135$ s and 229 s are used again to estimate the magnitude of the continuous faradaic background current as the slope of the weighted least-squares regression of $q(t) - q(t_i) - Q_2\{1 - \exp[-p(t - t_i)]\}$ on $(t - t_i)$. In the copper(II) electrolysis, this slope is 24.8 ± 0.2 ng s^{-1}. If it can be assumed that this same current was flowing from the beginning of the electrolysis, it can be calculated that $I_b t_i$ amounted to 0.003 mg of copper. The analyte end-point integral is thus $2.359 + 0.129 - 0.003 = 2.485$ mg, and if it is assumed that the $q(t)$ recorded data are precise to 0.0001 mg, the precision of the end-point integral can be estimated as $0.0001 + 0.0006 = 0.0007$ mg. The prediction of 2.485 mg is to be compared to a value of $2.49 \pm 0.3\%$ obtained by complete electrolysis. The prediction was made shortly after recording the data point at 229 s or 3.8 min, compared to the time for a complete electrolysis of approximately 10 min.

Table 2 summarizes the results of the application of the predictive coulometric methodology to all seven electrolyses. In each case, the agreement is excellent between the predicted Q_∞ and the value found by complete electrolysis in at least twice the time. The prediction is accurate for the uranium reduction, even though the mechanism involves a homogeneous disproportionation reaction, because a control potential was used that causes the overall process to be controlled by the rate of the electrode reaction [2].

TABLE 2

Comparisons of predicted end-point integral with results of complete electrolyses

Electrolysis	Timing (s)			Accumulated charge, in units of mg of analyte				
				By predictive methodology				By complete electrolysis
	t_i[a]	t_2[b]	t_∞[c]	$Q_i(\pm 0.0001)$[d]	$Q_2 \pm$ std. error	$I_b t_i$	Q_∞	$Q_\infty(\pm 0.3\%)$
1	210	393	960	4.987	1.054 ± 0.002	0.012	6.029	6.05
2	60	125	480	2.014	0.481 ± 0.003	nil[e]	2.585	2.59
3	110	189	360	2.384	0.170 ± 0.002	nil	2.554	2.55
4	90	269	900	1.710	0.857 ± 0.002	0.002	2.565	2.57
5	230	391	1200	3.940	0.897 ± 0.005	nil	4.837	4.84
6	135	229	600	2.359	0.129 ± 0.001	0.003	2.485	2.49
7	120	193	300	2.378	0.118 ± 0.001	−0.009	2.505	2.49

[a]Time of onset of ideal period. [b]Time of final recorded point used in prediction. [c]Approximate time for complete electrolysis. [d]Measured accumulated charge at time t_i. [e]Nil means that the quantity $I_b t_i$ is less than the standard error of Q_2.

However, because all seven electrolyses examined here are characterized by relatively small continuous faradaic currents, this was not an exacting test of the ability of the algorithm to handle such corrections. An additional feasibility study based on computer-synthesized data was therefore done to test the predictive algorithm in a severe case. An electrolysis current was synthesized in the following manner. For the first 60 s, a noise-free current is held constant at 5.0 mA in order to simulate resistance-control; after 60 s, the noise-free current is described by Eqn. 1 with I_0 = 5.0 mA, p = 0.0100 s^{-1} and I_b = 50 μA. Thus the ratio of analyte current to background current starts at 100:1 and decreases. This noise-free current $\bar{i}$ is computed at 0.1-s intervals and each such value is summed with random normally-distributed noise having zero mean and standard deviation s_i given by $1.0 \times 10^{-5} + 0.010|i|$ (in ampères), which is a typical electrolysis noise function as reported by Shia and Meites [10]. Trapezoidal numerical integration is used and the noisy instantaneous current values are integrated over 1.0-s intervals yielding instantaneous charge accumulation data. The instantaneous charge is then processed by the predictive algorithm in the same manner as the seven electrolyses described above. Figure 3 is a log i vs. t plot of these synthetic data after time-averaging over 1.0-s intervals. With data-processing parameter settings similar to those described for the copper(II) electrolysis, the algorithm calculates a sequence of group means $\bar{e}'$ as shown in Fig. 4 and selects groups 5—10, as bracketed, for a 97-s interval of ideal behavior. The first recorded point in group 5 is 60 s, at which time a charge of Q_i = 0.303 C has accumulated. Then the Guggenheim line in stage II computes Q_2 = 0.504 C, and in stage III the slope of the line yields a background current of 32 μA, which contributes 0.002 C to Q_i. The end-point integral predicted at 157 s into the run is 0.805 ± 0.010 C, which compares to the known true value 0.800 C.

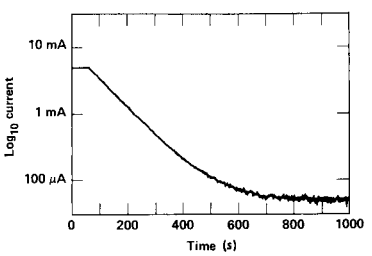

Fig. 3. Synthesized electrolysis current trace on log i vs. t coordinates.

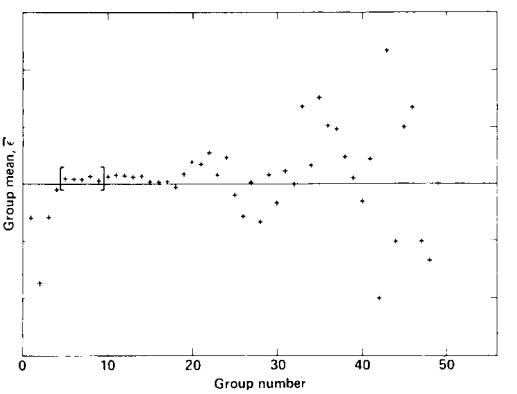

Fig. 4. Sequence of group means computed for the synthetic electrolysis data shown in Fig. 3. Brackets enclose the first 97 s of ideal behavior as detected by the algorithm.

CONCLUSIONS

It has been demonstrated that the first-order kinetic linearization technique can be utilized to predict the end-point integrals of controlled-potential coulometry with an accuracy and precision comparable to that obtainable in conventional coulometry. The technique is unaffected by transient departures of the current from first-order behavior during the initial stages of the electrolysis, provided that a region of ideal behavior of reasonable duration exists thereafter. The linearization technique yields an accuracy approaching that of conventional coulometry in about a third of the normal electrolysis time. The performance is similar to that of the method of Stephens et al. [2], when background currents are relatively low. However, because the method also automatically estimates and corrects for significant levels of continuous faradaic background current, the method is capable of greater utility and accuracy than conventional or previous methods of predictive coulometry when these background currents are relatively high. Efforts are now underway to interface coulometry instrumentation with a microcomputer to evaluate the predictive coulometry technique in real time.

This work was done in part at the Lawrence Livermore National Laboratory under the auspices of the U.S. Department of Energy under contract number W-7405-ENG-48.

REFERENCES

1 J. E. Harrar, in A. J. Bard (Ed.), Electroanalytical Chemistry, Vol. 8, M. Dekker, New York, 1975, Ch. 1.
2 F. B. Stephens, F. Jakob, L. P. Rigdon and J. E. Harrar, Anal. Chem., 42 (1970) 764.
3 L. Meites, Anal. Chem., 31 (1959) 1285.
4 C. L. Fellers and P. W. Seabaugh, Nucl. Instrum. Methods, 163 (1979) 499.
5 M. K. Holland, J. R. Weiss and C. E. Pietri, Anal. Chem., 50 (1978) 236.
6 T. A. Brubaker, R. Tracy and C. L. Pomernacki, Anal. Chem., 50 (1978) 1017A.
7 A. van den Bos, J. Phys. E, 10 (1977) 753.
8 G. R. Williams, L. M. Tolbert and F. J. Holler, Anal. Chem., 54 (1982) 256.
9 T. Meites and L. Meites, Talanta, 19 (1972) 1131.
10 G. A. Shia and L. Meites, J. Electroanal. Chem., 87 (1978) 369.
11 L. Meites, in E. Pungor and I. Buzas (Eds.), Coulometric Analysis, Akademia Kiado, Budapest, 1979, pp. 113—122.
12 L. M. Schwartz, Anal. Chem., 53 (1981) 206.
13 G. L. Booman, W. B. Holbrook and J. E. Rein, Anal. Chem., 29 (1957) 219.
14 G. W. C. Milner, A. J. Wood, G. Phillips and G. J. Weldrick, Fresenius Z. Anal. Chem., 224 (1967) 346.
15 L. P. Rigdon and J. E. Harrar, Anal. Chem., 43 (1971) 747.
16 W. D. Shults and P. F. Thomason, Anal. Chem., 31 (1959) 492.
17 J. E. Harrar and E. Behrin, Anal. Chem., 39 (1967) 1230.
18 J. J. Lingane, J. Am. Chem. Soc., 67 (1945) 1916.
19 O. L. Davies and P. L. Goldsmith, Statistical Methods in Research and Production, 4th edn., Oliver and Boyd, Edinburgh, 1972, Ch. 4.

Analytica Chimica Acta, 155 (1983) 79—87
Elsevier Science Publishers B.V., Amsterdam — Printed in The Netherlands

DETERMINATION OF TRACES OF WATER, HYDROXIDE, AND OXIDE IN METAL HALIDE SALTS BY COULOMETRIC KARL FISCHER TITRATION[a]

TIMOTHY R. BRUMLEVE

Anderson Physics Laboratories, Inc., 406 N. Busey Ave., Urbana, IL 61801 (U.S.A.)

(Received 18th May 1983)

SUMMARY

Coulometric Karl Fischer titrations are applied to the determination of trace quantities of oxygen- and hydrogen-containing impurities in high-purity metal halide salts such as those used in discharge lamps. The experimental setup is centered around a commercial coulometric titrator and a special inert gas/vacuum line for sample introduction. The solubilities of a number of metal halides in the reagent are evaluated, and several compounds causing interferences are identified. The technique gives useful results down to about 2 μg of water (200 ng g^{-1} for a 10-g sample), and quantifies all water from NaI/ScI_3 mixtures. Results for some typical metal halide mixtures are presented, and the effects of handling and storage on the determined water content are discussed.

Metal halide salts, particularly iodides, are used extensively as fill materials in metal halide discharge lamps. Trace amounts of oxygen- and hydrogen-containing impurities in the metal halides can have disastrous effects on the operation, reliability, and longevity of these lamps [1—3]. Accordingly, determination of the total oxygen and hydrogen contents in the metal halide is important.

The most successful techniques for quantitation of oxygen and hydrogen include reductive fusion with gas chromatographic separation [4—6] and 14-MeV neutron activation for oxygen [7]. It is also important to differentiate between molecular species such as H_2O, OH^-, H_2, O_2, oxyhalide, or oxide. In this way, sources of contamination can be identified and measures can be taken further to reduce impurity content. The most important impurity is probably water, because most metal halides used as lamp additives are exceedingly hygroscopic and sensitive to air.

The initial approach examined here was to detect H_2O/OH^- electrochemically in the molten salt during melt purification [8]. This approach, however, provides no information on subsequent contamination during handling or packaging of the material. Methods based on thermal evolution of water can

[a]Presented in part at the Third International Symposium on the Science and Technology of Light Sources, 18—21 April, 1983, Toulouse, France.

0003-2670/83/$03.00

provide high sensitivity and selectivity [9] but are totally inappropriate for the important rare earth iodides, which decompose on heating in the presence of water to give oxides or oxyiodides [10, 11].

Coulometric Karl Fischer (K.F.) titration with direct dissolution of the solid salts in the nonaqueous reagent was therefore examined. Complete details of the K.F. method are readily available [12]. This paper describes the application of the method to trace determination of water, hydroxide, and oxide in metal halide salts. The method responds to water at the 2 μg level, quantifies all water in rare earth/alkali metal iodide mixtures, and does not respond to rare earth oxides or oxyiodides. Typical results are presented for a number of rare-earth/alkali-metal iodide mixtures. Results for some selected samples are compared with results obtained with a fast neutron activation procedure.

EXPERIMENTAL

Instrumentation and materials

All results were obtained using a Mitsubishi Model CA-02 Moisture Meter (U.S. distributor, COSA Corp., Montvale, NJ). The titration reagents (Mitsubishi) were used as received.

Neutron activation (14-MeV) results were obtained from IRT Corporation, San Diego, CA.

Metal halide salts were prepared in-house. All rare earth iodides, ThI_4, FeI_2, SnI_2, InI, PbI_2, and CdI_2 were prepared from resublimed iodine and metal ($\geqslant$99.9% purity) as described previously [13]. All salts were handled under anhydrous conditions in a Vacuum Atmospheres drybox. These metal halides are of the same quality as the materials currently offered for sale for dosing of discharge lamps. The Sc_2O_3 (99.9%) and Dy_2O_3 (99.9%) were obtained from Research Chemicals, Phoenix, AZ.

Apparatus

To introduce solid hygroscopic samples into the titration cell, a special solid-sample inlet valve and an inert gas/vacuum line were constructed (Fig. 1). Vacuum was provided by a Precision Scientific Model DD-20 pump which is capable of an ultimate pressure of 0.05 torr. A trap of molecular sieve 13X was included to prevent back-streaming and internal damage to the pump. High-purity argon was dried as shown in Fig. 1 with calcium sulfate (Drierite), anhydrous magnesium perchlorate (Anhydrone), and phosphorus pentoxide. The phosphorus pentoxide was finely powdered and loosely packed, and movement of this powder served as a crude flowmeter. The water content of the gas was checked with the moisture meter by passing the gas through a small dispersion tube for 2 min at a flow rate of 500 ml min^{-1}. This drying scheme reduced the water content of the argon to below 2 $\mu g\ l^{-1}$.

The three-way stopcock shown in Fig. 1 permits either argon pressure or vacuum to be applied to the sample inlet valve. A flexible metal bellows

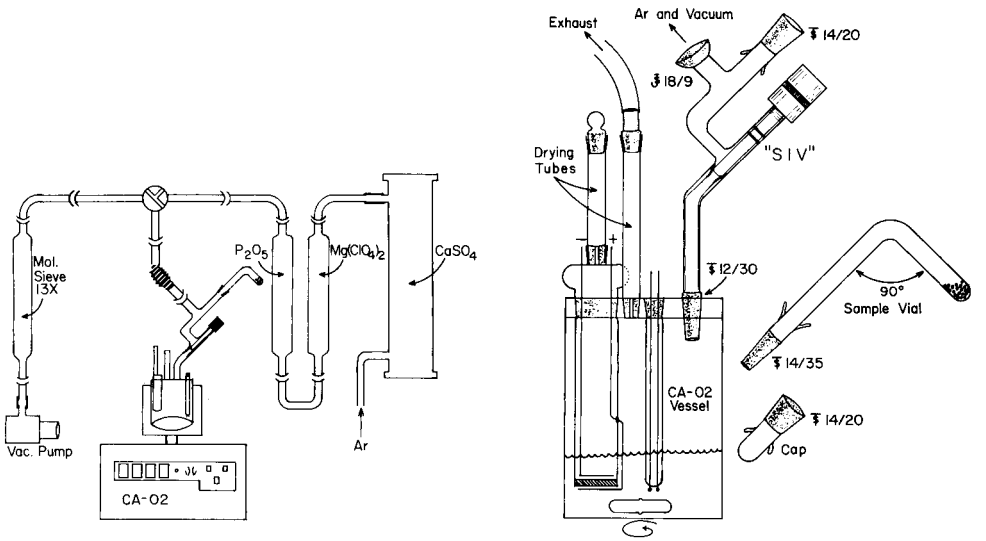

Fig. 1. Schematic diagram of the inert gas/vacuum line, sample inlet valve, and coulometric Karl Fischer titrator and cell.

Fig. 2. Detail of the sample inlet valve (SIV), sample vial and cap, and titration vessel. The inlet valve provides a vacuum-tight seal at the tip of the plunger, and dual O-rings seal the system from the outside atmosphere.

coupling (Cajon G321-8) with 18/9 ball and socket joints on each end permits easy connection to the valve assembly. The sample inlet valve (Fig. 2) is designed around a "low-holdup" valve (Kontes 826620) which seals off the titration vessel from the vacuum system and from the outside atmosphere.

Procedure

The titration cell is first filled with Mitsubishi reagents A and C (if necessary), and the instrument is turned on to pretitrate any water present in the vessel. The cleaned and dried sample inlet valve (Fig. 2) is installed with an empty vial in place with the valve securely closed. The system is evacuated for about 5 min, refilled with dry argon, and purged with a small argon flow (200—500 ml min^{-1}) until the titration current meter reads $\leqslant 1$ mA. This inlet valve is then closed.

The metal halide sample which has been loaded under argon into a capped, bent sample vial in the drybox is introduced as follows. With a positive flow of argon to the sample inlet valve, the empty vial is removed and the sample vial is quickly uncapped and placed on the assembly. Vacuum is immediately applied, and the system is pumped down to ca. 0.05 torr for 1 min. The system is refilled with argon, and the evacuation/fill cycle is repeated. The inlet valve is opened slightly, and a small amount of argon is allowed to flow through the vessel for 5—10 s. The titration current should remain below

1 mA; if it does not, the purge is continued. The argon flow is then stopped, the inlet valve is opened to the full 4-mm bore, and the sample vial is rotated 180° so that the sample falls into the vessel. (With the instrument used here, the "reset" button is pushed immediately before the sample is dropped. This sets the integrator to zero, stores the background current, and initiates the titration.) The sample inlet valve is then closed securely. It is important that no powder adhere to the glass near the teflon-glass seal because this would prevent further evacuation of the system. If this occurs, the entire assembly must be cleaned and dried for the next sample.

Some solid samples may be slow to dissolve, especially large spheres with low surface-area-to-mass ratio. In the CA-02 instrument, there is a 1-min timer internal to the instrument which may cause the titrator to signal the end-point prematurely when the H_2O/OH^- level is low (<100 μg). If this occurs, one of two procedures becomes necessary. The initial (premature) reading is recorded, and the "start" switch is turned off for 5 min or until the sample is dissolved. This stops the titration and resets the integrator, but retains the previously stored background current. The "start" switch is turned on, the titration is resumed, and the second reading is recorded. The background reading must be obtained by repeating the above procedure for the same length of "off time" after the sample has been completely dissolved (and the background current has returned to the initial value <1 mA). The initial and second readings are then totalled and the background reading is subtracted to compute total water.

Alternatively, after the initial end-point has been reached, the reading is recorded and the "start" switch is turned momentarily to off and then back to on without touching "reset". The instrument then automatically subtracts the initially-stored background current. When the next end-point has been reached, the reading is recorded, and the procedure is repeated until the sample is completely dissolved. All readings are then totalled. If very low levels are present, this procedure will require repetition every minute (set by the internal timer in the instrument). If more than two repetitions are required, this procedure may lead to "round-off" error from the digital display (±1 μg for each repetition), and the first procedure above should be used.

Subsequent samples can then be processed immediately. When the Mitsubishi A reagent is saturated with metal halide salts, it becomes very cloudy and must be renewed.

Recovery study

Known amounts of water were added to metal halide reference materials as follows. Bent sample vials were loaded in the drybox and capped with rubber septum closures. Argon saturated with water vapor at ambient temperature (18 ± 1°C) was drawn into a syringe with a 10-cm needle. The dry argon in the vials was slowly displaced with the contents of the syringe, and the samples were allowed to equilibrate with the wet argon for 1.5 h. The amount of water added was calculated from the temperature, barometric pressure, and the known vapor pressure of water.

RESULTS AND DISCUSSION

Solubility

Initially, the solubility of various metal iodides and bromides (particularly those used in discharge lamps) was studied. The coulometric Karl Fischer results for water in a number of metal halides soluble in the reagent, such as CdI_2, CsBr, FeI_2, LiI, NaI, ScI_3 and ThI_4, were found to vary from zero (CsI) to 6880 (unpurified NaI) $\mu g\ g^{-1}$. The K.F. reagent became quite turbid after about 10—12 g of NaI had been dissolved in about 100 ml of reagent; the reagent was always renewed at this point. The other iodides examined appear to have similar solubility limits. The sole bromide salt examined (CsBr) showed markedly lower solubility (<2 g/100 ml), but the determination was still easily done. Some preliminary results on chloride salts indicated even lower solubilities in the K.F. reagent.

Silver iodide and lead iodide were completely insoluble in the reagent; mercury(II) iodide dissolved quite readily, but a white crystalline precipitate appeared in the reagent after 24 h.

The dissolution rate of the metal iodides is dependent primarily on surface area-to-mass ratio of the spherical particles, and to some extent on the amount of iodide salt previously dissolved in the reagent. For example, 0.24 mm NaI spheres (60 $cm^2\ g^{-1}$) typically dissolved in 1—2 min, but larger spheres (1.8 mm, 10 $cm^2\ g^{-1}$) required 8—15 min. Because of the long dissolution times involved, the first of the titration procedures noted above was used for the results reported here.

Interferences

Three compounds used as lamp additives (TlI, SnI_2, and InI) were found to cause significant positive interferences in quantified H_2O content. In all three cases, the interfering reaction is caused by oxidation of the metal ion by the iodine generated in the K.F. titration. Because these are all two-electron oxidations, one mole of interfering salt appears as 1 mole of water in the titration. The theoretical values for these salts calculated on this basis agree quite well with the experimental data. Free halogens also interfere and act to decrease the apparent water content.

Reproducibility and detection limit

The reproducibility and detection limit of the technique were found to be primarily limited by the digital readout of the instrument ($\pm 1\ \mu g\ H_2O$). A more meaningful statistical test of the precision was made by pooling the standard deviation for all determinations made at low levels (less than 50 μg of water). Included were 15 separate materials involving 33 separate measurements, and the final pooled standard deviation was found to be 1 μg which was taken as a good approximation to the true standard deviation for the method [14]. For samples yielding results over 50 μg of water, it is estimated that the major error involved in the determination is weighing error, for which the standard deviation is estimated to be about 0.025 g.

The detection limit for this method can then be estimated in the usual fashion as twice the standard deviation of the background. The detection limit is thus reported as 2 μg, or for a 10-g sample (the maximum capacity of the sample vials) it is equal to 200 ng g^{-1}.

Dynamic range

One of the greatest advantages of the coulometric K.F. method is the dynamic range of the instrument, which allows determinations from as low as 1 μg up to 10 mg without changing scales or instrument settings. Data were obtained over the wide range of 0.7—6880 μg g^{-1} for sodium iodide, proving the utility of the technique in checking the purification and handling of sodium iodide. Before purification, reagent-grade sodium iodide showed a water concentration of about 0.7%. When outgassed, molten, and filtered only, the level dropped to 7 μg g^{-1}, probably because of residual sodium hydroxide to which the method also responds (see below). This was 10-fold higher than the average level of 0.7 μg g^{-1} for properly purified sodium iodide. Mishandling of the material is easily detected by the method; a purified sample stored in a polycarbonate vial in a drybox for 72 h had a water content of 25 μg g^{-1}. The use of plastic apparatus in the handling and storage of these materials is clearly not to be recommended.

Response to other oxygen- and hydrogen-containing species

It is well-established that the Karl Fischer method responds quantitatively to water in metal halides and in a wide variety of other inorganic matrices [12]. It is also well-established that metal hydroxides (e.g., sodium hydroxide) respond quantitatively [12]. The oxides show a wider range of behavior, the oxides of electropositive metals (e.g., Na_2O, MgO, CaO, etc.) reacting quantitatively [12]. The oxides of Cu(I), Zn(II), Ag(I), Hg(II), and Fe(III) are also readily converted [12]. Oxides that do not undergo reaction with the reagent include CuO and Al_2O_3. Some oxides such as NiO and PbO react, but not quantitatively [12]. Thus, of the compounds considered here, the oxides of Cd(II), Cs(I), Fe(III), Hg(II), Li(I), and Na(I) will show a response, and such oxide contamination (if present) will appear as apparent water.

The responses of the oxides of the rare earths have not been treated in the literature, although by analogy with Al_2O_3, one would expect no reaction. This was verified by direct addition of both Sc_2O_3 and Dy_2O_3 to the titration vessel in the usual fashion. Neither oxide showed a response, and both were totally insoluble in the reagent.

The oxyhalides are also well-known impurities in rare earth halides [10]. Oxyiodides were prepared by dissolving the pure rare earth trioxide in an excess of aqueous hydroiodic acid and dehydrating under vacuum at 1000°C; ScOI could not be prepared by this method [11]. However, DyOI was readily prepared (Dy found = 51.0%; theory 53.2%). It was found that DyOI was totally insoluble in the K.F. reagent and the compound yielded no response in the titration. Thus in the case of rare earth iodides, the procedure

appears to be selective for H_2O and OH^- with no response to oxides or oxyiodides.

Stability, recovery, and comparison of methods

The stability and recovery studies and the activation analysis were conducted on samples of NaI/ScI_3 mixture 347-28 which was used as reference material. In the stability study, the background water content was first established, and triplicate measurements on three 1-g samples yielded 22, 21, and 18 $\mu g\ g^{-1}$ water. After 24 h of storage in a sealed, bent sample vial on the bench, a fourth sample yielded 17 $\mu g\ g^{-1}$ water. After a 1.5-h exposure to the argon atmosphere of the drybox, a fifth sample yielded 20 $\mu g\ g^{-1}$. A sixth sample stored in a sealed pyrex ampoule for 4 months yielded 19 $\mu g\ g^{-1}$ water. The average of these 6 results yielded an average value of 19.5 $\mu g\ g^{-1}$ water. Thus, with appropriate handling, the material is quite stable.

Two additional samples were reserved for the recovery study, and were intentionally contaminated with known amounts of water. This was done to verify the quantitative nature of the method and to establish that irreversible reactions of the sort:

$$REI_3 + H_2O \rightarrow REOI + 2HI \quad (1)$$

$$2REI_3 + 3H_2O \rightarrow RE_2O_3 + 6HI \quad (2)$$

(RE = rare earth) do not occur at ambient temperature. For these samples, 90 μg of water was recovered when 82 μg was added, and 167 μg was recovered from a 164 μg addition, indicating quantitative recovery within the limits of experimental error.

Two samples of reference material 347-28 were also submitted for quantitation of oxygen via fast 14-MeV neutron activation. The results were 79 ± 12 and 88 ± 12 $\mu g\ g^{-1}$ oxygen (average 84 $\mu g\ g^{-1}$). If this contamination were all present as water, it would correspond to 95 $\mu g\ g^{-1}$ water, which is considerably higher than the value of 19.5 $\mu g\ g^{-1}$ found above from the K.F. titration. It must be concluded that there are other oxygen-containing species in the material (e.g., rare earth oxide or oxyhalide, or conceivably trace amounts of oxyanions such as silicate, iodate, sulfate, phosphate, or nitrate). No attempt has been made so far to quantify any of these species.

Typical results

Results for a variety of pure salts are available and will be supplied to interested readers. Results for purified NaI indicated that the water levels are at or near the detection limit in most cases.

Results for some mixtures are given in Table 1. In the case of mixtures of NaI and ScI_3 levels are higher, ranging from 9 to 145 $\mu g\ g^{-1}$. Clearly the addition of ScI_3 to NaI has a significant effect on the measured water content. For the 14 different samples of NaI/ScI_3 there is a weak correlation (r_1 = 0.29) between water content and ScI_3 concentration. The small negative

TABLE 1

Water content of some metal halide salt mixtures

Mixture	Water found ($\mu g\ g^{-1}$)			Correlation coefficient[a]	
	Mean	Low	High	r_1	r_2
(NaI)	0.7	0	2		
NaI/ScI_3[b]	47	9	145	0.29	−0.06
$NaI/ScI_3/ThI_4$[c]	64	24	118	0.46	0.63
MI/LnI_3[d]	132	29	279	—	—

[a] r_1 is the correlation coefficient for the concentration of water vs. $\%ScI_3$ or ThI_4; r_2 is the correlation coefficient for a plot of water vs. $m^{-1/3}$ where m is the mass per spherical pellet. [b] Range in ScI_3 was 10—50%; range in pellet mass was 0.2—10 mg; 14 samples. [c] Range in ThI_4 was 2—5% with 10% ScI_3; range in pellet mass was 0.2—10 mg; 10 samples. [d] M = Li, Na, Cs; Ln = Ce, Dy, Ho, Tm; range in LnI_3 was 33—80%; range in pellet mass was 0.5—2.0 mg; 12 samples.

value of r_2 is a bit puzzling, and indicates that water is not being picked up during handling or packaging.

The results for mixtures of NaI, ScI_3, and ThI_4 indicate a higher average water level of 64 $\mu g\ g^{-1}$. The ScI_3 content of all 10 samples was approximately equal. The correlation coefficient (r_1 = 0.46) in this case is that for the regression of water content versus $\%ThI_4$. This is consistent with the high water content (500 $\mu g\ g^{-1}$) of pure ThI_4. The high value of r_2 = 0.63 is also consistent with water contamination during packaging and handling.

Table 1 also contains results for the water content of some typical lanthanide iodide/alkali metal iodide mixtures. The range of compounds, compositions, and particle sizes considered was much too varied to establish any correlations with water content. It if of interest that the higher values reported may reflect the added difficulty in preparing ultra-dry lanthanide metal iodides.

The author thanks Scott Anderson for helpful discussions, Jim Schoolenberg and Harold Rodehaver for sample preparation, and Vernon Lewis for construction of glassware.

REFERENCES

1 J. F. Waymouth, Electric Discharge Lamps, MIT Press, Cambridge, MA, 1971, pp. 1—10, 260—278.
2 D. M. Speros, R. M. Caldwell and W. E. Smyser, High Temp. Sci., 4 (1972) 99.
3 P. C. Drop, J. J. De Groot, A. G. Jack and G. C. J. Rouweler, Light. Res. Technol., 6 (1974) 212.
4 P. Wiedijk, Anal. Chim. Acta, 81 (1976) 105.
5 L. Bruninx-Poesen and G. Solleveld, Paper presented at Second Int. Symp. Incoherent Light Sources, Enschede, 1979.

6 W. E. Dallman, in F. D. Snell and L. S. Ettre (Eds.), Encyclopedia of Industrial Chemical Analyses, Vol. 8, Wiley-Interscience, New York, 1968, pp. 613—693.
7 S. S. Nargolwalla and E. P. Przbylowicz, Activation Analysis with Neutron Generators, Wiley, New York, 1973.
8 H. A. Laitinen, W. Ferguson and R. Osteryoung, J. Electrochem. Soc., 104 (1957) 516.
9 J. Mitchell, Jr. and D. M. Smith, Aquametry, Part I, Wiley-Interscience, New York, 1977.
10 M. D. Taylor and C. P. Carter, J. Inorg. Nucl. Chem., 24 (1962) 387.
11 F. A. Cotton and G. W. Wilkinson, Advanced Inorganic Chemistry, 2nd edn., Interscience, New York, 1966, p. 1061.
12 J. Mitchell, Jr. and D. M. Smith, Aquametry, Part III, Wiley-Interscience, New York, 1980.
13 S. Anderson and R. B. Page, J. Light Vis. Environ., 5 (1981) 1.
14 D. A. Skoog and D. M. West, Analytical Chemistry, 2nd edn., Holt, Reinhart, and Winston, New York, 1974, p. 40.

Analytica Chimica Acta, 155 (1983) 89—102
Elsevier Science Publishers B.V., Amsterdam — Printed in The Netherlands

EXPERIMENTAL OPTIMIZATION PROCEDURES IN THE DETERMINATION OF PHOSPHATE BY FLOW-INJECTION ANALYSIS

T. A. H. M. JANSE*, P. F. A. VAN DER WIEL and G. KATEMAN

Department of Analytical Chemistry, Faculty of Sciences, University of Nijmegen, Toernooiveld, 6525 ED Nijmegen (The Netherlands)

(Received 14th June 1983)

SUMMARY

Flow injection analysis is attractive for handling large numbers of similar samples on a routine basis. In order to develop a procedure with a well defined performance in a relatively short time, application of experimental optimization procedures is useful. The two procedures evaluated are factorial design and simplex optimization. Criteria on the performance of a particular analytical method are formulated in terms of signal height, peak width, baseline noise and linearity of the calibration graph. As a demonstration of the general approach, the determination of phosphate in aqueous solution is discussed; the flow rates of the water carrier stream and the reagent streams, the injection volume and the lengths of coils are the parameters applied for optimization of the procedure.

In routine analytical practice, flow injection analysis (f.i.a.) is attractive because of the readily available low-cost instrumentation, the high sampling rate, fast response, reproducible and accurate results, and low detection limits. In the case study presented here, the latter was of particular interest. A reliable and stable procedure was required for the determination of inorganic phosphate in the concentration range 0.05—2 mg l^{-1}, such as is found in surface waters. The development of an optimal instrumental configuration may take considerable effort, because the influence of the various parameters is only partly predictable [1, 2]. In order to find a satisfactory configuration in a relatively short time, and to achieve better insight into the influence of different parameters, experimental optimization procedures are useful. Very little has been published on optimization procedures for f.i.a. itself although such procedures have been applied to the detection method [3] and to continuous flow analyzers [4]. The influence of the most important factors (injection volume, flow rate, coil length) has been investigated merely from a theoretical point of view. But complex interaction effects are to be expected; for example, dispersion is a complex function of flow rates, diameters, coil lengths, mixing devices, injection volume, etc. These interactions must be included in the development of an optimal analytical design.

0003-2670/83/$03.00

The application of experimental optimization procedures makes it possible to establish an optimal configuration for a particular purpose with a reduced number of experiments. The results of two different optimization procedures are described: factorial design experiments for some discrete factors, and simplex optimization for continuous factors.

EXPERIMENTAL

A commercially available f.i.a. instrument (Model 5005; BIFOK, Sweden) was used, with a sample injection valve, a flow system with replaceable units, and a photometric detection system consisting of an 18-μl flow-through cell with amplifier (Fig. 1). Solvents were pumped by three pumps (one Ismatec, and two Gilson Minipuls peristaltic pumps) for separate flow variation. Signals were recorded and processed by a HP-9820A desktop calculator.

The phosphate was determined by the heteropolymolybdenum blue method. After injection of the sample into a water stream, a yellow complex is formed with ammonium heptamolybdate in acidic medium. Upon reduction with a second reagent (ascorbic acid or tin(II) chloride) the molybdenum blue heteropoly complex is formed. The absorbance was measured at 670 nm. This is a modification of the widely-used flow-injection method for phosphate [1].

PERFORMANCE CRITERIA

In order to optimize a system, a performance criterion must be selected, i.e., in terms of optimization, a definition of response is needed. Various different definitions of response might be considered; a well-defined response function should fulfil the following requirements. First, it indicates whether a system functions "better" or "best", with respect to the desired goal, e.g., minimal detection limit, minimal variance of the analytical results, maximal

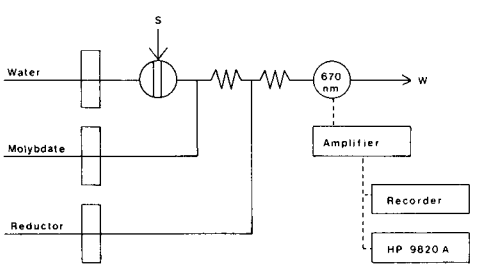

Fig. 1. Experimental configuration used in all experiments.

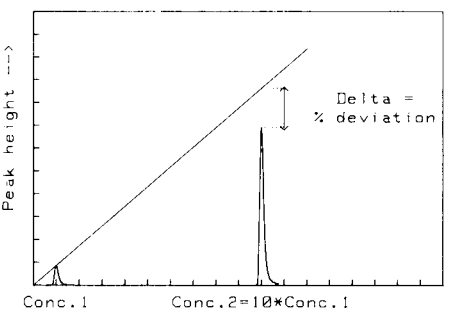

Fig. 2. Definition of delta-% used as a measure of linearity of the calibration graph.

linear working range. Secondly, it must be based on reliable and reproducible measurements. Sequential optimization procedures (e.g., simplex optimization) are affected particularly by drift, irregularities (shot noise), coloured noise and high noise levels in general. Thirdly, the response function must be measureable in a relatively short time. In order to prevent day-to-day effects, the criterion selected for this f.i.a. optimization was that measurements for one simplex optimization or one experimental design could be finished in one day.

Some response definitions considered for the f.i.a. system were as follows.

Maximization of peak height. On the assumption that calibration graphs pass through the origin, sensitivity is optimized.

Minimization of peak width. Minimization of dispersion permits more frequent injections, resulting in higher sample throughput.

Maximization of signal-to-noise ratio. Here optimization is aimed at accuracy. In order to obtain an accurate estimation of the standard deviation of the signal, a series of signals must be recorded. This requirement conflicts with the third requirement mentioned above. When the noise variance is considered to be equal to the baseline variance (for low sample concentrations), the detection limit is optimized. However, this requires an estimate of the baseline variance; unfortunately, a f.i.a. baseline often originates from a non-stationary process (e.g., drift, fluctuations in the pumps, spikes, etc.). Consequently, it takes some time to acquire a reliable estimate of this baseline variance. In unstable configurations (e.g., bad adjustment of the parameters), this response function operates rather well as a criterion for reliability, but it is poorly reproducible.

Maximization of the correlation coefficient of the calibration graph. This response function is a good criterion for linearity and residual variance. An optimal range can be selected by suitable choice of standards, but the number of standards must be dramatically increased to obtain a reliable estimate of the correlation coefficient, and again the third requirement is not met. An easier and less time-consuming, though less accurate, method of establishing linearity in a certain range, is simply to inject two sample concentrations. The regression is input from the first injection (as standard) and the response function involves minimization of the percentage deviation of the second injection from the calibration graph (see Fig. 2). Of course, it is essential that the calibration graph passes through the origin.

In most optimization procedures, several criteria should be combined in one response function. In the present work, a flow-injection method was required for the accurate determination of inorganic phosphate in natural waters. Analytically, this translated into a limit of determination of 0.05 mg l^{-1} phosphorus (as phosphate), a linear calibration graph from 0.0 to 2.0 mg l^{-1} P, with a sample injection rate as high as possible, a reagent consumption as low as possible, and of course with reliable and reproducible results.

If the calibration graph passes through the origin, the variance of the estimated results can be related [5] to the standard signal according to

the equation

$$\mathrm{Var}(C_{\hat{x}}) = \mathrm{Var}(y)\, C_s[(1/\hat{y}_s^2) + (\hat{y}_x^2/\hat{y}_s^4)]$$

where $\mathrm{Var}(y)$ is the variance of the signal (assumed to be independent of concentration, or equal to baseline variance), C_s is the concentration of the standard, $\hat{y}_s$ is the signal of the standard, and $\hat{y}_x$ is the signal of the unknown sample. Minimization of $\mathrm{Var}(y)/\hat{y}_s^2$ will provide the lowest variance in the final results; this normally corresponds to maximum peak heights, minimal detection limit and maximal sensitivity. Combination with the requirement of maximal sample rate (small peak widths) results in minimizing the response function peak width $*$ $\mathrm{Var}(y)/\hat{y}_s^2$.

However, as mentioned above, reliable estimations of the variance could not be obtained quickly. Therefore in the sequential optimization procedure the response used is peak width/(peak height^2). An advantage of the simultaneous optimization procedure is that one collects different responses at one time; the results do not influence the experimental design. The computations are done afterwards, and the interpretation might include a combination of optimal settings for different responses.

OPTIMIZATION PARAMETERS AND PROCEDURES

Table 1 shows the most important parameters that might affect the performance of the system. To obtain an optimal configuration and adjustment of the instrument for this analysis, all parameters could be studied in all combinations. This would mean, with n parameters on m levels, that m^n experiments would be needed. Various plans may be used, in order to reduce this to a feasible number of experiments.

First, the simplest and most frequently used plan is sequential stepwise optimization; for every parameter the optimal adjustment is selected by separate studies. As long as the influence of one parameter on the optimal adjustment of the others is not too large, this procedure functions quite well. However, if these interactions are not negligible, it is necessary to obtain the optimal adjustment of all parameters once, and then start again from the beginning. The number of experiments increases quickly, and optimizing in this way is a very unfortunate choice.

A far more economic sequential optimization procedure in such cases is the simplex method: every single experiment consists of a re-adjustment of all parameters towards an optimal configuration. Several simplex optimization procedures have been described in the literature [6, 7]. In the present paper, the super-modified simplex procedure (SMS) is applied for the three continuous flow parameters (Table 1). The procedure has been described in detail [8], and is used with a second-order fit between rejected, reflected and (estimated) reflection points. Boundary rules are incorporated in the software, as well as the $(N + 1)$ rule. A severe limitation of the simplex method is that all parameters must be continuously

TABLE 1

Optimization factors investigated, with the chosen levels (for discrete adjustable parameters) or ranges (for continuous adjustable parameters)

Factor	Adjustable	Levels/Range
Injection volume	discrete	30, 100, 200, 300 μl
Tube diameter (incl. coils)	discrete	0.5, 0.8 mm
Maximum pumping rate[a]	discrete	
for the water flow		1.6, 3, 4, 9.5, 15 ml min^{-1}
for the molybdate flow		1.6, 0.8, 0.5 ml min^{-1}
for the reductor flow		0.8, 0.5 ml min^{-1}
First coil length	discrete	40, 70, 100 cm
Second coil length	discrete	0, 40, 70 cm
Concentration molybdate	discrete	5, 7 g l^{-1}
Concentration reductor	discrete	2.5, 5 mM
Concentration acid		Only 0.6 M
Pumping rate : water stream	continuous	40—100% of max. flow
molybdate	continuous	10—100% of max. flow
reductor	continuous	10—100% of max. flow
Temperature	continuous	Only room temperature

[a]By choice of peristaltic pump tubing.

adjustable. For discrete adjustable parameters (from nature, or levelled for practical reasons, see Table 1), another plan must be chosen.

A completely different scheme of experimentation is obtained by using one of the simultaneous optimization procedures; a systematic approach results in a factorial design. However, a complete factorial design for the mentioned variables, on only two levels, leads to 2^{14} experiments. This number can be reduced rapidly by ignoring higher-order interaction effects and by splitting this design into different smaller designs, in a logical way. A thorough description of the application of factorial designs has been given by Box et al. [9]. The advantage of using this optimization technique is not only its ability to select the optimal response from the design, but also to achieve better understanding in the influence of the factors for the particular reaction. Effects can be estimated, arranged in order of importance, and tested for significance.

In f.i.a., indications for improvement of the method can be found in the dispersion rules [1]. Hereafter, optimal reaction conditions must be selected. Because the resulting response functions are complex, certain actions can have completely reversed effects when other parameter levels are changed. In a factorial design, this results in significant interaction effects.

If this optimization technique is applied before a simplex optimization, a rough improvement is obtained for the discrete adjustable parameters, and then the continuously adjustable settings can be refined by applying the simplex method.

RESULTS

Ascorbic acid as reductor

This method was studied with the basic configuration of Růžička and Stewart [10]. Apart from some higher reagent concentrations, only optimization to flows was investigated by the simplex method. As an example, a two-dimensional response surface is shown in Fig. 3A. It was necessary to rinse the system with 0.1 M NaOH, every time the $N + 1$ rule was applied. In Fig. 3B, the course of the simplex on the mentioned response surface is shown: the optimization procedure works but the real optimum is not reached in a limited number of experiments because of standard error in the response measurement of about 5%, an almost plain area in the surface, and a restricted mobility from the simplex after several consecutive expansions in one direction. Theoretical improvements in the simplex procedure might be considered at this point. Further optimization of this method for phosphate determination was not attempted because this reaction is not suitable for the lower concentrations, mainly because of the slowness of the reduction step. However, in the range above 1 mg l^{-1} phosphorus, this method is reliable, has perfect linear calibration graphs and a standard error of estimate of about 0.05 mg l^{-1} phosphorus.

Ascorbic acid as reductor, with potassium antimonyl tartrate as catalyst

Addition of a catalyst to the ascorbic acid solution greatly improves the sensitivity of the phosphate determination [11]. In Fig. 4, some signals are shown, all recorded on the same scale. Optimization of this method was very difficult: depending on the selection of the parameter settings, un-

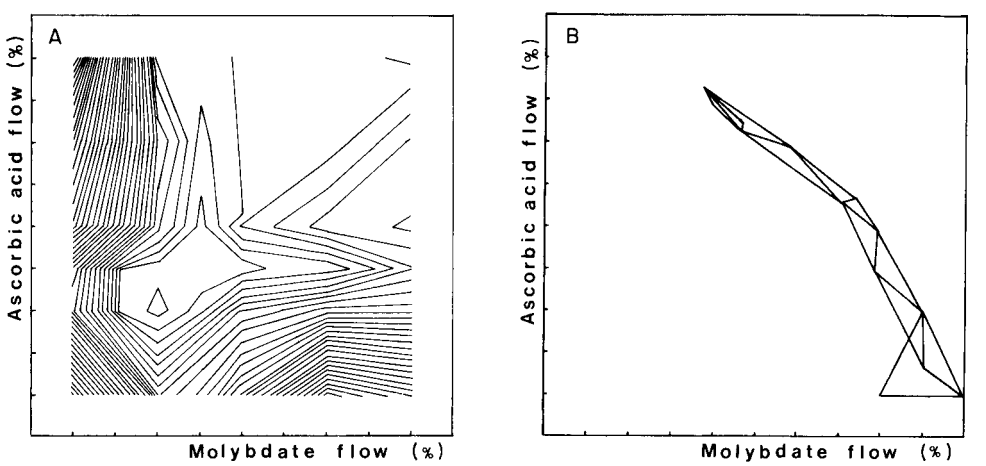

Fig. 3. (A) Two-dimensional response surface obtained by drawing equi-response lines (by linear interpolation) between measured points; the response function is peak width/(peak height^2). (B) Simplex optimization, under the same conditions as Fig. 3A.

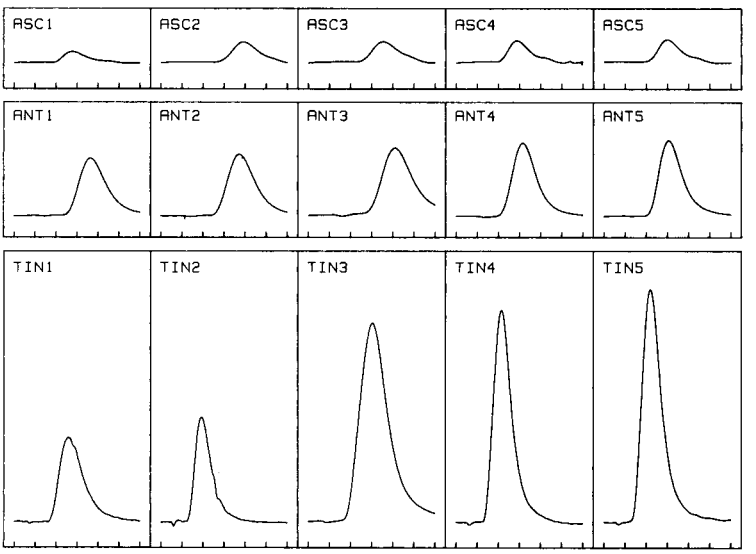

Fig. 4. Signals for 1 mg l^{-1} P solutions under various conditions. Top row, ascorbic acid as reductor; centre row, antimonyl tartrate as catalyst; bottom row, $SnCl_2$ as reductor.

stable configurations could be obtained giving relatively large drift, pump pulsation effects or poor peak-height reproducibilities. In such cases, it is hardly possible to use one of the more sophisticated optimization procedures. A stepwise approach is advisable, and so the number of experiments required to achieve optimal adjustment increases quickly. Over 60 experiments were needed to obtain the best reagent concentrations and coil lengths with respect to optimal sensitivity (peak height) and satisfactory stability (baseline variance). By recording a response surface (for peak heights), the flows were readjusted. In this way, "optimal" conditions for this method outlined in Table 2 were established.

Tin(II) chloride as reductor

In preliminary investigations, it was noticed that the sensitivity of the method was improved considerably when tin(II) chloride was used as the

TABLE 2

Best configuration obtained for potassium antimonyl tartrate as catalyst for reduction with ascorbic acid

Injection volume	30 µl	Flow rates (ml min^{-1})[a]	
Coil 1	0.7 m	Water	2.10
Coil 2	1.2 m	Molybdate	0.40
Tube diameter	0.8 mm	Ascorbic acid	1.0
		Catalyst	0.32

[a]Concentrations: 8 g l^{-1} molybdate, 12 g l^{-1} ascorbic acid, 1.8 g l^{-1} potassium antimonyl tartrate.

TABLE 3

A saturated factorial design, or "main effect plan"[a]

F1	L2	L1	F2	F3	C1	C2	PH	PW	PW/(PH²)
—	—	—	+	+	+	—	2.23	11.7	2.35
+	—	—	+	—	—	+	3.06	7.7	0.82
—	+	—	—	+	—	+	2.01	14.4	3.56
+	+	—	—	—	+	—	2.36	9.9	1.78
—	—	+	—	—	+	+	1.84	11.6	3.43
+	—	+	—	+	—	—	1.96	10.0	2.60
—	+	+	+	—	—	—	1.29	15.7	9.43
+	+	+	+	+	+	+	1.89	11.5	3.22

Factors

Abb.		Units	Levels		Main effects		
			+	—	PH	PW	PW/(PH²)
F1	Max. main flow	ml min^{-1}	3.0	2.1	0.48	−3.6	−2.59
L2	Coil 2 length	m	1.0	0.4	−0.39	2.6	2.20
L1	Coil 1 length	m	1.0	0.4	−0.67	1.3	2.54
F2	Max. flow molybd.	ml min^{-1}	1.2	0.8	0.08	0.2	1.11
F3	Max. flow $SnCl_2$	ml min^{-1}	1.2	0.8	−0.12	0.7	−0.93
C1	Conc. molybd.	g l^{-1}	7.0	5.0	0.00	−0.8	−1.41
C2	Conc. $SnCl_2$	g l^{-1}	0.8	0.4	0.24	−0.5	−1.28

[a]PH, peak height; PW, peak width.

reductant [11]. The main difficulty encountered was drift in the baseline, caused by the instability of the tin(II) chloride solution. This was solved by addition of hydrazinium sulphate as a stabilizer [12]. It is clearly shown in Fig. 4 that chemical optimization in this way is of utmost importance, and that no optimization procedure can counterbalance such fundamental improvements. In order to achieve the optimization with as few experiments as possible, the following plan was followed. First, a preliminary search was made by means of some saturated designs, to rank variables to importance. Then by considering high and low levels for the parameters, successive designs were set up. Finally, with the best settings for the discrete parameters, a simplex optimization procedure was applied for the three flows.

An example of a saturated design is given in Table 3. Care should be taken with such 2^{7-4} designs: main effects cannot be distinguished from interaction effects. The advantage is the minimal number of experiments, 8 experiments for 7 factors. Although no test criteria are present, a few conclusions can be drawn from this plan for establishing main effects. Thus a shorter length for coil 1 is favourable with respect to peak height, and a high flow rate for the water carrier stream is favourable, particularly with respect to peak width. Other saturated designs indicated that a smaller inner diameter for the connecting and coil tubing was very unfavourable, as

TABLE 4

Fractional factorial design[a]

IV	F1	F3	C2	L2	PW/(PH²) Injected: 0.10 ppm P	PW/(PH²) 2.0 ppm P	Delta (%)
—	—	—	—	+	1378	3.29	—1
+	—	—	—	—	458	1.42	—10
—	+	—	—	—	595	1.90	—19
+	+	—	—	+	201	1.71	—44
—	—	+	—	—	1190	3.25	—4
+	—	+	—	+	599	1.47	3
—	+	+	—	+	627	1.60	—3
+	+	+	—	—	286	0.80	—13
—	—	—	+	—	1007	2.51	2
+	—	—	+	+	355	1.00	—8
—	+	—	+	+	452	1.30	—14
+	+	—	+	—	186	0.58	—18
—	—	+	+	+	1468	3.10	6
+	—	+	+	—	389	1.08	—6
—	+	+	+	—	571	1.47	—7
+	+	+	+	+	181	0.56	—4

Factors

IV	Injection volume	Levels:	(—)	100	(+)	200 µl
F1	Main water flow	Levels:	(—)	1.6	(+)	3.0 ml min^{-1}
F3	$SnCl_2$ flow	Levels:	(—)	0.5	(+)	0.8 ml min^{-1}
C2	$SnCl_2$ conc.	Levels:	(—)	0.5	(+)	1.0 g l^{-1}
L2	Coil 2 length	Levels:	(—)	0.4	(+)	0.7 m

Effects

	Low conc. (0.10 ppm P)			High conc. (2.0 ppm P)			Delta (%)
	PH	PW	PW/(PH²)	PH	PW	PW/(PH²)	
Mean	0.250	28.7	621	4.46	28.0	1.69	—9
St. dv. ef.	0.007	1.1	36	0.06	0.4	0.06	2
IV	⟨0.122⟩	—0.2	⟨—579⟩	⟨1.81⟩	1.0	⟨—1.22⟩	—7
F1	⟨0.067⟩	⟨—6.4⟩	⟨—468⟩	⟨0.47⟩	⟨—8.8⟩	⟨—0.90⟩	⟨—13⟩
F3	⟨—0.034⟩	—2.9	85	0.00	⟨—1.9⟩	—0.05	⟨11⟩
C2	⟨0.027⟩	0.0	—90	⟨0.83⟩	—0.3	⟨—0.48⟩	—5
L2	—0.007	—1.2	72	—0.17	0.2	0.13	2
IV × F1	0.009	—0.7	⟨231⟩	—0.11	0.3	⟨0.59⟩	—1
IV × F3	0.007	1.2	—21	⟨0.22⟩	0.4	—0.15	—5
IV × C2	0.012	—1.0	—18	⟨0.45⟩	0.7	—0.06	—2
IV × L2	—0.002	—1.2	—68	⟨0.21⟩	0.2	0.09	—3
F1 × F3	—0.011	—0.8	—27	⟨0.24⟩	—0.4	⟨—0.22⟩	7
F1 × C2	—0.001	—0.9	11	⟨0.28⟩	—0.4	—0.05	4
F1 × L2	0.006	—1.9	—117	—0.11	0.1	—0.02	—3
F3 × C2	—0.009	—1.1	67	⟨—0.34⟩	0.3	⟨0.25⟩	—4
F3 × L2	—0.006	—0.3	37	0.19	—0.1	—0.10	6
C2 × L2	—0.003	—0.6	3	0.16	—0.8	—0.05	1

[a]⟨···⟩: Highly significant effects at the $\alpha = 0.002$ level.

was doubling the molybdate concentration. Raising the temperature decreased the baseline stability and was not considered further.

After inspection of these results, the next designs were constructed: in the first design (Table 4) the tin(II) chloride parameters are gathered (concentration, flow and second coil) together with injection volume and main flow; molybdate parameters are placed in a second design (Table 5); and flow interactions are considered in the third design (Table 6). The construction and the results of the first design are shown in Table 4. In order to reduce the number of experiments, a 2^{5-1} design is used; this results in confounding of main effects with fourth-order effects, and second-order with third-order effects. The influence on peak height, peak width and linearity of the calibration graph is shown. Duplicate runs were made to obtain a reliable estimate of the variance of the effects. The linearity of the calibration graph is expressed as "delta"-percentage (Fig. 2); this is the percentage deviation of the higher concentration, by using the regression coefficient at the lower concentration for a calibration graph through the origin.

Important conclusions are as follows. The second coil has little effect on peak width and peak height, and no significant influence on the calibration graph. However, the shorter coil might be superior and was used in the further investigations. The larger injection volume and higher water flow rates gave obviously higher and narrower peaks; but the higher water flow rate also gave a significant negative effect in the "delta" response, thus indicating a shorter linear working range. This could be almost completely compensated for by a higher reductant flow rate, although the higher flow lowered the peak height somewhat; this was shown at lower concentrations by the significant F3 effect, and at higher concentrations in combination with the (favourable) higher C2 concentration, regarding the F3 × C2 effect. The interpretation of these results was facilitated by expressing the optimization criteria as a function of the variables. For example, for the delta-%:

$$D = -9 - 13/2*(\mathrm{IV}) + 11/2*(\mathrm{F1})$$

and for the $PW/(PH^2)$ response at high concentrations:

$$R = 1.69 - 1.22/2*(\mathrm{IV}) - 0.90/2*(\mathrm{F1}) - 0.48/2*(\mathrm{C2}) + 0.59/2*(\mathrm{IV}*\mathrm{F1}) - 0.22/2*(\mathrm{F1}*\mathrm{F3}) + 0.25/2*(\mathrm{F3}*\mathrm{C2})$$

In these relations the parameter descriptors stand for +1 and −1, representing the higher or the lower level.

The more significant interaction effect, IV × F1, indicates that higher injection volumes result in less improvement in the system performance at the higher F1 level; this conclusion was simply verified by some tests with 300-μl injections. Other (second or third?) interaction effects are classified as significant. These indicate clearly the complex nature of the non-linear processes in a flow-injection system. However, they all seem not very important at the chosen levels, and the conclusions drawn so far are not changed by them.

TABLE 5

Complete factorial design with molybdate parameters. Measured effects for differences between two levels[a]

Factors

F1	Main water flow	Levels:	(—)	3.0	(+)	4.0 ml min^{-1}
C1	Molybdate conc.	Levels:	(—)	5.0	(+)	7.0 g l^{-1}
F2	Molybdate flow	Levels:	(—)	0.5	(+)	0.8 ml min^{-1}

Effects

	Low conc. (0.10 ppm P)			High conc. (2.0 ppm P)			Delta (%)
	PH	PW	PW/(PH^2)	PH	PW	PW/(PH^2)	
Mean	0.40	25	162	6.39	20.8	0.52	20
St. dv. eff.	0.01	2	72	0.11	0.8	0.09	4
F1	⟨0.06⟩	—3	—67	⟨0.43⟩	⟨—3.6⟩	—0.16	—6
C1	⟨0.06⟩	—3	—64	⟨0.42⟩	0.0	—0.06	—6
F2	0.01	1	13	0.08	—1.0	—0.03	0
F1 × C1	0.01	4	31	0.13	—0.4	—0.02	—1
F1 × F2	0.02	5	16	0.17	0.7	—0.01	—2
F2 × C1	0.03	—4	—51	0.20	—0.7	—0.05	—4
F1 × C1 × F2	—0.01	0	13	—0.22	0.2	0.05	—1

[a]⟨···⟩: Significant effects at the $\alpha = 0.001$ level.

TABLE 6

Complete factorial design with flow parameters. Measured effects for differences between two levels[a]

Factors

F1	Main water flow	Levels:	(—)	3.0	(+)	4.0 ml min^{-1}
F2	Molybdate flow	Levels:	(—)	0.5	(+)	0.8 ml min^{-1}
F3	$SnCl_2$ flow	Levels:	(—)	0.5	(+)	0.8 ml min^{-1}

Effects

	Low conc. (0.10 ppm P)			High conc. (2.0 ppm P)			Delta (%)
	PH	PW	PW/(PH^2)	PH	PW	PW/(PH^2)	
Mean	0.48	25	116	6.52	21.1	0.50	29
St. dv. eff.	0.01	2	72	0.11	0.8	0.09	4
F1	⟨0.07⟩	—6	—62	0.08	⟨—5.0⟩	—0.12	—11
F2	—0.01	—2	—14	⟨0.24⟩	—1.6	—0.08	1
F3	⟨—0.07⟩	1	38	0.16	—1.8	—0.06	⟨13⟩
F1 × F2	0	2	13	0.11	0.2	—0.01	3
F1 × F3	—0.01	1	—4	⟨0.42⟩	—0.2	—0.07	2
F2 × F3	0.03	—4	—34	0.06	0.7	0.01	—5
F1 × F2 × F3	—0.01	—1	10	—0.20	0.2	0.04	2

[a]⟨···⟩: Significant effects at the $\alpha = 0.01$ level.

Two other complete factorial designs were constructed. The results are shown in the Tables 5 and 6. Briefly, the main conclusions are as follows. Table 5 again shows that increasing the water flow rate gives better results, although the effect is less at this higher level. The higher molybdate concentration is favourable with regard to peak heights. Here, no effect is measurable for the molybdate flow. By looking at the three flows in Table 6, the main conclusion from the above was confirmed: higher water flows give higher or narrower peaks, and higher tin(II) chloride flows give a wider linear range. Increasing the molybdate flow significantly improves the peak height for the higher phosphate concentration.

The simplex optimization

Further improvement with respect to flow rates is more easily investigated by applying simplex optimization. In order to avoid complications with the procedure as mentioned above, the "next-to-worst" rule was reintroduced [8]. The discrete parameters were chosen, according to the above experiments, i.e., an injection-volume of 200 μl, two short coils of 40 cm length, and the two more concentrated reagent solutions.

The parameter boundaries are established by the chosen ranges for flow rates. These are reported in Table 7, together with the results. In particular, higher water flows were investigated, as they were indicated by the previous designs. As a minimization criterion, the peak width/peak height^2 value was again used. The injected sample concentration was taken at 1 mg l^{-1} P for two reasons: to reduce the noise on the measured response, and as a compromise between the lower and higher concentrations used above. Of course, a consequence of this optimization procedure is that the effect on linearity of the calibration graph may be influenced negatively by the adjustment of the flow parameters, but the risk is decreased by this compromise. A three-dimensional simplex optimization was done twice. Both times

TABLE 7

Results of the simplex optimization procedures for optimal flow adjustment (All flows are given in ml min^{-1})[a]

Optim. No.	Dimension	Flow ranges			Optimum found		
		Water	Molybdate	$SnCl_2$	Water	Molybdate	$SnCl_2$
1	3	6—15	0.16—0.8	0.16—0.8	9.4	0.76	0.30
2	2	6—15	0.16—0.8	0.56	8.3	0.76	(0.56)
3	2	6—15	0.16—0.8	0.56	9.0	0.76	(0.56)
4	3	4—10	0.32—1.6	0.16—0.8	9.1	1.2	0.20
5	2	4—10	0.32—1.6	0.56	8.1	1.3	(0.56)
6	2	4—10	0.32—1.6	0.56	8.6	1.2	(0.56)

[a]Other parameter levels: injection volume 200 μl, coil 1 40 cm, coil 2 40 cm, molybdate solution 7 g l^{-1}, tin(II) chloride solution 1.0 g l^{-1}, tube diameter 0.5 mm, room temperature.

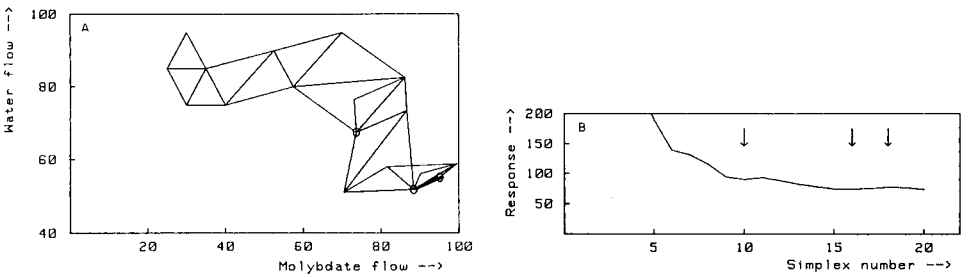

Fig. 5. Two dimensional simplex optimization with respect to the main water flow and the molybdate flow rates. (A) Course of the simplex; (B) mean response during the minimization. Circled points and arrows indicate occurrence of the $N + 1$ rule.

the procedure was stopped after about forty measurements. The results (Table 7) clearly indicate the tendency towards lower reductant flow rates, in agreement with the results from the experimental designs. The higher water flow rate resulted in a minimal response, because of higher and narrower peaks. The higher molybdate flow resulted in lower responses, mainly because of smaller peak widths. In order to maintain the widest possible linear range, the reductant flow was held constant in the other simplex optimizations. A graphical representation of a two-dimensional optimization procedure is given in Fig. 5. There is a good agreement between all results from Table 7, indicating only one "optimal" adjustment of flow rates. Of course, further improvement might be obtained by considering the discrete parameters at this point again. In fact, the results were satisfactory, with regard to the following characteristics for this flow-injection determination of inorganic phosphate: a detection limit of 0.01 mg l^{-1} P was achieved, with a limit of determination of 0.04 mg l^{-1}, a linear range from 0.04 to 2.50 mg l^{-1} P, and a speed of about 180 injections/hour.

CONCLUSIONS

From the many adjustable parameters in flow-injection analysis, it is possible to select the most significant ones by experimental design procedures, with respect to some carefully chosen optimization criteria. Despite the non-linear nature of most responses, a considerably improved configuration can be attained by a limited number of experiments. By ending the optimization scheme with the simplex optimization procedure, the original goal was reached.

Very recently, an article on the same subject appeared [13]. A very sensitive flow-injection determination of phosphate with malachite green and ammonium heptamolybdate as a complexing agent was described. Although this method has a lower limit of determination ("several ng ml^{-1}"), the reported frequency of analysis (40 h^{-1}) and the linear range (0.01—0.8 μg ml^{-1}) are comparatively poor. Of more interest is the way the parameter

settings were obtained: the classical approach used provides no "optimal adjustment", in particular because almost all interaction effects are ignored. Of course this is also an effective way of limiting the number of experiments.

Although many preliminary experiments were done in this research, the use of experimental designs, including continuously adjustable parameters, before application of the simplex optimization procedure is strongly recommended. The optimization scheme, as described above, takes only some days for experimentation. The time investment for the construction of the proper designs, combined with some additional software for the computations, virtually guarantees minimal effort in obtaining a desired configuration, wherever possible.

The authors thank Bert Doyen and Dini van de Kerkhof for their contribution to the experimental work.

REFERENCES

1 J. Růžička and E. H. Hansen, Flow Injection Analysis, Wiley, New York, 1981.
2 J. T. Vanderslice, K. K. Stewart, A. G. Rosenfeld and D. J. Higgs, Talanta, 28 (1981) 11.
3 C. Vanroelen, R. Smits, P. Van den Winkel and D. L. Massart, Fresenius Z. Anal. Chem., 280 (1976) 21.
4 See e.g., A. S. Olansky and S. N. Deming, Anal. Chim. Acta, 83 (1976) 241.
5 C. Liteanu and J. Rica, Statistical Theory and Methodology of Trace Analysis, Horwood, Chichester, 1980.
6 G. Kateman and F. W. Pijpers, Quality Control in Analytical Chemistry, Wiley, New York, 1981.
7 D. L. Massart, A. Dijkstra and L. Kaufman, Evaluation and Optimization of Laboratory Methods and Analytical Procedures, Elsevier, Amsterdam, 1978.
8 P. F. A. Van der Wiel, Anal. Chim. Acta, 122 (1980) 421.
9 G. E. P. Box, W. G. Hunter and J. S. Hunter, Statistics for Experimenters, Wiley, New York, 1978.
10 J. Růžička and J. W. B. Stewart, Anal. Chim. Acta, 79 (1975) 79.
11 J. Murphy and J. P. Riley, Anal. Chim. Acta, 27 (1962) 31.
12 I. Kolthoff, Treatise on Analytical Chemistry II, Vol. 3, Interscience, New York, 1961.
13 S. Motomizu, T. Wakimoto and K. Toei, Talanta, 30 (1983) 333.

Analytica Chimica Acta, 155 (1983) 103—111
Elsevier Science Publishers B.V., Amsterdam — Printed in The Netherlands

EVALUATION OF A SOLID-STATE PHOTODIODE-ARRAY SPECTROMETER WITH OPTICAL-FEEDBACK STABILIZATION

DAVID T. ROSSI and HARRY L. PARDUE*
Department of Chemistry, Purdue University, West Lafayette, IN 47907 (U.S.A.)
(Received 21st June 1983)

SUMMARY

An optical-feedback system is adapted for stabilization of a rapid-scanning spectrometer based on a solid-state photodiode array detector and its performance is evaluated. A beam-splitter is used to divert a fraction of source intensity to a phototransistor, the signal from which is used to control the output from a programmable power supply that controls source intensity. Any tendency for source intensity to change with time is compensated by the feedback system. The system reduces effects of short-term and long-term drift by more than an order of magnitude relative to the same system without optical feedback. Other features of the system including stray light and linearity are evaluated.

One of the significant developments in spectrometry in recent years has involved the use of imaging detectors for simultaneous monitoring of multiple wavelengths [1, 2]. To date, most applications of imaging detectors to spectrometry have involved single-beam systems that are subject to drift with time.

Earlier studies have demonstrated that the concept called "optical feedback" can be used to develop very stable single-beam photometers [3, 4]. In such systems, a portion of the light beam is diverted by a beam-splitter to a control detector that generates a signal that is used in a programmable power supply to control source intensity. Any drift in source intensity is detected and utilized to control power to the source to compensate for the drift.

A major purpose of this study was to evaluate the utility of the optical-feedback principle with a multiwavelength imaging detector. Results obtained in the visible region with a tungsten source are very encouraging. Reproducibility data for the system with feedback were more than an order of magnitude better than the system without feedback for 13.5-s, 5-min, and 1-h measurement intervals. Results with feedback compare favorably with results obtained with a commercially available double-beam system (Hewlett-Packard 8450A spectrophotometer). Several performance characteristics of the system are presented.

0003-2670/83/$03.00

EXPERIMENTAL

Instrumentation

Optical system. Figure 1 is a diagram of the optical system for the diode array spectrometer. The source housing contains a 12-V, 100-W tungsten lamp (FCR-Quartzline, General Electric Co.) and a 60-W deuterium lamp (96280, Beckman Instruments). The source housing may, optionally, be cooled by a 4-in. fan (Model 4800X, Pamotor). Separate regulated supplies are used to power the tungsten lamp (6267A power supply, Harrison Laboratories), and the deuterium lamp (Transistorized Hydrogen Lamp Power Supply, Beckman Instruments). The supply for the tungsten lamp is capable of voltage regulation of 0.01% when operated in a voltage programming mode.

Energy from either lamp is collected by a 3-in. spherical mirror and directed to a collimating lens (0.5 in., plano-convex, fused silica). A 0.5-in. iris-diaphragm, a beam splitter (MP-1022, McKee Pederson Instrument), a sample cell (fused silica 30-300, Perkin-Elmer), and a focusing lens (0.5 in., plano-convex, fused silica) follow the collimating lens in a linear arrangement. The focusing lens focuses the undispersed energy onto the entrance slit of the polychromator. The entrance slit is continuously variable from 0 to 6 mm and is calibrated in steps of 0.1 mm. Typical slit widths used in this work are from 0.05 to 2.5 mm. A commercial monochromator assembly (33-86-25, Bausch and Lomb) was modified by removal of the exit slit, thereby producing a broad band of spectrally dispersed radiation at the rear plane of the polychromator.

Three different diffraction gratings were used in the polychromator. The three gratings with 1350 grooves mm^{-1} blazed at 500 mm, 2700 grooves mm^{-1} blazed at 300 nm (both from Bausch and Lomb) and 1200 grooves mm^{-1} blazed at 2400 nm (Edmund Scientific) gave spectral ranges of about 170, 80, and 200 nm, respectively, on the active surface of the diode array. Any of the three gratings can be orientated to pass radiation anywhere in the range from 180 to 800 nm.

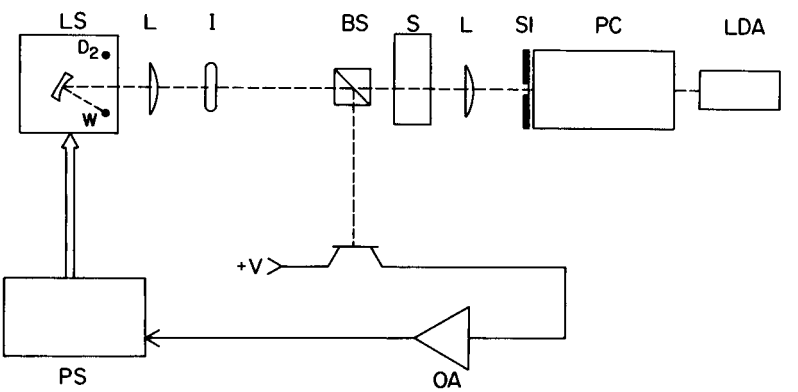

Fig. 1. Optical diagram for photodiode array spectrometer with optical feedback. LS, light source; L, lens; I, iris; BS, beam splitter; S, sample cell; SI, entrance slit; PC, polychromator; LDA, linear photodiode array; OA, operational amplifier; PS, programmable power supply.

The optical feedback arrangement is also shown in Fig. 1. A portion of the white light produced by the tungsten source is diverted by a beam splitter to a phototransistor (FPT10A, Fairchild Camera and Instrument). The response time for the phototransistor is about 10 μs, compared to a response time of 1 μs for a photodiode. The photocurrent generated by the phototransistor is converted to a proportional voltage that is used to control the output from the power supply used to drive the tungsten lamp.

Optical-feedback circuitry. Details of the circuitry for the feedback loop are shown in Fig. 2. The current from the phototransistor is proportional to radiation incident on the active surface of the phototransistor. This current is offset by a reference current from an operational amplifier (OA1), an integrated circuit voltage reference source, and a resistor network. The net current is sampled by a precision amplifier (OA2) in a current-to-voltage configuration. The output of OA2 is converted to current, added to a fixed offset, and sampled by a voltage follower, OA5. The output swing of OA5 is from 0 to 1.5 V, and is used to drive the voltage programming input of the power supply for the tungsten lamp.

Optical attenuators. Some linearity and dynamic range measurements were made with a precision optical attenuator (Technometrics). A sharp cut-off filter (No. 5031, Corning) was used for some of the stray light experiments.

Photometric measurements

Operational details for the silicon photodiode array detector and the solid-state detector controller (models 1412 and 1218, EG&G-Princeton Applied

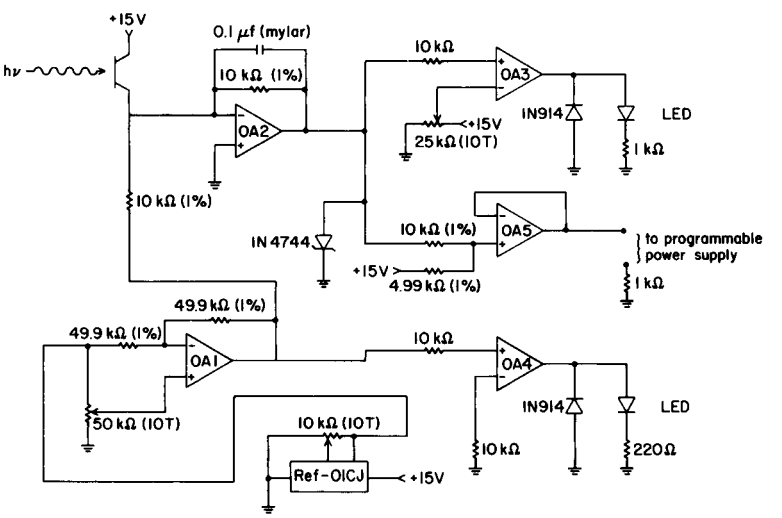

Fig. 2. Schematic diagram of optical-feedback circuitry: OA1, OA2 and OA5 are 714-C; OA3 and OA4 are 741-C.

Research) are supplied in the operating manual. The detector cooling apparatus was set to a nominal value of −20°C. Cold water (15°C) was circulated through the detector housing to provide heat exchange.

Two commercially available spectrophotometers (8450 UV/Vis spectrophotometer, Hewlett-Packard, and PE-320, Perkin-Elmer) were used in the photometric studies done for comparison purposes.

Data acquisition and instrument control

A detector controller accepts scan parameters from the instrument interface and uses these to control the interrogation parameters for each of the 1024 pixels in the diode array. Parameters such as integration time, scan initiation, scan termination, frame synchronization, and various pixel access modes are programmed into the controller. Controller instructions can be supplied manually through the switch register, or instructions can be downloaded from a computer (PDP-12/30, Digital Equipment Corporation). The controller for the detector is also responsible for digitization of data. It also provides an end-of-scan flag, which is useful for latching the data, and an external event flag, which echoes an external event to the controller.

Digitized data are transmitted in parallel from the controller through a row of latches to a fast memory module external to the computer. The external memory is used because of fast data acquisition requirements (1024 data points at a rate of 50 kHz). Data are then collected by the computer at a more leisurely rate (8 kHz) through a general purpose I/O port. When the data have been placed in core, they can be displayed on a storage scope or terminal, printed, or stored on a hard disk for subsequent processing and hardcopy readout.

Software

The basic scanning procedures for the diode array detector are downloaded from the PDP-12 computer to the detector controller under program control. A program, called BANDIT, written in FORTRAN with assembly language subroutines (SABR) allows the user to initiate scanning, execute one complete data scan, collect the data, terminate scanning, and store the data in one of four different formats on the hard disk. Another program, CAT1, works in much the same manner as BANDIT except that it allows data acquisition from 1 to 300 scans at repetition rates from 4 s to 10 000 s. This repetition rate is set by a programmable clock in the instrument interface. The maximum scan repetition rate is limited at the present time by bulk storage of data on the hard disk.

Another FORTRAN program, WAVCAL permits calibration of the wavelength scale with spectral data from a mercury pen lamp. The basic algorithm for the calibration is to find the pixel locations at which the emission intensity maxima occur and do a linear least-squares fit of pixel number (independent variable) vs. a reference table of known wavelengths of mercury emission lines (dependent variable). The slope and intercept for the resulting line are

calculated along with appropriate statistical information. Another program, ABSORB, is used to calculate absorbance and transmittance from a blank spectrum, a dark current spectrum, and raw intensity data. The program assumes equal integration times for the three spectra. Another program, INTEG, is similar but normalizes the data to account for different integration times. Spectral smoothing procedures were not used because it was felt that they would detract from an objective evaluation of the noise performance of the instrument system.

Chemicals

Reagent-grade chemicals and spectroscopic-grade solvents were used without further purification. Solution pH values were adjusted with certified buffer tablets (Perkin-Elmer) diluted to 100 ml in water. All aqueous solutions were prepared by dilution with distilled, deionized water.

Uric acid assays were done with a commercial reagent kit (A-gent Clinical Chemistry Uric Acid Assay; Abbott Laboratories, Diagnostic Division, South Pasadena, CA).

RESULTS AND DISCUSSION

Unless stated otherwise, uncertainties are reported as one standard deviation ($\pm s$).

Spectral characteristics

Figure 3 includes the spectra of a mercury pen lamp recorded with the diode-array spectrometer in two regions of the spectrum. Such spectra were used to evaluate different spectral characteristics of the system.

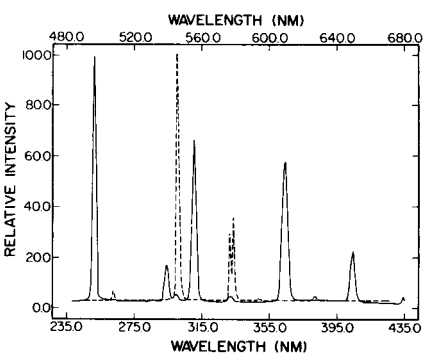

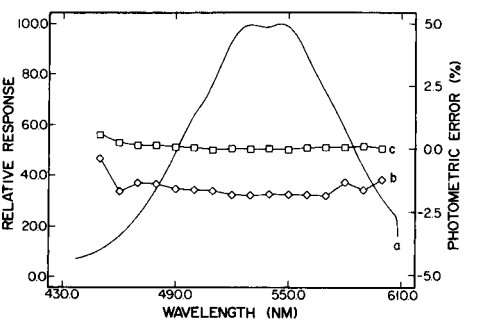

Fig. 3. Spectra for mercury pen lamp: (– – –) 235—435 nm; (——) 480—680 nm.

Fig. 4. Response curve for tungsten source with random and systematic errors: (a) relative response; (b) systematic error (% T); (c) standard deviation (% T, n = 10 for each point).

Wavelength calibration. For a typical wavelength calibration experiment in which five lines between 235 and 435 nm were used, a linear least-squares fit of wavelength vs. pixel number gave an intercept of 235.6 ± 0.6 nm and a slope of 0.195 ± 0.001 nm/pixel with a standard error of estimate (S_{yx}) of 0.68 nm and a correlation coefficient of 0.99995. For this particular configuration, the 1024 diodes correspond to a wavelength range of 235.6 to 435.3 nm. The statistics suggest excellent linearity for the calibration data. Standard errors of estimate for other five-point calibrations were in the range 0.3—0.7 nm.

The short-term repeatability of the wavelength calibration based on ten replicates during a 135-s period yielded relative standard deviations in slope, intercept, and wavelength range of 0.12, 0.047, and 0.13%, respectively.

Accuracy. Several experiments were conducted to check wavelength accuracy. For holmium oxide glass bands at 360.4 and 537.2 nm, differences between measured and expected peak positions were +0.4 and —0.8 nm, respectively. For deuterium, calcium, and manganese lamps with lines at 483.9, 422.8, and 403.3 nm, respectively, differences were +2.1, 0.1, and 0.0 nm, respectively. The larger differences associated with the holmium oxide glass and deuterium lamp result from the relative widths of the transmission bands for the former and the relatively low intensity of the emission band for the latter.

Resolution. The two lines at 577.0 and 579.1 nm (dashed curve in Fig. 3) provide a visual indication of the resolution of the system. Numerically, the resolution is estimated to be 1.1. This value is superior to the value of 3 to 4 reported for a silicon vidicon with a similar spectral range [5, 6].

Photometric characteristics

This section includes comparisons of photometric characteristics of the system developed in this study with characteristics of two commercial instruments (Hewlett-Packard 8450A and Perkin-Elmer 320). It should be noted that the integration time for the present system (0.018 s) is much shorter than the integration time for the HP-8450A (1 s) and the time constant for the PE-320 spectrophotometer. A linear transmittance system (LTS) was used to set desired absorbances in these studies.

Stability. With the exception of the HP-8450A spectrophotometer, most applications of imaging detectors to date have involved single-beam optical systems. A major objective of this study was to evaluate the viability of an optical-feedback approach [3, 4] with multiwavelength imaging detectors.

Table 1 compares time-dependent imprecisions obtained without and with optical feedback and with an HP-8450A spectrophotometer. Results with optical feedback are substantially improved in all cases relative to those without feedback. The long-term data suggest that the double-beam system (HP-8450A) may be more effective than the optical-feedback system in compensating for source drift; however, there are too many other differences between the systems to be very confident of this apparent conclusion. To

TABLE 1

Time-dependent reproducibility data without (A) and with (B) optical feedback, and with the Hewlett-Packard 8450 spectrophotometer (HP)

Wavelength (nm)	Standard deviation (% T)[a]								
	Short-term (13.5 s)			Intermediate (5 min)			Long-term (1 h)		
	A	B	HP	A	B	HP	A	B	HP
540	1.0	0.033	0.035	0.22	0.03	0.08	3	0.13	0.04
580	0.8	0.05	0.02	0.9	0.006	0.07	2.6	0.17	0.02
600	0.7	0.03	—	1.7	0.3	—	2.5	0.13	—

[a]All measurements were made with an optical attenuator set at 50% T; 10 replicates each for 13.5 s and 5 min, 8 replicates for 1 h.

put these data into perspective, an error of 0.1% T at 50% T corresponds to an error of about 0.0009 absorbance. Thus, the optical-feedback system permits absorbance measurements with random uncertainties in absorbance of about 0.001 in this range.

Imprecision data at several other wavelengths with optical feedback are included as curve (c) in Fig. 4.

All results reported in the remainder of this paper were obtained with optical feedback.

Photometric error. Curve (b) in Fig. 4 shows photometric error as a function of wavelength at 50% T. The estimated uncertainty associated with settings on the LTS unit is 1.5% T; most of the errors are at or within this limit. The average error for all the data is 0.86% T, which corresponds to an apparent absorbance error (at 50% T) of —0.0074. This compares favorably with a value of 0.8% T (—0.0069 absorbance) obtained for the HP-8450A spectrophotometer with a solution of potassium dichromate. It is probable that in each case the apparent error results at least as much from the "standard" as from the instrument.

Linearity. A least-squares fit of measured (A_m) vs. expected (A_e) absorbances between 0.1 and 2.1 (set with LTS) at 600 nm gave the equation

$$A_m = (0.966 \pm 0.04)A_e - 0.0075 \pm 0.005$$

with a standard error of estimate of 0.009 and a correlation coefficient of 0.99992. These statistics suggest good linearity in this range with slope and intercept different from the expected values of unity and zero. As noted in the previous subsection, this systematic difference may be inherent in the LTS. Similar results were obtained at 550 and 500 nm.

Serial dilutions (1.4×10^{-6} to 4×10^{-4} M) of a potassium dichromate solution in 0.05 M NaOH were used to evaluate the linearity at 257 nm for the absorbance range between 0.0019 and 1.57. A least-squares fit of absorbance vs. concentration gave the equation

$A = (3.88 \pm 0.05)\, C\,(\text{mM}) + 0.0003 \pm 0.0001$

with $S_{yx} = 0.5$ and $r = 0.9996$. Again, these statistics suggest good linearity.

In each case above, the plots bend toward the concentration axis for absorbances higher than the indicated upper limits (2 at 600 nm and 1.6 at 257 nm). This upper limit is imposed by stray energy in the present optical system. Some typical values of stray energy estimated with previously described procedures [7] were 0.64% T at 220 nm, 0.06% T at 265 nm and 0.004% T at 700 nm, with values between 0.01 and 0.05% T at intermediate wavelengths. Thus, the upper limit of the linear range is limited by the optical system rather than the detector.

Integration time. Figure 5 compares absorbance data obtained with two different integration times at relatively low intensities. The S/N enhancement at the longer integration time is quite apparent. Experiments with integration times between 0.0183 s and 0.293 s demonstrated an approximately linear increase in S/N with increasing integration time. For data similar to those in Fig. 5 with an absorbance of 2.6, the least-squares fit of S/N vs. time gave the equation S/N = 146.1 t (s) + 5.0 for the time range mentioned above. For higher intensities, there is a square-root dependence on integration time.

Use of longer integration times to gain additional improvements in S/N is complicated by the increase in dark current. For integration times below 2 s, dark current is influenced very little by integration time. However, above 2 s, dark current increased linearly with time. A least-square fit of the fraction (f) of dark current (relative to the full-scale current) vs. integration time between 2 and 100 s gave the equation $f = 0.007\ t$ (s) + 0.05. Effects of dark current can be reduced by operating at lower temperature.

Chemical applications

The photometer was evaluated for one equilibrium and one kinetic study.

Equilibrium study. Figure 6 shows the absorption spectra resulting from the addition of different amounts of pyridine to a fixed concentration of iodine in carbon tetrachloride. The band centered at 520 nm corresponds to absorption by molecular iodine and the band centered at 420 nm corresponds to the charge-transfer complex. Data such as these were used to evaluate the equilibrium constant for the reaction by procedures described earlier [8]. The value of the equilibrium constant determined at 25°C with the instrument described herein is 97 ± 1.5; this compares favorably with values of 92 ± 4 and 95 ± 0.4 determined with the HP-8450A and PE-320 spectrophotometers. A literature value for the constant is 101.2 [9].

Kinetic results. A two-point kinetic method for quantifying uric acid (see Experimental) was used to evaluate the performance of the system for long measurement times. The reaction involved enzymatic (uricase) oxidation of uric acid to allantoin followed by oxidation of nicotinamide adenine dinucleotide (NADH) to NAD [10]. The absorbance change at 340 nm during a 15-min reaction time was used to quantify uric acid. Results were

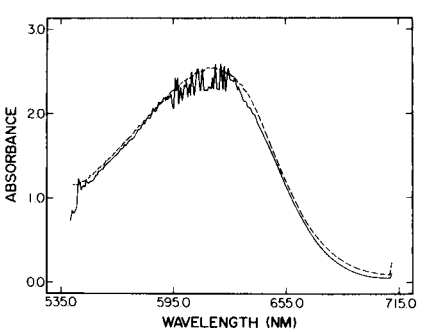

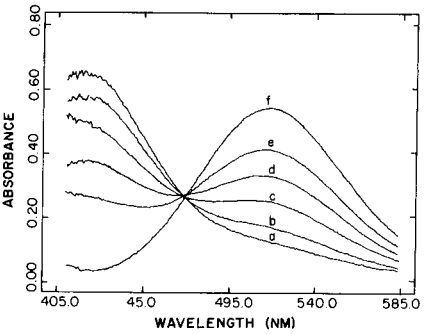

Fig. 5. Effect of integration time on the signal. Integration times are 18.3 ms (——) and 54.9 ms (— — —).

Fig. 6. Spectra for different concentrations of pyridine with a fixed concentration of iodine. Pyridine concentrations (a—f) are 0.0, 4.3, 8.6, 17.2, 34.4, and 68.8 mmol l^{-1}.

obtained with the instrument described here as well as with the HP-8450A spectrophotometer. For eight concentrations of uric acid between 2 and 12 g l^{-1}, a least-squares fit of absorbance changes (ΔA) measured with the two spectrophotometers yielded the expression

$$\Delta A_E = (0.974 \pm 0.040)\, \Delta A_{HP} + 0.039 \pm 0.004$$

with $S_{yx} = 0.25$ and $r = 0.995$. These statistics suggest excellent agreement between the two data sets.

Photometric drift in the system without optical feedback (see Table 1) would greatly degrade results obtained during such a long (15 min) measurement interval.

These results show that combination of optical feedback with the photodiode array detector can provide the combined advantages of rapid-scanning spectrophotometry with long-term stability. This capability should further enhance the utility of these detectors.

This work was supported in part by Grants DE-AC02-79EV10240 from the Department of Energy and CHE-7822456 from the National Science Foundation.

REFERENCES

1 Y. Talmi, Appl. Spectrosc., 36 (1982) 1.
2 H. L. Pardue, in J. K. Foreman and P. B. Stockwell (Eds.), Topics in Automatic Chemical Analysis, Horwood, Chichester, 1979, pp. 163—207.
3 H. L. Pardue and P. A. Rodriguez, Anal. Chem., 39 (1967) 901.
4 T. E. Hewitt and H. L. Pardue, Clin. Chem., 21 (1975) 249.
5 T. A. Nieman and C. G. Enke, Anal. Chem., 48 (1976) 619.
6 M. J. Milano and H. L. Pardue, Anal. Chem., 47 (1975) 25.
7 W. Slavin, Anal. Chem., 35 (1963) 561.
8 H. A. Benesi and J. H. Hildebrand, J. Am. Chem. Soc., 71 (1949) 2703.
9 A. I. Popov and R. H. J. Rygg, J. Am. Chem. Soc., 79 (1951) 4622.
10 T. Feichtmeir and H. Wienn, Am. J. Clin. Pathol., 25 (1955) 833.

Analytica Chimica Acta, 155 (1983) 113—121
Elsevier Science Publishers B.V., Amsterdam — Printed in The Netherlands

THE USE OF ULTRAVIOLET-VISIBLE SPECTROPHOTOMETRY IN THE DETERMINATION OF AVERAGE PROPERTIES OF NONYLPHENOL ETHYLENE OXIDE CONDENSATES

MIGUEL DE LA GUARDIA*, JUAN LUIS CARRIÓN and JULIO MEDINA

Departamento de Química Analítica, Facultad de Ciencias Químicas, Universidad de Valencia, Burjasot, Valencia (Spain)

(Received 23rd May 1983)

SUMMARY

Ultraviolet spectrophotometry is used in the determination of average molecular weight (M), average degree of polymerization (X), the hydrophilic-lipophilic balance (HLB) and ethylene oxide percentage of nonylphenol ethylene oxide condensates. The method is based on determination of the absorptivity a, expressed in g l^{-1} cm^{-1}, from the absorbances measured at 275 nm for a series of dilutions of an aqueous ethanolic solution (60:40, v/v) of a given product, followed by numerical interpolation of this value in the expressions a = f(HLB), log a = f(log M), and log a = f(log X). These expressions are obtained from reference samples or samples previously analyzed. The proposed method gives relative standard deviations of 1% for the estimation of M and X, and 0.5% for HLB and ethylene oxide percentage, with reasonable accuracy. Aqueous solutions can be used but the method is then restricted to samples with $HLB > 13$. For the estimation of M, the molar absorptivity can be used, because the value obtained for this parameter (1700) remains constant for a variety of degrees of polymerization.

Surfactants are extensively used to improve the characteristics of many analytical techniques [1]. This involves an interesting alternative to traditional sample preparation methods, but it requires strict characterization of the surfactant properties such as hydrophilic-lipophilic balance (HLB) [2] or degree of polymerization. However, most instrumental methods used in analyses for nonionic surfactants are centred on the determination of the compounds [3]. Chromatographic techniques, ultraviolet-visible spectrophotometry, atomic absorption spectrometry, x-ray fluorescence, potentiometry and polarography have been used. To characterize these surfactants, thin-layer chromatography has been employed, relating R_f values to molecular weights [4]. Danes and Casanovas [5] used mass spectrometry to characterize nonionic surfactants, determining their nature from the spectra and the degree of polymerization from the inlet temperature required to obtain a good spectrum.

Crutchfield et al. [6] proposed the use of nuclear magnetic resonance (n.m.r.) for nonionic surfactant characterization, obtaining the degree of polymerization and the alkyl radical composition from absolute integrals of

0003-2670/83/$03.00

the different types of hydrogen existing in the molecule. Bergueiro et al. [7] also employed n.m.r. to obtain the *HLB* of nonionic surfactants by means of an empirical equation, obtained from the relative integrations of lipophilic and hydrophilic hydrogens in the molecule and from literature *HLB* values.

In some preliminary work here, the molecular weight (M), degree of condensation (X), *HLB* and ethylene oxide percentage were determined by n.m.r. by means of empirical equations, and also by direct treatment of the spectral data of nonylphenol ethylene oxide condensates; it was concluded that the latter treatment is better than n.m.r., being capable of generalization to compounds of the same chemical nature but different manufacturer. Further, methods other than n.m.r. can be more cost-effective. Infrared spectroscopy was examined for the determination of the average properties of nonylphenol ethylene oxide condensates, by calculating the quotient between the heights of bands appearing at 1000 and 800 cm^{-1} (h_2/h_1). These values must be interpolated in the regression equation $\log h_2/h_1 = f(\log P)$ obtained from i.r. spectra of standard samples of this type or of previously analyzed compounds, which makes the method unattractive.

Ultraviolet-visible spectrophotometry was used by Greef et al. [8] in the determination of nonionic surfactants; the method is based on the formation of a blue complex between ammonium thiocyanatocobaltate and a polyethoxylated compound which is extracted into benzene from a saturated salt solution and measured at 320 nm, allowing the determination of 0—20 mg l^{-1} surfactant. The method is sensitive to condensates containing three or more molecules of ethylene oxide, but has apparently not been applied to characterize nonionic surfactants.

The present paper is concerned with the application of u.v.-visible spectrophotometry to the determination of average molecular weight, X, *HLB* and ethylene oxide percentage of nonylphenol ethylene oxide condensates; the analytical characteristics and possibilities are evaluated. It is important to realize that X, *HLB* and the percentage of ethylene oxide are alternative expressions of the same fundamental property, the average molecular weight.

EXPERIMENTAL

Apparatus and reagents

The Shimadzu UV-240 spectrophotometer used was equipped with a Graphic-Printer model PR-1 and 1-cm quartz cells. The n.m.r. data were obtained with a Perkin-Elmer model MS-12 spectrometer, equipped with a double resonance accessory.

To apply the standard method (UNE 55-518-75), the glassware was constructed as specified in the standard [9].

Aqueous and aqueous ethanolic solutions of nonylphenol ethylene oxide condensates were prepared from the series Nemol K-34, K-36, K-38, K-39, K-539, K-1030, K-1032, K-1033 and K-1035 (Masso and Carol), Renex 647,

697, 688, 690, 682 and 678 (ICI Pharmaceuticals) and Arkopal 40, 60 and 80 (Hoechst). Tetramethylsilane solution (3.5%, w/w) in distilled tetrachloromethane was used. Surfactant solutions (50%, w/w) were prepared in this solution.

Procedures

Standard method [9]. The standard method used to evaluate the accuracy was the UNE 55-518-75 method based on iodimetric determination of ethylene oxide groups. The surfactant (20—100 mg) was accurately weighed and then introduced into a round-bottomed flask; 3 g of potassium iodide is added and a condenser is connected to the flask. The system is purged with nitrogen for 20 min, and then placed in a glycerine bath at 165 ± 1°C for 30 min, without stopping the gas flow. An absorption tube containing 10 ml of 10% (w/v) potassium iodide solution is connected to the condenser. The flask is then allowed to cool to below 80°C, and the gas flow is stopped. The contents of the absorption tube are poured through the condenser into the flask, all the glassware and joints being rinsed with the iodide solution and with distilled water. The solution in the flask is titrated with 0.1 N sodium thiosulfate, using starch as indicator.

Ultraviolet method. The surfactant (0.1—0.2 g) is weighed and dissolved in ethanol (40%), and the solution is diluted to 50 ml. From this solution, aliquots of 1.25, 2.5, 3.75 and 5.0 ml are transferred to 50-ml volumetric flasks and these solutions are diluted to 50 ml with the same solvent. The absorbances are measured at 275 nm. The data obtained are plotted vs. the concentration of surfactant in g l^{-1}, and the slope is calculated, giving the absorptivity a. This value is interpolated into the equations that relate absorptivity to molecular weight (M), degree of polymerization (X) and HLB, obtained from samples previously analyzed (see Results and Discussion).

N.m.r. method. The surfactant (500 ± 1 mg) is weighed and dissolved in an equivalent amount of TMS solution and the n.m.r. spectrum is recorded between 0 and 10 ppm. From the integrated values of the three hydrogen types, the degree of polymerization and the alkyl radical composition can be calculated, because each surfactant molecule contains four hydrogens corresponding to the aromatic group, which can be used as an internal reference to calculate the number of hydrogens corresponding to the other peaks. From these calculated values, the molecular weight (X, HLB and percentage of ethylene oxide) can be estimated. This method was applied to a series of samples. The parameters obtained were used as standards to calculate the equations relating a to M, X and HLB.

RESULTS AND DISCUSSION

The u.v. spectrum of nonylphenol ethylene oxide condensates

Figure 1 shows the u.v. spectra of a condensate of 12 moles of ethylene oxide with nonylphenol. The spectrum has three bands corresponding to

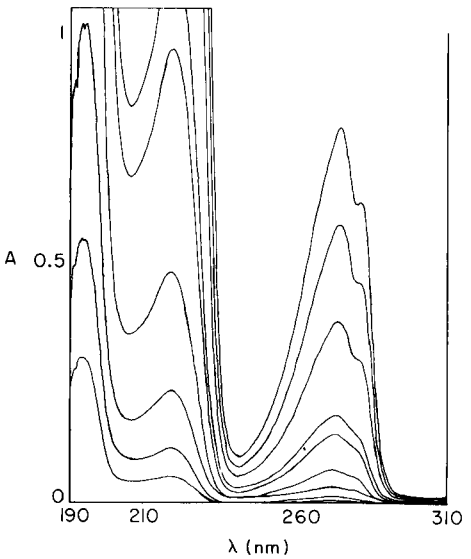

Fig. 1. Ultraviolet spectra of nonylphenol ethylene oxide condensate at concentrations of 0.01—0.1 g l^{-1}.

the aromatic group of the surfactant molecule. The bands at 195 and 222 nm are too intense, giving absorbance readings well above the zone of minimal photometric error in the range of usual working concentrations. The band at 275 nm is less intense, which allows a wider range of surfactant concentrations to be used; it was therefore chosen as the working wavelength.

To obtain such spectra, u.v.-transparent solutions are needed, so that water would be the ideal solvent. However, only the surfactants with high degrees of polymerization are water-soluble. In ethanolic and aqueous ethanolic solutions, a wider range of surfactants of both high and low molecular weight are soluble.

The influence of the percentage of ethanol on the absorbance reading is shown in Fig. 2 for a set of solutions containing 0.026% Nemol K-539; in all cases, the blank contained the same percentage of ethanol as the sample. As can be seen, the absorbance is minimal for a 30% ethanol solution. At higher ethanol percentages, the absorbance increases and tends to stabilize. As the concentration of surfactant is very low, near the critical micelle concentration (c.m.c.) expected for this type of compound, this could be interpreted as an increase in the c.m.c. caused by ethanol (or methanol) [10]. On the basis of these results, it was decided to use aqueous ethanolic solutions (60:40, v/v); this minimized the amount of solvent needed and gave only a slight loss of sensitivity, but allowed all the surfactants tested to dissolve. Moreover, around this ethanol percentage, the variation in absorbance remained within acceptable error limits.

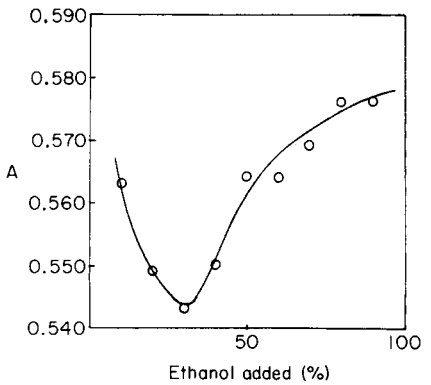

Fig. 2. Effect of ethanol concentration on the absorbance of an aqueous solution of Nemol K-539 at 275 nm.

Influence of time

In surfactant solutions at concentrations near the c.m.c., micelles are formed and are in dynamic equilibrium with their monomers. It is usually necessary to reach this equilibrium in order to study the properties of these solutions. The influence of the time of measurement on the absorbance readings was studied in order to establish to what extent micelle phenomena could influence the u.v. absorption of solutions of nonylphenol ethylene oxide condensates. Table 1 shows the values obtained for solutions of 0.024% Nemol K-539 in water/ethanol (60:40, v/v) measured at different times; the deviations observed are within the normal range of photometric error.

Deduction of empirical equations

From the absorbances found for each surfactant at different dilutions and from the concentrations in g l^{-1}, it is possible to obtain a calibration equation that differs from one compound to another in the absorptivity (a, i.e., slope) which depends on the molecular weight and decreases as the molecular weight increases. Table 2 shows the a values for 19 surfactants with different degrees of polymerization, as well as the standard deviations (s) corresponding to three independent assays for each compound.

In order to establish the relationship between the absorptivity a and the

TABLE 1

Effect of time on the absorbance of aqueous ethanolic solutions of Nemol K-539

Time (h)	0	1	5	24
A (275 nm)	0.526	0.528	0.528	0.529
Relative difference (%)[a]	—	0.38	0.38	0.57

[a]Calculated from 100 $(A_t - A_0)/A_t$.

TABLE 2

Average properties of the surfactants obtained by the u.v., n.m.r. and standard UNE methods

Sample	a[a]	s[b]	N.m.r. method						U.v. method								UNE method	
			M	*s*	*X*	*s*	*HLB*	*s*	*M*	*s*	*X*	*s*	*HLB*	*s*	*%EO*	*s*	*%EO*	*s*
K-34	3.57	0.02	440	30	4.6	0.3	9.9	0.2	440	4	4.68	0.07	9.83	0.08	46.9	0.3	42.9	0.3
K-36	2.90	0.02	560	10	7.2	0.1	11.88	0.07	550	3	6.80	0.07	11.85	0.05	54.2	0.2	—	—
K-38	2.41	0.01	690	20	10.0	0.4	13.3	0.1	680	4	9.4	0.1	13.30	0.04	61.6	0.2	59.0	0.5
K-39	2.271	0.009	710	20	10.7	0.3	13.68	0.04	720	3	10.5	0.07	13.72	0.03	64.2	0.2	—	—
K-539	2.214	0.002	770	20	12.0	0.8	14.2	0.2	770	5	11.8	0.1	14.15	0.04	67.3	0.3	65.0	0.4
K-539(N)	2.29	0.08	690	40	10.5	0.6	13.93	0.05	710	1	10.3	0.1	13.66	0.01	63.8	0.1	65.1	0.3
K-1030	2.090	0.005	800	20	12.4	0.4	14.1	0.1	790	2	12.22	0.05	14.26	0.01	68.0	0.1	—	—
K-1032	1.894	0.008	830	50	13.4	0.8	14.6	0.1	890	4	14.5	0.1	14.84	0.02	72.8	0.2	70.4	0.5
K-1033	1.758	0.005	940	50	16.0	1.0	15.1	0.1	950	3	16.57	0.08	15.25	0.01	76.6	0.1	—	—
K-1035(N)	1.70	0.03	1040	60	17.8	0.8	15.5	0.3	970	14	17.6	0.5	15.42	0.09	78.4	0.9	74.0	0.5
Renex																		
647	3.31	0.08	460	10	5.1	0.1	10.4	0.2	470	2	5.25	0.03	10.50	0.03	49.1	0.1	—	—
697	3.090	0.006	530	20	6.4	0.2	11.4	0.2	515	1	6.06	0.02	11.27	0.02	51.88	0.07	—	—
688	2.44	0.08	690	10	9.8	0.2	13.0	0.2	650	9	8.9	0.2	13.07	0.09	60.3	0.5	—	—
690	2.13	0.02	770	20	11.9	0.1	14.0	0.2	770	5	11.6	0.1	14.09	0.03	66.8	0.3	—	—
682	2.1	0.1	800	20	12.8	0.4	14.47	0.01	820	7	13.1	0.2	14.50	0.04	69.9	0.4	—	—
678	1.69	0.02	970	50	16.5	0.8	15.37	0.05	995	1	17.80	0.04	15.453	0.006	78.76	0.07	—	—
Arkopal																		
40	3.68	0.01	440	20	4.3	0.2	9.57	0.05	425	1	4.44	0.02	9.53	0.03	46.02	0.09	—	—
60	3.07	0.06	500	10	6.0	0.2	11.3	0.2	525	2	6.27	0.04	11.45	0.04	52.6	0.1	—	—
80	2.41	0.02	670	40	8.9	0.8	13.5	0.2	680	6	9.5	0.1	13.31	0.06	61.7	0.4	—	—

[a]Absorptivity. [b]Standard deviation.

average molecular weight (as well as X and HLB) of the test compound, regression equations were set up between the experimental parameter values and the values of M, X and HLB obtained by the n.m.r. method. The expressions for the absorbance of a solution as a function of the molar absorptivity (ϵ) and the absorptivity (a) with concentrations c in g l^{-1} are

$A = \epsilon\ b\ c\ M^{-1}$ and $A = a\ b\ c$

Thus $\epsilon\ b\ c\ M^{-1} = a\ b\ c$ and $M = \epsilon\ a^{-1}$, and taking logarithms,

$\log M = \log \epsilon - \log a$

A similar relationship is valid for X. Three regression models were tested for HLB: $a = f(HLB)$, $\log a = f(HLB)$, and $\log a = f(\log HLB)$. The simple model provides the best regression.

Table 3 shows the relationships derived between parameter a obtained experimentally by the u.v. method with M, X and HLB, previously obtained by n.m.r., as well as the regression coefficients (r^2).

Determination of M, X, HLB *and ethylene oxide percentage of nonylphenol ethylene oxide condensates*

Experimental values of parameter a of each of the compounds studied were interpolated into the empirical equations in Table 3, giving the corresponding values of M, X and HLB. Table 2 shows the results obtained with the standard deviations. As the standard method [9] provides only the ethylene oxide percentage (% EO), this value was calculated from the values of X and M obtained by u.v. by means of the equation $\%\ EO = 44.052 \times 100 \times X/M$. Table 2 shows the values found and the standard deviations.

The preceding treatment of data from u.v. spectra of nonylphenol ethylene oxide condensates was also applied to aqueous solutions of these condensates, but it was satisfactory only for compounds with more than 11 moles of ethylene oxide (HLB > 13). For aqueous solutions, the equations relating a to M, X and HLB were of the same type as those used for water/ethanol solutions. Water should be used as solvent if the products to be tested are completely soluble in it.

TABLE 3

Empirical equations used in the estimation of the average molecular weight (M), degree of polymerization (X) and HLB from the u.v. spectral data

Function	Equation	r^2
$\log a = f(\log M)$	$y = 2.968 - 0.914x$	0.99
$\log a = f(\log X)$	$y = 0.928 - 0.560x$	0.99
$a = f(HLB)$	$y = 6.866 - 0.335x$	0.99

Treatment of the data obtained with aqueous and aqueous ethanolic solutions as a function of the molar absorptivity

When the number of moles of ethylene oxide condensed with one mole of nonylphenol is increased, the number of aromatic groups within the molecule does not vary whereas the average molecular weight in grams increases considerably. Thus M can be determined for a given compound, if the band intensity at the working wavelength and the weight of dissolved compound are known, by means of the equation $M = \epsilon\ b\ c/A$.

From the data for M obtained for each compound by n.m.r. and from the pairs of values of A/c (g l^{-1}) obtained from the preceding experiments, the value of ϵ was calculated for both aqueous and aqueous ethanolic solutions at the working wavelength. It was found that the experimental values corresponding to each assay, for each compound and with different sample dilutions, belonged to the same population; the mean values were 1700 for aqueous solution with a standard deviation of 64 for 140 values, and 1600 for aqueous ethanolic solutions with a standard deviation of 60. It can be concluded that these values can be taken as constants for all the compounds studied. Accordingly, to determine the molecular weight of a new sample of nonylphenol ethylene oxide condensate, it would suffice to prepare an aqueous or aqueous ethanolic solution of the sample at an accurately known concentration (g l^{-1}), measure its absorbance at 275 nm, and calculate M as above. This procedure is very simple and provides sufficiently precise and accurate results for this type of compound.

To determine X and HLB by means of this procedure, it is necessary to assume that the average nature of the compound corresponds to a polyethoxylated nonylphenol; this is not strictly correct, so that the errors obtained for X and HLB are greater than those for M.

Precision and accuracy

The precision of the proposed u.v. method was evaluated for calculation of molecular weight, degree of polymerization, HLB and ethylene oxide percentage for two condensation levels and from nine independent assays. The relative standard deviations obtained in the molecular weight determination for condensation levels of 4.6 mol and 12 mol of ethylene oxide were 0.9% and 0.7%, respectively. The corresponding data for the degree of polymerization were 1.4% and 0.85%; for the HLB the deviations were 0.85% and 0.28% and for ethylene oxide percentages the deviations were 0.55% and 0.34%.

The accuracy of the method was evaluated by comparison of the ethylene oxide percentage values obtained by the UNE standard method and by the proposed method. Regression analysis [11] was applied to all the values found for six samples analyzed by u.v. and by the reference method [12]. Variances corresponding to each sample were shown to be homogeneous by the Hartley test. The analysis showed that the proposed method neither requires blank correction (the intercept is statistically equal to zero) nor

shows bias (the slope is statistically equal to one) for a probability level of 95%.

Conclusions

These studies suggest that the proposed procedure for the characterization of average properties of nonylphenol ethylene oxide condensates is easy, precise and accurate. Moreover, the empirical equations found fit any compound of this type from different manufacturers.

The use of aqueous ethanolic solutions for evaluating the absorptivity is necessary if all the samples are to be treated with the same equation, but for samples with *HLB* higher than 13, aqueous solutions can be used. For the average molecular weight determination, the molar absorptivity can be used, as it is constant at 275 nm for a variety of degrees of polymerization.

We are indebted to Masso and Carol S.A., ICI Pharmaceuticals and Hoechst for the provision of surfactant samples.

REFERENCES

1 K. L. Mittal, Solution Chemistry of Surfactants, Vol. 1, Plenum, New York, 1979.
2 W. C. Griffin, J. Soc. Cos. Chem., 1 (1949) 311.
3 R. A. Llenado and R. A. Jamieson, Anal. Chem., 53 (1981) 174R.
4 L. A. Safiullina, D. N. Asanbaeva and A. L. Shtangeev, Tr. Bashk. Gos. Nauchnoissled. Proektn. Inst. Neft. Prom. St., 53 (1978) 64.
5 H. J. Danes and A. M. Casanovas, Tenside Deterg., 16 (1979) 317.
6 M. M. Crutchfield, R. R. Irani and J. T. Yoder, J. Am. Oil Chem. Soc., 41 (1964) 129.
7 J. R. Bergueiro, M. Bao and J. J. Casares, Anal. Quim., 74 (1979) 529.
8 R. A. Greef, E. A. Setzkorn and W. D. Leslie, J. Am. Oil Chem. Soc., 42(3) (1965) 180–185.
9 Instituto Nacional de Racionalización y Normalización, Madrid, 1975, UNE 55-518-75.
10 N. Nishikido, Y. Moroi, H. Uehara and R. Matuura, Bull. Chem. Soc. Jpn., 47 (1974) 2634.
11 Commisariat à l'energie atomique, Statistique appliquée à l'exploitation de mesures, Masson, Paris, 1978.
12 M. de la Guardia, A. Salvador, V. Berenguer, Anal. Quim., 77B (1981) 129; V Encontro Anual da Sociedade Portuguesa de Quimica, Oporto, April, 1982.

Analytica Chimica Acta, 155 (1983) 123—129
Elsevier Science Publishers B.V., Amsterdam — Printed in The Netherlands

LUCIGENIN CHEMILUMINESCENCE AND BIOMOLECULES
Determination of Heparin

ROBERT A. STEEN[a] and TIMOTHY A. NIEMAN*
School of Chemical Sciences, University of Illinois, Urbana, IL 61801 (U.S.A.)
(Received 16th February 1983)

SUMMARY

Heparin, a polymer of glucosamine and uronic acids, is subjected to acid hydrolysis to be degraded to disaccharides which are in turn quantified by using a chemiluminescent reaction with lucigenin. The hydrolysis time used was 4 h in 0.25—0.5 M sulfuric acid at 90°C, and the optimum reagent concentrations for the chemiluminescent reaction were 1 mM lucigenin and 0.5 M KOH. The detection limit is 90 μg of heparin and the response is linear up to 10 mg of heparin. The relative standard deviation for the method is 10% with a 4-h hydrolysis and 4% with an 8-h hydrolysis; the relative standard deviation for the measurement step is 2%.

In earlier work in this laboratory, the chemiluminescent reaction of lucigenin (*N,N'*-dimethyldiacridinium nitrate) was investigated in basic solution with organic reductants and was found to be applicable to the quantitation of simple organic reductants of clinical significance, such as ascorbic acid, creatinine, uronic acids, and reducing sugars [1, 2]. It should be possible to extend this chemiluminescent procedure to determine other biomolecules that contain these simple reductants as subunits. One such molecule is heparin, a mucopolysaccharide important as a blood anticoagulant. Heparin (I) is composed of alternating D-glucosamine (mostly *N*-sulfonated) and uronic acid (mostly iduronic, the remainder glucuronic) residues with *O*-sulfonation at some iduronic acid and glucosamine residues [3—5]. Several recent reviews have covered the structure, function, and quantitation of heparin [6—9]. The molecular weight of heparin is reported to be between 5000 and 30 000 so that one molecule would contain 20—130 sugar residues. If heparin is hydrolyzed in acidic solution at elevated temperature, the glycosidic linkages are broken to yield a series of oligosaccharides, the smallest of which are the disaccharides (II). The length of hydrolysis determines the extent to which the heparin is depolymerized [10].

In the earlier work on lucigenin chemiluminescence, the detection limits were 10—20 mg l^{-1} for glucose and glucuronic acid [1]. If heparin could be

[a]Present address: American Can Co., Neenah Technical Center, 1915 Marathon Ave., Urbana, IL, U.S.A.

0003-2670/83/$03.00

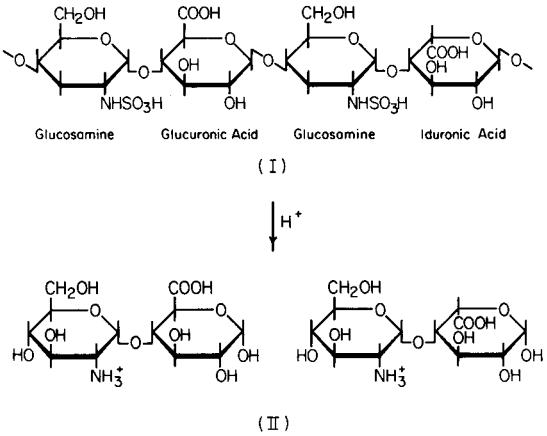

completely degraded and the residues determined by lucigenin chemiluminescence, then a detection limit on the order of 10—20 mg of heparin per liter would be expected. In this paper, the extension of lucigenin chemiluminescence to the determination of heparin is reported.

EXPERIMENTAL

All solutions were prepared from distilled-deionized water and reagent-grade chemicals. Sodium heparin was obtained from ICN Pharmaceuticals.

Procedures

Acid hydrolysis. The mixture used was 1—3 ml of water containing the desired amount of heparin plus 1 ml of 1 M H_2SO_4. The mixture was placed in a test tube and heated at 90°C in a water bath. Hydrolysis was stopped by removing the sample from the bath and adding 2 ml of 1 M NaOH to neutralize the solution. The hydrolyzed sample was diluted to 25 ml before the measurement of chemiluminescence.

Nitrous acid cleavage. The mixture used was 1—3 ml of water containing the desired amount of heparin, 1 ml of 1 M H_2SO_4, and 4 ml of 5.5 M sodium nitrite. The reaction proceeded in a test tube at room temperature and was stopped by addition of sodium hydroxide to neutralize the solution.

Chemiluminescence measurements. All measurements were made with a stopped-flow instrument as described by Veazey and Nieman [1]. There were separate drive syringes for the sample, lucigenin (1.0 mM), and potassium hydroxide (0.5 M) solutions. Reaction was initiated by simultaneously injecting the solutions from the three syringes through a mixer into the flow cell. The emission intensity was monitored with an IP28 photomultiplier tube biased at 900 V. The anode current was monitored on a strip-chart recorder until the maximum light intensity was observed (about 2 min). All signals reported are the maximum observed intensity (in nA) corrected for the background emission from a blank solution.

RESULTS AND DISCUSSION

Acid hydrolysis

Figure 1 shows the effect of hydrolysis time on the intensity of the chemiluminescence. At longer hydrolysis times, the emission intensity decreases. These observations are in agreement with earlier reports concerning the acid hydrolysis of heparin; at long times the uronic acid moiety is further degraded [10, 11]. The blank does not change with hydrolysis time. As a compromise between hydrolysis time and sensitivity, a 4-h hydrolysis time was preferred to the 6—8-h time that would correspond to complete hydrolysis.

Optimization of reagent concentrations

Several combinations of lucigenin (between 0.1 and 1 mM) and potassium hydroxide (between 0.5 and 2 M) concentrations were tried as reagents for a hydrolyzed heparin solution and a blank solution. The measured intensities are given in Table 1. Both the sample intensity and the blank intensity increase as either the potassium hydroxide or the lucigenin concentration increases. The sample intensity increases linearly with both the potassium hydroxide and lucigenin concentrations and therefore also linearly with the product of the concentrations as shown in Fig. 2. The ratio of sample intensity to blank intensity decreases with increasing reagent concentrations. This situation is appreciated by examining Fig. 2 which shows both the intensity for the sample and the sample-to-blank ratio as a function of the product of the alkali and lucigenin concentrations. The conditions chosen for subsequent work were 1 mM lucigenin and 0.5 M KOH for a concentration product of 5×10^{-4} M^2.

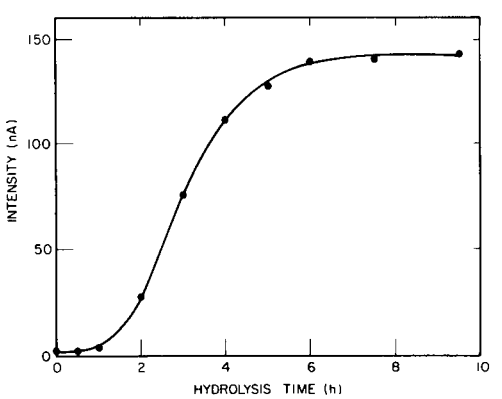

Fig. 1. Variation of chemiluminescent emission intensity with duration of acid hydrolysis for 25 mg of heparin.

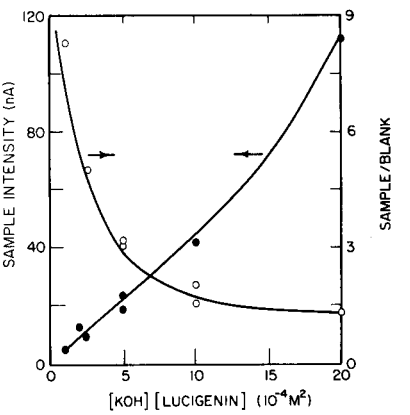

Fig. 2. Variation of chemiluminescent emission intensity with reagent concentrations: (•) emission intensity for sample; (○) emission intensity for sample divided by emission intensity for blank.

TABLE 1

Optimization of reagent concentrations

Concentrations		Signal intensity (nA)	
KOH (M)	Lucigenin (mM)	Blank	Sample
2	1	80.8	112.0
1	1	19.8	41.4
0.5	1	5.75	18.2
2	0.5	43.4	69.7
1	0.5	7.49	23.2
0.5	0.5	1.81	9.16
2	0.1	4.06	12.3
1	0.1	0.59	4.93

Calibration graph

Figure 3 shows a calibration graph for heparin samples from 60 μg to 10 mg. The data are linear over this range and yield a correlation coefficient of 0.9950. For a signal-to-noise ratio of 2, the detection limit is 90 μg of heparin. This concentration is in the 1—6 μM range depending on the molecular weight of heparin. The detection limit for this procedure is comparable to those for assay methods based on clotting time measurements [7], colorimetry of heparin-dye complexes [9], turbidimetric titration with polycations [12], chromatography [9, 13], and reaction rate-measurements [14].

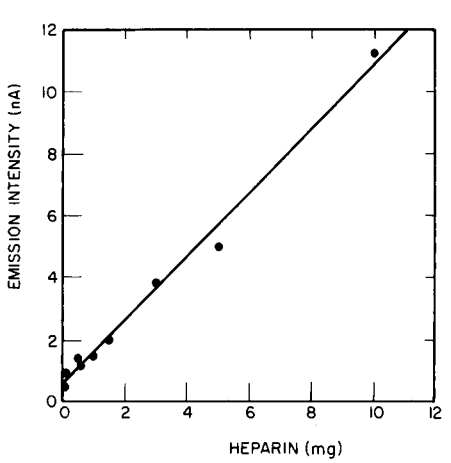

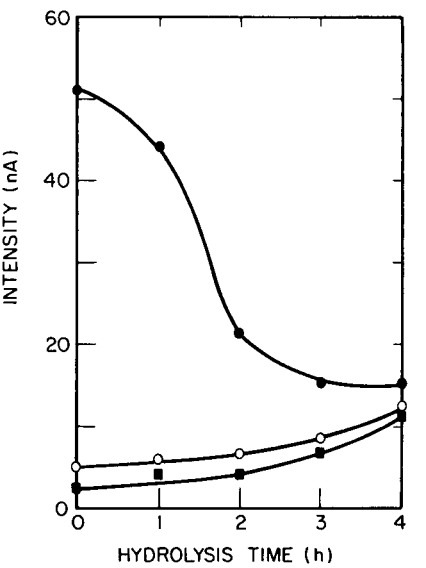

Fig. 3. Chemiluminescence calibration graph for heparin.

Fig. 4. Interferences: (▪) 1.25 mg heparin; (○) 1.25 mg heparin plus 3 mg glucose; (•) 1.25 mg heparin plus 0.5 mg ascorbic acid.

The precisions of both the chemiluminescence measurement step and the overall method are good. Repeated injections of the same hydrolyzed solution yielded a 2% relative standard deviation. To study the precision for the method, twelve samples, each containing 1.5 mg of heparin, were hydrolyzed separately (6 for 4 h and 6 for 8 h) and run through the entire procedure. The relative standard deviation was 10% for the 4-h hydrolysis and 4% for the 8-h hydrolysis.

Interferences

The concentration of free heparin in the blood is normally very low. A recent study has shown that the amount of endogeneous heparin, if any, in human blood is less than 2 ng ml^{-1} [8]. As a result, it is expected that chemical assay methods for heparin would find application with heparin preparations rather than for measurements in body fluids. However, the possible error introduced by the presence of other reductants that might be found in blood was examined.

Three batches of samples (each containing 1.25 mg of heparin) were subjected to acid hydrolysis for up to 4 h. The first batch contained only the heparin. The second batch also contained 3 mg of glucose in each sample, and the third also contained 0.5 mg of ascorbic acid in each sample. The concentrations were chosen to be representative of those found in body fluids. The results are shown in Fig. 4.

Ascorbic acid and glucose are typical of two different types of interference. Under the harsh conditions of hydrolysis used here, the ascorbic acid is unstable; both the absolute error and the relative error become very small as the hydrolysis time increases. Glucose is typical of an interference for which the signal is constant with time. Because the signal from heparin increases with time, the relative error from an interference like glucose decreases with time. If a milder degradation method were used (like the enzymatic procedure proposed later) then most or all interferences would behave like the glucose here. From the previous study of lucigenin and reductants, it was noted that the chemiluminescence intensity observed for a mixture of analytes was the sum of the intensities for each analyte separately [1]. Therefore, to discriminate against a constant interference, one can make chemiluminescence measurements on two portions of the same sample subjected to different degrees of heparin degradation and use the change in intensity rather than the absolute chemiluminescence intensities to quantify the heparin concentration.

Alternative degradation methods for heparin

Because almost all of the time required for the assay is needed for the hydrolysis, some consideration was given to alternative degradation methods. Nitrous acid depolymerizes heparin by cleaving the 2-amino-2-deoxy-D-glucosidic bonds. The reaction involves nitrosation of the amino groups, release of nitrogen, and ring contraction of the glucosamine groups to form

2,5-anhydro-D-mannose [15]. This reaction proceeds to completion in 10 min at room temperature [16]. Several heparin samples were treated with nitrous acid (generated in situ by adding sodium nitrite to sulfuric acid) and quantified by chemiluminescence. Only for samples containing 5—10 mg of heparin was the emission intensity significantly higher than the blank. Apparently, the product, 2,5-anhydro-D-mannose does not react well with lucigenin. Thus, although the nitrous acid degradation is far faster than the acid hydrolysis, the detection limit obtained with the acid hydrolysis is much lower.

An enzyme-catalyzed degradation would be more selective than the acid hydrolysis. By using a large enzyme concentration, the reaction time could be shortened sufficiently (say to 1 min) to make it practical to proceed all the way to complete degradation and thus obtain better sensitivity and precision. The enzyme, heparinase (EC.4.2.2.7), degrades heparin into reducing disaccharide units [6, 8, 9]. This enzyme has only just recently become commercially available. The present cost per unit is extremely high and it is fiscally impractical to consider use of large amounts of this enzyme at this time.

Conclusion

This work demonstrates that lucigenin-based chemiluminescence can be successfully applied to determinations of large biomolecules. For this investigation, stopped-flow instrumentation was chosen because of its general versatility and because it is then possible to examine the entire reaction profile. The chemiluminescence measurement can be done easily in a flow-injection system instead [17]. A flow-injection system would be particularly attractive if and when a more economical source of heparinase becomes available; a column of immobilized enzyme could be incorporated directly into the flow stream. We have had success using such a system with lucigenin chemiluminescence and other enzyme/substrate combinations. Detection limits and precisions are similar to those reported here, and a total time for the assay is about 5 min per sample.

This research was supported in part by the National Science Foundation (CHE-78-01614 and CHE-81-08816).

REFERENCES

1 R. L. Veazey and T. A. Nieman, Anal. Chem., 51 (1979) 2092.
2 R. L. Veazey and T. A. Nieman, J. Chromatogr., 200 (1980) 153.
3 S. R. Delaney, M. Leger and H. E. Conrad, Anal. Biochem., 106 (1980) 253.
4 K. Diem and C. Lentner (Eds.), Scientific Tables, Geigy Pharmaceuticals, Ardsley, NY, 1970, p. 327.
5 M. Windholz (Ed.), Merck Index, 9th edn., Merck & Co., Rahway, NJ, 1976, pp. 607—8.
6 J. Ehrlich and S. S. Stivala, J. Pharm. Sci., 62 (1973) 517.
7 D. Triplett, Ther. Drug Monit., 1 (1979) 173.

8 W. D. Comper, Heparin (and Related Polysaccharides), Gordon and Breach, New York, 1981.
9 L. B. Jaques, in D. Glick (Ed.), Methods of Biochemical Analysis, Vol. 24, Wiley, NJ, 1977, 203.
10 A. B. Foster and A. J. Huggard, in M. L. Wolfrom (Ed.), Advances in Carbohydrate Chemistry, Vol. 10, Academic Press, NY, 1955, 335.
11 M. L. Wolfrom and J. V. Karabinos, J. Am. Chem. Soc., 67 (1945) 679.
12 T. Katayama, K. Takai, R. Kariyama and Y. Kanemasa, Anal. Biochem., 88 (1978) 382.
13 R. Losito, H. Gattiker and G. Bilodeau, J. Chromatogr., 219 (1981) 61.
14 P. Band and A. Lukton, Anal. Biochem., 120 (1982) 19.
15 J. E. Shively and H. E. Conrad, Biochemistry, 15 (1976) 3932.
16 J. E. Shively and H. E. Conrad, Fed. Proc., 36 (1977) 28.
17 D. Pilosof and T. A. Nieman, Anal. Chem., 54 (1982) 1698.

Analytica Chimica Acta, 155 (1983) 131—138
Elsevier Science Publishers B.V., Amsterdam — Printed in The Netherlands

A SIMPLE PROCEDURE FOR STANDARD ADDITIONS IN FLOW INJECTION ANALYSIS
Spectrophotometric Determination of Nitrate in Plant Extracts

M. F. GINÉ, B. F. REIS, E. A. G. ZAGATTO, F. J. KRUG* and A. O. JACINTHO[a]

Centro de Energia Nuclear na Agricultura-USP, Caixa Postal 96, 13400 Piracicaba, SP (Brasil)

(Received 24th May 1983)

SUMMARY

The standard additions method with constant sample volumes is readily achieved in a flow injection system if zone sampling is used to select segments with different concentration levels from the dispersed zone of a known standard, and these segments are merged with the sample zone. This system requires a single standard solution, is suitable for routine large-scale analyses, and does not need complex equipment. The number, sequence and level of additions are chosen in accordance with the required sampling rate, the speed of the method and the mean analyte content in the samples. Details of system design, stability and potential are discussed. As an application, this system was used in the spectrophotometric determination of nitrate in plant extracts where the standard additions method is required to overcome the matrix effect. The results, based on twelve additions per sample (about 100 measurements per hour) agree with those obtained by the corresponding manual procedure.

Although the standard additions method is often necessary for improving accuracy, its usefulness in routine large-scale analyses is limited by the manipulations involved, which drastically reduce the sampling rate. Also, some applications require larger sample and reagent volumes. To minimize these drawbacks, there is a tendency to reduce the number of additions per sample, which diminishes the precision of the results [1]. The feasibility of using standard additions in flow injection analysis (f.i.a.) [2] was first reported by Giné et al. [3] and was demonstrated recently in atomic absorption [4, 5] and emission [6] spectrometry. In the latter application, a generalized standard additions method [7] with three levels of additions of all elements being determined was used to overcome both spectral interferences and matrix effects. The inherent high sampling rate of f.i.a., the low consumption of samples and reagents, and the good precision enable standard additions to be used without difficulty in routine work.

The standard additions method requires the preparation of a large set of

[a]Present address: Escola Superior de Agricultura "Luiz de Queiroz", Universidade de São Paulo, Brasil.

0003-2670/83/$03.00

standards to permit several levels of additions at different concentrations. In f.i.a. this can be done with the zone-sampling process [8]: several standard additions can be made at constant total volume so that the sample matrix effect is kept constant during the application of the standard additions. In this case, a standard A (Fig. 1A) is introduced into the first carrier stream (C_A) creating a zone which undergoes continuous dispersion while being pushed through the dispersion coil (D_C) by the carrier stream towards waste (W). After a time interval Δt, a small portion ΔA of the dispersed zone is resampled and introduced into the second carrier stream (C'_A). Simultaneously the sample (S) is injected into its carrier stream (C'_S), the two established zones merging at the confluence point y. This provides reproducible addition of the standard to the sample zone [6]. The coalesced zones are then directed towards the measurement system (M), participating in all the required physicochemical steps before detection. Each Δt value defines a given amount of standard [8] for the single standard solution A. Therefore, several standard additions can be achieved by selecting suitable Δt values. The mathematical treatment of this standard additions method at constant sample volume is given elsewhere [9]; the equations are adapted for the present situation in which there are no regular stepwise additions.

To illustrate the method, the spectrophotometric determination of nitrate in plant extracts is described. The procedure involves reduction of nitrate to nitrite, diazotization and coupling with *N*-(1-naphthyl)ethylenediammonium dihydrochloride [3]. The proposed system is used to overcome the sample matrix effect on this modified Griess reaction and on the efficiency of the reduction column when the earlier f.i.a. procedure for water analysis [3] is applied to plant extracts.

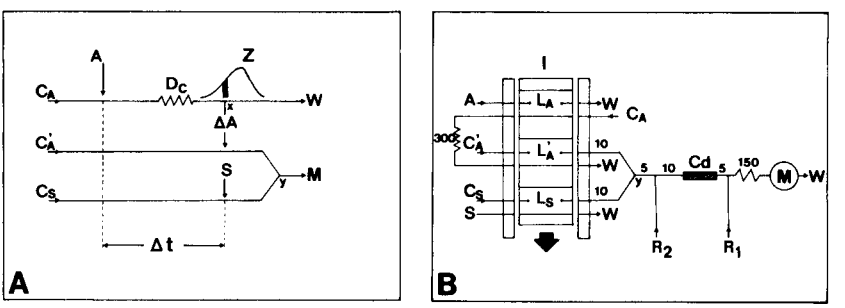

Fig. 1. A general f.i.a. system for standard additions (A) and the system designed for nitrate determination (B). S, aqueous sample at an aspiration rate of 2.0 ml min^{-1}; A, 15.0 mg l^{-1} NO_3^--N standard pumped at 2.0 ml min^{-1}; C_A, C'_A, C_S, water carrier streams flowing at 6.8, 2.5 and 2.5 ml min^{-1}, respectively; L_A, L'_A, L_S, 15-cm loops (ca. 75 μl); R_2, buffer solution at 1.0 ml min^{-1}; R_1, colour reagent at 1.0 ml min^{-1}; Cd, column packed with cadmium filings; M, spectrophotometer at 540 nm; I, injector/commutator; W, waste. Numbers represent tubing lengths, in cm; y indicates confluence points. For details, see text.

EXPERIMENTAL

Apparatus, reagents, standards and samples

All components of the f.i.a. system have already been described [8]. A microcomputer system based on the Intel SDK-85 was used to control the injector-commutator, generating the Δt scans, furnishing the preselected Δt values and specifying other parameters such as number of replications, number of additions, sequence, etc. Details of software, hardware and interfaces are available on request.

The reagents, including the cadmium filings for the reduction column were of analytical-reagent quality. Freshly distilled-deionized water was used throughout. The colour-forming reagent (R_1, Fig. 1B) was 2% (w/v) sulphanilamide, 0.1% (w/v) *N*-(1-naphthyl)ethylenediammonium dihydrochloride in 8% (v/v) phosphoric acid solution. The buffer solution (R_2) contained 10% (w/v) ammonium chloride, 2% (w/v) sodium tetraborate (12 H_2O) and 0.1% (w/v) Na_2EDTA. These solutions and the copperized cadmium filings were prepared as described earlier [3].

The aqueous 1000 mg l^{-1} NO_3^--N stock solution (6.07 g l^{-1} $NaNO_3$) and the 1000 mg l^{-1} NO_2^--N stock solution (4.92 g l^{-1} $NaNO_2$) were kept in a refrigerator; the latter solution was standardized against potassium permanganate. Nitrite standards were used from time to time to check the reduction efficiency.

The plant extracts were prepared by shaking 500 mg of dried ground leaves with 100 ml of hot water (ca. 80°C) for 5 min. After filtration, 10.0 ml of the extract was neutralized with sodium hydroxide and 0.2 ml of 36% (w/v) hydrogen peroxide was added. The mixture was evaporated to dryness, and the residue was taken up with 100 ml of water. Extracts containing more than 15 μg of nitrate-nitrogen were diluted appropriately with water.

The f.i.a. standard additions system

The system for the determination of nitrate in plant extracts (Fig. 1B) employs zone sampling [8] and merging zones, coupled to a flow injection system similar to that used for the simultaneous determination of nitrate and nitrite in natural waters [3]. The portions of the manifold related to nitrite determination were not necessary because the nitrite content in the samples was negligible after treatment with hydrogen peroxide, and the R_1 reagent was added continuously. The main carrier stream (5.0 ml min^{-1} in the earlier work [3]) was replaced by two confluent streams flowing at 2.5 ml min^{-1} each, to allow the standard additions via a symmetrical merging zones configuration, with a 50% dilution of the sample zone at point y (Fig. 1). This configuration was preferred because sensitivity was not a limiting factor. Also, mixing of the merging zones seems to be better in symmetrical systems.

It must be emphasized that the f.i.a. configuration used in the system proposed for evaluation of selectivities [10] was not employed here, because

the matrix effect would not be constant during the application of the standard additions method and perfect overlap between the sample and standard zones would probably not be attained.

The parts of the manifold related to the zone-sampling process had the following dimensions: the L'_A and L_S loops, which are identical in symmetrical systems, were fixed as 15 cm long (ca. 75 μl) in accordance with the mean nitrate contents in the samples and the sensitivity of the spectrophotometric method. The length of the D_C dispersion coil was 300 cm and the pumping rate for C_A was 6.8 ml min^{-1}. When D_C was only 50 or 100 cm long, erratic results were obtained. The length of D_C cannot, however, be increased at will, to avoid the need for excessive C_A pumping rates with consequent troubles related to the increased hydrodynamic pressure. Of course, if D_C is increased without increasing the C_A pumping rate, the frequency of sampling can be affected. Care is necessary to avoid pronounced concentration gradients along L'_A, as initial experiments indicated that when C_A was counterflow relative to C'_A, there were significant changes in the recorded peak shapes when L'_A was longer than 100 cm. Finally, the length of the L_A loop was chosen as 15 cm so that a relatively concentrated standard solution (15.0 mg l^{-1} NO_3^--N) could be used.

Procedure

Initially, nitrate standards in the range 0.00—5.00 mg l^{-1} NO_3^--N were measured in triplicate instead of the sample, with the A solution being water. Next, water was injected, simulating the sample, and the 15.0 mg l^{-1} NO_3^--N standard was restored in A (Fig. 1), to obtain measurements of the generated standard corresponding to the different Δt values. This procedure gives information about the linearity of the response, the distribution of the zone near point x (Fig. 1A) [8] and the exact amounts of added standards, regardless of the dispersion factors involved and a possible asymmetry of the merging zones configuration. In this experiment, the Δt values were varied in the range 10—30 s in steps of 0.5 s; the total sampling period (or cycle) was kept at 35 s (maximum) so that a measurement rate of about 100 h^{-1}, similar to the sampling rate of the earlier method [3], was achieved.

Thereafter twelve Δt values were selected in accordance with the expected nitrate contents in the extracts. Because of the number of levels of additions, replication was not necessary in treating the samples. After all the samples had been measured with twelve additions each, the R_1 reagent (Fig. 1A) was replaced by an 8% (v/v) phosphoric acid solution and the samples were run again, without additions (Δt = 4 s) in order to obtain the blank values. The net peak heights were then calculated by subtracting the peak heights corresponding to blank measurements from those originally recorded. This operation is necessary because the standard additions method requires the analytical signal to be zero in absence of the analyte [1], i.e., no blank is allowed.

The results were calculated by linear regression [5, 9]. The ordinate data

were the net peak heights measurements, in arbitrary units, and the corresponding abscissa, the added concentrations, in mg l^{-1} NO_3^--N, defined as above. No correction factor was employed because the mean volume of the sample zone was not affected by the additions. For comparison, standard additions (100 μl) of 0.00, 5.00, 10.0 and 15.0 μg of NO_3^--N were made to 10.0-ml aliquots of each sample manually with triplicate measurements.

RESULTS AND DISCUSSION

With the proposed system, standard additions can be made when 12.5 s < Δt < 30.0 s (Fig. 2). For lower Δt values, the standard dispersed zone does not reach L'_A before commutator switching, and for higher Δt values, L'_A is bypassed. If water replaces the sample, a picture corresponding to the different nitrate concentrations to be added is obtained (Fig. 2, left). A calibration

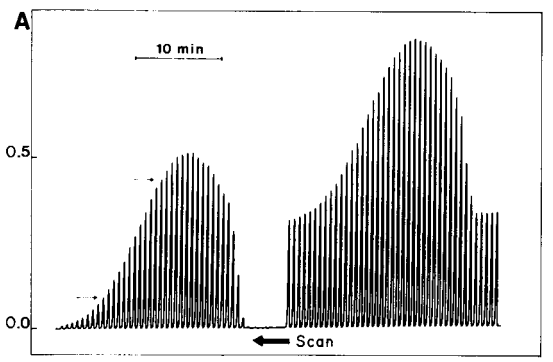

Fig. 2. Recorder outputs obtained with the system of Fig. 1 with Δt values of 10.0, 10.5, 11.0 ... 30.0 s. To the left is shown the output without samples. The series of 41 peaks to the right represents the output for the application of standard additions to an extract of lettuce leaves. The range within the arrows refers to Fig. 3.

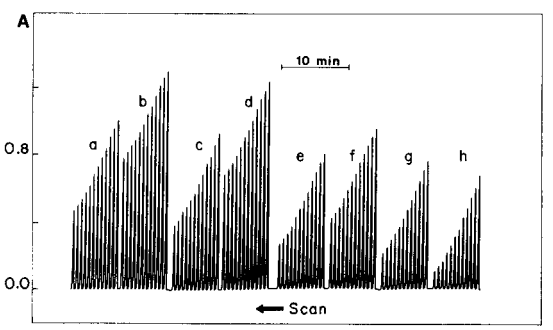

Fig. 3. Routine determination of nitrate in water and in aqueous plant extracts. In each case, the twelve measurements are set in the Δt range specified in Fig. 2; each series corresponds to one sample. Samples: (a) rice shoots; (b) soybean leaves; (c) CENA 1 (reference material from CENA); (d) coffee leaves; (e) cotton leaves; (f) lettuce leaves; (g) vine leaves; (h) water.

TABLE 1

Determination of nitrate in plant extracts (data refer to Fig. 3)

Δt values (s)	Added NO_3^--N (mg l^{-1})	Net peak heights[a] (mm)							
		Water	Vine	Lettuce[b]	Cotton	Coffee	CENA1	Soybean	Rice
10.0	0.2251	13	27	52.5	33	86	48	97	59
10.5	0.2597	15	31	56.5	37	89	52	10.2	63.5
11.0	0.3463	20	36	60	41	94	58	106.5	68
11.5	0.4675	27	41	67	46	99.5	62	110.5	72
12.0	0.5714	33	46	73	53	106	67	117	77
12.5	0.6753	39	53	80	60	113	72	122.5	85
13.0	0.7619	44	59	85.5	66	118	79	131	91
13.5	0.9264	53.5	67	94	72	126	86	136	98
14.0	1.0389	60	73	100	80	134.5	94	144	104
14.5	1.1861	68.5	80.5	107	86	141.5	99	152	113
15.0	1.3159	76	88	113.5	93.5	147	107	157	119
15.5	1.4718	85	95	119.5	99.5	154	116	162	126
Linear regression data	r	1.0000	0.9996	0.9991	0.9991	0.9993	0.9993	0.9983	0.9992
	Slope	57.75	54.27	54.47	53.75	55.45	52.89	52.90	53.64
Nitrate content[c] (mg l^{-1} NO_3^--N)	Proposed method	—	0.30	0.77	0.42	1.35	0.71	1.65	0.90
	Manual method	—	0.29	0.83	0.41	1.45	0.70	1.60	0.86

[a]12.5 mm = 0.100 absorbance. The peak heights relate to a sample of distilled water put through the procedure (to indicate later matrix effects) and to extracts from various leaf samples. [b]After 100-fold dilution with water. [c]Referred to extracts.

graph was used to evaluate the effective added concentrations and to check the linearity up to an absorbance of 1.8 (r = 0.9997, N = 15). The peak heights of Fig. 2 (left) correspond to the exact added concentrations related to the different Δt values. Relative standard deviations (r.s.d.) of the peak height measurements were calculated by replicating the Δt scan six times during a total 6-h working period, so that system stability could be evaluated. As expected, the r.s.d. is higher (4.5—15.7%) when 12.5 s $< \Delta t <$ 14.0 s because this situation causes the sampling of the frontal portion of the standard zones (Z, Fig. 1A), in which the concentration gradient is more pronounced and the time available for dispersion is shorter than for other portions. Small r.s.d. values (<2.3%) were attained near the top of the peak (14.5 s $< \Delta t <$ 20.5 s) because the concentration gradient diminishes, leading to a more stable situation. Similar r.s.d. values were calculated for the tailed portion of the Z zone, i.e., 20.5 s $< \Delta t <$ 26.0 s. For $\Delta t >$ 26.0 s, measurement precision deteriorated because the signal available for measurement, corresponding to the most dilute tailed portion of the dispersed zone, fell outside the range of the spectrophotometric method. It must be stressed that the above values indicate the short-term (6 h) stability of the system, and do not reflect the precision of measurement, for which the r.s.d. was <0.5% when 14.5 s $< \Delta t <$ 26.0 s.

The right-hand portion of Fig. 2 was obtained similarly, with a plant extract as sample. As can be seen, this output is essentially the same as the standard additions output, superimposed on the sample signal, with small variations caused by the matrix effect. The measurement of the sample without additions is characterized by the four peaks to the right.

Figure 3 is a sequence of eight samples taken through the proposed method with 20.5 s $< \Delta t <$ 26.0 s; the corresponding results are presented in Table 1. The usefulness of the standard additions method is validated by the linear regression data; the slopes indicate clearly the magnitude of the matrix effect. The results obtained by the proposed method agree well with those obtained by the manual standard addition procedure, no significant statistical difference between methods being found at the 99% level.

Partial support of this research by FINEP (Financiadora de Estudos e Projetos) and CNPq (Conselho Nacional de Desenvolvimento Científico e Tecnológico) is greatly appreciated. The authors thank Célio Pasquini and M. C. U. Araújo for critical comments, O. E. S. Godinho for providing equipment and P. B. Vose for correcting the manuscript.

REFERENCES

1 J. Kragten and A. Parczewski, Talanta, 28 (1981) 901.
2 J. Růžička and E. H. Hansen, Flow Injection Analysis, Wiley-Interscience, New York, 1981.
3 M. F. Giné, H. Bergamin F^{q}, E. A. G. Zagatto and B. F. Reis, Anal. Chim. Acta, 114 (1980) 191.

4 J. F. Tyson, Anal. Proc., 18 (1981) 542.
5 J. F. Tyson, J. M. Appleton and A. B. Idris, Anal. Chim. Acta, 145 (1983) 159.
6 E. A. G. Zagatto, A. O. Jacintho, F. J. Krug, B. F. Reis, R. E. Bruns and M. C. U. Araújo, Anal. Chim. Acta, 145 (1983) 169.
7 B. E. H. Saxberg and B. R. Kowalski, Anal. Chem., 51 (1979) 1031.
8 B. F. Reis, A. O. Jacintho, J. Mortatti, F. J. Krug, E. A. G. Zagatto, H. Bergamin F° and L. C. R. Pessenda, Anal. Chim. Acta, 123 (1981) 221.
9 M. Bader, J. Chem. Ed., 57 (1980) 703.
10 E. H. Hansen, J. Růžička, F. J. Krug and E. A. G. Zagatto, Anal. Chim. Acta, 148 (1983) 111.

Analytica Chimica Acta, 155 (1983) 139—150
Elsevier Science Publishers B.V., Amsterdam — Printed in The Netherlands

SPECTROPHOTOMETRIC DETERMINATION OF HYDROGEN PEROXIDE AND ORGANIC HYDROPEROXIDES AT LOW CONCENTRATIONS IN AQUEOUS SOLUTION

JANE E. FREW, PETER JONES* and GEORGE SCHOLES

Radiation and Biophysical Chemistry Laboratory, School of Chemistry, University of Newcastle upon Tyne, Newcastle upon Tyne, NE1 7RU (Great Britain)

(Received 13th June 1983)

SUMMARY

Five procedures are presented for the determination of hydrogen peroxide and organic hydroperoxides (including organic peroxyacids) at concentrations of 1—10 μM in aqueous solution. All five are spectrophotometric methods, based on formation of phenolphthalein or triiodide, catalytic dye bleaching, coupled oxidation of NADPH, and horseradish peroxidase-coupled oxidations. Each is evaluated in terms of sensitivity, selectivity and reliability. The method based on coupled oxidation of NADPH is the most widely applicable to peroxidic species, whereas the horseradish peroxidase method can be made highly selective for hydrogen peroxide.

Techniques for the identification and determination of peroxides find application in diverse analytical situations. This is exemplified by the multitude of procedures to be found in the literature (for reviews, see refs. 1—3) ranging from those designed for industrial purposes to clinical assays employed in monitoring the composition of body fluids. However, few have proven suitable or reliable when dealing with peroxides at concentrations as low as 1—10 μM (10^{-6}—10^{-5} mol dm^{-3}). The primary objective of this work was the development of quantitative spectrophotometric methods for the determination of peroxides in this concentration range.

The investigation was motivated by a need for sensitive techniques to identify and measure yields of peroxidic species in the γ-radiolysis of aqueous systems. Such experiments require the detection of small amounts of hydrogen peroxide and organic peroxidic material in the presence of other radiolysis products and unmodified solute. Previous workers in this field employed three principal techniques. The first of these, developed by Eisenberg in 1943 is based on the formation of a yellow complex on reaction of H_2O_2 with titanium(IV) sulphate under acidic conditions [4]. At room temperature the reagent is highly selective for H_2O_2, but somewhat insensitive with ϵ = 720 l mol^{-1} cm^{-1} at 410 nm [5]. Oxidation of iodide ions by peroxides and measurements of iodine as triiodide is considerably more sensitive; according to Allen et al. [6], $\epsilon(I_3^-)$ at 350 nm is 2.5 × 10^4 l mol^{-1} cm^{-1}; a

0003-2670/83/$03.00

slightly lower value of 2.3×10^4 l mol^{-1} cm^{-1} at 352 nm is reported here. This method has commonly been used to assess peroxide (particularly hydrogen peroxide) in irradiated systems; however, as discussed below, problems can arise as a result of interference by other solutes in the system. The xylenol orange method, which involves the oxidation of iron(II) ions to iron(III) and subsequent formation of a coloured complex with xylenol orange [7—9], is also sensitive (ϵ for the Fe(III)-complex at 540 nm is 2.68×10^4 l mol^{-1} cm^{-1}) but can be unreliable in some systems where chain processes can ensue [10]. More recently [11], the copper(II) ion-catalysed peroxidic oxidation of phenolphthalin to phenolphthalein [1] has been used to estimate peroxidic material formed in irradiated solutions of nucleic acid components.

The aims of the present investigation were to modify existing analytical procedures and to devise new methods for measurement of 1—10 μM peroxidic material. In order to assess these methods, hydrogen peroxide, cumene and t-butyl hydroperoxides, peracetic acid and *m*-chloroperoxybenzoic acid were used as test materials. An evaluation of the advantages and disadvantages of each assay for these particular peroxides is presented.

PHENOLPHTHALIN METHOD

Peroxides will oxidise phenolphthalin to the common indicator phenolphthalein in the presence of a Cu^{2+} catalyst [1]. Under alkaline conditions the resultant phenolphthalein can be measured spectrophotometrically at 552 nm and related to peroxide concentration. This technique has previously been employed in an industrial capacity to estimate oxidants in air [12, 13] and has also formed the basis of an automatic colorimetric method for peroxide analysis [14].

Experimental

Reagents. Materials should be of analytical-reagent grade whenever possible and triple-distilled water used for the preparation of reagent solutions and in all dilutions (this also applies to the other methods examined).

Phenolphthalin stock solution is prepared as follows: 1 g of phenolphthalein, 10 g of sodium hydroxide, 5 g of zinc dust and 20 ml of water are refluxed together on a boiling water bath until the solution is colourless. After cooling, the solution is filtered through a No. 4 sintered glass crucible and then diluted with 50 ml of distilled water. The phenolphthalin is stored over granulated zinc in a closed bottle, in the dark, at 4°C.

Phenolphthalin/copper sulphate reagent is prepared by adding 0.24 ml of the phenolphthalin stock solution to approximately 80 ml of water; after addition of 0.48 ml of 0.01 M copper sulphate solution, the volume is made up to 100 ml. This reagent should be freshly prepared on the day of use.

Peroxides. Samples of the following peroxides were obtained from Laporte Industries Ltd., General Chemicals Division, Widnes, Cheshire. The

standard analytical method used to estimate the concentrations of stock peroxides is given in parentheses: hydrogen peroxide (titration with cerium-(IV) to a ferroin end-point [15]); cumene and t-butyl hydroperoxides (reduction with iodide in acetic acid/chloroform [16]); peracetic acid and *m*-chloroperoxybenzoic acid (iodimetric titration [17]). Approximately 10^{-5} M solutions were prepared by quantitative dilution of $\approx 10^{-3}$ M stock solutions.

Apparatus. A Pye-Unicam SP1800 u.v.-visible recording spectrophotometer was used with thermostatted cell compartments.

Procedure. The peroxide solution is added to 5 ml of the phenolphthalin/copper sulphate reagent and the volume made up to 10 ml with water. The solution is maintained at 25°C during the period required for maximum colour development (this may be 40 min or longer depending on the peroxide). The absorbance of each solution is then recorded over the range 520—570 nm, a maximum being observed at 552 nm. A blank containing no peroxide is prepared with each series of samples and serves as a reference for the spectrophotometric measurements.

Results and discussion

Calibration graphs of absorbance versus peroxide concentration for H_2O_2 and *m*-chloroperoxybenzoic acid are shown in Fig. 1. Colour formation was too slow with cumene and t-butyl hydroperoxides to allow meaningful results to be obtained. The solid line corresponds to a molar absorptivity of 3.3×10^4 l mol^{-1} cm^{-1} at 552 nm determined from the spectrum of phenolphthalein in a solution containing phenolphthalin, copper sulphate and sodium hydroxide at the concentrations used in the assay (the literature value for the molar absorptivity of phenolphthalein in the range 550—555 nm is 2.66×10^4 l mol^{-1} cm^{-1} [18]). The non-linearity, particularly of the H_2O_2 calibration graph, is probably due to a copper-catalysed decomposition of peroxide which becomes increasingly significant at higher peroxide concentrations. Copper salts are known to catalyse H_2O_2 decomposition [19] and other possible explanations such as catalyst inactivation were eliminated through experiment. Attempts to find an alternative catalyst for the assay have as yet proved unsuccessful.

A severe limitation on the use of the phenolphthalin method is that colour development is relatively slow with the accessible range of catalyst concentration. The alkaline nature of the reagent leads to the formation of a gelatinous precipitate at elevated Cu^{2+} concentrations. Heat cannot be used to increase the rate of reaction as this results in the oxidation of phenolphthalin in the absence of peroxide.

The use of this system in the analysis of mixtures of peroxides is complicated by the fact that coincident calibration graphs may not be obtained with different peroxidic species (Fig. 1). So, although this technique has found important industrial and environmental applications, it is not easily made quantitative under the conditions required when H_2O_2 is present. The high sensitivity of the assay, however, may render it a useful tool for the determination of given peroxides.

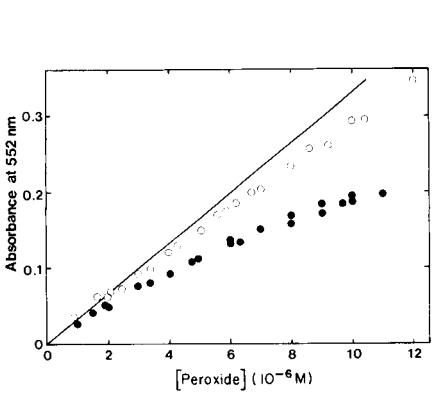

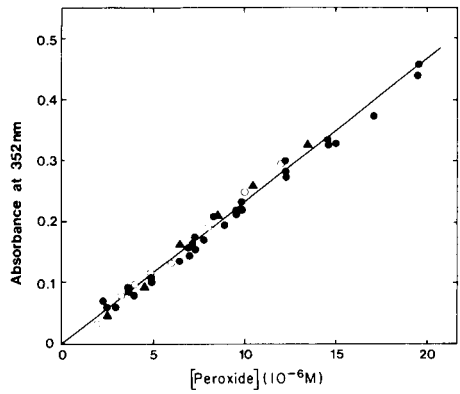

Fig. 1. Phenolphthalin method. Calibration graphs: (•) H_2O_2; (○) *m*-chloroperoxybenzoic acid. The solid line corresponds to the molar absorptivity for phenolphthalein determined by experiment (see text for details).

Fig. 2. Iodide method. Calibration graph: (•) H_2O_2; (○) *m*-chloroperoxybenzoic acid; (▲) peracetic acid—H_2O_2 mixtures.

IODIDE METHOD

Oxidation of iodide is the most widely used of all the reactions for peroxide determinations. Various iodide procedures have been designed, each attempting to remedy earlier deficiencies [2]. The method described here is based on that of Allen et al. [6] and involves oxidation of potassium iodide by H_2O_2 and organic hydroperoxides in the presence of an ammonium molybdate catalyst; the liberated iodine is determined spectrophotometrically as I_3^- at 352 nm.

Experimental

Reagents. Solution A (500 ml) contains 33 g of potassium iodide, 1 g of sodium hydroxide and 0.1 g of ammonium heptamolybdate. Solution B (500 ml) contains 10 g of potassium hydrogenphthalate. Peroxides were the same as for the phenolphthalin method.

Procedure. Solutions A and B (2 ml each) and an appropriate quantity of peroxide solution are mixed in a total volume of 10 ml. The liberated iodine is then measured as triiodide by recording the absorbance of the solution at 352 nm and 25°C.

Results and discussion

In the presence of ammonium molybdate catalyst, rapid oxidation of iodide occurs with H_2O_2 and the more reactive hydroperoxides. Figure 2 shows the calibration graph obtained with H_2O_2, *m*-chloroperoxybenzoic acid and peracetic acid—H_2O_2 mixtures. Reaction of cumene or t-butyl hydroperoxide with iodide is too slow under the above experimental conditions.

From these data a molar absorptivity of 2.3×10^4 l mol^{-1} cm^{-1} at 352 nm is obtained (trace reducing impurities in the reagents can lead to variations in the measured absorptivity).

Despite the advantages of high sensitivity and a linear calibration, there are limitations on the use of the iodide method. Any species in solution which can react with iodide (to enhance iodine production) or iodine (resulting in bleaching of the iodine colour) will interfere. This problem was encountered in the determination of peroxide yields in the γ-radiolysis of oxygenated solutions of pyrimidines, dihydropyrimidines and polynucleotides where reaction products such as barbituric acid can react with the liberated iodine, leading to a rapid bleaching [20]. In a given system, therefore, it may be necessary to check the results by independent means.

CATALYTIC DYE BLEACHING

Iron—porphyrin complexes (ferrihaems) are efficient catalysts in the decomposition of peroxides [21]. The catalyst is activated by reaction with hydroperoxide forming an oxidised iron—porphyrin intermediate which can then react with suitable donor molecules in a one-electron oxidation of substrate:

$$\underset{\text{Iron—porphyrin}}{2Fe(III)} + ROOH \rightarrow \underset{\text{Intermediate}}{2Fe(IV)} + ROH$$

$$Fe(IV) + \underset{\text{Donor}}{D} \rightarrow Fe(III) + D^+$$

This reaction sequence forms the basis of a determination of peroxides by measuring the extent of the oxidation of the donor. The iron(III) complex of deuteroporphyrin-IX, deuteroferrihaem (I) was chosen as catalyst because its reactions are well characterised [21], with a coal tar dyestuff, Black PN (II) as substrate. The oxidation products of the latter are colourless and the bleaching can be monitored spectrophotometrically. The reaction between ferrihaem and hydroperoxide is strongly pH-dependent, RO_2^- being the reactive species [22]. The determination is therefore done at pH >10 to increase the rate of intermediate formation, and hence, dye bleaching.

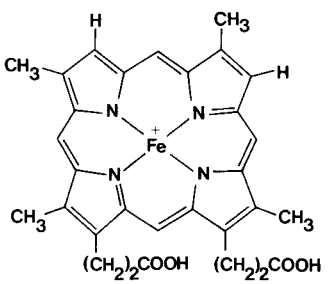

(I)

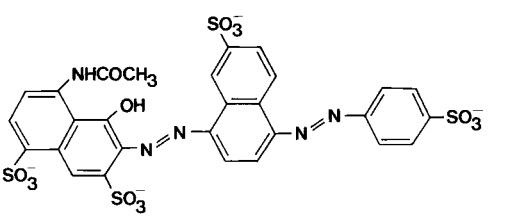

(II)

Experimental

Reagents. A stock solution (1.56 mg ml^{-1}) of Black PN (L. J. Pointing and Sons Ltd., Newcastle upon Tyne) is prepared in water. Chlorodeuteroferrihaem is prepared from chloroprotoferrihaem (haemin chloride, purum; Fluka A.G., Buchs, Switzerland) by the resorcinol melt method [23]. A stock deuteroferrihaem solution (ca. 170 μM) is prepared by dissolving the appropriate quantity of the solid in 2 ml of 0.1 M sodium hydroxide and then adding water to make up the volume required.

The 0.5 M carbonate buffer, pH 10.1 contains 19.03 g of sodium carbonate (anhydrous) and 5.92 g of sodium hydrogencarbonate (anhydrous) per 500 ml.

The dye—deuteroferrihaem reagent (100 ml) contains 3 ml of stock Black PN solution, 60 μM deuteroferrihaem and 0.2 M carbonate buffer.

Procedure. The peroxide is added to 5 ml of the dye/ferrihaem solution contained in a 10-ml volumetric flask and the volume is completed with water. Anomalous results are obtained in the presence of oxygen, so rigorous deaeration of all solutions is necessary. This is achieved by bubbling with nitrogen before and after mixing of components. The peroxide—reagent mixture is transferred to a stoppered 2-cm pathlength cuvette (nitrogen flushed) and the bleaching of Black PN is monitored at 576 nm (25°C). The test solution is placed in the reference compartment of the spectrophotometer with a dye/ferrihaem solution in the sample compartment, so that bleaching of the dye results in an increase in absorbance.

Results and discussion

The calibration graph obtained for a range of peroxides is shown in Fig. 3. The relationship between the extent of dye bleaching and peroxide concentration is given by the equation ΔAbsorbance = 10.7×10^3 [Peroxide] $- 0.019$. The loss of peroxide implied by the negative intercept is considered to be due to an impurity in the dye. The calibration should therefore be checked for each batch of Black PN.

This technique provides a rapid method of assaying both H_2O_2 and organic hydroperoxides; the bleaching is complete within 2—5 min at 25°C for the more reactive peroxides. A range of dyestuffs can be employed which have different absorption spectra [24] providing some flexibility in the monitoring wavelength.

COUPLED OXIDATION OF NADPH

Glutathione peroxidase, EC 1.11.1.9., catalyses the reduction of hydroperoxides with glutathione (GSH) as the reductant:

$$2GSH + ROOH \xrightarrow[\text{Peroxidase}]{\text{Glutathione}} ROH + GSSG + H_2O$$

where R may be H or an organic residue. The enzyme exhibits a pronounced

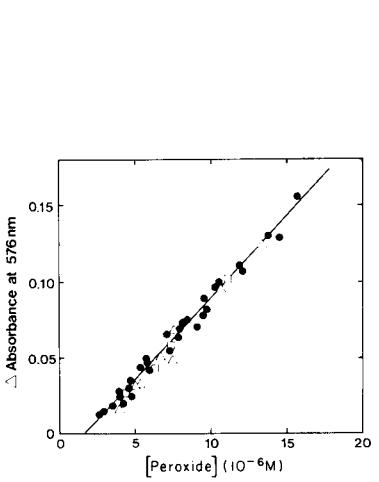

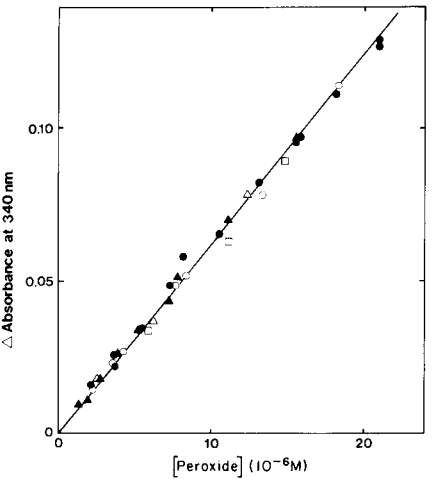

Fig. 3. Catalytic dye bleaching. Calibration graph: (•) H_2O_2; (□) t-butyl hydroperoxide; (△) cumene hydroperoxide.

Fig. 4. Coupled oxidation of NADPH. Calibration graph: (•) H_2O_2; (○) *m*-chloroperoxybenzoic acid; (□) t-butyl hydroperoxide; (△) cumene hydroperoxide; (▲) peracetic acid—H_2O_2 mixtures.

lack of selectivity towards acceptor substrates which range in complexity from H_2O_2 to nucleic acid and steroid hydroperoxides [25]. This reaction can be followed by measuring the coupled oxidation of NADPH in the presence of glutathione reductase:

$$GSSG + NADPH + H^+ \xrightarrow[\text{Reductase}]{\text{Glutathione}} 2GSH + NADP^+$$

The procedure described is based on a number of published methods [26—28].

Experimental

Reagents. Aqueous stock solutions of reduced glutathione, glutathione reductase (type III, yeast) and NADPH (tetrasodium salt, type X) (all from Sigma Chemical Company) and glutathione peroxidase (from bovine erythrocytes, crystalline form; Boehringer Mannheim) are prepared on the day of use.

Procedure. The components (except the peroxide) are mixed in a 1-cm pathlength cuvette in a total volume of 2 ml (see Table 1 for details). The solution is flushed with nitrogen for 5 min to minimise the natural oxidation of glutathione. The cuvette is then stoppered and the NADPH absorption at 340 nm recorded. An aliquot (0.5 ml) of peroxide solution (saturated with nitrogen) is added to the cuvette and the extent of NADPH oxidation is monitored. For each series of analyses, the hydroperoxide-independent

TABLE 1

Coupled oxidation of NADPH. Solutions added

Reagent	Volume (ml)	Final concentration
0.1 M phosphate buffer, pH 7.75	1.0	0.04 M
0.01 M EDTA	0.1	4×10^{-4} M
0.052 M sodium azide	0.2	4.2×10^{-3} M
~1×10^{-6} M glutathione peroxidase	0.2	~8×10^{-8} M
0.038 M reduced glutathione	0.2	3×10^{-3} M
1.4×10^{-3} M NADPH	0.1	5.6×10^{-5} M
Glutathione reductase (5 U ml^{-1})	0.2	1 U
Peroxide sample	0.5	

consumption of NADPH is measured in a solution to which 0.5 ml of water has been added instead of peroxide. For all spectrophotometric measurements, solutions are thermostatted at 25°C.

Results and discussion

The calibration is linear for the peroxides studied (Fig. 4) and the experimental data is a good fit to a line of slope equal to the published molar absorptivity for NADPH, i.e., 6.2×10^3 l mol^{-1} cm^{-1} at 340 nm [29].

Oxidation of NADPH is complete within 2—5 min at 25°C with most peroxides; 20—30 min is required with the less reactive cumene and t-butyl hydroperoxides. Sodium azide is an essential component of the assay system as it inhibits the activity of traces of catalase present in the commercial glutathione peroxidase preparation. This method provides a rapid means of determining peroxides at near physiological pH (the final pH of the reaction mixture is about 7.5) in contrast to the extremes of pH employed in the three methods described above.

HORSERADISH PEROXIDASE-COUPLED OXIDATIONS

The clinical determination of glucose, urate and cholesterol generally involves assaying the H_2O_2 formed by specific oxidase action by the peroxidase- or catalase-coupled oxidation of a donor substrate system yielding a coloured product, e.g.,

$$\text{Glucose} + O_2 \xrightarrow[\text{oxidase}]{\text{Glucose}} \text{Gluconate} + H_2O_2$$

$$H_2O_2 + \text{donor substrate} \xrightarrow{\text{Peroxidase}} \text{coloured product}$$

Commonly used substrates included benzidine, *o*-tolidine, *o*-toluidine and *o*-dianisidine until these compounds were shown to be carcinogenic. A search then commenced for alternative, less hazardous chromogens. A system devised by Trinder [30] and Barham and Trinder [31] for the determination of blood glucose utilises 4-aminoantipyrine and phenol as donor substrates.

$$2H_2O_2 + \text{4-aminoantipyrine} + \text{phenol} \xrightarrow{\text{Peroxidase}} \text{coloured product} + 4H_2O$$

The hydrogen peroxide oxidatively couples with 4-aminoantipyrine and phenol, in the presence of peroxidase to yield a chromogen (a quinoneimine dye) with a maximum absorption at 505 nm.

The following procedure is based on Trinder's method with modifications to optimise the system for detection of micromolar peroxide.

Experimental

Reagents. Horseradish peroxidase (type VI) and 4-aminoantipyrine (both from Sigma Chemical Company) and phenol (AnalaR; Hopkin and Williams) were used as received. The reagent solution (100 ml) contains 0.234 g of phenol, 0.10 g of 4-aminoantipyrine, 1 ml of 0.1 M phosphate buffer pH 6.9, about 2×10^{-8} M horseradish peroxidase, and about 2.5 μM H_2O_2.

Procedure. The 4-aminoantipyrine/phenol reagent (4 ml) is mixed with the peroxide in a total volume of 10 ml. The absorbance of the resulting solution is scanned over the range 490—520 nm until no further increase is observed (generally 2—5 min at 25°C). A reagent/water mixture serves as a reference for the spectrophotometric measurements.

Results and discussion

A trace impurity in the 4-aminoantipyrine samples interfered in preliminary calibration experiments leading to linear calibration curves with a negative y-intercept. Inclusion of a small quantity of H_2O_2 (ca. 2.5 μM) in the 4-aminoantipyrine/phenol reagent (used both for assay and blank) eliminates the problem. The calibration obtained with H_2O_2 (Fig. 5) yields a molar absorptivity of 6.4×10^3 l mol^{-1} cm^{-1} at 505 nm. Variation of the pH and/or the concentration of phosphate buffer employed has only a small effect on the molar absorptivity, but can lead to a decreased stability of the coloured complex. The conditions quoted were found to be the most suitable for maximum colour stability.

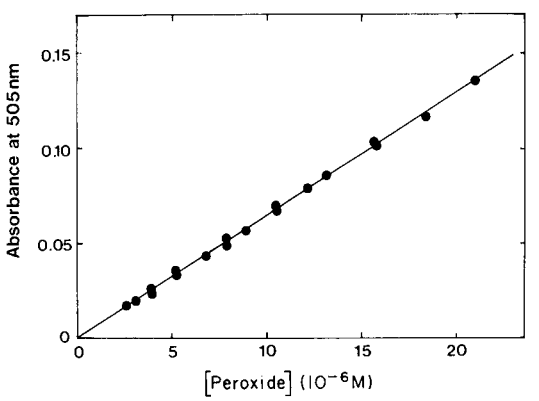

Fig. 5. Horseradish peroxidase-coupled oxidation. Calibration graph with H_2O_2.

The use of horseradish peroxidase as catalyst in this chromogenic system would be expected to confer some degree of peroxide substrate selectivity in the assay. The active site of the enzyme discriminates between hydroperoxides on electrostatic and/or steric grounds [32]. No reaction was observed with cumene and t-butyl hydroperoxides. An additional source of substrate selectivity probably arises from the high concentration of phenol (ca. 10^{-2} M) in the assay mixture relative to the enzyme concentration (ca. 8×10^{-9} M). Under such conditions, phenol binds to the enzyme [33] putting severe constraints on the entry of the hydroperoxide to the active site. There is, however, the possibility of reaction with unhindered peroxybenzoic acids which are exceptionally efficient substrates for horseradish peroxidase [32], reacting at a diffusion-controlled rate [34]. Colour production occurred on reaction with *m*-chloroperoxybenzoic acid although the reaction appeared incomplete in that lower absorbance charges were observed than with comparable concentrations of H_2O_2. The effect was not due to the formation of H_2O_2 by hydrolysis of the peroxyacid, nor to direct reaction of peroxyacid with the chromogen.

With this exception the 4-aminoantipyrine/phenol chromogenic system provides a rapid, sensitive method, performed at physiological pH, which is very highly selective for H_2O_2.

GENERAL DISCUSSION

Although the first four methods tested will all measure total peroxide (i.e., H_2O_2 plus organic hydroperoxide), the coupled oxidation of NADPH seems the most widely applicable because of the lack of substrate selectivity exhibited by glutathione peroxidase. Another favourable feature of this method is that the system is buffered at about pH 7.5, in contrast to the extreme acid or alkaline conditions of the three non-enzymatic methods. This is important in view of the instability of peroxides; of particular relevance is the observation that hydroperoxides undergo uncatalysed decomposition in aqueous alkali. Studies with aromatic peroxyacids have shown that the decomposition process involves attack of the peroxyacid anion on the unionised peroxyacid [35], a maximum rate being observed at a pH corresponding to the pK_a of the peroxyacid. It seems probable, therefore, that cross-reactions between HO_2^- (pK_a (H_2O_2) $\approx$ 11.6) and other hydroperoxides could occur in test solutions, lowering the apparent yield of these species. Such reactions are unlikely to interfere with assays in which the final state is rapidly attained, but are perhaps of more relevance in the phenolphthalin method where solutions are incubated for considerable times before measurements can be made.

The 4-aminoantipyrine/phenol reagent, with its high selectivity for H_2O_2, allows determination of H_2O_2 alone, in mixtures of peroxides. Previously, such measurements generally involved the use of either the H_2O_2-specific titanium sulphate reagent, or an unselective reagent before and after

enzymatic scavenging of the H_2O_2 by catalase. Commercial (beef liver) catalase requires further purification [36] to avoid non-specific peroxide decomposition. Bacterial catalase [37] may prove better suited for this purpose because of its greater stability in solution compared to the beef liver enzyme. Furthermore, immobilisation [38] of the bacterial catalase should overcome such problems by allowing its removal before determination of organic peroxide.

Sellers [39] has described the development of a spectrophotometric method for the determination of H_2O_2 using potassium titanium(IV) oxalate. A titanium(IV)—peroxide complex is produced, with an absorption maximum of about 400 nm and ϵ = 935 l mol^{-1} cm^{-1} at this wavelength. Although this is an improvement on the original titanium sulphate assay, it is not sufficiently sensitive to be of use with micromolar concentrations of substrate. The 4-aminoantipyrine/phenol reagent would therefore seem the most appropriate for use with <10 μM peroxide. Alternative donor substrates have been described for the clinical assay systems [40—45] and might prove useful if they could be incorporated into an assay of increased sensitivity.

The five analytical systems described were designed specifically to estimate 1—10 μM peroxide. When dealing with such low concentrations of species as reactive as peroxides, trace amounts of impurities in any reagent may cause interference; it is therefore essential to perform a calibration experiment with each reagent batch. From this investigation, it is also evident that analytical results should be confirmed by using more than one method, as no procedure can be guaranteed immune from interference by other solutes that may be present.

We gratefully acknowledge support of this work by a grant from the North of England Cancer Research Campaign and valuable discussions with Dr. D. J. Deeble.

REFERENCES

1 A. J. Martin in J. Mitchell, Jr. (Ed.), Organic Analysis, Interscience, New York, 1960, p. 1.
2 R. D. Mair and R. T. Hall in I. M. Kolthoff and P. J. Elving (Eds.), Treatise on Analytical Chemistry, Part II, Vol. 14, Wiley-Interscience, New York, 1971, p. 295.
3 S. Siggia, Quantitative Analysis via Functional Groups, Wiley, New York, 1963, p. 255.
4 G. M. Eisenberg, Ind. Eng. Chem., Anal. Ed., 15 (1943) 327.
5 R. A. Basson and T. A. du Plessis, Radiat. Res., 33 (1968) 183.
6 A. O. Allen, C. J. Hochanadel, J. A. Ghormley and T. W. Davis, J. Phys. Chem., 56 (1952) 575.
7 B. L. Gupta, Microchem. J., 18 (1973) 363.
8 B. L. Gupta, R. M. Bhat, K. R. Gomathy and B. Susheela, Radiat. Res., 75 (1978) 269.
9 H. B. Michaels and J. W. Hunt, Anal. Biochem., 87 (1978) 135.
10 M. I. Al-Sheikhly, Ph.D. Thesis, University of Newcastle upon Tyne, 1981.

11 A. A. L. Abdul Rahman and D. J. Deeble, unpublished results.
12 L. C. McCabe, Ind. Eng. Chem., 45 (1953) 111A.
13 N. J. Chalkley and C. Whalley, Proc. Anal. Div. Chem. Soc., 15 (1978) 327.
14 E. K. Dukes and M. L. Hyder, Anal. Chem., 36 (1964) 1689.
15 E. C. Hurdis and H. Romeyn, Jr., Anal. Chem., 26 (1954) 320.
16 D. K. Banerjee and C. C. Budke, Anal. Chem., 36 (1964) 792.
17 D. Swern in D. Swern (Ed.), Organic Peroxides, Vol. 1, Wiley-Interscience, New York, 1970.
18 P. Talalay, W. H. Fishman and C. Huggins, J. Biol. Chem., 166 (1946) 757.
19 J. H. Baxendale, Adv. Catal., 4 (1952) 31.
20 A. A. L. Abdul Rahman, M. I. Al-Sheikhly and D. J. Deeble, unpublished results.
21 P. Jones and I. Wilson, in H. Sigel (Ed.), Metal Ions in Biological Systems, Vol. 7, M. Dekker, 1978, p. 185.
22 H. C. Kelly, D. M. Davies, M. J. King and P. Jones, Biochemistry, 16 (1977) 3543.
23 J. E. Falk, Porphyrins and Metalloporphyrins, Elsevier, Amsterdam, 1964.
24 T. Robson, Ph.D. Thesis, University of Newcastle upon Tyne, 1973.
25 L. Flohé and W. A. Günzler in L. Flohé, H. Ch. Benohr, H. Sies, H. D. Waller and A. Wendel (Eds.), Glutathione, Georg. Thieme Publ., Stuttgart, 1974, p. 132.
26 D. E. Paglia and W. N. Valentine, J. Lab. Clin. Med., 70 (1967) 158.
27 L. Flohé and I. Brand, Z. Klin. Chem. Klin. Biochem., 2 (1970) 156.
28 W. A. Günzler, H. Kremers and L. Flohé, Z. Klin. Chem. Klin. Biochem., 10 (1974) 444.
29 B. L. Horecker and A. Kornberg, J. Biol. Chem., 17 (1948) 385.
30 P. Trinder, Ann. Clin. Biochem., 6 (1969) 24.
31 D. Barham and P. Trinder, Analyst, 97 (1972) 142.
32 D. M. Davies, P. Jones and D. Mantle, Biochem. J., 157 (1976) 247.
33 G. R. Schonbaum, J. Biol. Chem., 248 (1973) 502.
34 H. B. Dunford and W. D. Hewson, Biochemistry, 16 (1977) 2949.
35 J. F. Goodman, P. Robson and E. R. Wilson, Trans. Faraday Soc., 58 (1962) 1846.
36 M. L. Kremer, Biochim. Biophys. Acta, 198 (1970) 199.
37 D. N. Middlemiss, Ph.D. Thesis, Newcastle upon Tyne, 1973.
38 A. Schejter and A. Bar-Eli, Arch. Biochem. Biophys., 136 (1970) 325.
39 R. M. Sellers, Analyst, 105 (1980) 950.
40 W. Werner, H. G. Rey and H. Wielinger, Z. Anal. Chem., 252 (1970) 224.
41 N. Gochman and J. M. Schmitz, Clin. Chem., 17 (1971) 1154.
42 F. Meiattini, L. Prencipe, F. Bardelli, G. Giannini and P. Tarli, Clin. Chem., 24 (1978) 2161.
43 M. Sugiura and K. Hirano, Clin. Chim. Acta, 75 (1977) 387.
44 T. T. Ngo and H. M. Lenhoff, Anal. Biochem., 105 (1980) 389.
45 R. H. White-Stevens and L. R. Stover, Clin. Chem., 28 (1982) 589.

Analytica Chimica Acta, 155 (1983) 151—158
Elsevier Science Publishers B.V., Amsterdam — Printed in The Netherlands

THE PREPARATIVE SCALE SEPARATION AND THE IDENTIFICATION OF CONSTITUENTS OF ANTHRAQUINONE-DERIVED DYE MIXTURES
Part 3. Products from the Combustion of Red and Violet Smoke Mixtures

I. B. RUBIN*, M. V. BUCHANAN and J. H. MONEYHUN

Bio/Organic Analysis Section, Analytical Chemistry Division, Oak Ridge National Laboratory, P.O. Box X, Oak Ridge, TN 37830 (U.S.A.)

(Received 19th May 1983)

SUMMARY

Two colored-smoke grenades, red and violet, were detonated and the particulate and vapor phase portions were collected and analyzed. The original dye mixes were also analyzed for comparison. The chloroform-soluble portion of each dye mix was fractionated by liquid chromatography on silica gel as was the original red dye mix, while the original violet smoke mix was fractionated by differential solubility. Major components were collected in essentially pure fractions while the impurities were concentrated in other fractions. The dye portion of the red smoke mix was substantially unchanged on combustion, with the major component remaining as 1-methylaminoanthraquinone. A significant amount (>5%) of 1-aminoanthraquinone was formed, however. The dye portion of the violet smoke mix was quantitatively converted from 1,4-diamino-2,3-dihydroanthraquinone to 1,4-diaminoanthraquinone upon combustion. The nonvolatile and/or chloroform-insoluble portions consisted mainly of sodium and potassium chlorides, elemental sulfur, and undifferentiated carbonaceous matter. Major constituents of the vapor phases were carbon disulfide, toluene, C_2-benzenes, styrene, chloromethylbenzene and naphthalene. Aliphatic and aromatic hydrocarbons, alkylbenzenes, and thiophenes, as well as a number of other compounds were detected in smaller quantities.

Dyes derived from anthraquinone have been used for a variety of purposes, among which are their inclusion in colored signal-smoke grenades [1]. The chemistry of several of these dyes which are used as colored smokes has been elucidated [2, 3]. A number of anthraquinone derivatives have shown bacterial mutagenic activity [4] and the biological effects of some of the dyes, as well as the whole smoke mixes, used in the signal smoke grenades have been reviewed [1]. In that earlier study of the smoke mixtures, both red and violet grenades were exploded and the dispersed smoke particulates were collected and examined spectrophotometrically [1]. It was found that the red smoke mix exhibited no change in the visible or ultraviolet regions when compared to the original, but that the violet mix showed substantial changes in both regions. At that time, no further chemical information was reported. With the increasing awareness and interest in environmental

contamination and the resulting health considerations for those who might be exposed to the disseminated smoke products, a study was devised to collect and evaluate the content of the smoke after detonation of a grenade, and to compare the composition of the combustion products with that of the original smoke mix. The grenades contain not only the dyes, but also pyrotechnic fuel, cooling and starter mixes consisting mainly of potassium chlorate and nitrate, sodium hydrogencarbonate, and sulfur. The dyes are volatilized at temperatures up to 500—550°C during the burn time, so that it was expected that the dyes might be subjected to oxidative and pyrolytic reactions that could result in a variety of reaction by-products.

In the present study, the smoke mixes were studied both before and after combustion in order to evaluate the differences in composition caused by combustion. Samples of the dispersed combusted products, both particulate and vapor phase, were trapped in various types of collectors. The particulates were fractionated by open-column liquid chromatography and by combined gas chromatography/mass spectrometry (g.c./m.s.), while the vapor phase samples were studied by g.c./m.s. after desorption from the traps.

EXPERIMENTAL

Samples and reagents

Red and violet M18 colored-smoke grenades were provided by the Pine Bluff Arsenal, as were red and violet smoke mixes from the same batches from which the grenades were filled. The standard dyes, 1-methylamino-anthraquinone [MAA; 1-(methylamino)-9,10-anthracenedione; CAS Registry No. 82-38-2] and 1,4-diamino-2,3-dihydroanthraquinone [DDA; 1,4-diamino-2,3-dihydro-9,10-anthracenedione; CAS 81-63-0] were obtained from the U.S. Army Armament Research Development Command, Aberdeen Proving Ground, MD. The 1,4-diaminoanthraquinone [DAA; 1,4-diamino-9,10-anthracenedione; CAS 128-95-0] was separated from the violet dye mix by preparative-scale thin-layer chromatography (t.l.c.). All solvents, with the exception of the methylethylketone (butan-2-one) used in the t.l.c. studies, were glass-distilled reagents (Burdick and Jackson). Tetramethylsilane and deuterated chloroform (Aldrich) were used for the nuclear magnetic resonance spectrometry (n.m.r.). The Amberlite XAD-2 and Tenax-GC used to trap the vapor-phase constituents were obtained from Polysciences and Applied Science Division, Milton Roy Laboratories, respectively. Silica gel (60—200 mesh, grade 950; Davison Chemical Co.) was used for open-column liquid chromatography. Thin-layer plates (SIL-N-HR (0.20 mm) and SIL-G-200 UV 254 (2.0 mm); Brinkman Instruments) were used for analytical and preparative-scale t.l.c., respectively.

Procedures

The colored-smoke grenades were detonated in separate canvas tents which were used as the combustion and sampling chambers. Sampling ports

of teflon tubing were inserted through the tent walls and airborne particulate matter was collected on pre-washed fiber glass filters while particulate matter fallout was collected in glass trays placed on the tent floor. The red smoke products and the original (uncombusted) red smoke mix were fractionated by the vacuum sublimation technique described previously [2] while the original violet smoke mix was fractionated by a differential solubility procedure [2]. The combusted red and violet products, as well as the original red smoke mix, were also separated by open-column liquid chromatography on silica gel by elution with chloroform [5]. Most of the analytical procedures have been described previously [2], and a detailed account of the sampling and additional analytical techniques used for the combusted dye studies is available [5].

RESULTS AND DISCUSSION

In this present work, red and violet smoke grenades were detonated and the products were collected and examined. The smoke grenades are composed of about 40% of the dye or dye mix and 60% of a combustion mixture composed of sodium hydrogencarbonate, potassium chlorate and sulfur. A mixture (60 g) of potassium nitrate, sodium hydrogencarbonate, sulfur, and cornstarch with a small amount of nitrocellulose binder is included in the grenade as a starter mixture [1]. It has already been noted that there is no spectrophotometrically detectable change in the red smoke mix, but a gross spectrophotometric change in the violet smoke mix after combustion [1]; however, this does not preclude the formation of other constituents that would not be spectrophotometrically detected in the presence of the major components. Because of the high temperature needed to volatilize the dyes, and the presence of oxidizing agents, the effects of the grenade detonation on the dye would be expected to result in some unknown oxidation or pyrolysis products which would include a number of compounds not found in the original dye mix. In order to facilitate sampling, the grenades had to be set off within an enclosed chamber. This might have caused some modifications in the reaction parameters, when compared to detonation in the open where the products would be readily dispersed.

Red smoke mix

The red smoke mix is formulated to contain only one dye component, 1-methylaminoanthraquinone (MAA) [1]. Spectrophotometrically, the combusted and original smoke mixes were virtually identical in both the visible and ultraviolet ranges, and were essentially the same as the reference MAA. The water-soluble portion of the whole combusted smoke mix was 3.5%. The chloroform-soluble portion represented 94% of the total material, compared to about 87% for the original.

When the red smoke mixes were fractionated by a vacuum sublimation procedure [2], several differences between the original and combusted

products were obvious. In the combusted mix, there was an orange compound apparently sublimed on top of the red MAA in fraction 2; there was an insoluble yellow film adhering to the condenser after the dye was dissolved; and the involatile residue was a compact black or dark brown material instead of a fluffy purple substance. The insoluble material was scraped off the condenser and its mass spectrum was obtained by using a direct insertion probe. It was identified as sulfur (S_8).

The involatile residue from the combusted smoke mix was examined by scanning electron microscopy, x-ray diffraction, Ag $K\alpha$-induced x-ray fluorescence and electron-induced energy-dispersive x-ray spectrometry. The crystalline material was found to be mainly potassium chloride with some sodium chloride also. Some partially graphitized carbon was detected, but no crystalline sulfur compounds were noted. A sulfur map showed that sulfur was coincident with potassium and chlorine, which would indicate that amorphous sulfur was deposited on the potassium chloride crystals. Very minor quantities of iron, lead, zinc and zirconium were detected.

Because so few impurities were found in the vacuum-sublimation fractions, and because of the effectiveness of t.l.c. on silica gel plates for separation, it was decided to try a chromatographic separation of the smoke mixes on a silica gel column. This technique proved very successful, yielding bands which were easily detected visually and were separated by color. The comparative results, by g.c./m.s., of the chloroform-soluble portion of the original and combusted smoke mixes after chromatography on silica gel are shown in Table 1, along with the gravimetric results. Band 1 in both cases was pure MAA, while band 2 of the combusted mix was an almost pure aminoanthraquinone (AA) with a minor amount of MAA present. The other two bands contained a number of constituents, some of which could not be unequivocally identified. Band 4 contained the material washed off with acetone after all of the substances eluted by chloroform had been collected. Band 3 consisted of several sub-bands, the largest of which was yellow. In a second column chromatographic separation, the yellow band was collected and designated as band 3b. On a weight basis, band 3b was 70% of band 3, and thus, about 4.4% of the total sample. A comparison of bands 2 and 3b by g.c./m.s. indicated the molecular weight of aminoanthraquinone (223) for each, but that band 3b had a longer retention time than band 2 and contained minor impurities corresponding to MAA and to band 2. Carbon-13 n.m.r. spectra obtained for bands 2 and 3b confirmed that the substance of band 2 was 1-aminoanthraquinone and of band 3b was 2-aminoanthraquinone. It has been reported that 1-aminoanthraquinone shows an orange spot and the 2-isomer a yellow spot on alumina t.l.c. plates [6]. In fraction 4, an estimate of comparative peak areas indicated that 1-aminoanthraquinone comprised about 75% of the total. The major chemical effect that appears to take place during the combustion of the red smoke mix is a partial demethylation of the MAA to give 1-aminoanthraquinone along with some rearrangement to 2-aminoanthraquinone.

TABLE 1

Summary of comparative composition of uncombusted and combusted red smoke mix[a]

Uncombusted			Combusted	
Band	Component	Wt. %[b]	Component	Wt. %[b]
1	*1-MAA*	98.1	*1-MAA*	85.6
2	*1-AA* 1-MAA Hydrocarbon Siloxanes	0.6	*1-AA* 1-MAA	6.4
3	*1-AA* *Aliphatic Amide* Hydrocarbons Cyclic or unsaturated hydrocarbons Other amides	1.3	*2-AA* 1-AA Cyanoanthraquinone Hydrocarbon 1-MAA	6.4
4		0.0	*1-AA* 2-AA Aliphatic amides Phthalate	3.4
		100.0		101.8

[a]Largest components in italics. AA = aminoanthraquinone.
[b]Weight percent of sample chromatographed, for whole band.

Vapor-phase samples were collected on Tenax-GC. The samples were analyzed by capillary column g.c. and then by g.c./m.s. after thermal desorption [7]. A list of tentatively identified compounds is presented in Table 2. In general, the alkanes seemed to be of the order of C_9 to C_{12} or larger. In many instances, chromatographic peaks were not well resolved, which made mass spectral interpretation difficult, if not impossible. The compounds listed below the alkanes were present in relatively small quantities, between 5 and 10% as large as the toluene peak, while a number of other constituents were present in very minor quantities.

Violet smoke mix

The violet smoke mix is formulated to contain two dyes, 20% MAA and 80% 1,4-diamino-2,3-dihydroanthraquinone (DDA) and the same combustion and starter mixes as the red grenades [1]. Prior studies indicated that the major effect of the grenade detonation was expected to be a conversion of DDA to DAA [1, 2]; however, other oxidation or combustion products might also be present as with the red smoke mix. Spectrophotometrically, the combusted smoke mix was substantially different from the original; this was obvious visually, as the original was a brownish powder while the combusted mix was a bright purple. The spectra are similar to those of DDA (original) and DAA (combusted) [2], with modifications caused by the

TABLE 2

Tentative identification of vapor-phase combustion products of red and violet smoke mixes[a]

Red[b]	Violet[b]	Violet[c]
Toluene	*Carbon disulfide*	*Naphthalene*
Styrene	*C_2-Benzenes*	C_1-Indanes
Chloromethylbenzene	*Toluene*	C_4-Benzenes
Alkanes	C_3-Benzenes	Dihydronaphthalene
Benzaldehyde	Alkanes	Benzene
Dichlorobenzene	C_4-Benzene	Methylbenzoate
Phenol	C_2-Thiophene	C_1-Indene
Cyanobenzene	Acetophenone	Benzothiophene
Acetophenone	Phenylacetaldehyde	C_2-Indanes
Phenylacetylene		C_5-Benzenes
C_{10}-Alkenes		C_7-Benzenes
Naphthalene		Methylbenzothiophene
Benzothiophene		Methylnaphthalenes
C_8-Benzenes		C_3-Indanes
Biphenyl/Acenaphthene		Biphenyl/Acenaphthene
		C_2-Naphthalene
		C_4-Indanes
		Methylbiphenyls

[a]Largest components in italics. [b]Tenax trapping. [c]XAD-2 trapping.

presence of 20% MAA. Solubility tests indicated that the chloroform-soluble portion of the combusted mix amounted to 83% of the total. A direct test of water solubility was not made, but 24% of the chloroform-insoluble portion was water-soluble, which represents about 4% of the whole combusted mix.

The combusted violet smoke mix was relatively soluble in chloroform, so that column chromatography on silica gel was used to fractionate this sample also. Because DDA is only very slightly soluble, the original violet smoke mix could not be chromatographed, and was separated by a differential solubility technique [2]. Consequently, the compositions of the two smoke mixes could not be compared fraction-to-fraction as the red smoke mixes were. The compositions of the various fractions of the violet smoke mixes, as they were separated, are shown in Table 3. Band 1 of the combusted products is essentially pure MAA, band 2 is predominantly 1-aminoanthraquinone while band 4 is pure DAA. Bands 3 and 5 were mixtures of a variety of compounds, that for the most part could not be unequivocally identified. Only a trace of DDA was detected in band 5. Band 5 contained material that was washed off the column with 900 ml of acetone followed by 300 ml of methanol after all the compounds eluted by chloroform had been collected. The chloroform-insoluble portion of the combusted mix was not examined further because it was assumed to be similar in composition to the involatile portion of the

TABLE 3

Summary of comparative compositions of uncombusted and combusted violet smoke mix[a]

Combusted (silica gel chromatography)			Uncombusted (Differential Solubility)	
Band	Component	Wt. %[b]	Fraction	Component
1	*1-MAA*	28.1	1	*1-MAA*
2	*1-AA*	3.5		DDA
	1-MAA			DAA
	Phthalate			Azobenzene
	Hydrocarbon			Anthraquinone
3	*C_{12} Hexene or Olefin*	1.1	2	*1-MAA*
	1-MAA			DDA
	1-AA			DAA
	2-MAA		3	*DAA*
	Cyanoanthraquinone			DDA
	Hydrocarbons			1-MAA
4	*DAA*	64.4	4	*DDA*
5	*$C_9H_{19}OH$ (Mass 157)*	11.7		(DAA)
	Phthalic anhydride			(Carbonaceous matter)
	AA		Insoluble residue: Carbonaceous matter, sulfur, KCl, NaCl	
	DAA			
	Hydrocarbons			
	Aliphatic amides			
	Phthalate			
		108.8		

[a]Largest component italicized. [b]Weight percent of sample chromatographed, for whole band.

combusted red smoke mix; this residue appeared to be formed mainly from the pyrotechnic fuel mixtures.

The only impurities detected in the original violet smoke mix were azobenzene and anthraquinone in fraction 1. Fraction 3 would have been expected to be predominately DDA [2], but the majority of it was apparently oxidized to DAA during the drying stage even though the solvent was evaporated under flowing nitrogen. Fraction 4 would have been expected to be mainly the carbonaceous residue rather than DDA [2], but there was a sufficient amount of DDA present that its direct-probe mass spectrum overwhelmed the more diffuse spectra of the carbon residue. From the results of these tests, it can also be seen that the major effect of the grenade detonation was to convert DDA to DAA quantitatively. Because the dye mix also contained 20% MAA, there was also some production of 1-aminoanthraquinone.

Vapor-phase samples from this grenade test were collected on Tenax-GC and XAD-2 traps. The Tenax samples were separated by capillary column g.c. and by g.c./m.s. after thermal desorption [7]. The major components are shown in Table 2. The compounds listed from C_3-benzene down were present in relatively small quantities, i.e., peak heights from 5 to 10% as large as the

carbon disulfide peak, while a number of other compounds were present in trace quantities. The XAD samples were extracted from the resin with dichloromethane and were examined by the normal g.c./m.s. method after evaporation of most of the solvent under flowing nitrogen with natural evaporative cooling. A list of compounds detected is shown in Table 2. Naphthalene was the only major compound found. In both the Tenax and XAD sample chromatograms, there were several overlapping peaks that made mass spectral identification difficult.

The x-ray and microscopy examinations were done by L. D. Hulett, Ms. F. L. Ball and H. W. Dunn of the Analytical Methodology Section, Analytical Chemistry Division, ORNL. Research was supported under Army Project Order No. 9600 by the U.S. Army Medical Research and Development Command, Fort Detrick, Frederick, MD 21701, and performed at Oak Ridge National Laboratory under U.S. Department of Energy Contract W-7405-eng-26 with the Union Carbide Corporation.

REFERENCES

1 E. J. Owens and D. M. Ward, Rep. AD/A-003827, Dec., 1974, NTIS, U.S. Dept. of Commerce, Springfield, VA.
2 I. B. Rubin, M. V. Buchanan and G. Olerich, Anal. Chim. Acta, 135 (1982) 111.
3 I. B. Rubin and M. V. Buchanan, Anal. Chim. Acta, 135 (1982) 121.
4 J. P. Brown and R. J. Brown, Mutat. Res., 40 (1976) 203.
5 I. B. Rubin, M. V. Buchanan and J. H. Moneyhun, ORNL/TM-8810, July, 1983, Oak Ridge National Laboratory, Oak Ridge, TN; National Technical Information Service, U.S. Dept. of Commerce, Springfield, VA 22161.
6 J. Franc and M. Hajkova, J. Chromatogr., 16 (1964) 345.
7 C. E. Higgins, Anal. Chem., 53 (1981) 932.

Analytica Chimica Acta, 155 (1983) 159—171
Elsevier Science Publishers B.V., Amsterdam — Printed in The Netherlands

LIQUID CHROMATOGRAPHIC DETECTION OF CARDIAC GLYCOSIDES, SACCHARIDES AND HYDROCORTISONE BASED ON THE PHOTOREDUCTION OF 2-TERT-BUTYLANTHRAQUINONE

M. S. GANDELMAN[a] and J. W. BIRKS*

Department of Chemistry and Cooperative Institute for Research in Environmental Sciences (CIRES), University of Colorado, Boulder, CO 80309 (U.S.A.)

(Received 27th July 1983)

SUMMARY

The photoreduction fluorescence detector, a postcolumn liquid chromatographic reaction detector, functions by generating fluorescent products from alcohols, aldehydes, ethers, and amines via a photochemical reaction. The fluorescent product is produced in the photoreduction of 2-tert-butylanthraquinone (t-BAQ) by analytes containing the above-mentioned functional groups. The photochemical reaction only requires t-BAQ to absorb light, and thus many analytes with extremely low ultraviolet-visible absorptivities can be determined with good sensitivity. Because the t-BAQ is added precolumn, no reagent-addition pumps or mixing cells are needed in the detection scheme. The photochemical reactor is simply inserted between the liquid chromatographic column and a conventional fluorimeter. To demonstrate the capabilities of the detector involatile compounds were chosen (cardiac glycosides, saccharides, and steroids), some of which exhibit extremely low u.v.-visible absorptivities. The detection limits for the cardiac glycosides and hydrocortisone were found to be about 2 ng whereas the detection limits for the saccharides were about 80 ng.

The application of high-performance liquid chromatography (h.p.l.c.) to the determination of compounds lacking chromophores or electrophores is presently limited by the availability of sensitive and selective detectors. Recently, postcolumn reaction detectors have been used successfully to improve the selectivity and sensitivity of conventional h.p.l.c. detectors [1—4], especially for the determination of nonabsorbing and electrochemically inactive compounds. Photochemical reactions have played an active role in the postcolumn reaction detector field [5—15] because they have characteristics that are well suited to postcolumn reactor technology. First, photochemical reactions only require the addition of photons; thus reagent-addition pumps and mixing cells, which cause additional band broadening, are not needed. Second, because many photochemical reactions proceed via free radical intermediates, the reactions are rapid, and lengthy reaction times usually can be avoided. Finally, monochromators and filters can be used to

[a]Present Address: University of Connecticut, School of Medicine, Farmington, CT 06032, U.S.A.

0003-2670/83/$03.00

add selectivity to photochemical reactors by limiting the spectral output of the photochemical source.

Earlier applications of postcolumn photochemical reactions have required that the analyte absorb light. This has limited the technique to compounds for which there is already a means of detection, i.e., u.v. absorption or fluorescence. In recent work, photochemical reactions that do not require the analyte to absorb light have been used and thus the applicability of the method has been greatly broadened [16—18]. The detection systems used a photochemical reagent (an anthraquinone) that absorbs u.v. energy and subsequently reacts with the analytes to produce a detectable product. The lowest triplet state, $T_1(n,\pi^*)$, of anthraquinone is the photoreactive state and can be populated by absorption of 254-nm or 360-nm radiation. Absorption of 360-nm radiation representing an $n \rightarrow \pi^*$ transition populates the lowest singlet state, $S_1(n,\pi^*)$, which rapidly exhibits intersystem crossing to produce the lowest triplet state, $T_1(n,\pi^*)$. Radiation at 254 nm excites the next highest singlet state, $S_2(\pi,\pi^*)$, which rapidly internally converts to the $S_1(n,\pi^*)$ state, and the S_1 state crosses to the $T_1(n,\pi^*)$ state as in the 360 nm absorption process [19].

The $T_1(n,\pi^*)$ state has a diradical character, and these excited-state molecules react with hydrogen-atom-donating (HAD) substrates, e.g., alcohols, aldehydes, amines, and ethers [19]. Such compounds contain a weak C—H bond because of the resonance effect of the heteroatom within the molecule [20], and thus readily react with the diradical triplet state by hydrogen abstraction to produce two radical intermediates.

$$Q + h\nu \rightarrow Q^* \text{ (singlet, } S)$$

$$Q^*(S) \rightarrow Q^* \text{ (triplet, } T)$$

$$Q^*(T) + CH_3CH_2OH \rightarrow QH\cdot + CH_3\dot{C}HOH$$

where Q is anthraquinone and QH· is the semiquinone radical.

The two radical intermediates, the semiquinone radical and the α-hydroxyalkyl radical (for an alcoholic substrate), have two possible reaction paths, depending on the experimental conditions: under aerobic conditions, the two radical intermediates will react with oxygen at diffusion-limited rates to produce H_2O_2, the anthraquinone, and the oxidized form of the original analyte [21, 22].

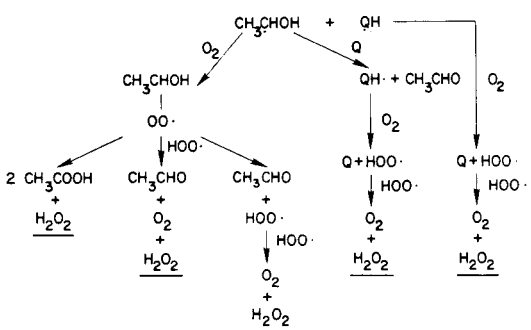

In other words, the analyte is oxidized, the oxygen is reduced, and the anthraquinone is regenerated. This photochemical reaction scheme is called photooxygenation, because the analyte or substrate is photochemically oxidized by oxygen. In contrast, in an anaerobic environment, the two radical intermediates rapidly disproportionate and produce the oxidized form of the analyte and the reduced form of the quinone (dihydroanthraquinone) [23—26]

$$CH_3\dot{C}HOH + Q \rightarrow QH\cdot + CH_3CHO$$

$$2QH\cdot \rightarrow Q + QH_2$$

This photochemical reaction pathway can be referred to as photoreduction, because the quinone is reduced.

Dihydroanthraquinone is a highly efficient fluorescent molecule with a quantum yield (Φ_F) of about 0.7, whereas anthraquinone has a Φ_F less than 10^{-5} [27]. This vast difference in photophysical properties of the two molecules is caused by dissimilarities in their electronic structures. The extremely low fluorescence quantum yield of anthraquinone and many other carbonyl compounds is caused by the inability of the fluorescence to compete with the rapid intersystem crossing from S_1 to T_1. This rapid intersystem crossing is caused by the proximity in energy of the $S_1(\dot{n},\pi^*)$ and $T_1(\dot{n},\pi^*)$ states [19]. In anthraquinone, this separation is about 4 kcal mol^{-1}. In other words, the depopulation of the excited state in anthraquinone proceeds through the T_1 state by a nonradiative decay rather than by fluorescence from S_1. In contrast, because the dihydroanthraquinone does not contain a carbonyl group, the molecule does not have a low lying $S_1(\dot{n},\pi^*)$ state, and there exists a much larger singlet-triplet energy gap in comparison to anthraquinone. This larger gap reduces the rate of intersystem crossing, so that fluorescence can compete with intersystem crossing. In other words, approximately 70% of the excited singlet state molecules are deactivated by fluorescence emission in the dihydroanthraquinone, while the vast majority of the excited state anthraquinone molecules are deactivated by intersystem crossing to T_1.

Two postcolumn reaction detectors using the two different photochemical reactions (photooxygenation and photoreduction) have been demonstrated and applied in this laboratory. The first detection system, referred to as the photooxygenation chemiluminescence detector makes use of an aerobic chemical environment. In this detector, the HAD analytes generate H_2O_2, which is subsequently detected in a luminol chemiluminescent reaction [16]. The second detection system, referred to as the photoreduction fluorescence (PRF) detector, generates dihydroanthraquinone from the HAD analytes under anaerobic conditions [17, 18]. The dihydroanthraquinone subsequently is detected by a fluorimeter. Work has been continued only with the PRF detector, because it exhibited superior detection limits (1—2 orders of magnitude), and allowed the use of a simpler detection scheme (no postcolumn reagent needed).

The detection limits of both the photooxygenation chemiluminescence and PRF detectors are confined by a background reaction. Presently it is not clear whether trace contaminants in the acetonitrile (e.g., methanol), direct reaction of the excited-state quinone with the mobile phase, or a reaction between an excited-state anthraquinone and a ground-state anthraquinone, is responsible for the background signal. Background reactions for anthraquinone-2,6-disulfonate are well documented [27, 28] and it is likely that these reactions can occur with other anthraquinones. A probable mechanism, the Stonehill mechanism [28], for the production of a background signal in the photoreduction detector is as follows

$$Q^*(T) + H_2O \rightleftharpoons (Q \cdot H_2O)$$

$$(Q \cdot H_2O) + Q \rightarrow QOH\cdot + QH\cdot$$

$$2QH\cdot \rightarrow Q + QH_2$$

where $(Q \cdot H_2O)$ is the photosolvation adduct of anthraquinone and QH_2 is dihydroanthraquinone. The mechanism is based on the photosolvation of excited $T_1(n,\pi^*)$ molecules to form adducts with water, which subsequently react with a ground-state anthraquinone to produce radical intermediates. These radical intermediates rapidly react to produce the detectable products, H_2O_2 in the aerobic environment or the reduced quinone in the anaerobic environment.

In this paper, improvements to the PRF detector and a new application are reported. In the first study using the PRF detector [17] aliphatic alcohols, aldehydes, and ethers were chosen as model compounds to test the performance of the detector toward these specific functional groups. Detection limits (S/N = 3) of a few nanograms were reported for all these compounds. However, the usefulness of the PRF detector in the determination of such volatile aliphatic compounds is questionable because gas chromatography (g.c.) is still a superior method for quantifying these compounds. In a further paper [18], cardiac glycosides and saccharides were quantified; these compounds represent more practical choices to demonstrate the capabilities of the PRF detector, because these compounds are difficult to determine by both g.c. and h.p.l.c. The difficulties in g.c. arise from the involatility of the compounds, whereas in h.p.l.c., the absorption maximum of the chromophore ($\approx$220 nm) presents problems in selectivity and sensitivity. In the present study, the photochemical reagent, anthraquinone-2,6-disulfonate, was replaced by 2-tert-butylanthraquinone (t-BAQ), and a previously constructed reactor containing a 360-nm fluorescent lamp was compared with a new photochemical reactor utilizing an intense 254-nm irradiation source. Both reactors show about 40-fold improved detection limits in relation to previous work. In addition, the application of the PRF detector is demonstrated for the determination of the synthetic corticosteroid hydrocortisone which, like the cardiac glycosides and the saccharides, can be difficult to determine by either g.c. or h.p.l.c.

EXPERIMENTAL

Reagents and chromatographic apparatus

The 2-tert-butylanthraquinone (Aldrich, Milwaukee, WI) was recrystallized from hot 80% acetonitrile/water and washed with deionized water. A stock solution containing 2.0 g of t-BAQ per liter of acetonitrile (7.6×10^{-3} M) was prepared and stored in a brown glass bottle. All acetonitrile used in the h.p.l.c. mobile phase and in the recrystallization of t-BAQ was h.p.l.c. grade (Fisher, Denver, CO).

The chromatographic system used for the optimization and the detection of hydrocortisone and the cardiac glycosides contained an Altex 110A pump, a Rheodyne 7120 injector with a 20-μl loop, and an Alltech 10-μm particle diameter, C_{18} column (250 × 4.6 mm). For chromatography of the saccharides, the C_{18} column was replaced by an IBM 5-μm particle diameter amino column (250 × 4.6 mm). The chromatographic system used for the comparative u.v. detection limits consisted of two Altex 110 A pumps, an Altex 5-μm particle diameter C_{18} column, an Altex injector with a 20-μl loop, and a Hitachi model 100—10 u.v.-visible variable-wavelength detector.

Photochemical reactors

Two photochemical reactors were used in this study. One reactor was identical to the reactor used in a previous study [17] and was constructed from 12.5 m of 0.25 mm i.d. polytetrafluoroethylene (PTFE) tubing (Omnifit, Biolab, Cambridge, Great Britain), which was knitted into a cylindrical shape and placed over the fluorescent lamp. The other reactor (Fig. 1) was constructed around an Ultra-Torr union (A) (Cajon model SS-12UT-6, Cleveland, Ohio), fitted with a 13-mm adapter (B) (Cajon model SS-8UT-A-12). A 13-mm o.d. quartz tube (C) was inserted through the Ultra-Torr fitting and connected to the nitrogen cylinder (D). The 13-mm o.d. quartz tube (C) was flared to 19 mm o.d. (E) after it emerged from the Ultra-Torr union (A).

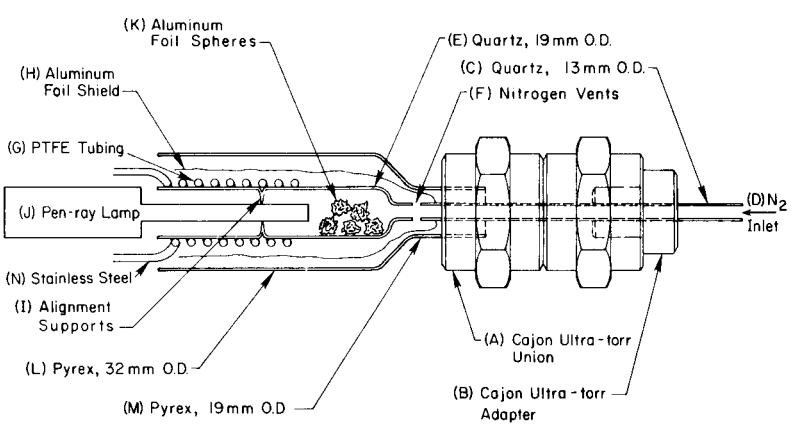

Fig. 1. Representation of the pen-ray photochemical reactor.

Prior to the flare, two vents (F) were cut into the quartz tube to allow the nitrogen to flow also over the surface of the 19 mm o.d. quartz tube (E). Approximately 0.8 m of 1.5-mm o.d., 0.50-mm i.d. PTFE tubing (G) was coiled around the 19-mm o.d. quartz tube (E), and the PTFE coils were covered with aluminum foil (H) to increase the photon flux by reflection. Three alignment supports (I) were placed on the inner surface of the 19-mm o.d. quartz tube (E) to center the pen-ray lamp (J) (Ultra-Violet Products, San Gabriel, CA), which was placed down the center of the 19-mm o.d. quartz tube (E). Near the head of the lamp, five small aluminum foil balls (K) were placed in E to increase the flow of nitrogen through the vents (F) by adding back-pressure to the flow of nitrogen down the center of E. Finally, a large-diameter pyrex tube (L) (32-mm o.d.) was placed over the 19-mm o.d. quartz tube (E) and reduced to 19-mm o.d. (M) in order to fit into the Cajon union (A). The larger pyrex cylinder (L) excluded oxygen from contact with the PTFE coils when the nitrogen stream was vented through C and F. The metal-to-PTFE junctions (N) were made within the space between L and E. To establish an anaerobic environment within the PTFE tubes of the reactor, it was imperative to exclude PTFE from contact with oxygen, because the material is permeable to oxygen. A smaller fraction of the nitrogen stream also passed directly through C in order to cool the lamp (J). The entire apparatus was held by two clamps, one around the pen-ray lamp and a second clamp positioned on the Cajon fitting.

The reactors were placed in-line between the column and the fluorimeter. No reagent-addition pumps or mixing cells were required in this detection system. A Schoeffel FS 970 fluorimeter with the excitation wavelength set at 375 nm and with a 470-nm filter on the emission side was used to detect the dihydroanthraquinone product.

Procedure and sample preparation

Nitrogen was bubbled through the mobile phase contained in a gas scrubber. Nitrogen flow was started 20 min prior to sample injection and continued throughout the chromatographic process. However, no sample deoxygenation was required before injection into the h.p.l.c. Sample preparation for the hydrocortisone cream consisted of a dichloromethane extraction, a back-extraction with water to remove the polyhydroxy polymer base, evaporation of the dichloromethane, and redissolution of the solid product in 80% acetonitrile.

The detection limits were evaluated by comparing the peak heights of the injected analytes with the peak-to-peak noise, and extrapolating the signal-to-noise (S/N) ratio to 3. The detection limits of the cardiac glycosides and the hydrocortisone were determined by injecting 20 ng of each sample, while the detection limits for the saccharides were calculated from 2-μg injections.

RESULTS AND DISCUSSION

Optimization

Both reactors were optimized for maximum S/N by injecting 157-ng samples of 2-propanol. Plots of S/N vs. residence time for various concentrations of t-BAQ are shown in Figs. 2 and 3 for the knitted and pen-ray reactors, respectively. The relative shapes and positions of these curves are difficult to explain, because they are complex functions of the photoreduction, background signals, and scavenging of residual oxygen. The higher concentrations of t-BAQ should exhibit the highest reactivity toward the analyte, because the H-abstraction (the rate-limiting step) is first order in the concentration of t-BAQ triplets. However, higher t-BAQ concentrations also produce a larger background signal. Consequently, the S/N can be optimized at a t-BAQ concentration that produces less than the maximum signal. Additionally, the lower quinone concentrations suffer from an oxygen-scavenging problem. Because the mobile phase contains traces of oxygen, some of the radicals and dihydroquinone generated in the photochemical reaction will be scavenged by reacting with this oxygen. The background reaction will lower the amount of residual oxygen in the mobile phase by reducing it to H_2O_2 in the photooxygenation mechanism. As a result, the

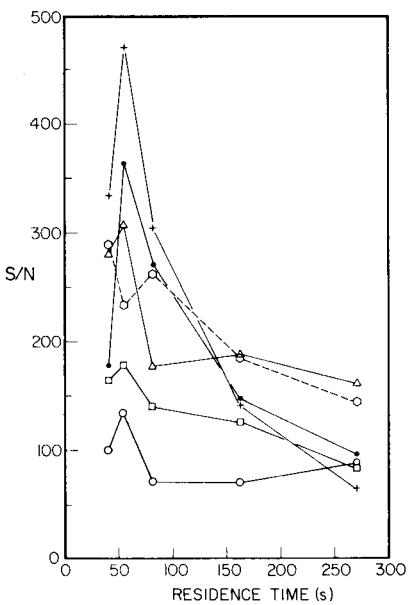

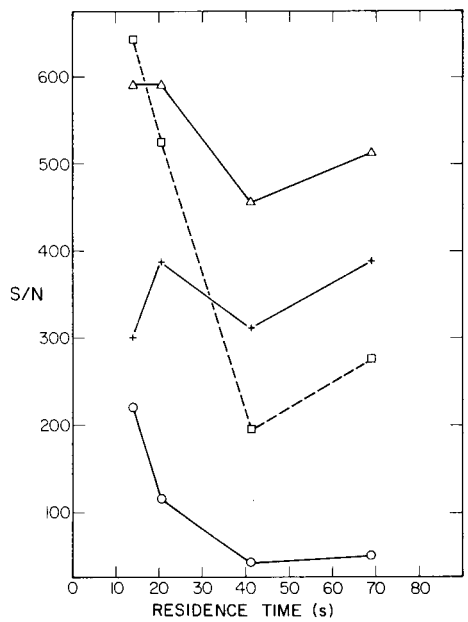

Fig. 2. Optimization curve for the knitted reactor. Concentration of t-BAQ: (○) 5.1×10^{-5} M; (□) 1×10^{-4} M; (△) 2.5×10^{-4} M; (+) 5.1×10^{-4} M; (◇) 1×10^{-3} M; (●) 2×10^{-3} M.

Fig. 3. Optimization curve for the pen-ray reactor. Concentration of t-BAQ: (○) 1×10^{-4} M; (□) 2.5×10^{-4} M; (△) 5.1×10^{-4} M; (+) 1.0×10^{-3} M.

amount of fluorescent product will be decreased if the residual level of oxygen is not reduced by the background reaction. Therefore, in the final procedure, the optimum concentration of t-BAQ is the best compromise of the previously discussed conditions. It was observed that in the knitted reactor, a t-BAQ concentration of 5.1×10^{-4} M gave the optimal S/N at a flow rate of 1.5 ml min^{-1} (Fig. 2), whereas in the pen-ray reactor, an optimal concentration of 2.5×10^{-4} M was found. Even though in the pen-ray reactor, 5.1×10^{-4} M t-BAQ gave a slightly better S/N as compared to 2.5×10^{-4} M at the desired flow rate, the difference in the S/N for the two concentrations was small, and the lower concentration of t-BAQ was chosen for the pen-ray reactor.

Detection limits

It was observed that the HAD substrates fall into two groups based on their detectability in the PRF detector. Substrates that do not have a high density of α-CH functional groups (aldehyde, ether, or hydroxy) are extremely reactive toward H-abstraction, and these compounds represent the first group of HAD substrates, e.g., aliphatic alcohols, aldehydes, ethers, cardiac glycosides, and steroids. The second group of HAD substrates consists of polyfunctional molecules such as saccharides, which exhibit significantly lower reactivity. The saccharides were found to have higher detection limits by 1—2 orders of magnitude in comparison to the less densely substituted substrates. The most probable explanation for this difference in photochemical reactivity involves the degree of solvation of the substrates. The polyfunctional molecules have a much higher degree of solvation in polar solvents compared to the less substituted substrates. Consequently, the rate-limiting hydrogen transfer between the saccharide substrate and the photoreactive state of the quinone is sterically hindered by the large solvent envelope of the polyfunctional substrate [22]. However, a second possible explanation for the lower reactivity of the saccharides might involve a destabilizing effect of the polyhydroxy groups on the transition state for H-abstraction.

Because both reactors exhibited almost identical detection limits for 2-propanol, only the pen-ray reactor was used in quantifying the less densely substituted analytes. This decision was made solely on the basis of time, because the pen-ray reactor required only 1/4 the residence time of the knitted reactor. The detection limits for hydrocortisone and the non-class A cardiac glycosides were 2 ng. Quantitation of the saccharides was a different matter, because the knitted reactor demonstrated a 6-fold improvement in detection limits relative to the pen-ray reactor. For the knitted reactor, detection limits of 80 ng were calculated for the common food saccharides, whereas the detection limits (S/N = 3) were about 500 ng for the same compounds with the pen-ray reactor. There are at least two factors that may contribute to this difference. First, the greater flux of the pen-ray lamp results in higher steady-state radical concentrations. As a result, second-

ary radical reactions are expected to be more important. Another difference between the two reactors is the wavelength of excitation. Hydrogen peroxide, formed from residual oxygen, is rapidly photolyzed at 254 nm to produce the highly reactive hydroxyl radical: $H_2O_2 + h\nu \rightarrow 2OH$. The "black lamp" is filtered by pyrex so that there is no significant flux of radiation shorter than about 320 nm. Plug injections of hydrogen peroxide showed that H_2O_2 is nearly completely photodissociated within the pen-ray reactor, but unaffected by the black lamp.

Chromatography

The only detrimental effect of coupling a postcolumn reactor to an h.p.l.c. column involves the problem of peak or band broadening within the reactor capillary and any required mixing units. In comparison to a fixed-wavelength (254 nm) u.v. detector, the knitted reactor exhibited only 3% additional band broadening, whereas the pen-ray reactor produced about 20% additional band broadening.

Unfortunately, the PRF detector is not linear over a wide concentration range; the calibration curve for hydrocortisone was only linear for one order of magnitude. This finding is consistent with previous experience. However, this nonlinearity does not rule out its use as a quantitative tool.

The PRF detector suffers from a classic problem of postcolumn reaction detectors, namely the difficulty of finding a mobile phase composition that will perform an adequate separation while allowing the chemical reaction to proceed at a usable rate. Unfortunately, the energy levels of the excited triplet states of t-BAQ undergo mixing as the solvent becomes more polar or the H-bonding strength of the solvent increases. In other words, the energy level of the (n,π^*) triplet state, the photoactive state, is increased under such conditions, because the nonbonding electrons become more associated with the solvent, and it requires more energy to promote these nonbonding electrons to an excited state. The $T_2(\pi,\pi^*)$ excited state does not experience the same solvent effects, and thus the energy gap between $T_1(n,\pi^*)$ and $T_2(\pi,\pi^*)$ is reduced. This decrease in the energy gap of the two triplet states causes a mixing of the state configurations, (n,π^*) with (π,π^*). Because the (π,π^*) configuration has no photochemical reactivity, its contribution will produce a hybrid T_1 state that is less reactive than a pure $T_1(n,\pi^*)$. Thus, the efficiency of the photochemical reaction will drop drastically as the triplet-state mixing increases. A 60% acetonitrile/water mix was found to be the most polar mobile phase that would still allow adequate photochemical efficiency.

Even though some difficulty exists in finding a solvent system that is a good compromise for the separation and the postcolumn reaction, it was possible easily to separate and quantify synthetic standards and two commercial pharmaceutical products. Figures 4 and 5 are chromatograms of synthetic standards of two cardiac glycosides and hydrocortisone, respectively, and Fig. 6 (A and B) shows chromatograms of two pharmaceutical products, a digoxin tablet and hydrocortisone cream.

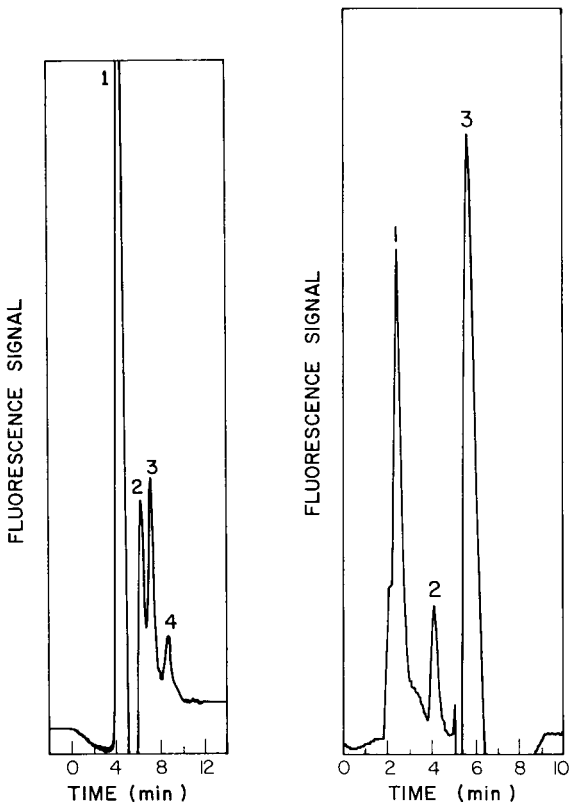

Fig. 4. Chromatogram of diginatin and digoxin. Peaks: (1) solvent; (2) 20 ng of diginatin; (3) 20 ng of digoxin; (4) solvent impurity. Conditions: flow rate 0.5 ml min^{-1}, residence time 42 s, pen-ray reactor, mobile phase 60% acetonitrile/water.

Fig. 5. Chromatogram of hydrocortisone. Peaks: (1) solvent; (2) 20 ng of hydrocortisone; (3) solvent impurity. Conditions: flow rate 1 ml min^{-1}, residence time 21 s, pen-ray reactor, mobile phase 60% acetonitrile/water.

Less difficulty was encountered in finding a mobile phase that is compatible with the photochemistry and chromatography when polar bonded-phase columns (amino and cyano) are used. These polar-bonded phases require nonpolar mobile phases for most types of separation and consequently a compromise solvent system can be avoided. Figure 6C demonstrates quantitation of components in a carbonated beverage using 87% acetonitrile and an amino column. This system represents a significant improvement over the previously reported PRF detection scheme for the determination of saccharides. In the earlier system, a post-column reagent pump was required; the anthraquinone-2,6-disulfonate could not be added to the mobile phase because its ionic groups interfered with the separation.

The reproducibility of the pen-ray photochemical reactor was evaluated

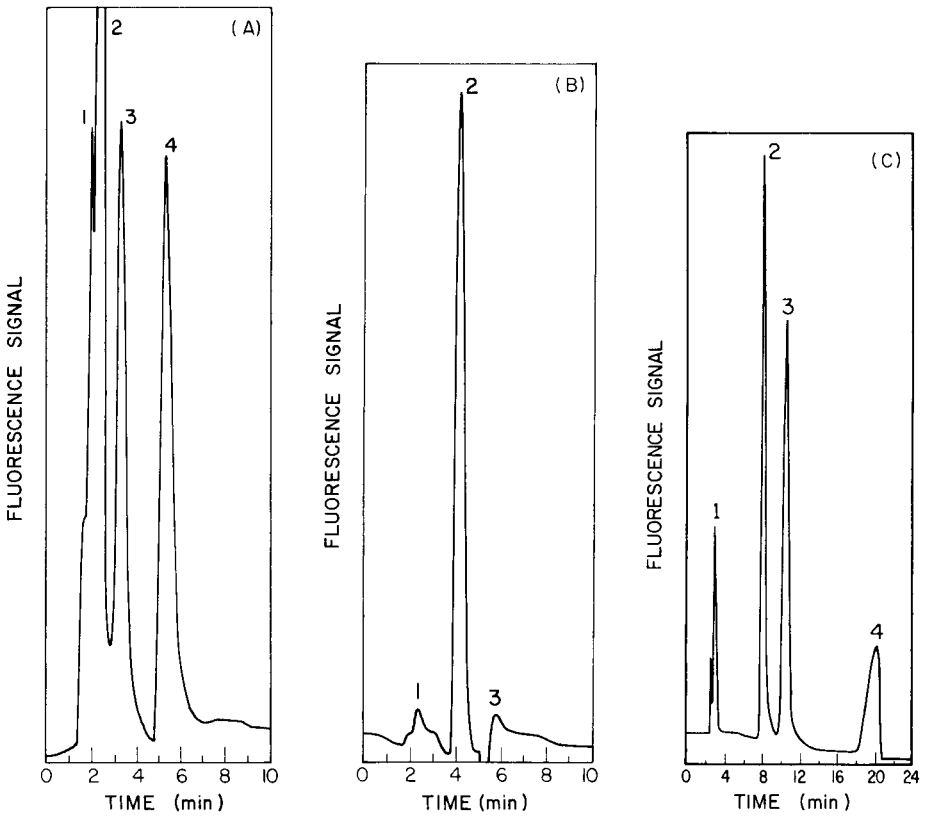

Fig. 6. Chromatograms of commercial products. (A) Digoxin tablet; peaks (1) solvent; (2) lactose; (3) 200 ng of digoxin; (4) solvent impurity; flow rate 1 ml min^{-1}, residence time 21 s, pen-ray reactor, mobile phase 60% acetonitrile/water. (B) Extracted hydrocortisone cream: peaks (1) solvent; (2) hydrocortisone; (3) solvent impurity; conditions as for (A). (C) Carbonated beverage: peaks (1) solvent; (2) fructose; (3) glucose; (4) sucrose; flow rate 1.5 ml min^{-1}, residence time 60 s, knitted reactor, mobile phase 87% acetonitrile/water.

by comparing the peak heights of ten repetitive 150-ng injections of hydrocortisone. The relative standard deviation was calculated to be 3.3%.

Comparison with conventional h.p.l.c. detectors

The performance of the PRF detector was compared to a u.v.-visible absorption detector for the determination of the cardiac glycosides and the hydrocortisone, whereas a refractive index detector was used for comparison in the case of the saccharide samples. The PRF detector exhibits slightly lower detection limits for the cardiac glycosides in comparison to the u.v.-visible detector, but the u.v.-visible detector provided greater selectivity for the digoxin tablet, because it did not respond to the lactose, an inert ingredient in the tablet. In contrast, the PRF detector, because of its sensitivity

toward saccharides, allows the quantitation of the active ingredient, digoxin, along with one of the major inert ingredients, lactose. Consequently both compounds can be quantified in one sample with the PRF detector, whereas the same information could not be obtained with the u.v.-visible detector. For the determination of hydrocortisone, the u.v.-visible detector exhibited slightly better detection limits than the PRF detector. However, for steroids such as cholesterol, cholic acid, lanosterol, and for the metabolic products of many steroid hormones that do not have the highly absorptive C=C—C=O chromophore, the PRF detector should exhibit significantly lower detection limits. Finally, the PRF detector exhibited 2—3 orders of magnitude lower detection limits and greater selectivity for saccharides in comparison to a refractive index detector attached to the same chromatographic system. Although the detection limits quoted by the manufacturers for refractive index detectors are not significantly higher than the values quoted here for the PRF detector, the detection limits obtained using a refractive index detector is considerably reduced when it is combined in a chromatographic system with single-piston, reciprocating pumps. These pumps can generate considerable flow-rate fluctuations that produce a much higher noise level in all detectors.

Conclusion

It has been found that 2-tert-butylanthraquinone provides a lower background and better detection limits in the PRF detector than does anthraquinone-2,6-disulfonate. This sensitizer also has the advantage that it can be added to the h.p.l.c. solvent reservoir without affecting the chromatography of an amino column, which is presently a popular method for separating common food saccharides.

Future work will involve further experimentation with quinone photochemistry in the hope of finding photoreactive quinones that exhibit extremely low backgrounds, and rigorous purification of acetonitrile to remove any trace quantities of HAD substrates which also would raise the background signal. It is expected that further improvements in the detection limits can be made, and thus it is likely that the ultimate detection limits of the PRF detector will be considerably lower than the u.v.-visible detector for both steroids and cardiac glycosides.

REFERENCES

1 R. W. Frei, in R. W. Frei and J. F. Lawrence (Eds.), Chemical Derivatization in Analytical Chemistry, Vol. 1, Plenum, New York, 1981, pp. 211—340.
2 R. W. Frei and A. H. M. T. Scholten, J. Chromatogr. Sci., 17 (1979) 152.
3 R. S. Deelder, M. G. F. Kroll, A. J. B. Beeren and J. H. M. Van Den Berg, J. Chromatogr., 149 (1978) 669.
4 R. W. Frei, Chromatographia, 15 (1982) 161.
5 J. W. Birks and R. W. Frei, Trends in Anal. Chem., 1 (1982) 361.
6 P. J. Twitchett, P. L. Williams and A. C. Moffat, J. Chromatogr., 149 (1978) 683.
7 P. J. Harman and G. L. Blackman, J. Chromatogr., 225 (1981) 131.

8 A. T. Rhys Williams, S. A. Winfield and R. C. Belloli, J. Chromatogr., 235 (1982) 461.
9 A. H. M. T. Scholten, U. A. Th. Brinkman and R. W. Frei, Anal. Chim. Acta, 114 (1980) 137.
10 A. H. M. T. Scholten, P. L. M. Welling, U. A. Th. Brinkman, and R. W. Frei, J. Chromatogr., 199 (1980) 239.
11 U. A. Th. Brinkman, P. L. M. Welling, G. De Vries, A. H. M. T. Scholten and R. W. Frei, J. Chromatogr., 217 (1981) 463.
12 M. Uihlein and E. Schwab, Chromatographia, 15 (1982) 140.
13 M. F. Lefevere, R. W. Frei, A. H. M. T. Scholten and U. A. Th. Brinkman, Chromatographia, 15 (1982) 459.
14 W. Iwaoka and S. R. Tannenbaum, IARC Sci. Publ., 14 (1976) 51.
15 D. J. Popvich, J. B. Dixon and B. J. Ehrlich, J. Chromatogr. Sci., 17 (1979) 643.
16 M. S. Gandelman and J. W. Birks, J. Chromatogr., 242 (1982) 21.
17 M. S. Gandelman and J. W. Birks, Anal. Chem., 54 (1982) 2131.
18 M. S. Gandelman, J. W. Birks, U. A. Th. Brinkman and R. W. Frei, J. Chromatogr., in press.
19 N. J. Turro, Modern Molecular Photochemistry, Benjamin-Cummings, Menlo Park, CA, 1978.
20 H. G. Viehe, R. Merenyi, L. Stella and Z. Janouseh, Angew. Chem. Int. Ed. Engl., 18 (1978) 917.
21 J. L. Bolland and H. R. Cooper, Proc. R. Soc., London, Ser. A, 225 (1954) 405.
22 C. F. Wells, Trans. Faraday Soc., 57 (1961) 1703, 1719.
23 F. Wilkinson, J. Phys. Chem., 66 (1962) 2569.
24 K. Tickle and F. Wilkinson, Trans. Faraday Soc., 61 (1965) 1981.
25 J. Beutel, R. J. Ruszkay and J. F. Brennan, J. Phys. Chem., 73 (1969) 3240.
26 A. Ledwith, G. Ndaalio and A. R. Taylor, Macromolecules, 8 (1975) 1.
27 A. Harriman and A. Mills, Photochem. Photobiol., 33 (1981) 619.
28 K. P. Clark and H. I. Stonehill, Trans. Faraday Soc. I, 68 (1972) 578, 1676.

Analytica Chimica Acta, 155 (1983) 173—181
Elsevier Science Publishers B.V., Amsterdam — Printed in The Netherlands

IDENTIFICATION OF FIBRES AND FIBRE BLENDS BY PYROLYSIS GAS CHROMATOGRAPHY

P. PERLSTEIN

Organic Materials Division, National Building Research Institute, C.S.I.R., P.O. Box 395, Pretoria 0001 (Republic of South Africa)

(Received 14th June 1983)

SUMMARY

The identification of single fibres and fibre blends by means of pyrolysis gas chromatography is described. The pyrograms are interpreted with the aid of identified peaks which are diagnostic for each fibre rather than by the pattern recognition method. This method of diagnostic peaks is especially useful for the identification of fibre blends.

The usefulness of pyrolysis gas chromatography (p.g.c.) for the identification of individual fibres has been demonstrated by several authors [1—5]. In certain cases, fibre blends were also analysed by the p.g.c. technique [2—4]. The gas chromatograms obtained from the pyrolysis products, the pyrograms, were interpreted by the "fingerprint" method. Numerous textiles used in carpeting, as well as nonwoven geofabrics used in dam construction and waterproofing, are currently evaluated in this Institute. A method was required for the identification of these fibres and fibre blends; p.g.c. was found to be the most reliable technique.

Most fibres exhibit in their pyrograms one or more main peaks which are characteristic of the particular fibre. Most of these diagnostic peaks are known, having been identified by absolute methods. The gases and liquids with low boiling points emanating from the pyrolysis of fibres are mostly non-specific. More useful decomposition products are the liquids with higher boiling points and certain solids which are of structural importance. A Carbowax 20M liquid phase gives excellent separation of the peaks characteristic of fibres and exhibits a very long lifetime, i.e., the retention times and the resolution are not significantly changed with time. Such a column has been in continuous use in this laboratory for over two years. The presence of the diagnostic peaks in the different pyrograms was confirmed by retention times on at least two columns, first on Carbowax 20M liquid phase and second either on a Porapak QS column or on an OV-225 liquid phase.

This method of interpreting the pyrograms, by diagnostic peaks rather than by their patterns or fingerprints, was applied by May et al. for identification of thermoplastic and thermosetting polymers [6]. These authors included a collection of pyrograms of such polymers, obtained by using

0003-2670/83/$03.00

Porapak Q as a column packing material. For fibre blends, the interpretation of pyrograms by using diagnostic peaks readily reveals the presence of the components. Once the fibres are known a full quantitative analysis can be completed by dissolving one of the components in a specific solvent and weighing the dried residue of the remaining constituents.

EXPERIMENTAL

For p.g.c., the instrumentation consisted of a Pye-Unicam Curie Point Pyrolyser mounted on the injector of a dual-column Pye-Unicam Series 204 gas chromatograph with flame ionization detectors, a Philips PM-8252 recorder and a Pye-Unicam DP-88 computing integrator. The recorder chart speed was 15 mm min^{-1}.

For pyrolysis, an iron wire (100 mm long, 0.55 mm diameter) was used, giving a temperature of 770°C at the Curie point. One end of the wire, approximately 10 mm in length, was flattened to a width of 1.5 mm and bent to form a hook about 2 mm long. The fibres were placed in this hook, which was securely pinched together and the loose ends of the fibres were removed. The wire was weighed before and after the insertion of the fibre, using a microbalance readable to ±1 μg. The weight of fibre on the wire was 100—300 μg. A glass tube (6 cm long) was inserted through the injector head into the end of the column. The ferromagnetic wire was then inserted through the septum in the glass tube which protects the walls of the column from contamination by heavy pyrolysis products. For every pyrolysis a new glass tube was used. The pyrolysis time was 8 s. The conditions of the gas chromatograph are given in Table 1. The pyrolysis and the temperature programme of the gas chromatograph were started simultaneously.

The first 8-cm length of the g.c. columns was filled with glass wool to protect the column from becoming clogged by pyrolysis residues.

The materials used as standards to ascertain the retention times of diagnostic peaks were of reagent grade. Vinyl benzoate was prepared in this laboratory by the vinyl interchange reaction of benzoic acid with vinyl acetate in the presence of mercury(II) ions and fuming sulphuric acid [7].

TABLE 1

Gas chromatographic conditions

Column packing	10% Carbowax 20 M on Chromosorb W 80-100	5% OV-225 on Chromosorb W-HP-100-120	Porapak QS
Column (glass)	2.1 m × 0.4 mm i.d.	1.5 m × 0.4 mm i.d.	1.6 m × 0.4 mm i.d.
Injector temp. (°C)	125	125	125
Detector temp. (°C)	200	200	250
Nitrogen carrier flow rate (ml min^{-1})	30	30	60
Temperature programme	70°C for 10 min, 70—180°C at 16°C/min, hold at 180°C for 35 min.		120—250°C at 12°C/min, hold at 250°C for 35 min.

RESULTS AND DISCUSSION

Diagnostic peaks used for the identification of fibres

Twenty-seven compounds were used; the presence of one or more of these in the pyrogram of a given fibre or fibre blend indicated the presence of a certain fibre. The retention times of these compounds on a Carbowax 20M column are given in Table 2. To ascertain the presence of the compounds

TABLE 2

Retention data for the diagnostic peaks used in the identification of fibres[a]

Compound	Retention time (min)		Peak appears in pyrogram from
	Carbowax 20M	Porapak QS	
Acetaldehyde	1.65	3.15	Polyvinyl alcohol, polyester, wool, silk, cellulosics
Vinylidenechloride	1.85	5.85	Polyvinylidenechloride (d)
Acetone	2.50	5.85	Polyvinyl alcohol, cellulosics
1-Octene	3.05	12.80	Polyethylene
Benzene	4.70	9.20	Polyester(m), aramids
1-Nonene	5.10	15.90	Polyethylene
Acrylonitrile	6.10	6.05	PAN and copolyacrylonitriles (d)
Acetonitrile	6.65	5.15	PAN and copolyacrylonitriles, silk (d), wool (d)
Toluene	8.35	11.35	Wool (d), silk (d), polyester, aramids
Crotonaldehyde	8.45	9.10	Polyvinylalcohol (m,d)
1-Decene	9.10	20.90	Polyethylene (d)
Cyclopentanone	13.75	11.75	Polyamide 66 (m,d), polyamide 6
Styrene	15.00	14.60	Polyester
1-Dodecene	15.05	42.45	Polyethylene
Hydroxyacetone	15.65	9.45	Cellulosics (d)
Acetic acid	17.10	7.50	Poly(acrylonitrile-vinyl acetate) (d), cellulose acetate (m,d)
m-Dichlorobenzene	17.15	17.95	Polyvinylidenechloride
Furfural	17.55	12.40	Cellulosics (d)
Pyrrole	18.10	10.30	Wool (d), silk (d)
1,3,5-Trichlorobenzene	18.50	25.50	Polyvinylidenechloride (m,d)
Benzonitrile[b]	19.75	18.05	Aramids (d)
Vinyl benzoate	20.40	31.25	Polyester (d)
Acetophenone	20.55	23.35	Polyvinylalcohol (d), polyester
Aniline[c]	22.05	—	Aramids
Biphenyl[c]	31.40	—	Polyester
p-Cresol	34.25	22.05	Wool (d), silk (d)
ϵ-Caprolactam[c]	43.65	—	Polyamide 6 (m,d)

[a]Gas chromatographic conditions are given in Experimental. d = Diagnostic; if present it immediately indicates the particular fibre. m = Main peak in the pyrogram. [b]Retention time on OV-225 is 12.6 min. [c]Does not elute when injected on Porapak QS column. The retention times (min) on OV-225 column (see Experimental) are: aniline 11.80, biphenyl 17.40, and ϵ-caprolactam 17.60.

which are characteristic of particular fibres, the pyrograms of all the fibres and fibre blends were done on both the Carbowax 20M and the Porapak QS columns. The retention times of these diagnostic compounds on the Porapak QS column are also listed in Table 2. The retention times of aniline, biphenyl and ϵ-caprolactam were recorded on OV-225, because they did not elute on Porapak QS.

Polyethyleneterephthalate (PETP). Benzene is the main product of the pyrolysis; very characteristic is the presence of vinyl benzoate and biphenyl.

Polyamides. For polyamide 6, the main peak is the monomer ϵ-caprolactam; for polyamide 66, the main peak is cyclopentanone, originating from the adipic acid component. The main peaks in the pyrolysis of the aromatic polyamides, poly-*m*-phenylene isophthalamide (Nomex) and poly-*p*-phenylene terephthalamide (Kevlar) have been identified by Brown and Power [8]. On the Carbowax 20M column, the main peaks are benzonitrile, benzene and aniline, the presence of which was also confirmed on Porapak QS for benzene and benzonitrile and on OV-225 for all three peaks.

The two aramids may be differentiated by the fact that in the case of Nomex the benzonitrile and benzene peaks are of comparable area, whereas in the pyrogram of Kevlar the benzonitrile peak is about double the area of the benzene peak. Another differentiating feature, shown in Table 3, is the low pyrolysis yield of Kevlar at 770°C. At 980°C, both aramids give similar yields.

Acrylonitrile fibres. A large acrylonitrile peak at 6.1 min and close to it a much smaller acetonitrile peak at 6.65 min are strongly indicative of PAN (Orlon). The poly(acrylonitrile-vinyl acetate) copolymer (Acrilan) shows the same features, but in addition it exhibits a strong acetic acid peak.

Polyolefins. Polyethylene is known to yield α-olefins, α,ω-dienes and n-paraffins when pyrolysed at high temperatures. In the present experimental set-up, 1-nonene, 1-decene and 1-dodecene are characteristic. The pyrograms of low- and high-density polyethylene are identical.

Polypropylene is the only fibre for which the fingerprint method of interpretation of the pyrogram was used. Very prominent are the main peak at 3.75 min and the doublet appearing at 16.2 and 16.45 min.

TABLE 3

Characteristic peak areas and yields of aramid pyrograms at different temperatures

	$\frac{\text{Benzene}}{\text{Benzonitrile}}$ (770°C)	Pyrolysis yield (%)[a]	
		770°C	980°C[b]
Nomex	>1	53	55
Kevlar	0.5	24	57

[a]Defined as Yield (%) = [(Mass of wire + fibre) − (Mass of wire + char)/Mass of fibre] × 100. [b]Fe/Co (50:50) wire.

Polyvinyl alcohol. The presence in the pyrogram of crotonaldehyde as the main peak, and of acetaldehyde together with acetone and acetophenone permit the identification of polyvinyl alcohol.

Polyvinylidenechloride. The main peak of the pyrogram is 1,3,5-trichlorobenzene, which is known to result from pyrolytic dehydrochlorination followed by cyclisation. Characteristic are also the vinylidene chloride monomer and *m*-dichlorobenzene.

Cellulose fibres. The pyrolysis of cellulose and the identity of its degradation products were studied by Lipska and Wodley [9]. In the present case, the main peaks useful for the identification of cotton are hydroxyacetone, furfural, acetaldehyde and acetone (Fig. 1).

To distinguish between natural cotton and rayon, the unidentified shoulder at 16.15 min is used. This shoulder is much larger in the pyrogram of rayon than in that of natural cotton. The ratio of the peak area at 16.15 min versus the hydroxyacetone peak is 0.73 for natural cotton and 1.3 for rayon. Mercerized cotton gives a pyrogram identical to that of rayon, a regenerated cellulose. To distinguish between these two fibres, microscopy is required. When this technique is used, natural and mercerised cotton show twists or convolutions, whereas the regenerated cellulose fibres have a straight rod-like shape with occasional striations in the fibre direction.

Protein fibres. Several organic products derived from the pyrolysis of wool and silk were identified by Hiramatsu [10]. Among the higher-boiling products, nitrogen-containing products or phenols were not detected. Ingham [11] studied the pyrolysis of wool at 550°C, but identified only the gases evolved.

The pyrogram of wool is shown in Fig. 2. The diagnostic peaks are acetaldehyde, acetonitrile, toluene, pyrrole and *p*-cresol. The amino acid compositions of both wool [12] and silk [13] are well known. The pyrolysis products of amino acids [14] and of derivatised amino acids [15] have been studied and largely identified. Table 4 summarizes the main pyrolysis products of amino acids found in the composition of wool and silk.

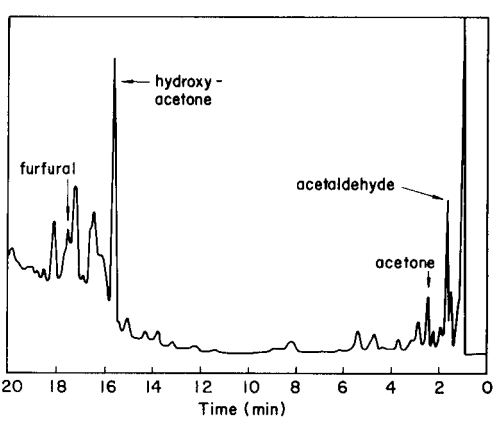

Fig. 1. Pyrogram of natural cotton.

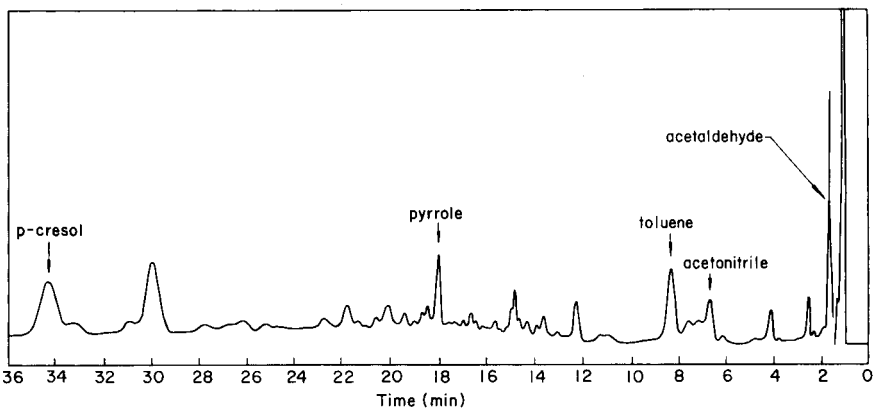

Fig. 2. Pyrogram of wool.

Wool and silk may be differentiated by marked and reproducible differences in their pyrograms. From wool, the acetonitrile peak is much smaller than the toluene peak, whereas from silk the acetonitrile peak is about three times larger than the toluene peak. This may be explained by the significant decrease in the phenylalanine content (producing toluene on pyrolysis) and the increase in the serine content (producing acetonitrile on pyrolysis) in the composition of silk. Pyrrole also decreases in intensity, because of the much lower proline content of silk.

Identification of fibre blends

Polyethylene terephthalate/wool. The pyrogram of a PETP/wool of a nominal composition of 65/35 is shown in Fig. 3. Benzene and vinyl benzoate originate from PETP. The presence of wool is revealed by the pyrrole peak and also by a significantly intensified toluene peak, of which the greater part originates from the wool fibre. The ratio between the peak areas

TABLE 4

The pyrolysis products of amino acids known to be present in wool and silk

Amino acid	Percentage by mass in		Pyrolysis product
	wool	silk[a]	
Threonine	6.4	0.97	Acetaldehyde[b]
Serine	9.1	18.1	Acetonitrile[b]
Phenylalanine	3.9	0.5	Toluene[c]
Proline	6.8	0.4	Pyrrole[b]
Tyrosine	5.8	4.6	*p*-Cresol[b]

[a]Weighted average between fibroin and sericine, knowing that silk is composed of about 76% fibroin and 24% sericine. [b]Product of the pyrolysis of the phenylthiohydantoin derivative of the respective amino acid [15]. [c]See Völlmin et al. [14].

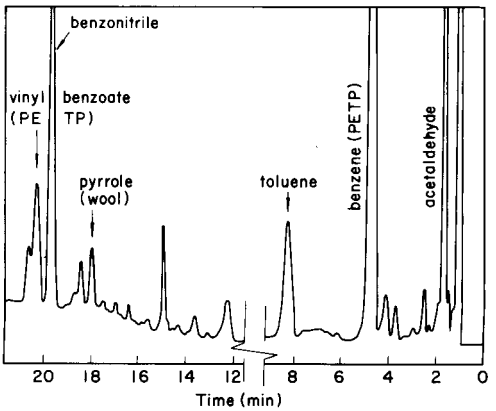

Fig. 3. Pyrogram of a PETP (65%)/wool (35%) fibre blend.

of toluene and benzene in PETP is 1/20 whereas in the 65/35 PETP/wool blend it is 1/8.

An interesting feature of the pyrogram of this mixture is the appearance of an intense peak at 19.75 min, corresponding to benzonitrile. The identity of this peak was verified by running the p.g.c. on the three different columns used in this work. As benzonitrile is not present in the pyrogram of wool, a reaction between reactive intermediates formed during the pyrolysis of the two different fibres has to be postulated. Benzene radicals are present in abundance when PETP is pyrolysed. These radicals, provided with a long enough lifetime, can encounter nitrile-containing molecules such as HCN, CH_3CN or their radical precursors resulting from the pyrolysis of wool, giving benzonitrile.

PETP/cotton. The pyrogram of a 65/35 blend of PETP with cotton is shown in Fig. 4. PETP is evidenced by the dominant peak of benzene and vinyl benzoate. Cotton is revealed by the typical region between 15.3 and

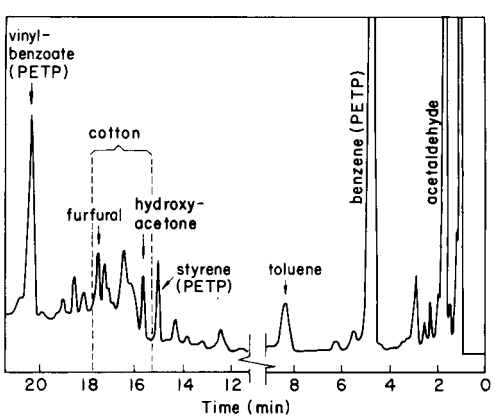

Fig. 4. Pyrogram of a PETP (65%)/cotton (35%) fibre blend.

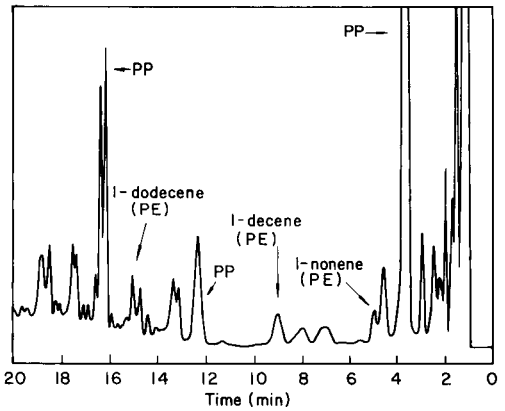

Fig. 5. Pyrogram of a polypropylene (55%)/low-density polyethylene (45%) fibre blend.

17.8 min. It is similar to a "fingerprint" for cotton, the diagnostic peaks of hydroxyacetone, furfural and the shoulder at 16.15 min showing the presence of cotton.

PETP/polypropylene. The peaks diagnostic for PETP are the same as in the two previous blends. For polypropylene the diagnostic peaks are an unidentified very large peak at 3.75 min and the doublet at 16.2 and 16.45 min.

Blends of polyamide 66 with poly(acrylonitrile-vinyl acetate), polypropylene and wool. The pyrograms of polyamide 66 blends with poly(acrylonitrile-vinyl acetate), polypropylene and wool present no special identification problems. The diagnostic peaks are well separated.

Blends of polypropylene with poly(acrylonitrile-vinyl acetate) or polyethylene fibres. In the pyrogram of the polypropylene/poly(acrylonitrile-vinyl acetate) blend the diagnostic peaks of both fibres are evident.

The pyrogram of the polypropylene/low-density polyethylene blend (Fig. 5) exhibits the above-mentioned characteristic peaks for polypropylene (PP) and the three diagnostic peaks showing the presence of polyethylene (PE): 1-nonene, 1-decene and 1-dodecene. The fact that the blend contained low-density polyethylene was revealed by thermal analysis.

The author thanks Dr. H. M. Saayman for many helpful discussions, Messrs. R. Cromarty and M. Smit for kindly providing the fibre samples, and Messrs. V. de Melo and P. Orme for doing part of the experimental work.

REFERENCES

1 H. Haase and J. Rau, Melliand Textilber., (1966) 434.
2 U. Gokcen and D. M. Cates, Appl. Polym. Symp., 2 (1966) 15.
3 J. Derminot and C. Rabourdin-Belin, Bull. Inst. Text. Fr., 25 (1971) 721.

4 B. Focher, A. Seves and M. Bollini, Tinctoria, 12 (1972) 411.
5 W. Günther, K. Koukoudimos and F. Schlegelmilch, Melliand Textilber., (1979) 501.
6 R. W. May, E. F. Pearson and D. Scothern, Pyrolysis—Gas Chromatography, The Chemical Society, London, 1977.
7 R. L. Adelman, J. Org. Chem., (1949) 1057.
8 J. R. Brown and A. J. Power, Polym. Degradation Stab., 4 (1982) 379.
9 A. E. Lipska and F. A. Wodley, J. Appl. Polym. Sci., 13 (1969) 851.
10 K. Hiramatsu, Mass Spectrosc. (Tokyo), 14 (1966) 285.
11 P. E. Ingham, J. Appl. Polym. Sci., 15 (1971) 3025.
12 W. v. Bergen (Ed.), Wool Handbook, Vol. 1, Interscience, New York, 1963, p. 225.
13 Ullmanns Encyklopädie der Technischen Chemie, Vol. 21, Verlag Chemie, Weinheim, 1982, p. 203.
14 J. Völlmin, P. Kriemler, I. Omura, J. Seibl and W. Simon, Microchem. J., 11 (1966) 73.
15 C. Merritt, C. Di Pietro, D. H. Robertson and E. J. Levy, J. Chromatogr. Sci., 12 (1974) 668.

Analytica Chimica Acta, 155 (1983) 183—189
Elsevier Science Publishers B.V., Amsterdam — Printed in The Netherlands

A UNIVERSAL MICROCOMPUTER INTERFACE FOR THE RAPID ACQUISITION OF DATA FROM ATOMIC ABSORPTION SPECTROMETERS

K. LUM
National Water Research Institute, Burlington, Ontario (Canada)
D. NARANJIT
Department of Chemistry, University of Toronto, Toronto, Ontario (Canada)
B. RADZIUK* and Y. THOMASSEN
Institute of Occupational Health, P.O. Box 8149 Dep, Oslo 1 (Norway)

(Received 2nd May 1983)

SUMMARY

A universal data acquisition interface for atomic absorption spectrometers is described. A minimum of electronic circuitry is required. The software is designed for flexibility and simple operation. Photomultiplier response is monitored directly so that separate plots of total absorbance, background absorbance and corrected atomic absorbance, as a function of time, can be produced for each measurement. Thus more information is provided than is normally available from the digital communications link of most such instruments. Use of the system to interface an Apple II microcomputer with Perkin-Elmer 5000 and Zeeman 5000 instruments is described and examples of results are given.

Many of the sampling techniques used for atomic spectrometric determinations, notably those involving a graphite furnace, give rise to variations in detected light intensity too rapid to be followed accurately by a conventional analog recorder. Storage oscilloscopes [1, 2] and more recently computer systems have been used for studies of atom generation mechanisms [3, 4] in order to provide undistorted information on the time-dependence of these variations. Such information is also essential in the systematic development of methods for routine analysis. Several manufacturers of atomic absorption spectrometers now offer video and/or graphics accessories for this purpose.

Self-contained microcomputers, now commonplace in the laboratory and used primarily for the statistical manipulation of data, are sometimes interfaced by means of a digital communications link to an analytical instrument with a built-in microprocessor. It is often the case that the digital values are

0003-2670/83/$03.00

obtained at the end of the analog processing chain and are thus dependent on the operating mode of the instrument.

The interface described in this paper was designed for the rapid acquisition of raw analog data from virtually any atomic absorption spectrometer, using a basic microcomputer. Very little electronic circuitry is required, and by means of minor modifications in software the interface can be adapted to a wide variety of specific applications. Intensity variations resulting from both atomic and non-specific absorption are monitored, with a time-resolution limited only by the inherent characteristics of the instrument. These data are then manipulated to produce individual plots of line absorbance, non-specific absorbance, as well as "corrected" atomic absorbance, vs. time. Use of the interface in no way affects the operation of the spectrometer.

For the work described here, an Apple II microcomputer was interfaced with a Perkin-Elmer 5000 atomic absorption spectrometer. The capabilities of the interface are illustrated and compared to those of the graphics system offered by the manufacturer. To demonstrate the flexibility, the use of an Apple II—Perkin-Elmer Zeeman system is also described.

EXPERIMENTAL

The interface is shown schematically in Fig. 1. It consists of an electronic circuit for analog signal conditioning and integration (Fig. 2), an analog-to-digital converter (12-bit resolution, 0.78-ms conversion time; Analog I/O 801, Datateknikk AS, Skedsmokorset, Norway) and a program written in 6502 machine code, summarized in Table 1.

For operation with a PE-5000 (also applicable to the PE-4000), three

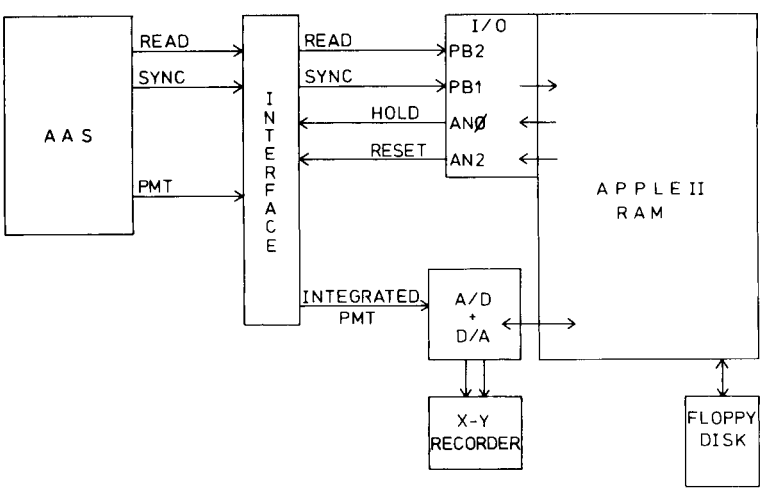

Fig. 1. Block diagram of interface for atomic absorption spectrometer with an Apple II microcomputer.

TABLE 1

Program steps for timing and data acquisition

1. Initialize data buffers, Y-index register and Page counter
2. If not in gain/zero calibration mode, wait for PB2 to become low
3. Wait for first falling edge in optical synchronization wave train at PB1
4. Sequence of 7 delays to produce HOLD and RESET pulses shown in Fig. 3
   Length of a delay is determined by the value assigned to the X-index register
   After each integration period start conversion, wait for end of conversion, store the 12 bits of each value in two locations indexed by Y
5. Wait for next falling edge at PB1 to ensure that synchronization is maintained
6. Check counters to determine whether or not sufficient data have been acquired; if yes, return to BASIC
7. Increment counters and buffer addresses
8. Return to beginning of data collection cycle (step 4)

signals from the instrument are used: (1) the "read" signal available at an external connector; (2) a 50-Hz square wave (jumper SP4, analog receiver board), optically coupled to the rotation of the chopper; and (3) the output of the photomultiplier preamplifier (TP3, analog receiver board). Signals 1 and 2 are buffered and applied to single bit (PB) inputs of the Apple I/O connector. The state of these inputs is monitored in, and controls execution of, the program. During the measurement period, which begins when the state of PB2 changes to low, "hold" and "reset" pulses synchronized with the 50-Hz square wave are generated at annunciator (AN) outputs by program instructions. These pulses are timed by means of programmed delays to coincide with the desired integration intervals.

In this case, for each 20-ms measurement cycle of the instrument (i.e., for a half rotation of the chopper), there are four such integration intervals, yielding values corresponding to the intensity of the line source sample, the continuum source sample, the line source reference, and the continuum source reference beams. The timing relationships are shown schematically in Fig. 3.

All values obtained for each 20-ms cycle during an observation period of up to 20 s are stored and may be transferred to disk for later recovery and/or manipulated after completion of the measurement cycle. A program to control the operating sequence and for data handling was written in Applesoft BASIC and compiled (microsoft TASC compiler) to increase speed of execution. Total absorbance, background-only absorbance and corrected atomic absorbance (total minus background) may be plotted against a program-generated time axis with a resolution of 20 ms. Peak area and peak height may also be calculated. Reference values measured within each cycle are incorporated into the calculations in order to compensate for source intensity fluctuations and furnace emission.

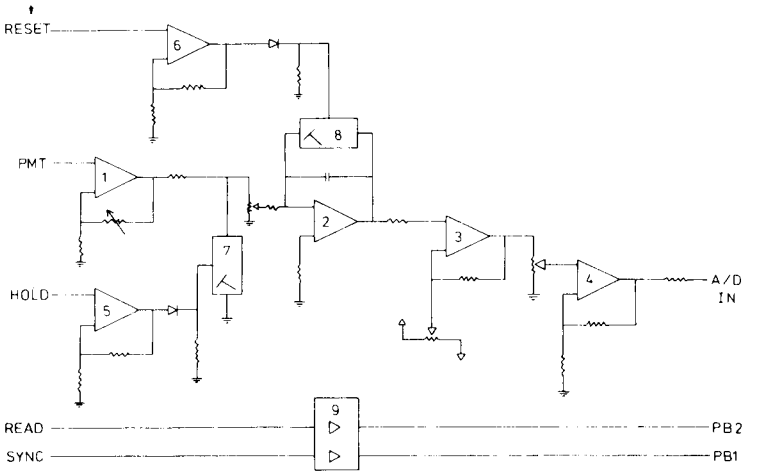

Fig. 2. Schematic diagram of analog signal processing circuit:

Integrated circuit		Function
1	TL071	Gain stage
2	TL071	Integrator, RC = 2.2 ms
3, 4	LM324	Offset & gain stage
5, 6	LM324	Buffer, TTL-CMOS
7, 8	CD4066	FET analog switch
9	CD4050	Buffer, CMOS-TTL

RESULTS AND DISCUSSION

The data acquisition system based on Apple II was developed for a study of matrix modification methods for the reduction of spectral interferences in the determination of selenium and arsenic by graphite-furnace atomic absorption spectrometry, which will be reported at a later date. The system can be used in addition to, but independently of, any other interface device without affecting the results obtained on the instrument display, at the output for the analog recorder or through the communications port. Conversely, data for all source beams are acquired, regardless of the mode of operation of the instrument. A direct comparison of the output with a Data Station display of information which was acquired through the RSC 232 communications port is presented in Fig. 4. There is more baseline noise apparent in the plot generated by the Apple II system (Fig. 4a) than in the printer plot (Fig. 4b). This is due primarily to the fact that digital values obtained with 12-bit A/D converter resolution, rather than analog signals, are used in the logarithmic conversion and subtraction operations. The signal-to-noise disadvantage is more than adequately compensated, however, by the provision of considerably more analytical information per measurement than is normally available at the communications port. For example, an

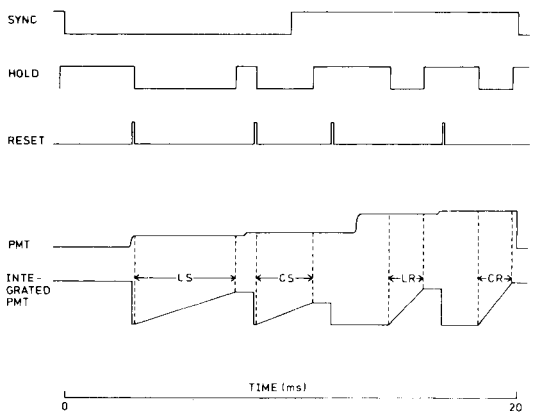

Fig. 3. One cycle of 50-Hz optical synchronization signal (PE-5000). Integration intervals: LS, line source sample beam; CS, continuum source sample beam; LR, line source reference beam; CR, continuum source reference beam.

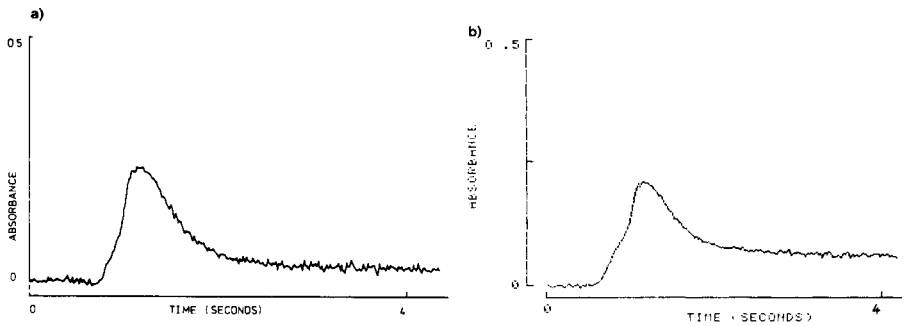

Fig. 4. Plots of atomic absorbance corrected for non-specific absorbance vs. time for the same determination of manganese in aqueous solution: (a) Apple II with X-Y recorder (Houston Omniscribe); (b) Perkin-Elmer 3600 Data Station with printer (PE-PR100).

apparent negative absorbance obtained with the PE-5000 operated in the "AA-BG" mode can be resolved into line and non-specific absorbances, as shown in Fig. 5. From this, it is clear that the "over-compensation" results, in fact, from the presence of species which absorb more strongly in other regions of the spectral bandpass than at the analyte line.

The BASIC program was written to make operation of the system simple but flexible. The raw data for a series of measurements may be stored on disk, and the three data sets calculated for each may be plotted, by pressing the space bar on the keyboard in response to the flashing cursor on the screen. Options may be selected by pressing specific keys at certain points in the program. The plotting step may be omitted entirely, or data, either the last collected or that retrieved from a disk file, can be plotted using various time and absorbance ranges, zero offsets and/or degrees of smoothing.

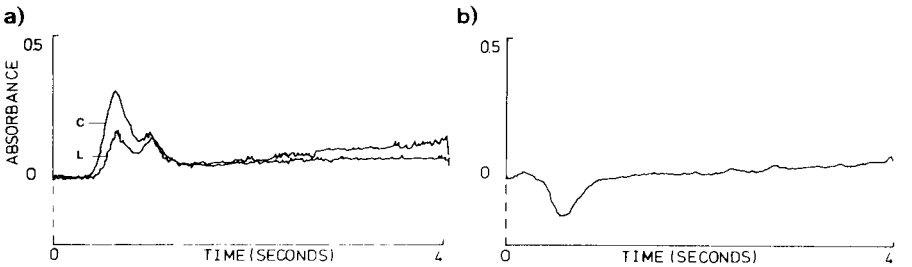

Fig. 5. Absorbance vs. time plots obtained with 0.025% (w/w) phosphate in aqueous solution at 196.0 nm using a selenium electrodeless discharge lamp. (a) Superimposed plots of line absorbance (L) and continuum absorbance (C). (b) "Atomic" absorbance minus "background" absorbance (here, a four-point running average was used for smoothing).

Peak height and peak area for any desired time intervals may be calculated. Calibration procedures may also be implemented.

The design of the Apple II microcomputer makes possible an especially straightforward interface, but the concepts described here can be applied similarly to other 6502 processor-based microcomputers (e.g., Commodore 8000 series, BASIS, Sirius, AIM) and, with appropriate software changes, to computers based on other processors. The data acquisition program has, in fact, been translated for use with an INTEL 8088 processor.

The choice of electronic components is not critical; yet it should be noted that the A/D and D/A card used in this study was not ideal. The conversions occupied 20% of each measurement cycle, which affected the signal-to-noise ratio slightly. There are many similar plug-in cards available for the Apple, including 12-bit A/D converters with conversion times under 100 μs. Alternatively, an A/D and D/A circuit, along with the analog circuit shown in Fig. 2, can be assembled on a plug-in prototype board.

For plotting, precise control of the time/absorbance relationship may be achieved with a 2-channel D/A converter, one channel for generating the time axis and the other for absorbance values. Should an X-Y recorder not be available, one D/A channel and a standard strip-chart recorder may be used.

High-resolution graphics, facilitating the display of data on a monitor screen, are either built into or available for most microcomputers. In the authors' experience it is more convenient simply to obtain recorder hard copy than to use the screen display and optional print-out.

For Zeeman operation of the PE-5000, the source is electronically modulated at 100 Hz, twice the frequency of the magnetic field modulation. In order to use the described system with this instrument, it was necessary only to adjust the delays so that, of the four integration intervals per measurement cycle, two correspond to lamp ON periods. Corrected atomic absorbance in good agreement with that obtained using a PE Data Station was calculated by subtracting pairs of values corresponding to magnet off (total)

and magnet on (background only) periods. When background absorption is significant, however, it is not possible to acquire separate, accurate data for total and non-specific absorption because of the automatic gain control circuit used in the instrument. Methods used to circumvent this problem, previously encountered in work with a Hitachi-170-70 Zeeman atomic absorption spectrophotometer, will be discussed at a later date.

The data acquisition system is now in routine use in a practical laboratory and will be subject to long-term evaluation. Further applications are under investigation.

The authors are indebted to Dr. Y. Thomassen for providing the opportunity to complete this work, and to his co-workers at the Institute for Occupational Health in Oslo for their cooperation and assistance. B. Radziuk gratefully acknowledges the financial support of the Alexander von Humboldt-Stiftung, Bundesrepublik Deutschland, for the part of the work which was carried out in Oslo.

REFERENCES

1 R. E. Sturgeon and C. L. Chakrabarti, Prog. Anal. At. Spectrosc., 1 (1978) 5.
2 J. P. Maney and V. J. Luciano, Anal. Chim. Acta, 125 (1981) 183.
3 E. Lundberg and W. Frech, Anal. Chem., 53 (1981) 1437.
4 M. Suzuki, K. Ohta and T. Yamakita, Anal. Chim. Acta, 133 (1981) 209.

Analytica Chimica Acta, 155 (1983) 191—198
Elsevier Science Publishers B.V., Amsterdam — Printed in The Netherlands

ANALYSIS OF THIN METALLIC FILMS BY GLOW DISCHARGE MASS SPECTROMETRY

M. HECQ*, A. HECQ and M. FONTIGNIES

Université de l'Etat à Mons, Laboratoire de Chimie Inorganique, 23, Avenue Maistriau, 7000 Mons (Belgium)

(Received 1st June 1983)

SUMMARY

Copper targets covered by a sequence of thin metallic films are analysed by glow discharge mass spectrometry. The sensitivity is inversely proportional to the ion mass. An oxygen plasma leads to a higher sensitivity than an argon plasma. When different metallic targets are sputtered in an argon plasma, the metal ion currents are proportional to the deposition rate. It is suggested that the ionization of the sputtered species in an oxygen plasma can be explained by charge-transfer reactions. For all the metals studied in a given gas, the ionization cross-sections are of the same order of magnitude.

Glow discharge mass spectrometry (g.d.m.s.) is a simple and sensitive method for the determination of target composition and a convenient method for investigating reactive sputtering processes [1]. In this method, positive ions bombard a target containing the material to be analysed and eject particles (ions, neutral species, electrons) from the surface. Some sputtered neutral species become ionized in the plasma. In the case of an argon discharge, it has been shown that Penning ionization is the dominant process [2, 3] for the sputtered species ionization. The general reaction is $Ar^m + M \rightarrow Ar + M^+ + e^-$, where M is the sputtered species and Ar^m is a metastable argon atom. Gas particles are ionized by electron impact [4]. Plasma ions pass through a hole located in the anode and are detected with a quadrupole mass spectrometer. Unlike secondary-ion mass spectrometry, the ions are formed after their ejection from the target outside the cathodic sheath and no matrix effects are found. Many authors [1] assume that the ionization efficiency of the sputtered species is independent of their ionization potential energy. In order to apply this technique to quantitative measurements, we have checked the mass discrimination of the system, the influence of the nature of the gas (argon, oxygen or mixtures of both gases) on the ionization efficiency and the relation between the deposition rate and the ionic current. An interpretation of the ionization mode in an oxygen discharge is given.

0003-2670/83/$03.00

EXPERIMENTAL

The experimental system is shown in Fig. 1. It has two parts, one containing the ion source and the second the quadrupole mass spectrometer. Ions are produced in a glow discharge by a planar sputtering system. The low-pressure enclosure containing the quadrupole filter is separated from the high-pressure side by a diaphragm with a hole 0.5 mm in diameter. The diaphragm is an earthed metal disc. The electrical power is not a pure r.f. system but the waveform is more or less rectangular and asymmetric [5].

The frequency is adjusted to ≈2000 Hz. In the negative phase of the alternating system, the equipment acts by classical d.c. sputtering. The positive phase is of shorter duration and may thus be considered as a sampling phase. The sputtering voltage is the bias arising from the rectified voltage. Between the hole and the mass filter there is a cross-beam ionization source but during measurements by glow discharge mass spectrometry (g.d.m.s.) the filament is not used. The acceleration voltage used was 100 V; extraction voltage, 150 V; formation voltage, 40 V; field axis potential, 25 V.

At the exit of the mass filter are a 90° deflector, an electron multiplier and an electrometer. The electron multiplier consists of ten Cu-Be dynodes and 2000 V is usually applied to the first dynode. The crossed-beam ionization source can be replaced by an extraction electrode and a cylindrical focussing electrode. The extraction electrode is required to remove the space

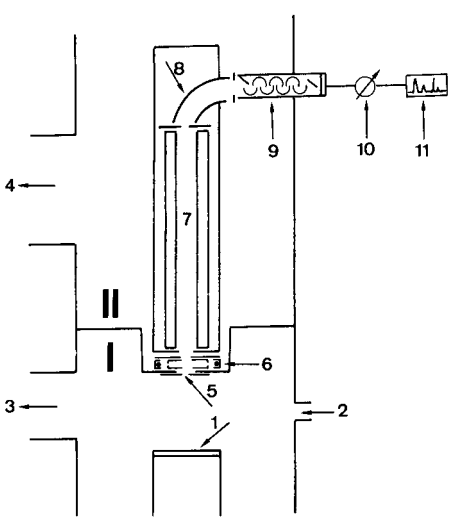

Fig. 1. The experimental system: (I) sputtering chamber; (II) mass spectrometer chamber. (1) Cathode; (2) gas inlet; (3, 4) to the turbo-molecular pumps; (5) diaphragm; (6) crossed-beam ion source; (7) mass filter; (8) deflector; (9) electron multiplier; (10) electrometer; (11) recorder.

charges. Gas is introduced into the sputtering chamber through a monitored magnetically-controlled valve. The working pressure of the glow discharge was read with an ionization gauge control unit (iridium filament).

The deposition rate is followed in situ with a quartz crystal oscillator. The material to be analyzed is a metal disk which is brazed onto a copper cathode. In some experiments, the cathode is covered by successive metallic films. The amount of deposited material is determined by means of x-ray fluorescence spectrometry. Before measurements, the discharge is stabilized for 20 min; all the ionic currents decrease by a factor of 3 during this period.

RESULTS AND DISCUSSION

Deflector voltage

Under the above experimental conditions, the ion beam energy is different from the values usually reported. From the results of Coburn and Kay [6], the mean energy in r.f. or d.c. discharges is around a few tens of eV, depending on the plasma potential. In the present system [5], because of the low frequency of the electric field (2 kHz), the ions "see" the electric field and during the positive cathode phase, the walls are bombarded by positive ions.

Figure 2 shows the Ar^+ and Cu^+ signals as a function of the deflector voltage. If it is assumed that the ion speed in the axial direction is not modified by the quadrupole filter, and that there is no substantial influence of the multiplier voltage, and if the curvature of the deflector and the applied field are known, then the energy of the extracted ions can be estimated. The mean energy of Cu^+ (sputtered species) and Ar^+ (gas) are 350 eV and 230 eV, respectively. In the same electrical discharge conditions, for every metal and oxygen ion, the maximum current is found at a deflector potential of 350 ± 10 V. In oxygen discharges, the mean energies of O^+ and O_2^+ are 310 and 280 eV, respectively. In Ar/O_2 mixtures where oxygen is 1% of the total pressure, the mean energies of O^+ and O_2^+ are 320 eV. The maximum ion energy depends on the voltage during the reversed period, which can be decreased by symmetrical charge-transfer reactions [7] such as $Ar^+ + Ar \rightarrow Ar + Ar^+$. When the probability of such reactions is lower, the energy of

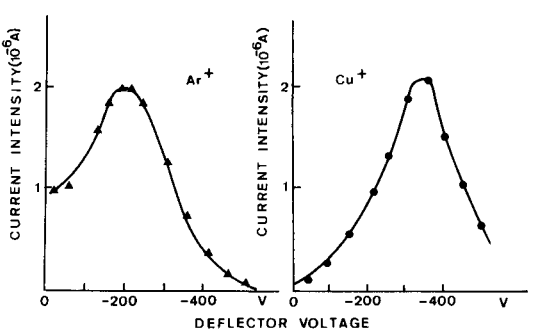

Fig. 2. Ion currents as a function of the deflector voltage.

the ions is higher. The ratio between different ionic species can vary with the deflector potential; e.g., I_{Cu^+}/I_{Ar^+} is 0.05 for −230 V and 0.4 for −350 V. In this work, energy spectra are recorded with a deflector voltage of −350 V.

Transmission of the system

In order to study the transmission factor of ions in the present experimental system, the cathode was covered by a sequence of thin films of metal. This cathode was then analyzed by g.d.m.s. The ion signals were recorded as a function of time. A sensitivity signal (S) is defined as $S = N^{-1}\int_0^\infty I_{M^+}(t)dt$, where N is the number of metal atoms in the films and $I_{M^+}(t)$ is the signal intensity as a function of time. The units of S are Å min atom^{-1}.

The nature and the thickness of the films were chosen as a function of the eventual interferences from impurities in the spectra and the sputtering yield. In order to have a pre-sputtering time to stabilize the signals, the films are covered by a protective film of silver or gold. In Fig. 3, the M^+ signal is plotted as a function of time for a copper target covered by tantalum (5750 Å), silver (19700 Å), gold (10200 Å), cobalt (5500 Å) and finally a protective coating of silver. S for a particular M^+ is obtained from the area of the M^+ curve divided by N. S depends on the ionization efficiency of the discharge, the extractive efficiency of the hole, the transmission into the filter and the gain of the electron multiplier.

Figure 4 shows the sensitivity as a function of the ion mass for different experimental conditions. Every curve has the same trend; S decreases when the ion mass increases. At a pressure of 6×10^{-2} torr, the sensitivity in oxygen is four times the sensitivity in argon. As the metal ion energy is the same in oxygen and argon discharges, the transmission of the mass filter is similar in oxygen and argon. The higher sensitivity is due to a more efficient ionization process in an oxygen discharge. However, at a total pressure of 6×10^{-2} torr, the addition of small amounts (1%) of oxygen to argon decreases the sensitivity. This effect is negligible at a total pressure of 1.5×10^{-1} torr. This has been already reported [8] and is considered as being due to the quenching

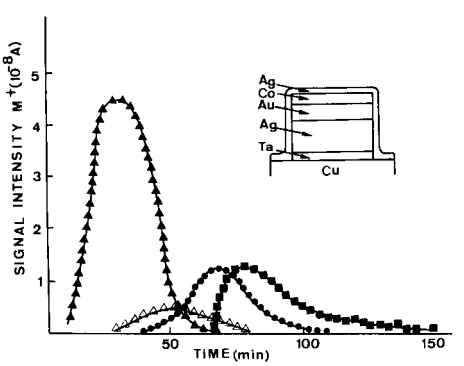

Fig. 3. Analysis by g.d.m.s. of a copper target covered by a sequence of thin metallic films: (▲) Co; (△) Au; (●) Ag; (■) Ta.

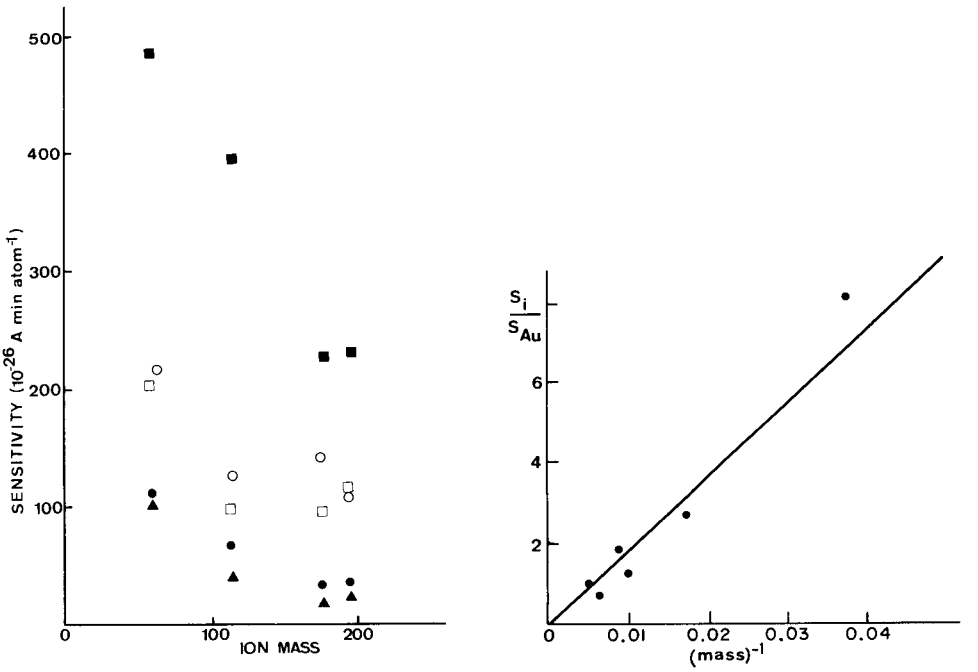

Fig. 4. Sensitivity as a function of the ion mass under different experimental conditions. At 6×10^{-2} torr: (■) 100% O_2; (●) 100% Ar; (▲) 99% Ar, 1% O_2. At 0.15 torr: (○) 100% Ar; (□) 99% Ar, 1% O_2.

Fig. 5. Sensitivity normalized to the gold sensitivity as a function of the reciprocal of the mass (argon at 7×10^{-2} torr).

of the argon metastable atoms by oxygen. In argon, the sensitivity increases with an increase in the pressure, as has already been reported by Coburn et al. [9].

In order to study the variation of the sensitivity with the ion mass a cathode was prepared covered by a sequence of six films (Al, Mo, Ta, Ag, Au, Co). This cathode was sputtered in argon at a pressure of 7×10^{-2} torr. The results are summarized in Fig. 5, where the sensitivity is plotted as a function of the reciprocal of the mass. An inverse linear relationship between sensitivity and ion mass is observed.

If it is assumed that the ionization efficiency is independent of the ionization potential of the particle, the relation between the current (i) measured at the detector and the plasma current (j) is nevertheless complex [10], and can be summarized by

$$i = jT_1T_2T_3T_4T_5 \qquad (1)$$

where T denotes the transmission and geometry factors for the various parts of the sampling system (T_1 ≐ sheath effects, T_2 = orifice effect, T_3 = down-

stream orifice effect, T_4 = mass filter effect, T_5 = electron multiplier effect). It is very difficult to evaluate the correct relations for each effect but if the mass discrimination is considered, there is apparently no discrimination in the mass filter in the low-pressure mode [11]. The attenuation of the ion beam in the low-pressure chamber depends only on the orifice diameter and discharge pressure [12]. The orifice effect can be decreased if a very thin orifice is used and if it is assumed that the ions flow towards the wall and the hole in a free-fall condition. The sheath effects are simplified by using the theory of the Langmuir probe; in this case, the mass current and ion density are related by the simple relation [13]

$$j = An^+v^+/4 = An^+(2E/m^+)^{1/2}/4$$

where n^+ is the ion density, E the ion energy and m^+ the ion mass. The mass dependence of the detector yield, however, follows an $m^{-1/2}$ relation, suggesting that kinetic extraction is the primary supplier of secondary electrons in the collisions of the ions with the first dynode [14]. This relation was checked by comparison of the ion current of the first dynode of the electron multiplier to the electron current at the last dynode, when the first is at −2 kV (Fig. 6). In the present experimental conditions, Eqn. 1 is simplified to

$$i = kn^+(2E)^{1/2}/4m^+ \qquad (2)$$

which can explain the results shown in Fig. 4.

In the case of an argon discharge at a pressure of 6×10^{-2} torr and a cobalt target, the total transmission (including the ionization process) was calculated to be 2.4×10^{-7} ion atom^{-1} and the instrumental transmission was 4×10^{-5}. The ionization efficiency is thus about 6×10^{-3} ion atom^{-1}. Bentz

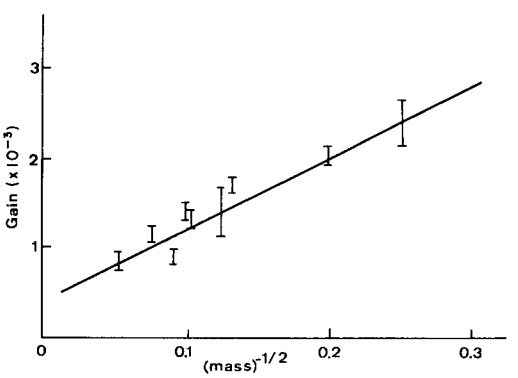

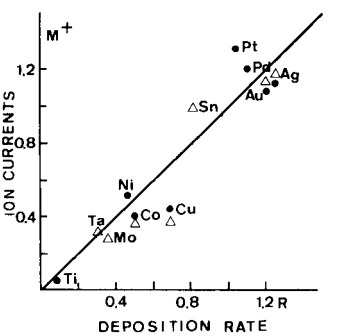

Fig. 6. Electron multiplier gain as a function of (ion mass)$^{-1/2}$ (potential applied to first dynode is 2 kV).

Fig. 7. Ion currents vs. deposition rate (argon at 8×10^{-2} torr): (•) measured with the crossed-beam source; (△) measured with the electrode system. Corrected current and deposition rate are given in arbitrary units.

et al. [15] found, for different experimental conditions, a value of 1.3×10^{-4} ion atom^{-1}.

Relation between the ion current and the deposition rate

Different metal targets were sputtered in an argon plasma. The ion currents of M^+ and the deposition rate were measured by the quartz oscillator method. Previously, the quartz method was calibrated by x-ray fluorescence and optical methods. The ion currents corrected by the simplified Eqn. 2 (Fig. 7) show a linear relation between the plasma current and the deposition rate. Similar results were obtained when the same metal targets were sputtered in an oxygen plasma [8]. However, the ion currents are higher in spite of lower deposition rates.

For a given gas, the ionization cross-sections of the different metal species are thus of the same order of magnitude but they are higher in an oxygen discharge than in an argon discharge. A comment must be made on this point because, although it is accepted that Penning ionization is the dominant process [2, 3] for the ionization of the sputtered species in an argon discharge, the ionization mode in an oxygen plasma is not well understood. Penning ionization is not valid because the energies of metastable oxygen states (O_2^m: 0.98 and 1.63 eV and 3 metastable states between 4.2 and 4.5 eV) are lower than the ionization potentials of most of the metals studied.

Electron impact ionization cannot explain the large difference between the ionization efficiency of oxygen (8.5×10^{-6} ion atom^{-1} at 6×10^{-2} torr) [16] and of the neutral sputtered particle ($\approx 10^{-2}$ ion atom^{-1}) [16]. However, sputtered species could be ionized by a charge-transfer process: $O_2^+ + M \rightarrow M^+ + O_2$. Table 1 shows some cross-sections for charge transfer between O_2^+ and a metal ion; they are of the order of the gas kinetic cross-sections for gas molecules. It is known [21] that the cross-sections for charge transfer between atoms of low atomic number are small when the ionization potentials differ widely. But they can be larger when molecular or atoms of high atomic number or both participate in the reaction. The excess of energy is dissipated in the rotational and vibrational excited states of the molecule or in electronic excited states of the atoms or both [22]. The reaction can then be considered to be "quasi-resonant" in energy.

TABLE 1

Charge-transfer cross-sections for O_2^+ and O^+ for some metals

Reaction	Cross-section (10^{-16} cm^2)	Ref.
$O_2^+ + Ca \rightarrow O_2 + Ca^+$	170 (ion energy = 2 eV)	17
$O_2^+ + Mg \rightarrow O_2 + Mg^+$	150 (ion energy = 2 eV)	18
$O_2^+ + Fe \rightarrow O_2 + Fe^+$	28 (ion energy = 2 eV)	19
$O^+ + U \rightarrow O + U^+$	30 (ion energy = 2 eV)	20
$O^+ + Th \rightarrow O + Th^+$	25 (ion energy = 5 eV)	20

REFERENCES

1 J. W. Coburn and W. W. Harrison, Appl. Spectrosc. Rev., 17 (1981) 95.
2 J. W. Coburn and E. Kay, Appl. Phys. Lett., 18 (1971) 435.
3 E. W. Eckstein, J. W. Coburn and E. Kay, Int. J. Mass Spectrom. Ion Phys., 17 (1975) 129.
4 P. F. Knewstubb and A. W. Tickner, J. Chem. Phys., 36 (1962) 674.
5 M. Hecq, A. Hecq and M. Liemans, J. Appl. Phys., 49 (1978) 6176.
6 J. W. Coburn and E. Kay, J. Appl. Phys., 43 (1972) 4965.
7 W. D. Davis and T. A. Vanderslice, Phys. Rev., 131 (1963) 219.
8 M. Hecq and A. Hecq, Thin Solid Films, 76 (1981) 35.
9 J. W. Coburn, E. Taglauer and E. Kay, J. Appl. Phys., 45 (1974) 1779.
10 H. Helm, T. D. Mark and W. Lindinger, Pure Appl. Chem., 52 (1980) 1739.
11 F. Howarka, J. Chem. Phys., 68 (1978) 804.
12 J. W. Coburn and E. Kay, J. Vac. Sci. Technol., 8 (1971) 738.
13 J. B. Hasted, Int. J. Mass Spectrom. Ion Phys., 16 (1975) 3.
14 M. A. Rudat and G. H. Morrison, Int. Mass Spectrom. Ion Phys., 27 (1978) 249.
15 B. L. Bentz, C. G. Bruhn and W. W. Harrison, Int. J. Mass Spectrom. Ion Phys., 28 (1978) 409.
16 A. Hecq, Doctorate Thesis, Mons University, 1981, unpublished.
17 J. A. Rutherford, R. F. Mathis, B. R. Turner and D. A. Vroom, J. Chem. Phys., 57 (1972) 3087.
18 J. A. Rutherford, R. F. Mathis, B. R. Turner and D. A. Vroom, J. Chem. Phys., 55 (1971) 3785.
19 J. A. Rutherford and D. A. Vroom, J. Chem. Phys., 57 (1972) 3091.
20 J. A. Rutherford and D. A. Vroom, J. Chem. Phys., 69 (1978) 332.
21 J. B. Hasted, Physics of Atomic Collisions, Elsevier, New York, 1972, pp. 621—627.
22 K. Tanaka, J. Durup, T. Kato and I. Koyano, J. Chem. Phys., 74 (1981) 5561.

Analytica Chimica Acta, 155 (1983) 199—207
Elsevier Science Publishers B.V., Amsterdam — Printed in The Netherlands

DETERMINATION OF LEAD AND NICKEL IN EPITHELIAL TISSUE BY ELECTROTHERMAL ATOMIC ABSORPTION SPECTROMETRY

J. F. ALDER* and M. C. C. BATOREU[a]

Department of Instrumentation and Analytical Science, UMIST, Manchester M60 1QD (Great Britain)

(Received 31st May 1983)

SUMMARY

The atomic absorption spectrometric determination of lead and nickel in epithelial tissue sections by solid injection into the graphite furnace is described. Matrix interference is minimised by using as small a sample of tissue (ca. 1 μg) as possible. Although this is good for biopsy analysis where sample size is limited, the advantages obtained by decreasing the sample size are compromised by the difficulties in handling and weighing. Hair, nail and skin sections were analysed by using doped gelatin and NBS bovine liver as reference materials. Profiles of element concentration in these matrices are presented.

Nickel is of considerable interest in dermatological studies. It is well known to be responsible for contact dermatitis [1] although the mechanism of its reaction is not known. Nickel applied to the skin permeates the stratum corneum and epidermis and can reach the dermis [1]. The profile of nickel concentration through the skin is therefore of some consequence in the study of dermatitis reactions. Because samples of the skin have to be taken from humans in vivo, the quantities available for analysis are small. The skin depth is about 2—3 mm in areas where biopsies can be taken readily and 20-μm thick sections are needed to give reasonable profile detail. The analytical technique for nickel determination has, therefore, to be sensitive and accurate to give meaningful results and the calibration procedure must reflect the nature of the matrix as closely as possible. In this study, graphite-furnace atomic absorption spectrometry (a.a.s.) was employed in order to establish an overall picture of nickel distribution in the body. The level of nickel in more easily obtained samples is also of interest. Hair and nails can be obtained more readily than skin. Although there is no evidence for any connection between the concentrations in these different tissues, methods for these determinations are required.

Lead is always of interest in discussing human metabolism, but is not an easy element to determine by electrothermal a.a.s., because of the volatile

[a]Present address: Faculdade de Farmácia, Universidade de Lisboa, Av. das Forças Armadas, 1699 Lisboa Codex, Portugal.

0003-2670/83/$03.00

nature of both the metal and its compounds, and the high temperature required for complete pyrolysis of the tissue matrix.

One of the most important aspects of this problem is to find a matrix which matches that of skin in its behaviour in the graphite furnace and also in the pretreatment steps. Skin biopsies are presented to the analyst on a glass microscope slide as 20-μm sections. The procedure adopted in this work was to roll the skin sample into a ball on the slide and transfer the 50—70-μg ball with a vacuum pipette to an ultramicrobalance for weighing. After weighing, the skin ball was transferred to the furnace and atomised directly.

The principal organic component of skin is collagen, which accounts for about 30% of all body protein. Gelatin is produced by the hydrolysis of collagen from animal skin, tendons and bones and if carefully prepared it may be regarded chemically as a pure form of collagen. Gelatin contains trace quantities of the elements which one would expect to encounter in animal tissue and is therefore attractive as a reference material in determining trace elements in human tissues [2]. It is readily available, a variety of elements can easily be incorporated into the matrix, and the readily prepared thin films can be treated and handled as tissue [3].

Anderson et al. [2] used gelatin as a matrix for a mercury reference material, preparing later a new gelatin reference material containing 25 trace elements ranging in concentrations from 27 to 62 $\mu g\ g^{-1}$ which was analysed by atomic absorption spectrometry and neutron activation analysis by 11 independent laboratories [4].

Roomans and Seveus [5] studied the use of gelatin and albumin as organic matrices doped with mineral salts to be applied as standards in quantitative x-ray microprobe analysis. Gelatin gave better results with respect to the homogeneity of the standard. As a freezing preservative, 5% glycerol was added to a 20% gelatin solution and it was possible to dope this mixture with high concentrations of mineral salts without losing the homogeneity required of standards. This standard was used later by Roomans et al. to determine different elements in guinea pig skin by electron microprobe analysis [6]. Burns-Bellhorn and File [3] prepared standards of gelatin to determine the capability of secondary ion mass spectrometry (s.i.m.s.) for determining metals in soft biological tissues, showing the possibility of quantifying the distribution of several elements. Zhu et al. [7] proposed the same standard for s.i.m.s. on the assumption that the matrix effects of gelatin would be similar to those of soft tissues. By use of computer-controlled data acquisition techniques, they were able to reduce to 2—15 $\mu g\ g^{-1}$ the detection limits for six trace elements (B, Ba, Cu, Mn, Rb and Sr).

In this paper, methods for the determination of lead and nickel in hair, skin and nail by electrothermal a.a.s. are described. Gelatin is used as reference material for nickel in skin and NBS bovine liver for lead.

EXPERIMENTAL

Samples and standards

Gelatin (powder form; BDH) solutions (20% w/v) were made in distilled water at ca. 80°C and combined with known volumes of nickel salt solution to give a metal content of $\leqslant 2\ \mu g\ ml^{-1}$. A water repellent (Repelcote, Hopkin and Williams; dimethyldichlorosilane in trichloroethane) was used as a coating material for the glass surface of some slides. On the dried glass surface were applied, with a Pasteur pipette, several drops of doped gelatin. Blank drops of undoped gelatin were also applied in different slides. These slides were dried at 60°C for 2 h. The doped gelatin in the form of small balls was easily removed from the slide surface with the vacuum pipette and weighed on a Perkin-Elmer AD2 ultramicrobalance.

The NBS bovine liver (SRM 1577) was kept tightly closed and stored in a cool dark place. Prior to analysis, portions of sample were dried in a vacuum desiccator over silica gel for 2 h. A stock 1000 mg l^{-1} aqueous lead solution was prepared by dissolving lead nitrate in twice-distilled water. All solutions were prepared by serial dilution of the 1000-mg l^{-1} stock solution with twice-distilled water immediately prior to use.

Instrumentation and procedure

A Perkin-Elmer HGA70 carbon furnace was used with a Perkin-Elmer 305 AA spectrometer with output to a Servoscribe 210 strip-chart recorder. The operating conditions are summarised in Table 1. For the lead determinations a modified L'vov platform [8] was used in the graphite furnace. The platform was made in-house, by cutting the two ends of a Perkin-Elmer HGA70 graphite tube (7 × 5 mm) and making grooved, curved sections. A blade was used to make two perpendicular cuts parallel to the tube axis into the ends

TABLE 1

Instrumental conditions for a.a.s. of hair, nail and skin and for nickel in gelatin

Element	Line[a] (nm)	Drying[b] temp. (°C)	Ashing		Atomisation		Ar flow (l min^{-1})
			Time (s)	Temp. (°C)	Time (s)	Temp. (°C)	
Cu	324.7	110	30	1400	3	2600	3
Al[c]	309.2	110	30	1200	3	2700	3
Ni[c]	232.0	170	30	1200	5	2650	2
Mn[c]	279.5	110	30	1000	3	2500	2
Pb[c,d]	283.3	110	40	500	3	2100	3
Zn[d]	213.9	110	40	400	3	2000	3
Ni[c,e]	232.0	110	20	1200	4	2650	4

[a]Lamps operated according to manufacturer's instructions; background correction employed. Bandpass 0.3 nm, except for Pb and Zn (0.4 nm). [b]For 30 s. [c]Gas-stop mode. [d]Furnace cooled for 10 s before next injection. [e]In gelatin.

of the tube. A narrow piece of masking tape was wrapped around the ends, and a third cut was made perpendicular to the tube axis and 7 mm in from the end, giving four platforms. The platform was placed into the graphite tube and centred within the tube using a graphite rod.

A solid sampling device to introduce the powder samples was made using a 10-cm graphite rod with a groove machined at one end of it. The gelatin and skin balls were transferred to the furnace with a vacuum pipette.

The temperature programme conditions (Table 1) were optimised with the aqueous standard solutions of lead nitrate. As most of the problems in determining lead in biological samples are thought to arise because of metal lost as lead(II) chloride during the charring stage [9], the temperature used for the charring stage was checked with the aqueous lead solution in the presence of chloride. The absorbance of lead added as nitrate with and without added chloride (5 μl of 1% hydrochloric acid) was measured at different charring temperatures. No decrease in the measured absorbance was found until 700°C, after which the peak intensity continuously decreased. A temperature of 500°C, therefore, was employed as it was sufficient to remove the organic material of the microsample.

RESULTS AND DISCUSSION

Nickel

The results obtained from 20 samples of doped gelatin containing 2 μg g^{-1} nickel showed a relative standard deviation of 10% and good agreement between the expected value and the value measured, when aqueous solutions were used for calibration. This shows that there is no measurable matrix interference at this scale of sample weight, rendering it possible to calibrate the skin samples against aqueous solutions. It is remarkable and significant that the precision for direct graphite-furnace a.a.s. with the gelatin standard is in agreement with the values obtained with doped beads of resin [10], confirming that for this size of sample the matrix interferences are compensated by the background correction and it is possible to calibrate procedures for direct analysis of solids with aqueous solutions of metal. Figure 1 confirms that the response from nickel is directly proportional to the amount of gelatin, and that larger amounts of matrix do not depress the signal.

The variation of nickel concentration along individual hairs from root to tip and in pooled small sections of finger- or toe-nails, as well as in ordered layers of the same fingernail, was studied by direct solid injection. In the first stage of this study, a main objective was to elaborate a comparison of the nickel content of hair, nail and skin of the same individual, as a possible indicator in detecting cases of contact dermatitis produced after occupational or accidental exposure. The individual samples of hair and pieces of a pool of finger- or toe-nails obtained from the same individual were washed with diethyl ether separately in a silica beaker with manual shaking and then dried, cut and weighed as previously described [10]. The individual samples of hair or nail were injected afterwards into the furnace.

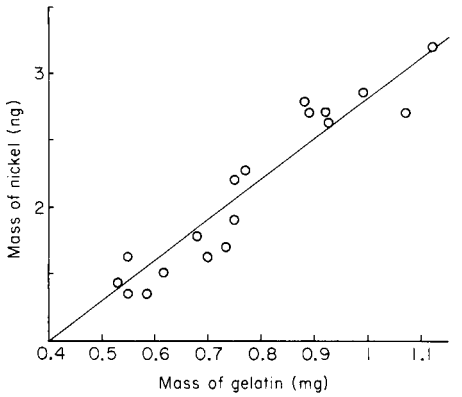

Fig. 1. Nickel content determined in doped gelatin against aqueous calibration standards vs. mass of doped gelatin introduced into the furnace.

The ashing conditions chosen after experiments with aqueous standards of nickel were checked by measuring the signals from solid samples of hair and nail at a nearby non-absorbing line. No signal was observed, which confirmed that the ashing programme chosen was adequate for the micro samples used and the background correction was complete. The aqueous calibration graph for nickel was linear in the range 0—1.5 ng of nickel. The detection limit was 0.2 ng of nickel.

Nickel determinations in fingernails were made on two pools of nails (from different fingers) belonging to two individuals. One (Female 1) showed 2.43 ± 0.41 $\mu g\ g^{-1}$ ($n = 20$); another (Male 3) gave 2.91 ± 1.7 $\mu g\ g^{-1}$ ($n = 17$). Figure 2 shows the results obtained for the distribution of nickel in two layers of one fingernail corresponding to Male 3. Figure 3 shows the distribu-

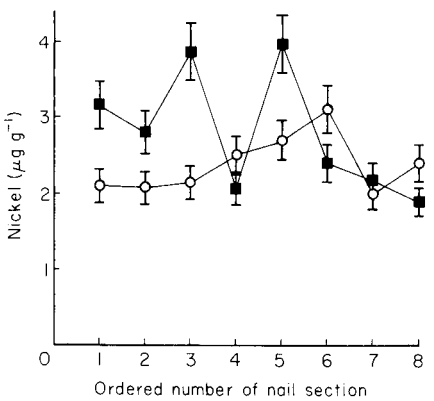

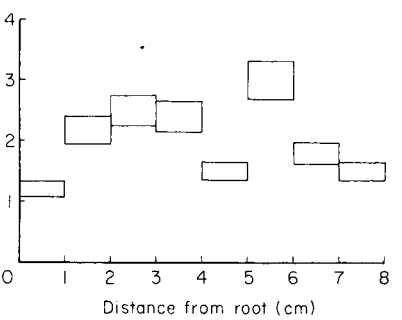

Fig. 2. Nickel concentration along ordered transverse sections in two layers of one fingernail from Male 3.

Fig. 3. Nickel concentration along the length of one head hair from Male 3 taken from root to tip.

tion of nickel in a single head hair from the same individual. The 10% r.s.d. on the points is that found using gelatin as the solid standard.

The mean value of the nickel content of skin biopsies from two sets of four individuals was measured by this technique. The results obtained from fifty biopsy sections from each group were 2.88 ± 1.65 $\mu g\ g^{-1}$ nickel and 4.45 ± 2.96 $\mu g\ g^{-1}$ nickel, respectively.

Although the hair, nail and gelatin samples were cut with stainless steel instruments, no evidence of contamination by the nickel content of the steel was observed. It is appreciated that such contamination is difficult to prove when no absolute reference material is available. Neither in this nor previous work [11] was either iron or nickel contamination arising from cutting instruments ever shown when teflon, glass or porcelain was used as the cutting board, and scissors were employed.

Lead

Aqueous solutions containing 0—0.5 ng lead were injected into the furnace with and without the L'vov platform. This experiment was repeated several times in order to establish the calibration graph for lead with and without the platform, but no significant differences were observed between them. However, the L'vov platform was found to be very useful in direct solid injection, as it was possible to place the sample reliably in the same position within the furnace thus ensuring better reproducibility in the results.

The reliability of the method was checked by using the NBS bovine liver standard reference material. A solid sample of bovine liver weighing around 1 mg was weighed in the solid-sampling rod and the sample was delivered on to the platform inside the graphite tube. The rod was reweighed to determine the weight of sample introduced. The analysis was done six times and the concentration of lead in bovine liver was determined from the calibration with aqueous standards and the platform. The mean value obtained (0.36 ± 0.03 $\mu g\ g^{-1}$ Pb) closely agreed with the certified value (0.34 ± 0.08). When the weight of bovine liver was increased to above 1 mg, the ashing temperature and time were not sufficient to destroy the organic matrix.

Nail and hair

Samples were washed, cut and weighed as previously described, and nail and hair were injected with the vacuum micropipette and solid injector microsyringe, respectively, inside the graphite tube onto the L'vov platform. The absorbance was measured using the same programme conditions as for bovine liver. The corresponding concentrations were measured from the aqueous calibration graphs for two single head hairs and in two layers of one fingernail belonging to the same person. These are reported in Figs. 4 and 5, respectively. The results obtained for the pools of fingernails from three individuals were: Male 4, 3.36 ± 0.62 $\mu g\ g^{-1}$ Pb (n = 17); Male 5, 5.10 ± 0.9 $\mu g\ g^{-1}$ (n = 10); Female 2, 1.95 ± 0.45 $\mu g\ g^{-1}$ (n = 15). A pool of toenails from Male 6 gave 2.29 ± 0.59 $\mu g\ g^{-1}$ (n = 20).

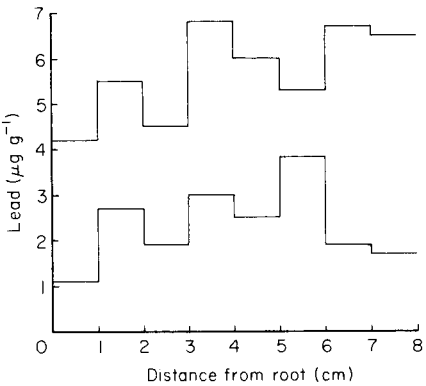

Fig. 4. Lead concentration along the length of two head hairs from Male 4 taken from root to tip.

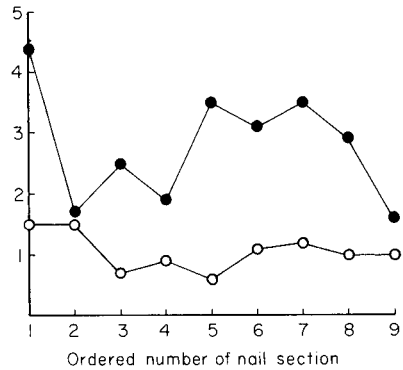

Fig. 5. Lead concentration along ordered transverse sections of two layers of one fingernail from Male 4.

Interferences from background absorption were checked by injecting several samples of nail in the furnace using the closest spectral line to the absorbing working line (i.e., 282.0 nm). No signal was observed at this second line. In the determination of lead in hair and nail, where volatilisation interferences were expected to be more apparent, no problem was found when the L'vov platform was used with a lower temperature than that corresponding to the volatilisation of the lead, possibly as a chloride species. Low-temperature ashing was possible because of the small weight of sample taken. The low charring temperature was enough to remove most of the matrix and the deuterium background correction could cope with the small residual non-atomic absorption.

The small number of donors involved, four in this study for the determination of lead in nails, precluded the possibility of obtaining any meaningful biological conclusion. The mean values obtained for nail pools vary in a range 1.95—5.1 $\mu g\ g^{-1}$ with a large r.s.d. (18—26%) in each pool, which shows the scatter of concentrations between nail pieces for the same individual and the errors of the method. When ordered transverse sections of one fingernail were examined in two subsequent weeks (first layer and second layer Fig. 5) a variation of lead content was seen from section to section and with time. The correlation between time and trace element content in fingernails, however, requires a study over a period of at least 12 months of the same donor. This is the main reason why hair is more often used when there is interest in analysing these epithelial tissues as a possible biological calendar.

Several hairs were analysed in order to quantify the distribution of lead along the length of single hairs. In Fig. 4, the variation of lead content along two hairs shows a slight increase towards the tip. Renshaw et al. [12] as well as Samuel [11] found an increase in lead content from root to tip when

analysing sections of single hairs by direct graphite-furnace a.a.s. This trend towards the tip was also found by Obrusnik et al. [13] using neutron activation analysis. There is no reported work on the determination of lead in fingernails by graphite-furnace a.a.s. The values found by Goldblum et al. [14] in 1953 (atomic emission) are very high (97—240 $\mu g\ g^{-1}$) compared with the results obtained by Harrison and Clemena [15] who used spark-source mass spectrometry and found a range of 1.7—64 $\mu g\ g^{-1}$ in the fingernails of 17 donors.

In this and previous work using ion-exchange beads [10] and gelatin, matrix interferences were completely compensated by the background corrector when copper, aluminium and nickel were determined. The expected validity of these results has been now extended to lead determination by using a standard reference material, bovine liver. Again, it can be concluded that one of the most important factors determining the reliability and efficiency of the method employed in the present study is the small size of the sample. However, the biological and analytical advantages obtained by decreasing the sample size are counteracted by the increased difficulties in handling (with the possibility of irretrievable loss of the sample) and of higher relative errors in weighing. Although the fact that eventually the method will be limited by the sensitivity of the a.a.s. measurement and all the compounded errors of handling and weighing cannot be ignored, it is clear that the minimum sample size possible is likely to be the optimum from the viewpoint of reproducibility and matrix interferences.

Concerning the distribution of trace elements in the biological matrices studied, it is necessary to differentiate between the analytical and biological aspects. Obviously the latter are completely dependent on the former. It was not the aim of this study to reach any biological conclusion, but rather to establish reliable analytical methods to permit such conclusions to be drawn. From the analytical viewpoint, any inhomogeneity of metal content has significance if the measured value differs from the mean value by more than a predetermined multiple of the standard deviation of the method. Thus a fundamental prerequisite for any meaningful discussion is a valid standard deviation of the method, so that some indication of the inhomogeneity of the biological distribution can be given. In this context, the selection of a proper washing step for the sample to remove surface contamination plays a fundamental role in establishing confidence in the results obtained.

The practical biological and forensic applications of the increased information achieved by this direct method, where it is possible to quantify the distribution of trace element in these tissues, are circumscribed by the difficulty in discriminating between the endogeneous and exogeneous sources of metal content. Their variations as a result of age, sex, geographic location etc., make the whole system rather complex. The quantitative consequences of all these variables are difficult to rationalise, and it is likely that the influence of each factor would be more easily interpreted in abnormal conditions, for example, in heavily polluted environments or in extreme metal-deficiency

conditions. It is nonetheless important that reliable analytical methods should be available and that some indicator of the complex trace element distribution is possible.

This work has gone some way in providing an analytical method which is sufficiently precise and accurate for this work, and is practically feasible for clinical laboratories. The fact that any dissolution step has been avoided is important in this respect as the time taken in such procedures and the contamination risk are such that electrothermal a.a.s. methods for hair and nails based on them are often not practically viable.

M. C. C. Batoreu was supported by the Instituto Nacional de Investigação Cientifica, Portugal.

REFERENCES

1 E. Cronin, Contact Dermatitis, Churchill Livingstone, London, 1980.
2 D. H. Anderson, J. J. Murphy and W. W. White, Anal. Chem., 44 (1972) 2099.
3 M. Burns-Bellhorn and D. M. File, Anal. Biochem., 92 (1979) 213.
4 D. H. Anderson, J. J. Murphy and W. W. White, Anal. Chem., 48 (1976) 116.
5 G. M. Roomans and L. A. Seveus, J. Submicrosc. Cytol., 9 (1977) 31.
6 Xu Wei, G. Roomans and B. Forslind, private communication.
7 D. Zhu, W. C. Harris and G. H. Morrison, Anal. Chem., 54 (1982) 419.
8 M. L. Kaiser, S. R. Koirtyohann, E. J. Hinderberger and H. E. Taylor, Spectrochim. Acta, Part B, 36 (1981) 773.
9 W. Slavin and D. C. Manning, Anal. Chem., 51 (1979) 262.
10 J. F. Alder and M. C. C. Batoreu, Anal. Chim. Acta, 135 (1982) 229.
11 A. J. Samuel, Ph.D. Thesis, University of London, 1977.
12 G. D. Renshaw, C. A. Pounds and E. F. Pearson, Nature, 238 (1972) 162.
13 I. Obrusnik, J. Gislason, D. Maes, D. K. McMillan, J. D'Auria and B. D. Pate, J. Radioanal. Chem., 15 (1973) 115.
14 R. W. Goldblum, S. Derby and A. B. Lerner, J. Invest. Dermatol., 20 (1953) 13.
15 W. W. Harrison and G. G. Clemena, Clin. Chim. Acta, 36 (1972) 485.

Analytica Chimica Acta, 155 (1983) 209—218
Elsevier Science Publishers B.V., Amsterdam — Printed in The Netherlands

WAVELENGTH-DISPERSIVE X-RAY FLUORESCENCE SPECTROMETRY OF LANTHANUM AND CERIUM IN NODULAR CAST IRON

F. ALLUYN, J. BILLIET, R. DAMS and J. HOSTE*

Institute of Nuclear Sciences, Rijksuniversiteit Gent Proeftuinstraat 86, B-9000 Gent (Belgium)

(Received 13th June 1983)

SUMMARY

Cerium and lanthanum can be determined in cast iron samples by wavelength-dispersive x-ray fluorescence spectrometry (x.r.f.). Excitation and detection conditions are evaluated, as is the required degree of surface finish of the castings. Standard samples for x.r.f. were obtained by careful determination of the cerium and lanthanum contents of specimen cast iron samples by neutron activation—γ-spectrometry. The calibration graphs obtained with these reference samples and tungsten tube excitation were linear for the ranges 3—30 mg kg^{-1} lanthanum and 3—60 mg kg^{-1} cerium. The relative standard deviations of the determinations, for 400-s counting times, ranged from 15% for samples containing 4 mg kg^{-1} La to 4% for samples containing 30 mg kg^{-1}. For cerium, the corresponding numbers were 15% for 3 mg kg^{-1} and 2% for 60 mg kg^{-1}. For unknown samples, the results obtained with these calibration graphs agreed within 3% with the neutron activation results.

The superior mechanical properties of spheroidal graphite iron compared to flake grey iron are due to the spheroidal shape of the graphite particles or nodules which are imbedded in the metal matrix. The favorable effects of adding well-dosed amounts, at the mg kg^{-1} level, of rare earth metals, especially cerium and lanthanum, on nodule count and graphite structure in magnesium-treated ductile iron castings have been repeatedly described in the literature. The most important reason for their application is to neutralize excesses of inhibitors such as Pb, Bi, Sb, Ti, etc. [1—3] in the melt that cannot be completely neutralized by magnesium but can cause nodule degeneration during solidification of the iron. Another reason is that the presence of appropriate amounts of rare earth metals in the melt increases nodule count and therefore decreases the chilling tendency of the iron. Excessive additions of rare earth metals, however, reduce the nodule count again and may even cause mottled or white cast iron structures to be formed, owing to the carbide-stabilizing behavior of these elements. Additionally, the rare earth metals themselves may be a reason of graphite deterioration, especially in heavy-section and austenitic spheroidal graphite iron castings. This degeneration can be avoided by addition of proper amounts

0003-2670/83/$03.00

of inhibitors such as Sb, Bi or Pb [4]. It follows that mutual neutralization is possible between the elements of both groups, i.e., the rare earth metals and the inhibitors, provided that the amounts available in the liquid iron are suitably chosen. Inexplicable variations in the structure and properties of nodular cast iron may thus be due to unforeseen changes in the concentrations of the trace elements in the raw materials used.

Precise determinations of these elements at the mg kg^{-1} level in the raw material and in the castings may thus lead to a better understanding of the solidification process, and thence to a better control of the production.

Several authors have dealt with analyses for cerium and lanthanum in cast iron, using techniques such as amperometry [5, 6], x-ray fluorescence spectrometry [7, 8], polarography [9] and spectrophotometry [10—13], often preceded by an ion-exchange separation [14, 15]. Each of these methods, however, requires the complete dissolution of the samples and is therefore time-consuming.

This paper describes the nondestructive determination of lanthanum and cerium by x-ray fluorescence (x.r.f.) on the cast iron samples, with a minimum of sample preparation, so that the technique can be considered as fast and suitable for production control. Quantitative x-ray fluorescence spectrometry usually requires the use of standards chemically and physically analogous to the samples. As no standard reference cast irons with certified La and Ce values in the usual range are readily available, work commenced with the accurate determination of the Ce and La contents of a series of cast iron samples by instrumental neutron activation analysis, with a view to their later use as x-ray fluorescence standards.

EXPERIMENTAL

Preparation of the cast iron samples

The samples examined were produced by the CRIF (Centre for Scientific and Technical Research of the Metalworking Industry in Belgium). After addition of magnesium and a Fe—Si alloy containing lanthanides, the melt was poured into a cylindrical casting mould of sand (60 mm in diameter). A fraction of the dissolved carbon in the melt precipitated as graphite nodules during the slow solidification. In this way, a grey cast iron cylinder was obtained. Disks (4 cm diameter, 4 mm thick) were cut from the cylinder. These disks fitted the sample holders and were infinitely thick for x-ray spectrometry.

As only an area with a diameter of 3 cm of these samples was irradiated during x-ray spectrometry, some material was machined away from the rim of the disks and the turnings were used for neutron activation analysis. This ensured that the neutron activation was done on the same samples as those to be used as standards for x.r.f. later. For neutron activation, the turnings were mixed, after size reduction, with reagent-grade iron carbonyl powder in a 1:1 ratio, and pressed to a circular pellet (12 mm diameter, 3 mm thick), weighing about 2 g.

Neutron activation—γ-spectrometry

The iron samples, together with standards were irradiated for 3 h at a neutron flux of 4.8×10^{11} n cm^{-2} s^{-1} in the Thetis reactor of the Institute for Nuclear Sciences. The standards were prepared by spotting known amounts of lanthanum and cerium in HNO_3—H_2O_2 solution on reagent-grade iron carbonyl powder. After drying in a furnace for 10 h at 110°C, the mixture was ground and homogenized with a mortar and a turbula mixer and subsequently pressed into the pellets of the same size as the samples.

The γ-ray intensities of the isotopes ^{140}La and ^{143}Ce were then measured at least one day after irradiation to allow for the decay of ^{56}Mn ($t_{1/2}$ = 2.58 h) produced by the (n, p) reaction on ^{56}Fe. After a decay time of 15 days, the γ-activity of the long-lived ^{141}Ce isotope was also measured. The specific activity of the isotope ^{59}Fe was used to monitor the relative neutron flux differences between samples and standards, because the concentration of this matrix element was nearly constant in all samples, allowing it to be used as an internal standard. The appropriate nuclear data of these isotopes are summarized in Table 1. Counting was done with Ge(Li) detectors with a relative efficiency of approximately 20% and a resolution of 1.9 keV for the 1332.4-keV photopeak of ^{60}Co. For the detection of the 145.4-keV photopeak of ^{141}Ce, a low-energy photon detector (LEPD) with a resolution of 190 eV for the 5.9-keV Mn K_α x-ray was used. This was necessary to avoid the interference of the ^{59}Fe photopeak at 142.3 keV.

X-ray fluorescence spectrometry

For x-ray fluorescence, a PW-1450 spectrometer was used in the hardware version. A fixed primary collimator diaphragm was fitted, increasing the peak-to-background ratio by eliminating scatter radiation from the sample holder and mask, and limiting the area examined to a diameter of 28 mm or an area of 6.16 cm^2. The detection system of the apparatus is equipped with a pulse-height compensation circuit including different attenuators for different diffraction crystals and a sin θ potentiometer so that all first-order

TABLE 1

Nuclear data for the isotopes of interest

Nuclide	$t_{1/2}$	γ-energy (keV)	Decay time (days)
^{59}Fe	45.1 d	142.3	1; 4; 15
		1099.0	
^{140}La	40.3 h	328.7	1; 4
		487.3	
		815.5	
		1595.5	
^{141}Ce	32.5 d	145.4	15
^{143}Ce	33.0 h	293.3	1; 4

x-ray photons deliver a pulse in the detector, centered around an amplitude of 500 mV.

The x-rays measured were the La L_α and Ce L_α lines. For the excitation, tungsten and chromium tubes were used. The excitation and detection conditions are summarized in Table 2. All measurements were done under vacuum conditions.

RESULTS AND DISCUSSION

Neutron activation analysis

Standard preparation. To check the reliability of the synthetic standards used for neutron activation, the homogeneity of the distribution of La and Ce over the iron carbonyl powder was first measured. To do so, 5 pellets were prepared from 10 g of standard powder and measured after irradiation. The results showed that heterogeneity was <2%. The reproducibility of the entire standard preparation method was then evaluated by analyzing four samples of grey cast iron against three independently prepared standards after different irradiations. All the results obtained were within one standard deviation of the mean and agreed with the reproducibility expected from counting statistics, as can be seen from Table 3.

Investigation of possible gradients in the castings. Neutron activation analysis was also applied to detect possible gradients of La and Ce in the castings. After careful casting, no horizontal, vertical or radial gradients could be detected in grey cast iron in cylinders of 140 mm diameter and 120 mm length.

Analysis of the standards for x.r.f. For the preparation of a calibration graph for x.r.f. seven samples of grey cast iron of a typical composition (3.8% C, 2% Si, 0.8% Ni and <0.1% the sum of Mn, P and S) but with increasing La and Ce content, were carefully analyzed. The concentrations are summarized in Table 4. The relative standard deviations of these determinations were ca. 2% for La and 5% for Ce.

TABLE 2

Excitation and detection parameters for x.r.f.[a]

Tube	X-ray	Discrim. window (mV)	Peak angle	Backgr. angle 1	Backgr. angle 2
Cr	Ce L_α	350—650	79°00	78°25	80°00
W	La L_α	400—600	82°90	82°00	83°50
	Ce L_α	400—600	79°00	78°25	80°00

[a]In all cases, the other conditions were as follows: tube voltage 60 kV; tube current 40 mA; LiF-200 diffraction crystal; flow counter, P-10; collimator at coarse, 0.4°.

TABLE 3

Reproducibility of the standard preparation for neutron activation checked for 4 samples

Sample	La found (mg kg^{-1})				Mean
	1	2	3	4	
Standard 1	15.0 ± 0.4	15.5 ± 0.4	14.8 ± 0.4	15.2 ± 0.4	15.2 ± 0.3
Standard 2	14.8 ± 0.4	14.6 ± 0.4	15.0 ± 0.4	14.8 ± 0.4	14.8 ± 0.2
Standard 3	14.9 ± 0.5	14.1 ± 1.3	15.6 ± 0.9	14.0 ± 0.5	14.7 ± 0.8
Mean	14.9 ± 0.1	14.7 ± 0.7	15.1 ± 0.2	14.7 ± 0.4	
Sample	Ce found (mg kg^{-1})				Mean
	1	2	3	4	
Standard 1	288 ± 8	293 ± 10	287 ± 8	292 ± 10	290 ± 3
Standard 2	283 ± 8	284 ± 8	278 ± 8	282 ± 8	282 ± 3
Standard 3	289 ± 10	297 ± 11	287 ± 9	277 ± 12	288 ± 8
Mean	287 ± 3	291 ± 7	284 ± 5	284 ± 8	

TABLE 4

Determination of lanthanum and cerium in the cast iron samples by neutron activation—γ-spectrometry

Sample	La content (mg kg^{-1} ± 1 s.d.)	Ce content (mg kg^{-1} ± 1 s.d.)
1	5.1 ± 0.1	7.9 ± 0.4
2	7.2 ± 0.1	11.0 ± 0.6
3	9.4 ± 0.2	14.4 ± 0.6
4	13.5 ± 0.2	21.2 ± 1.1
5	19.2 ± 0.3	29.5 ± 1.5
6	24.0 ± 0.5	36.9 ± 1.9
7	30.6 ± 0.2	57.6 ± 2.0

X-ray fluorescence spectrometry

Choice of excitation tube. Two x-ray tubes were considered for the excitation of La L_α (L III$_{ab}$ = 5.57 keV) and Ce L_α (L III$_{ab}$ = 5.81 keV). With a tungsten tube, the WL lines (from 7.4 to 11.7 keV) contributed to a large extent to the excitation, whereas with the chromium tube, especially the Cr K$_\beta$ (5.95 keV) line is well suited for excitation. However, with both tubes interferences must be considered.

With the chromium tube, the measurement of the Ce L_α posed no problem in spite of the very large Ti K_β and V K_α peak adjacent, as can be seen from Fig. 1. The measurement of the La L_α line, however, was impossible because of the interference of a resonant Raman x-ray scattering peak present in the samples (see Fig. 1).

With tungsten tube excitation, the measurement of the La L_α line was straightforward, but the Ce L_α line suffered interference from the second-

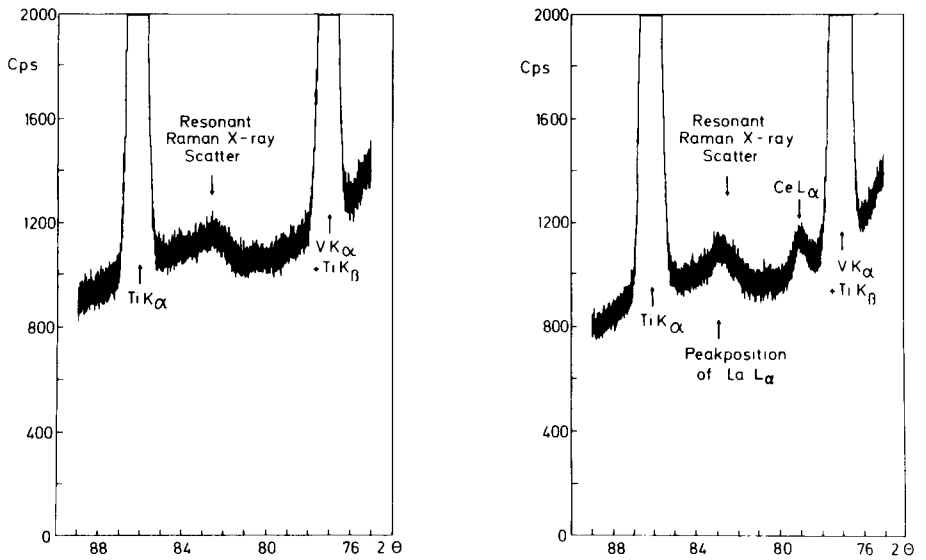

Fig. 1. Part of the spectrum from a 2θ scan of a grey cast iron blank and sample containing 58 $\mu g\ g^{-1}$ Ce and 30 $\mu g\ g^{-1}$ La. (Cr tube excitation).

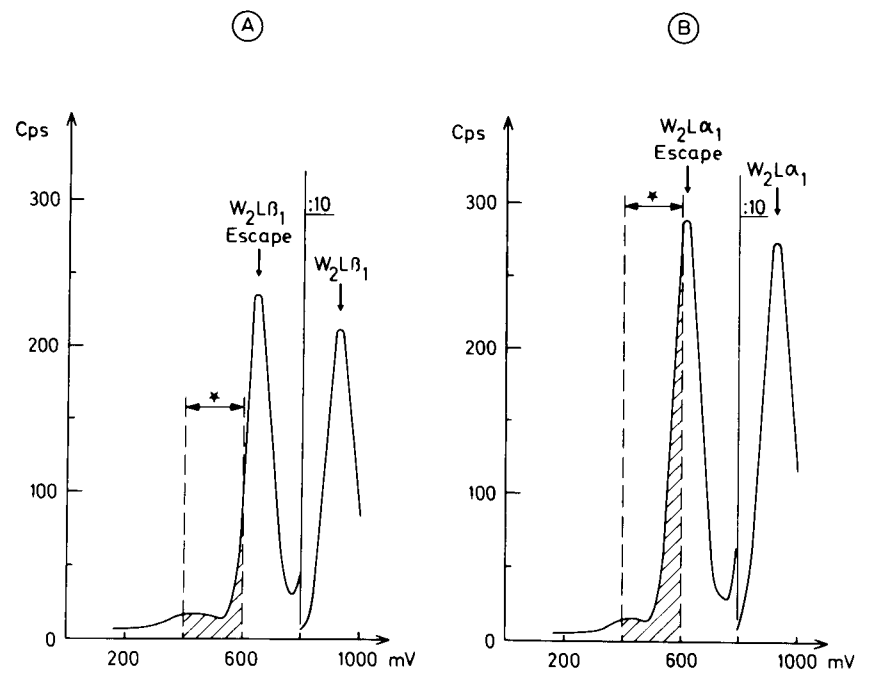

Fig. 2. Pulse-height distributions of the second-order tungsten L_{β_1} (A) and tungsten L_{α_1} (B) lines with the discriminator window used for the detection of first-order peaks. The range starred is the discriminator window.

order tungsten L_{β_1} line of the tube, scattered by the sample. As this is second-order scattering of an energy (9.67 keV) above the K-absorption edge of iron (7.11 keV), the scattering of the cast iron sample was rather limited and the interference could be greatly reduced by pulse-height discrimination. However, because of the presence of an escape peak in the flow counter a correction is still required. Figure 2 is a detailed view of the pulse-height distribution in the gas flow detector of the second-order tungsten L_{β_1} and L_{α_1} lines together with the discriminator window used for the detection of the first-order Ce L_α. It is clear from this figure that it is impossible to correct for the interference of W_2 L_{β_1} on Ce L_α in the 2θ scan, by using the ratio W_2 L_{α_1}/W_2 L_{β_1} and measuring W_2 L_α in the 2θ spectra of the samples, or by subtracting a constant value for W_2 L_{β_1} determined once from a blank sample. Indeed, the discriminator settings are so critical that the detector resolution plays an important part in the amount of interference that is actually measured. Determination of the interference by means of a blank sample must therefore be done for each series of analyses; ten apparently blank values measured from the same blank sample with a discriminator window from 400 to 600 mV varied from 2.1 to 35.2 cps.

A comparison of the excitation efficiency of both tubes is thus only possible for cerium. Table 5 summarizes the net intensities obtained for Ce L_α from several samples on irradiation with chromium or tungsten tubes. The tungsten tube is a factor of 2.5 more effective. As it is also the only tube that allows the measurement of both elements, it was chosen for all further work.

Sample finish. As the sample finish is always an important factor in x-ray fluorescence, appropriate tests were done on the grey cast iron. A selected sample of high Ce and La content was polished in several steps to varying degrees of smoothness, using a belt grinder followed by a disk grinder with silicon carbide disks of decreasing particle size and finally 6-μm diamond paste. After each step, the La L_α and Ce L_α intensities were measured using the tungsten tube, under the conditions mentioned earlier.

TABLE 5

Comparison of the Ce L_α net intensities obtained with Cr-tube and W-tube excitation, and the La L_α intensities obtained with W-tube excitation[a]

Sample	Ce by n.a.a. ($\mu g\ g^{-1}$)	Ce L_α (cps)[b] Cr tube	W tube	Ratio W/Cr	La by n.a.a. ($\mu g\ g^{-1}$)	La L_α (cps)[b]
1	7.9 ± 0.4	12.6 ± 0.3	37.1 ± 0.8	2.9 ± 0.1	5.1 ± 0.1	14.7 ± 0.5
2	11.0 ± 0.6	19.6 ± 1.1	52.8 ± 0.8	2.7 ± 0.1	7.2 ± 0.1	22.4 ± 0.7
3	14.4 ± 0.6	32.2 ± 1.1	75.2 ± 0.9	2.3 ± 0.1	9.4 ± 0.2	30.5 ± 0.9
4	21.2 ± 1.1	45.1 ± 1.0	115 ± 1	2.6 ± 0.1	13.5 ± 0.2	47.0 ± 0.9
5	29.5 ± 1.5	67.1 ± 1.1	159 ± 1	2.4 ± 0.1	19.2 ± 0.3	67.5 ± 0.8
6	36.9 ± 1.9	83.6 ± 3.0	208 ± 1	2.5 ± 0.1	24.0 ± 0.5	87.5 ± 0.6
7	57.6 ± 2.0	134 ± 4	316 ± 2	2.4 ± 0.1	30.6 ± 0.2	116 ± 1
			Mean ratio:	2.5 ± 0.2		

[a]Other conditions as in Table 2. [b]Counting time 400 s.

For the determination of the Ce L_α intensity, the W_2 L_{β_1} interference was determined for each step with a blank sample undergoing the same surface treatment. After each step, the second-order Fe K_{β_1} line was measured for use as an internal standard to correct for instrumental drift as a function of time. Plots of the cerium and lanthanum line intensities recorded after each step showed that polishing with 500-mesh grinding disks was sufficient to obtain reliable intensities.

Calibration graphs. Measurement of the La L_α and Ce L_α intensities of the seven samples previously analyzed by neutron activation—γ-spectrometry allowed the construction of calibration lines for La and Ce by means of the least-squares method. Figure 3 shows the part of the spectrum with the La and Ce lines obtained by excitation with a tungsten tube and recorded with a fine collimator and a coarse collimator. It can be seen that no new spectral interferences are induced by the use of a coarse collimator, while the intensity is increased by a factor of almost 4. This allows shorter measuring times for a similar precision.

Net intensities were calculated from three consecutive peak height measurements, one at the peak maximum and two at background positions before (b_1) and after (b_2) the peak; the latter two allow the calculation by linear interpolation of the background (b) at the peak position. The precision obtained on the measurement of the La L_α and Ce L_α lines in the samples is almost entirely determined by the large background (see Fig. 3) originating from scattering by the sample of first-order continuum radiation from the tube. A fixed counting time of 400 s for peak and background measurements

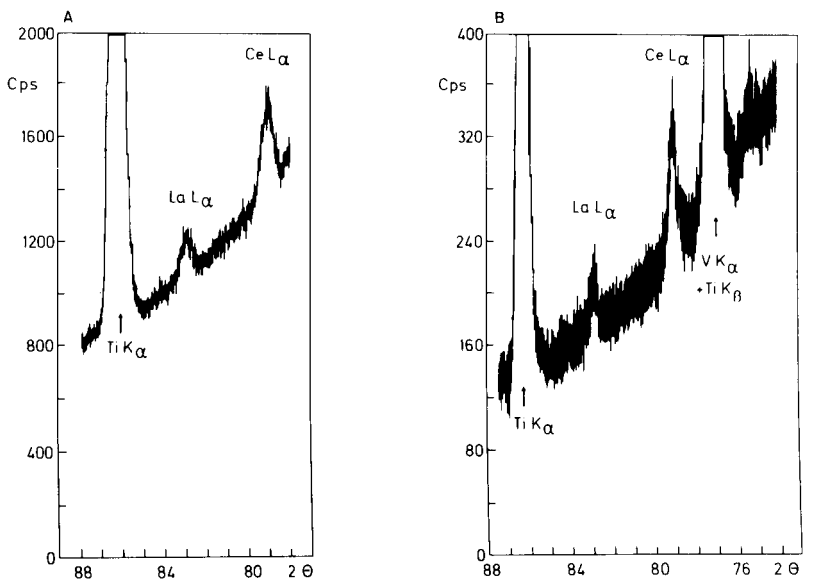

Fig. 3. Part of the spectrum from a 2θ scan of a grey cast iron sample (58 μg g^{-1} Ce and 30 μg g^{-1} La) recorded with (A) a coarse and (B) a fine collimator.

was thus adopted for all measurements. To improve the precision, the measurements were repeated 5—10 times for each sample, yielding the precisions indicated in Table 5.

The actual calibration lines obtained from these data had the equations: $y = (5.6202 \pm 0.0655)x - (5.98 \pm 2.28)$ for cerium, and $y = (4.0089 \pm 0.043)x - (7.03 \pm 1.04)$ for lanthanum, where y is $\mu g\ g^{-1}$ of the element (from neutron activation) and x is cps. The small errors on the slopes and the small intercepts of the lines illustrate the validity of the fits. No matrix influences were detected for concentrations up to 30 $\mu g\ g^{-1}$ La and 60 $\mu g\ g^{-1}$ Ce.

Detection limits. In accordance with Currie's definition [16], the detection limit (DL) is given as twice the standard deviation of the noise. For measurements during t_m seconds of the peak and the backgrounds, and determination of a single blank value, the detection limit is calculated as follows:

$$DL(t_m) = 2[(t_m \times B(\text{cps}) + b(t_m) + s^2_{b(t_m)} + s^2_{B(\text{cps})})/t^2_m]^{1/2} + s_B(\text{cps})$$

where t_m is the measuring time; B(cps) is the blank value in cps (e.g. ±7 for Ce from $W_2\ L_{\beta_1}$ interference, 0 for La); s^2_B is the variance of the blank, estimated from counting statistics only; b is the background at the peak position [$= b_1 - (\Delta p/\Delta)(b_1 - b_2)$, with $\Delta = 2\theta$ difference between b_1 and b_2 and $\Delta p = 2\theta$ difference between the peak position and b_1]; and $s^2_{b(t_m)} = b_1 + (\Delta p/\Delta)^2\ (b_1 + b_2)$. The term $s_{B(\text{cps})}$ is added here to increase the detection limit to compensate for the fact that only one blank is measured so that a systematic error ΔB is estimated by the standard deviation on B, might have been introduced [17]. For measuring times of 3 × 400 s, this leads to a detection limit of 11 cps for both the La L_α and Ce L_α lines, which means a detection limit of 3.1 $\mu g\ g^{-1}$ Ce and 3.7 $\mu g\ g^{-1}$ La.

X-ray fluorescence spectrometry of unknown samples

The above calibration graphs were applied in the analysis of grey iron samples of different castings. Four samples of four special castings with increasing additions of bismuth to the melt were analyzed as well as 15 samples from a single casting. The results are summarized in Tables 6 and 7, along with results obtained by the neutron activation method. The agreement of the results by the two methods proves the feasibility of the wavelength-

TABLE 6

Determination of lanthanum and cerium by neutron activation and x.r.f. in four cast irons with different amounts of bismuth in the melt

Sample No.	Bi added (mg kg^{-1})	La found (mg kg^{-1})		Ce found (mg kg^{-1})	
		N.a.a.	X.r.f.	N.a.a.	X.r.f.
1	5	8.6 ± 0.2	9.9 ± 0.4	13.6 ± 1.0	13.7 ± 0.5
2	10	9.2 ± 0.2	8.8 ± 0.3	14.6 ± 1.0	12.9 ± 0.4
3	100	8.5 ± 0.2	8.4 ± 0.2	12.1 ± 1.0	12.3 ± 0.4
4	300	9.2 ± 0.2	8.5 ± 0.3	11.2 ± 1.0	12.4 ± 0.4

TABLE 7

Determination of lanthanum and cerium in 15 disks from one grey iron casting

	La found (mg kg^{-1})		Ce found (mg kg^{-1})	
	N.a.a.	X.r.f.	N.a.a.	X.r.f.
Mean	13.3 ± 0.1	13.3 ± 0.2	23.9 ± 0.6	22.4 ± 0.2
Standard deviation	0.2	0.7	2.4	0.5
Relative standard deviation (%)	1.5	5.3	10	2.2

dispersive x-ray technique for cerium and lanthanum in grey iron samples "as cast" provided that a few standard samples are available.

The authors are indebted to Ir. Lietaert and Dr. Ir. Defrancq of the CRIF (Centre for Scientific and Technical Research of the Metal-working Industry in Belgium) for preparing the specimen cast iron samples and for fruitful discussions. The investigation is a part of a research program sponsored by the Instituut voor Wetenschappelijk Onderzoek in de Nijverheid en de Landbouw and the CRIF-Gieterijcentrum.

REFERENCES

1 H. Morrogh, A. E. S. Trans., 56 (1948) 72.
2 H. D. Merchant, Solidification of Cast Iron — A review of literature, in Recent Research on Cast Iron, Gordon and Breach, New York, 1964, pp. 1—100.
3 M. J. Lalich, Metallurgy of Cast Iron, Georgi, Switzerland, 1975, p. 561.
4 E. Campomanes, Giesserei, 65 (1978) 535.
5 Yu. I. Usatenkov, L. F. D'Yachenko and V. I. Kravatsova, Zavod. Lab., 41 (1975) 645.
6 D. Henriet and P. de Gelis, Chim. Anal., 50 (1968) 519.
7 I. M. Krasil'nikov, I. D. Shorova, A. V. Sholomov, P. A. Konstantinov and A. P. Matyushin, At. Energy, 48 (1980) 120.
8 A. T. Kashuba and C. R. Hines, Anal. Chem., 43 (1971) 1758.
9 F. M. Skolets and V. A. Chernyi, Zavod. Lab., 30 (1964) 147.
10 U. Gerulin and R. Olerhauser, Materialprüfung, 20 (1978) 233.
11 Z. I. Koroblinikova, M. N. Tropkina, V. G. Tatskova and Yu. G. Eremin, Zavod. Lab., 36 (1970) 159.
12 J. E. Roberts and M. J. Ruyterband, Anal. Chem., 37 (1965) 1585.
13 R. N. Smith, Modern Castings, an AFS Chemical Analysis Committee (12-F) Report October 1981.
14 L. S. Serdyuk and V. S. Smirnaya, Izv. Vyssh. Ucheb. Zaved., Khim. Khim. Tekhnol., 10(5) (1967) 509.
15 A. A. Amsheeva and D. V. Bezuglyi, Zh. Anal. Khim., 16 (1961) 683.
16 L. A. Currie, Anal. Chem., 40 (1968) 586.
17 J. Op de Beeck, J. De Donder, INW G-CHEM 3, Internal Report, 1977.

Analytica Chimica Acta, 155 (1983) 219—224
Elsevier Science Publishers B.V., Amsterdam — Printed in The Netherlands

Short Communication

DIRECT POTENTIOMETRIC MONITORING OF PROTEINS

M. L. HITCHMAN*, F. W. M. NYASULU, A. AZIZ and D. D. K. CHINGAKULE

Department of Chemistry and Applied Chemistry and Thin Film and Surface Research Centre, University of Salford, Salford M5 4WT (Great Britain)

(Received 13th July 1983)

Summary. A simple, reliable, rapid and inexpensive method of monitoring proteins is based on direct potentiometry with metal electrodes which are electrochemically treated before each measurement. The principles behind the treatment processes are discussed and the results are illustrated with an application to protein chromatography.

The monitoring of proteins and amino acids by potentiometric techniques has been studied frequently in recent years [1—5]. These studies have shown that, in principle, direct potentiometry can be used for protein determination, but that in practice the technique suffers from the problems of sluggish response to changes in protein concentrations (Fig. 1, curve A), lack of reproducibility (Table 1) and a marked dependence on the history and pretreatment of the electrode (Fig. 2a). The problem of poor reproducibility can be overcome by titrating the protein and monitoring the end-point with an electrode sensitive to the titrant [1], but the problem of slow response of indicator electrodes in the presence of proteins can still remain. Thus, for both direct and indirect potentiometry, electrodes with faster responses to protein concentration changes would be desirable; and better reproducibility is needed for direct potentiometry, which would be the preferred technique for many applications because small volumes can be used and the proteins are not destroyed.

If one considers a metal electrode in contact with a protein-containing solution, then the potential-determining process will undoubtedly involve the formation of a metal—protein complex. This complex could be considered as being adsorbed on the surface, e.g.,

$$Ag(s) + RS^-(aq) \rightleftharpoons AgSR\ (ads) + e^- \qquad (R1)$$

where RS^- is the anion of a thiol-containing protein. Alternatively, it could be considered as being formed in solution close to the electrode, e.g.,

$$Cu(s) \rightleftharpoons Cu^{2+}(aq) + 2e^- \qquad (R2)$$

$$Cu^{2+}(aq) + 2RCH(NH_2)COO^-(aq) \rightleftharpoons Cu\left(\begin{array}{c} NH_2{-}CH{-}R \\ \diagup \quad | \\ O{-}C{=}O \end{array}\right)_2 (aq) \qquad (R3)$$

0003-2670/83/$03.00

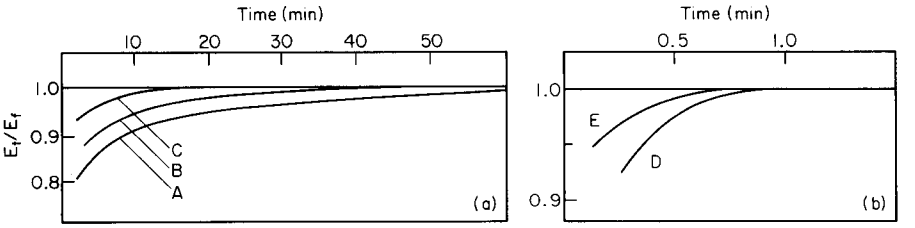

Fig. 1. Stabilisation times for electrode potentials. (The ratio of the potential at time t (E_t) to the final equilibrium potential (E_f) is plotted.) Silver electrode response to bovine serum albumin (0.5 mg ml^{-1}; pH 8.4): (A) without cleaning; (B) chemical cleaning; (C) cathodic cleaning; (D) with alkaline pretreatment, cathodic cleaning and anodisation. (E) Copper electrode response to γ-globulin (1 mg ml^{-1}; pH 9) with cathodic cleaning.

Whichever process is considered, it is clear that the electrode response will depend markedly on the rate of attainment of a heterogeneous equilibrium and this, in turn, will be influenced by any surface contamination. Improved response would be expected for a clean electrode, and this has been found to be so for silver [1] and copper [5] electrodes. For silver, cleaning with ammonia solution was effective, which indicates the removal of a surface layer by formation of a diammine complex:

$$Ag(s)/AgX\ (ads) + 2NH_4OH\ (aq) \rightarrow Ag(s) + Ag(NH_3)_2^+\ (aq) + 2H_2O + X^-\ (aq) \qquad (R4)$$

This idea suggests the use of cathodic electrochemical cleaning to achieve the same end:

$$Ag(s)/AgX\ (ads) + e^- \rightarrow Ag(s)/Ag\ (ads) + X^-\ (aq) \qquad (R5)$$

TABLE 1

Reproducibility of potentials[a] for the silver electrode

[Bovine albumin] (mg ml^{-1})	Electrode potential (mV vs. Ag/AgCl)							
	No cleaning		Cathodic cleaning				Full treatment[b]	
	$-E_1$	$-E_2$	$-E_1$	ΔE_1	$-E_2$	ΔE_2	$-E_1$	$-E_2$
0.01	51	31	80	12	73	14	80	78
0.05	70	54	110	43	103	42	125	124
0.10	76	62	126	57	124	60	154	152
0.50	100	79	147	79	137	78	199	201
1.00	113	92	170	104	166	106	236	233

[a] E_1 and E_2 denote actual potentials measured for two separate runs, while ΔE_1 and ΔE_2 denote the differences between potentials measured in a protein solution and those measured in the buffer solution for two runs. [b] Alkaline pretreatment, cathodic cleaning and anodisation.

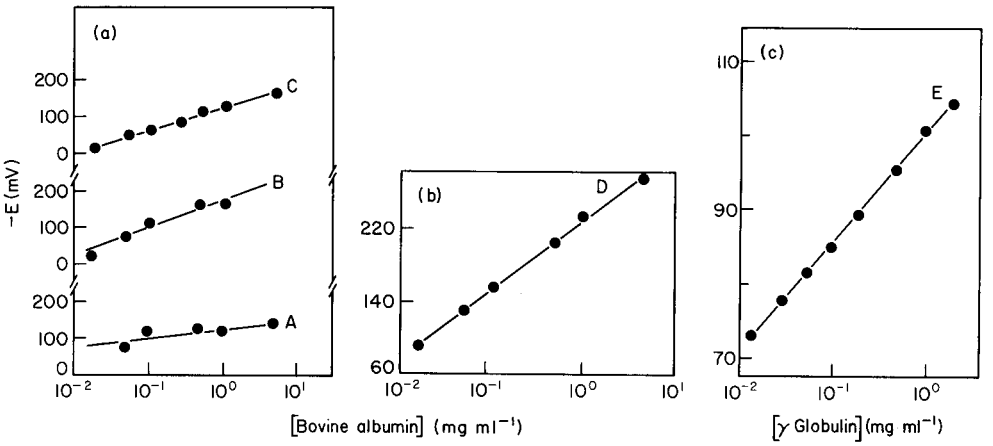

Fig. 2. Nernst plots. Lines A—E correspond to the conditions listed for Fig. 1. All potentials are with respect to Ag/AgCl reference electrode.

Experimental

Conventional potentiometric monitoring techniques were used. Potential variations with time were monitored on a recorder with the aid of a high-impedance voltage follower to ensure minimum electronic disturbance of the electrodes. Indicator electrodes used were high-purity silver and copper wires (diameter 1—2 mm) and silver and copper tubes (internal diameters 1—2 mm). Electrochemical pretreatment of electrodes was done with simple d.c. circuitry and with a platinum foil as the auxiliary electrode. Gel chromatography was done using Sephacryl S300 with commercial peristaltic pumping and u.v. monitoring systems.

Results and discussion

Figure 1(a) compares the stabilisation of the potential of a silver wire electrode on introducing it into a solution of bovine serum albumin (0.5 mg ml^{-1}) at pH 8.4 without precleaning (curve A), after chemical cleaning with ammonia solution (curve B), and after cathodic cleaning in the buffer solution (ca. 3 μA for 15 s) (curve C). The dramatic improvement in the stabilisation of the electrode potential after cathodic pretreatment is readily seen. Figure 2(a) shows the Nernst plots corresponding to the three cases; again the improved behaviour of the electrochemically pretreated electrode is apparent. Similar improvements were obtained at other pH values and with other thiol-containing proteins. However, even with cathodic cleaning attainment of an equilibrium potential is still relatively slow (ca. 18 min), and the reproducibility from run to run is not good, although it can be improved by taking the difference (ΔE) between the potential measured in the presence of protein and that measured in the buffer solution alone (Table 1). Finally, the slope of the Nernst plot is —60 mV/decade corresponding to 1 SH/protein molecule whereas one would expect —84 mV/decade corresponding to 0.7 SH/molecule [6].

Equations (R1) and (R2) suggest that the potential-determining processes require the presence of a higher oxidation state of the metal. Accordingly, the establishment of equilibrium conditions could be facilitated by a short period of anodisation of the electrode prior to measurement. When the cathodic cleaning as before was followed by anodisation (ca. 3 μA for 5 s) of the silver electrode in the protein test solution, the stabilisation time was reduced to about 7 min, but there was no significant improvement in either the reproducibility of measured potentials or in the slope of the Nernst plot. Nevertheless, the oxidation of the silver obviously changed the electrode response; and it was expected that this effect would be enhanced by running the oxidation in a protein solution at a pH significantly greater than the pK_a of the SH-group because this would ensure the presence of the anion RS^- during anodisation. The same procedure as before was tried except that the anodisation was made at pH 13. This technique gave a slightly faster stabilisation time still, but neither reproducibility nor Nernst slope were improved further. However, during these investigations it was discovered that simply allowing the electrode to stand for a short time (ca. 5 min) in an alkaline solution (e.g., 1—10 M NaOH) without protein, followed by cathodic cleaning and anodisation in the protein test solution at a normal pH (e.g., pH 4—9) led not only to fast stabilisation of electrode potential (Fig. 1b) but also to much more reproducible results (Table 1) and a Nernst slope of —82 mV/decade (Fig. 2b), which is closer to that expected on the basis of the number of SH groups available for complexation.

The cathodic cleaning and anodisation can obviously be done on a continuous basis between measurements, and this procedure was, in fact, used in obtaining the results in Figs. 1(b) and 2(b). However, soaking an electrode in a high pH solution between measurements is inconvenient. Further studies showed that there was no significant deterioration in electrode behaviour over a period of several hours, and if the electrode was kept in buffer solution with an anodic voltage (about 0.35 V) applied to it between measurements, then no alkaline treatment was necessary for periods in excess of 12 h. These results indicate that the alkaline pretreatment provides a persistent high local pH at the electrode surface, possibly through the formation of silver oxide sites. This effect is currently being studied in more detail.

Although all the above results relate to measurements with a silver electrode and bovine serum albumin, similar results were obtained with other albumins as well as for a number of globulins; all these are thiol-containing proteins. Alexander et al. [4, 5] have recently reported that bright copper electrodes respond to a wide range of amino acids. However, the response to amino acid concentration was generally non-Nernstian and the potential response of an electrode deteriorated with time, especially in the presence of a thiol group.

The use of the pretreatment techniques was therefore investigated with copper electrodes. It was found that cathodic cleaning alone was adequate to give acceptable behaviour in terms of stabilisation time, reproducibility and

TABLE 2

Reproducibility of potentials for the copper electrode with cathodic cleaning

[γ-Globulin] (mg ml^{-1})	0.01	0.05	0.10	0.50	1.00	2.00
$-E_1$[a]	70	81	85	95	101	105
$-E_2$[a]	71	81	83	94	100	103

[a]Electrode potential (mV vs. Ag/AgCl).

Nernstian slope. Figure 1 (curve E) is a typical stabilisation plot for a copper electrode, Fig. 2(c) is the corresponding Nernst plot and Table 2 indicates the run-to-run reproducibility; the Nernstian slope is understandable in terms of the complexing of copper with a globulin.

Figure 3 illustrates the application of the electrochemical pretreatment of copper and silver tube electrodes to the monitoring of mixtures of proteins eluting from a gel chromatographic column. The signals obtained are similar to those of the more sophisticated and much more expensive u.v. detector.

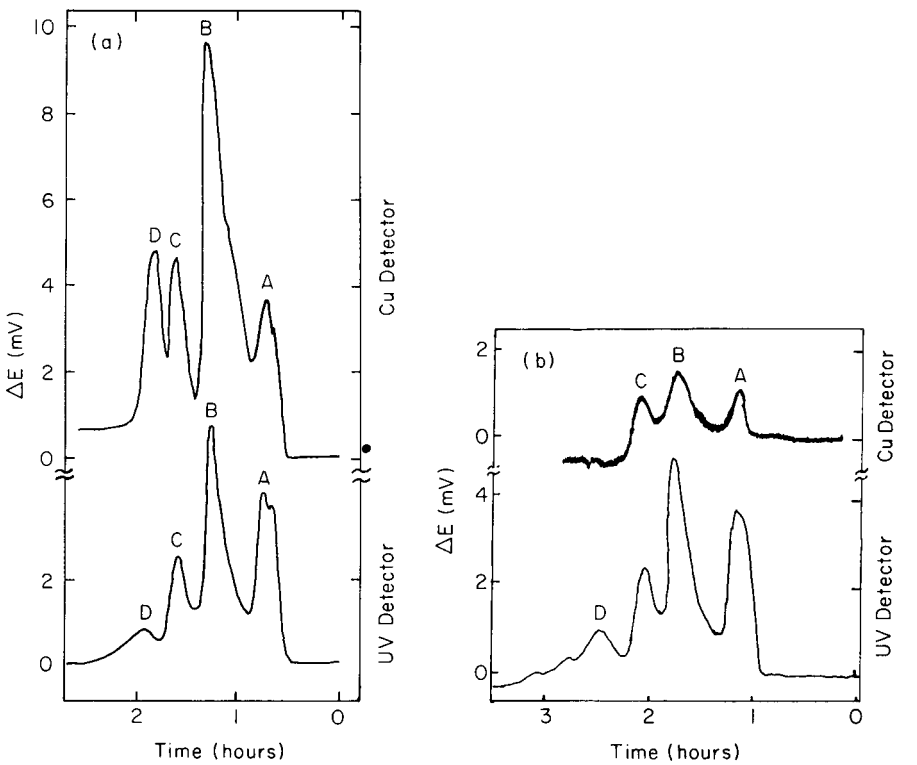

Fig. 3. Chromatograms for protein separations (Sephacryl S300 column, pH 6.7). (a) Copper tube electrode (flow rate 21 ml h^{-1}): A, thyroglobulin; B, catalase; C, human serum albumin; D, ribonuclease. (b) Silver tube electrode (flow rate 15 ml h^{-1}): A, thyroglobulin; B, α-globulin; C, human serum albumin; D, ribonuclease. Chromatograms obtained by u.v. detection are also shown.

There is no signal for ribonuclease with the silver electrode because this protein contains no thiol group. The different forms of complexation with different metals suggests the possibility of a detector with several different metal electrodes for identifying a protein as well as simply detecting its presence. Initial investigations on this have given promising results. The use of direct potentiometry with metal electrodes treated electrochemically before measurement would seem to offer the basis of a simple, rapid and reliable method for protein monitoring.

We acknowledge the provision of materials and equipment for this work by Pharmacia Fine Chemicals AB, Uppsala, Sweden.

REFERENCES

1 T. Y. Toribara and L. Koval, Talanta, 17 (1970) 1003.
2 P. D'Orazio and G. A. Rechnitz, Anal. Chem., 49 (1977) 41.
3 P. W. Alexander and G. A. Rechnitz, Anal. Chem., 46 (1974) 250, 860.
4 P. W. Alexander, P. R. Haddad, G. K. C. Low and C. Maitra, J. Chromatogr., 209 (1981) 29.
5 P. W. Alexander and C. W. Maitra, Anal. Chem., 53 (1981) 1590.
6 T. P. King, J. Biol. Chem., 236 (1961) PC5.

Analytica Chimica Acta, 155 (1983) 225—229
Elsevier Science Publishers B.V., Amsterdam — Printed in The Netherlands

Short Communication

A POLYMER SUPPORT FOR PYRIDOXINE HYDROCHLORIDE USED AS A SORBENT FOR THE PIEZOELECTRIC QUARTZ CRYSTAL DETECTION OF AMMONIA

G. J. MOODY, J. D. R. THOMAS* and M. A. YARMO[a]

Applied Chemistry Department, Redwood Building, UWIST, Cardiff CF1 3XA (Great Britain)

(Received 1st June 1983)

Summary. A high molecular mass polyalkoxylate, Antarox CO-880 (nonylphenoxypolyethoxylate with 30 ethoxylate units) is a suitable matrix for supporting pyridoxine hydrochloride (an ammonia sorbent) on a quartz piezoelectric crystal detector. The matrix helps considerably to extend the useful lifetime of the detector from ca. 10 to >53 days.

The scope of the piezoelectric crystal detector in analytical chemistry is greatly widened by using absorbent coatings of appropriate selectivity and sensitivity on the quartz crystal [1]. The analyte is selectively sorbed by the coating, thereby increasing the mass on the crystal and decreasing the frequency of vibration. The frequency change is linearly related to the mass sorbed according to $\Delta F = -\Delta m F/Adt$, which by substituting appropriate parameters for commercially available crystals simplifies to $\Delta F = -2.3 \times 10^6 F^2 \Delta m/A$, where ΔF is the change in frequency (Hz), F is the initial frequency of the quartz plate (MHz), Δm is the mass sorbed (g), A is the area of the coating (cm^2), d is the density of the quartz (g cm^{-3}) and t is the thickness of the crystal (cm). Thus, for a particular experimental set-up, the change in frequency can be expressed as $\Delta F = KC$, where C is the analyte concentration (mg dm^{-3}) and K is a constant which includes the basic frequency of the quartz crystal, the area coated and a factor to convert the mass of analyte sorbed to its gas-phase concentration.

For the detection of ammonia in air, Ucon 75-H-90,000 and Ucon LB-3000X were first used and found to have good sensitivity [2]. These were followed by coatings of extracts of *Capsicum annum* pods and ascorbic acid, with and without silver nitrate [3], and later by L-glutamic acid hydrochloride and pyridoxine hydrochloride (vitamin B6 hydrochloride) [4], which showed exceptional sensitivity.

---

[a]Present address: Chemistry Department, National University of Malaysia, Bangi, Selangor, Malaysia.

0003-2670/83/$03.00

During evaluation of a laboratory-constructed piezoelectric apparatus, [5], it was found that simply coating the quartz crystal with pyridoxine hydrochloride from an ethanol/water solution led to a coating with an effective lifetime of only ca. 10 days. However, application of the pyridoxine hydrochloride in a matrix of nonylphenoxypolyethoxylate (Antarox CO-880) gave greatly improved stability over a much longer period.

Experimental

Apparatus and detector design. The measuring unit consisted of a frequency oscillator with a buffered output powered by a Weir 400 power supply set at 9 V d.c. The frequency output from the oscillator was measured by a Marconi type 2431A 200-MHz digital frequency meter. A digital-to-analog converter selected the last two digits of the frequency meter output for conversion to an analog signal to a Bryans Model 28000 chart recorder, reading to ±1 Hz. The quartz crystal (AT-cut) with gold electrode (Quartz Crystal Co., Wellington Crescent, New Malden, Surrey) had a resonant frequency of 9 MHz. The detector cell incorporating this crystal was based on the design of Karmarkar and Guilbault [6] wherein the gas sample was split into two streams impinging directly on opposite faces of the coated crystal. The glass-encased cell detector was immersed in a water bath at 25 ± 0.1°C.

Crystal coatings. A saturated solution of 1% (w/v) pyridoxine hydrochloride in ethanol/water (1 + 1) was dip-coated on the quartz crystal for the first series of experiments. For the second series, the solution for dip-coating consisted of a (1 + 1) mixture of a 0.2% (w/v) solution of pyridoxine hydrochloride in ethanol and a 0.2% (w/v) solution of Antarox CO-880 in acetone. Each coating was readily removed by soaking the crystal in ethanol. The crystal was dried before re-coating.

Ammonia test samples. The ammonia gas test samples were obtained from ammonia vapour over ammonia liquor equilibrated at 25°C. Serial dilution of the headspace gas was effected by syringe dilution [7] with ambient air. Successive dilutions were delayed by 30—60 s in order to allow ammonia to diffuse throughout the air in the syringe. The concentration of ammonia was checked by titration. For example, 3, 5 and 10-cm^3 samples removed from the headspace over the ammonia liquor were taken by syringe and slowly injected into 20 cm^3 of 0.025 M sulphuric acid. The excess of sulphuric acid was titrated with 0.1 M sodium hydroxide using methyl orange as indicator. Ten replicate samples of 5 and 10 cm^3 of the headspace gas contained 30.8 ± 0.2 and 30.4 ± 0.2 mg dm^{-3} (mean ± std. dev.), respectively, of ammonia. Diluted headspace gas samples were similarly checked; for example, 4 cm^3 of headspace gas diluted to 10 cm^3 was found to contain 12.1 ± 0.1 mg dm^{-3} ammonia.

The responses of the coated crystal were tested on triplicate 1-cm^3 samples of appropriate dilutions of the headspace ammonia test samples and the mean decrease in frequency was measured. The diluted samples were injected into a carrier stream of dry (anhydrous calcium chloride) air, and passed

through the crystal compartment at 30 cm^3 min^{-1} by the pump of a Pitman Instruments model 7069 air sampler.

Results and discussion

The sample injection method essentially results in a gas-phase flow injection mode of analysis. Typical responses are shown in Fig. 1, from which the fast response of the detector is evident. There is a fast initial return of the frequency towards the baseline for 20 s after the sample has passed through the detector, although full return to the original frequency takes much longer depending on the concentration of ammonia in the sample (at least 30 min for the higher concentrations). Both modes of detector behaved similarly with regard to response speed and desorption rate. For 6 and 12 mg dm^{-3} ammonia, the desorption times were of the order of 10 min for both modes. These correspond to response times of <30 s and desorption times of ca. 4 min noted by Hlavay and Guilbault [4] for $\leqslant 1$ mg dm^{-3} ammonia. However, fresh samples may be injected before return to the baseline frequency for it is the immediate decrease in frequency caused by the injected sample that is analytically significant (Fig. 2). Of course, injections of aliquots of samples greater than the 1 cm^3 used here would lead to larger frequency changes as observed in other studies of pyroxidine hydrochloride coatings [4]. Slowing the air carrier stream would be expected to have a similar effect, but at the expense of longer times required to sweep the previous sample away.

This study was expressly devoted to the effect of the polymer (Antarox CO-880) matrix to support the sorbent. Figure 2(b) shows clearly that the use of Antarox CO-880 as a supporting matrix helps to maintain the effective sensitivity of the pyridoxine hydrochloride coating on the crystal for a prolonged period; there was only slight loss of sensitivity (0.14 Hz dm^3 mg^{-1}) between the attainment of equilibrium by the crystal (day 3) and the end of

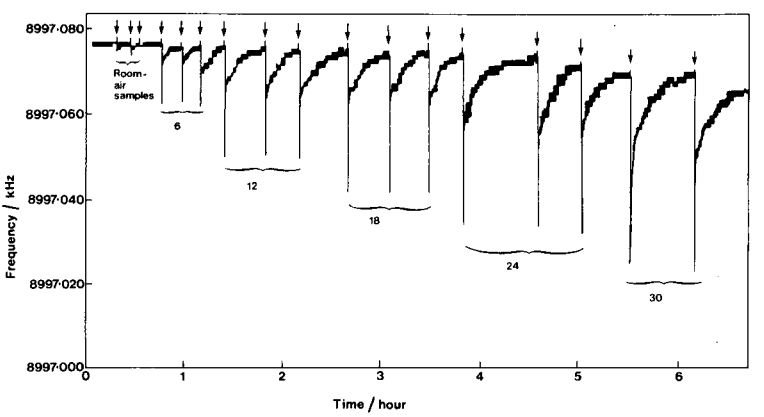

Fig. 1. Example of calibration responses to ammonia gas of quartz crystal coated only with pyroxidine hydrochloride (day 6). Arrows indicate the injection points. Air carrier at 30 cm^3 min^{-1}. Numbers on outputs are mg dm^{-3} ammonia.

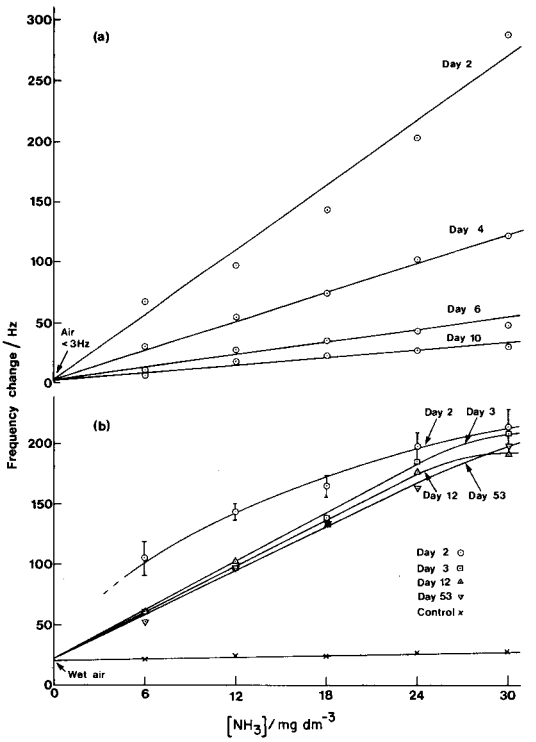

Fig. 2. Calibration with ammonia gas of quartz crystal coated with pyroxidine hydrochloride: (a) alone; (b) in a matrix of Antarox CO-880. (×) Control on crystal coated with Antarox CO-880 on day 5. The correlation coefficient (Fig. 2b) for 6, 12, 18 and 24 mg dm^{-3} NH_3 for days 3—12 together (from runs on day 3, 5, 6, 7, 8, 10 and 12) is 0.9912 ($\Delta Hz = 6.41\ [NH_3] + 20.0$); the correlation coefficient for the same NH_3 concentration for day 53 is 0.9856 ($\Delta Hz = 6.27\ [NH_3] + 20.4$).

the study period (day 53). The pyridoxine hydrochloride-coated crystal without the polymer support steadily and quickly lost its sensitivity, until at day 10 there was a mere 30 Hz decrease in frequency for the 30 mg dm^{-3} sample (Fig. 2a) compared with 198 Hz for the crystal with pyroxidine hydrochloride supported by Antarox CO-880. The response of the crystal with the Antarox support tended to approach a limiting value above 24 mg dm^{-3} ammonia.

The blank of ca. 20 Hz for the crystal with the Antarox matrix containing pyridoxine hydrochloride is attributed to background moisture, for such a reading was obtained by injecting 1-cm^3 control samples of uncontaminated air equilibrated over water. Dry air gave blank readings of <3 Hz. A control experiment with Antarox CO-880 coated on the crystal without any pyridoxine hydrochloride confirmed that the polymer matrix was not significantly involved in ammonia sorption but did sorb water (Fig. 2b).

Conclusions

A polyethoxylate polymer of high relative molecular mass, such as the Antarox CO-880 used here, is a suitable matrix for maintaining the useful life of piezoelectric crystal detectors coated with selective sorbents. Its humectant properties cause responses to sample moisture, but methods are available for overcoming this, such as the use of a gas chromatographic pre-column packed with an appropriate drying agent placed between the sample injection port and the crystal.

The National University of Malaysia, Kuala Lumpur, Malaysia is thanked for financial support to M.A.Y.

REFERENCES

1 G. G. Guilbault, Ion-Selective Electrode Rev., 2 (1980) 3.
2 K. H. Karmarkar and G. G. Guilbault, Anal. Chim. Acta, 75 (1975) 111.
3 L. M. Webber and G. G. Guilbault, Anal. Chem., 48 (1976) 2244.
4 J. Hlavay and G. G. Guilbault, Anal. Chem., 50 (1978) 1044.
5 A. J. Cannard, G. J. Moody, J. D. R. Thomas and M. A. Yarmo, unpublished work, 1983.
6 K. H. Karmarkar and G. G. Guilbault, Anal. Chim. Acta, 71 (1974) 419.
7 F. W. Karasek and J. W. Tienay, J. Chromatogr., 89 (1974) 31.

Analytica Chimica Acta, 155 (1983) 231—234
Elsevier Science Publishers B.V., Amsterdam — Printed in The Netherlands

Short Communication

INTERNAL ELECTROLYTIC DETERMINATION OF SILVER IN SOLUTION WITH A PIEZOELECTRIC QUARTZ CRYSTAL

T. NOMURA* and T. NAGAMUNE

Department of Chemistry, Faculty of Science, Shinshu University, Asahi, Matsumoto 390 (Japan)

(Received 20th May 1983)

Summary. The piezoelectric quartz crystal is connected to an oscillator constructed with an integrated circuit, which has insufficient potential between the electrodes to electrodeposit metal ions spontaneously from the solution. Silver (10^{-5}—10^{-6} M) in solution is determined by internal electrodeposition on the platinum electrodes of the crystal connected to a zinc rod immersed in the same solution.

A piezoelectric quartz crystal connected to a transistor-based oscillator oscillates in liquids [1]. The frequency shift depends on the specific conductivity and density of the solution [2]. Metal ions, however, electrodeposit on one of the electrodes because there is a potential of about 1.5 V between the electrodes [2]. One electrode on the crystal, therefore, should be covered to avoid electrodeposition of metal ions from the solution by electrolysis when the crystal is used. An oscillator constructed with an integrated circuit (i.c.) [3] also allowed the crystal to oscillate in liquids. It was found that no metal ion spontaneously electrodeposited on the electrodes, but the crystal otherwise behaved similarly to that connected to the transistor-based circuit. Internal electrolysis of silver in solution, therefore, was possible by using the crystal connected to the i.c. oscillator. Internal electrolysis [4] is now rarely used for the determination of metal ions because it is time-consuming, and cannot be used to determine minute amounts of metal ions. Shiobara [5] determined silver which is electrodeposited on a weighed platinum electrode against copper wire, using a potassium nitrate/agar bridge. In this communication, micromolar concentrations of silver are determined in an experiment lasting several minutes by using a zinc rod for the counter electrode.

Experimental

Apparatus and reagents. The piezoelectric quartz crystal was as described previously [6], and was set in a flow cell as shown in Fig. 1. A zinc rod, (2 mm diameter, 30 mm long) was used as a counter electrode to the platinum electrode of the crystal, 1 mm apart, and connected to the platinum electrode with a copper wire. The oscillator was built with an integrated circuit

0003-2670/83/$03.00

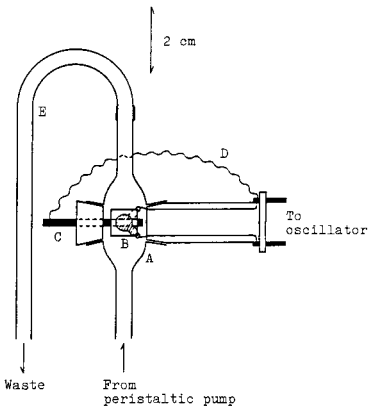

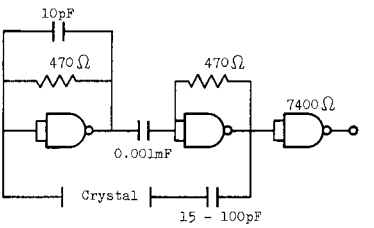

Fig. 1. Vertical section of the flow cell: (A) cell; (B) crystal; (C) zinc rod; (D) leading wire; (E) silicone tubing.

Fig. 2. Oscillator circuit [3].

as shown in Fig. 2 [3]. The digital counter, recorder, air bath and peristaltic pump were used as described previously [6].

A silver stock solution (0.1 M) was prepared by dissolving 1.6987 g of silver nitrate in water and, diluting to 100 ml with water; it was stored in an amber-coloured bottle. The pH was adjusted with 0.1 M tartaric acid and sodium tartrate solutions.

Determination of silver (10^{-5}—10^{-6} M). Transfer the sample or standard solution, which is 1×10^{-3} M in EDTA and 5×10^{-3} M in tartrate buffer (pH 3.9), and the reagent blank solution to their respective containers. Pass the reagent blank solution through the cell at 10.4 ml min^{-1}. When the crystal frequency has become constant (F_1), pass the sample solution for exactly 10 min (or 5 min for 10^{-5} M silver), and then pass the reagent blank solution again until the frequency is constant (F_2). The frequency change, $\Delta F = F_1 - F_2$, is proportional to the concentration of silver, and a calibration graph may be constructed on this basis. After several experiments, the electrode with deposited silver is removed from the cell, dipped in 6 M nitric acid for 5 s, washed with water and acetone, and dried. The zinc rod is cleaned by the same method, but with 6 M hydrochloric acid instead of nitric acid.

Results and discussion

Behavior of the crystal immersed in aqueous solution. The frequency shift of the crystal connected to the i.c. oscillator when the whole crystal was immersed in aqueous solution was investigated by the same method as described previously [2]. The frequency of the crystal in water decreased from that in air by about 6400 Hz, depending on the position of the crystal with regard to the water surface. Frequency shifts resulting from the specific con-

ductance of the medium are shown in Table 1. The frequency decreased with increasing specific conductance whereas it increased when the transistorized oscillator was used [2]. The changes were much greater than that of the latter [2]. On the other hand, the frequency decreased with increasing density, similarly to the transistorized circuit (Table 2). The frequency also changed with the water temperature; the change from 24°C to 25°C was 30 Hz (the transistorized circuit gave 75 Hz). Some metal ions spontaneously deposited on the electrode of the crystal connected to the transistorized oscillator when the whole crystal was immersed in solution because of the potential between the electrodes on the crystal. However, the frequency of the crystal connected to the i.c. oscillator did not change in solutions of silver, copper(II), cadmium, lead or nickel (which deposited on the crystal connected to the transistorized oscillator) in 0.01 M acetate buffer (pH 4.7). It was expected that the electrodes connected to the i.c. oscillator would have a smaller potential difference so that metal ions would not electrodeposit.

Internal electrolytic determination of silver. In order to determine silver selectively by internal electrodeposition, it is necessary to use a counter metal electrode having a slightly larger oxidation potential than silver [5]. Determination of silver using the platinum electrode of the crystal was initially examined with similar equipment to that in the earlier paper [5]. However, micromolar concentrations of silver did not electrodeposit on the crystal because the potential difference between the platinum electrode and the copper counter electrode was too small to overcome the junction

TABLE 1

Frequency shifts of the crystal when changing from water to potassium chloride solutions

KCl conc. ($\times 10^{-4}$ M)	Specific conductance ($\times 10^{-5}$ Ω^{-1} cm^{-1})	Frequency shift (Hz)	KCl conc. ($\times 10^{-4}$ M)	Specific conductance ($\times 10^{-5}$ Ω^{-1} cm^{-1})	Frequency shift (Hz)
1	1.48	−13	8	11.8	−661
1.5	2.23	−41	10	14.7	−850
2	2.96	−70	20	29.2	−1540
3	4.44	−153	50	71.8	Unstable
5	7.39	−352			

TABLE 2

Frequency shifts when changing from water to sucrose solutions

Sucrose conc. (% w/v)	Density difference (mg cm^{-3})	Frequency shift (Hz)	Sucrose conc. (% w/v)	Density difference (mg cm^{-3})	Frequency shift (Hz)
0.5	1.99	−75	4	16.60	−356
1	3.95	−161	6	24.38	−423
2	8.59	−221	8	32.28	−536

TABLE 3

Tolerance limits for ions in the determination of 1×10^{-5} M silver

Tolerance limit (Ion:silver mole ratio)	Ions
10	Fe(III), Co(II), Ni(II), Pb(II), Cd(II), Zn(II) SO_4^{2-}, NO_3^-, CN^-, CO_3^{2-}
1	Hg(II), Cu(II) $S_2O_3^{2-}$
0.1	SCN^-, Cl^-, Br^-, I^-, S^{2-}

potential of the agar bridge. When the copper counter rod was connected to the platinum electrode in the same solution, silver deposited on both surfaces of the platinum electrode and the copper rod and changed the frequency of the crystal. However, silver could not be determined because the frequency change had a plateau resulting from covering the copper rod with silver. The frequency changes were small or poorly reproducible when lead, aluminium or tin was used as the counter rod. Zinc rod was finally chosen for this purpose.

Dependence of the frequency change on pH and flow rate. Frequency changes depending on the electrodeposition of silver were constant in the range of pH 3.4—5.4 (tartrate buffers); above this pH, silver formed its hydroxide. Frequency changes were exactly proportional to the flow rate for 2.1—15.2 ml min^{-1} and for electrodeposition times in the range 0.5—10 min examined. Electrodeposition for 10 min was used for the determination of micromolar silver solutions, and 5 min for larger concentrations.

Calibration and reproducibility. The calibration graph of frequency change (ΔF) against silver concentration for 10-min electrolysis was linear for 1×10^{-6}—1×10^{-5} M and is described by the equation $[Ag] = (\Delta F/23.8) \times 10^{-6}$ M, where ΔF is measured in Hz. The standard deviation was 11.9 Hz (5.0%) for 5 determinations of 1×10^{-5} M silver.

Effect of other ions. The effect of various ions on the determination of 1×10^{-5} M silver was investigated; changes of frequency of more than ±8% were considered to result from interferences. The tolerance limits found are shown in Table 3. Interferences of mercury(II) and copper(II) arose from electrodeposition on the electrode, thus giving positive errors. Interferences of anions, except for thiosulfate, which formed a soluble silver complex, arose from the formation of precipitates of silver, giving negative errors. These anions preventing electrodeposition of silver would be eliminated by the method described previously [6].

REFERENCES

1 T. Nomura and M. Okuhara, Anal. Chim. Acta, 142 (1982) 281.
2 T. Nomura and M. Maruyama, Anal. Chim. Acta, 147 (1983) 365.
3 S. Nakajima, Transistor Gijutsu, 19 (1982) 348.
4 See, e.g., A. J. Bard, Anal. Chem., 36 (1964) 70R.
5 Y. Shiobara, Bunseki Kagaku, 10 (1961) 1290.
6 T. Nomura and M. Iijima, Anal. Chim. Acta, 131 (1981) 97.

Analytica Chimica Acta, 155 (1983) 235—242
Elsevier Science Publishers B.V., Amsterdam — Printed in The Netherlands

Short Communication

SOME ALKYLPHOSPHORIC ACID ESTERS FOR USE IN COATED-WIRE CALCIUM-SELECTIVE ELECTRODES
Part 3. Structural Characteristics of Calcium Di(octylphenyl)phosphate

R. W. CATTRALL* and M. J. NEWLANDS[a]

Department of Inorganic and Analytical Chemistry, La Trobe University, Bundoora 3083, Victoria (Australia)

M. F. MACKAY

Department of Physical Chemistry, La Trobe University, Bundoora 3083, Victoria (Australia)

(Received 17th May 1983)

Summary. The materials previously believed to be calcium salts of 4-(n-octyl)phenyl- and bis-4-(n-octyl)-phenylphosphoric acids are shown to be the calcium salts of 4-(1',1',3',3'-tetramethylbutyl)-phenyl- and bis-[4-(1',1',3',3'-tetramethylbutyl)phenyl]phosphoric acids. The latter compound is shown not to contain chelating phosphate groups in the solid state.

In earlier parts of this series [1, 2], calcium octylphenylphosphates were used in the preparation of calcium-selective electrodes. These salts were prepared from an industrial material which was believed to be a mixture of mono- and di-n-octylphenylphosphoric acids. However, the physical characteristics of the individual acids reported by different authors [1, 3—6] were remarkably varied and details of preparative methods were inadequate until 1978 [7]. Because doubt remained about the nature of the octyl groups in the commercial octylphenylphosphoric acids, the present study was done to remove the confusion.

Experimental

Chemicals. The calcium salts of the mixed octylphenylphosphoric acids were prepared from a 70/30 mixture of the acids (octylphenyl acid phosphate; Mobil Chemical Co., Richmond, VA) as reported earlier [1], with the exception that it was found to be convenient to separate the mixed calcium salts from excess of calcium hydroxide by Soxhlet extraction with ethanol. An authentic sample of calcium bis-[4-(1',1',3',3'-tetramethylbutyl)-phenyl]phosphate was kindly supplied by Dr. J. D. R. Thomas, University of Wales Institute of Technology, Cardiff.

[a]On sabbatical leave from the Department of Chemistry, Memorial University of Newfoundland, St. John's, Newfoundland, A1C 3X7, Canada.

0003-2670/83/$03.00

Preparation of octylphenol. A sample of the mixed acids (47 g, 100 mmol) was dissolved in ethanol (150 cm^3) and potassium hydroxide (15 g, 330 mmol) in ethanol (50 cm^3) was added. The mixture was refluxed for 2.5 h, more potassium hydroxide was added (10 g, 220 mmol), and the mixture was further refluxed for 3 h. On cooling, potassium octylphenoxide separated (29.98 g, 122 mmol; 72% yield). The material was recrystallized from ethanol. Because the potassium salt was insufficiently soluble in deuterochloroform for ^{13}C-n.m.r. studies, a sample (5.0 g, 20 mmol) was converted to the phenol by dissolution in water, acidification of the solution with hydrochloric acid, and filtering off the white phenol. The phenol is soluble in ethanol but difficult to crystallise.

Carbon-13 n.m.r. spectroscopy. The ^{13}C-n.m.r. spectra were recorded on a JEOL FX-200 multinuclear spectrometer operating at 50.1 MHz. All solutions were prepared in deuterochloroform and spectra were referenced either to the solvent or to added tetramethylsilane. Both ^{1}H-coupled and ^{1}H-decoupled spectra were recorded.

X-ray crystallography. The crystal structure of calcium bis[4-(1′,1′,3′,3′-tetramethylbutyl)phenyl] phosphate trihydrate, $[Ca^{2+}] \cdot 2[(C_{14}H_{21}O_2)_2P^-] \cdot 3H_2O$, was determined. The compound formed orthorhombic crystals belonging to the space group $C222_1$, with a = 21.268(6), b = 27.735(10), c = 21.643(6) Å and V = 12766.5 Å^3; M = 1041.3, D_m = 1.10 (flotation), D_c = 1.08 g cm^{-3}, Z = 8, $F(000)$ = 4512, μ(Cu $K\alpha$) = 16.4 cm^{-1}.

Intensity data were measured with Cu $K\alpha$ radiation (graphite crystal monochromator, $\bar{\lambda}$ = 1.5418 Å) at 289 K on a Rigaku-AFC diffractometer. The intensities were recorded by an $\omega - 2\theta$ scan from a crystal ca. 0.23 × 0.25 × 0.26 mm. Of the 5901 non-equivalent terms measured to a 2θ maximum of 130°, the 3170 for which $|F_o| > 5\sigma|F_o|$ were used for the structure refinement. The intensities were corrected for Lorentz and polarization factors but not for absorption.

The sites of the two calcium ions in the asymmetric unit with site symmetry 2 were derived from the vector map, and the P, O and C atom sites were located on subsequent Fourier maps. With indications of disorder in the structure, constraints were imposed in the final refinements: the benzene ring C atoms were constrained to form regular hexagons of side 1.395 Å; in the tetramethylbutyl groups, the bond lengths were constrained to 1.53 ± 0.05 Å and the bond angles to approximately tetrahedral values. With anisotropic temperature factors given to the calcium ions and phosphate atoms, and isotropic factors given to the remainder, a reliability index, R = 0.149 was attained. The least-squares refinements were made with SHELX-76 [8] and the function minimised was $\Sigma(|F_o| - |F_c|)^2$. Final atomic coordinates are given in Table 1 while an ORTEP drawing [9] of the anion with the atom numbering is shown in Fig. 1(a). Bond lengths and angles involving the phosphate group are given in Table 2, and the coordination of the calcium ions is illustrated in Fig. 1(b). Complete data on the observed and calculated structure amplitudes are available on request.

TABLE 1

Final atomic coordinates[a] ($\times 10^4$) and isotropic temperature factors[b]. Estimated standard deviations are given in parentheses

	x	y	z	B (Å^2)
Ca(1)	23(4)	0	0	4.3(3)
Ca(2)	0	35(3)	2500	4.3(3)
P(1A)	343(3)	868(2)	1252(3)	4.9(3)
P(1B)	1117(3)	182(2)	6246(3)	4.7(3)
O(1A)	450(10)	555(7)	1805(7)	5.8(8)
O(2A)	266(9)	650(5)	646(8)	4.3(6)
O(3A)	927(8)	1217(5)	1169(6)	4.3(6)
O(4A)	−224(9)	1222(6)	1388(6)	4.7(7)
O(1B)	734(9)	237(7)	5692(8)	6.1(9)
O(2B)	827(8)	82(7)	6851(7)	5.5(8)
O(3B)	1527(8)	656(6)	6357(7)	5.0(9)
O(4B)	1620(7)	−217(6)	6086(9)	5.0(9)
OW(1)	480(11)	608(8)	8099(11)	9.4(6)
OW(2)	842(11)	391(8)	9393(11)	9.7(6)
OW(3)[c]	1315(26)	1277(21)	9836(27)	11.8(17)
OW(4)[c]	1669(27)	801(19)	7742(26)	11.3(16)
C(1A)	1187	1529	1592	5.6(7)
C(2A)	1666	1830	1380	5.9(7)
C(3A)	1942	2164	1779	6.5(8)
C(4A)	1739	2197	2390	6.8(7)
C(5A)	1260	1896	2603	6.3(7)
C(6A)	984	1563	2204	4.5(5)
C(7A)	2044	2582	2815	7.3(7)
C(8A)	1951	2409	3476	11.4(10)
C(9A)	2775	2593	2701	13.7(11)
C(10A)	1904	3114	2747	16.0(13)
C(11A)	1260	3325	2726	17.3(13)
C(12A)	964	3412	3364	19.8(14)
C(13A)	1344	3847	2467	17.3(13)
C(14A)	833	3070	2276	14.5(12)
C(15A)	−428	1559	969	5.1(5)
C(16A)	−153	2013	913	5.6(6)
C(17A)	−379	2339	476	5.6(6)
C(18A)	−880	2210	93	5.9(6)
C(19A)	−1154	1756	149	9.1(7)
C(20A)	−928	1430	587	6.1(7)
C(21A)	−1077	2549	−448	8.6(8)
C(22A)	−660	3000	−493	15.8(13)
C(23A)	−1755	2701	−314	13.5(12)
C(24A)	−1087	2314	−1087	15.2(12)
C(25A)	−441	2177	−1346	15.2(11)
C(26A)	−22	2602	−1533	14.8(11)
C(27A)	−59	1840	−927	17.3(12)
C(28A)	−614	1905	−1950	19.3(14)
C(1B)	1935	877	5947	4.9(5)
C(2B)	2309	1236	6208	5.7(6)

TABLE 1 (continued)

	x	y	z	B (Å²)
C(3B)	2779	1456	5857	6.0(6)
C(4B)	2875	1316	5245	7.8(8)
C(5B)	2501	957	4984	6.0(6)
C(6B)	2031	737	5335	3.8(4)
C(7B)	3401	1550	4865	9.2(8)
C(8B)	3294	1484	4171	16.5(13)
C(9B)	3424	2095	5024	13.0(10)
C(10B)	4053	1412	5059	17.7(13)
C(11B)	4302	930	5232	13.6(11)
C(12B)	4655	725	4670	15.7(13)
C(13B)	4820	1042	5721	17.6(14)
C(14B)	3883	551	5528	11.2(10)
C(15B)	2066	−341	6522	4.9(6)
C(16B)	2663	−134	6505	8.0(8)
C(17B)	3136	−307	6893	9.2(8)
C(18B)	3011	−686	7298	8.1(8)
C(19B)	2413	−893	7315	7.0(7)
C(20B)	1941	−720	6927	5.9(6)
C(21B)	3492	−811	7829	12.7(11)
C(22B)	4098	−501	7900	13.6(11)
C(23B)	3683	−1318	7618	16.3(13)
C(24B)	3209	−873	8475	17.4(12)
C(25B)	2976	−427	8823	18.1(12)
C(26B)	3509	−75	8973	18.0(13)
C(27B)	2417	−158	8518	22.8(15)
C(28B)	2657	−636	9428	21.1(14)

[a]Coordinates of the C atoms were constrained in refinement. [b]For Ca and P, refer to the equivalent isotropic temperature factors. [c]Included with a site occupancy factor of 0.5.

Results and discussion

Details of the ^{13}C-n.m.r. spectra obtained from an authentic sample of calcium bis-[4-(1′,1′,3′,3′-tetramethylbutyl)phenyl] phosphate (I), calcium salts of the Mobil mixed acids (II), and 4-octylphenol derived from the Mobil product (III), are compared in Table 3 with spectra calculated for the 4-(1′,1′,3′,3′-tetramethylbutyl)phenyl group [10, 11]. Spectral parameters were also calculated for six other isomeric 4-octylphenylphosphates but none of the calculated spectra resembled the observed spectra.

The results show clearly that the phenol derived from the Mobil mixed acids is 4-(1′,1′,3′,3′-tetramethylbutyl)phenol and this specifies the octyl side-chain unambiguously. The spectrum of I agrees well with that calculated except that there appear to be two resonances corresponding to the two methyl groups attached to the side-chain carbon in the α-position to the ring. A space-filling model suggests that there may be restricted rotation at this position, but it is difficult to see why this should appear in the calcium salts and not in the corresponding phenol. Spectrum II consists of super-

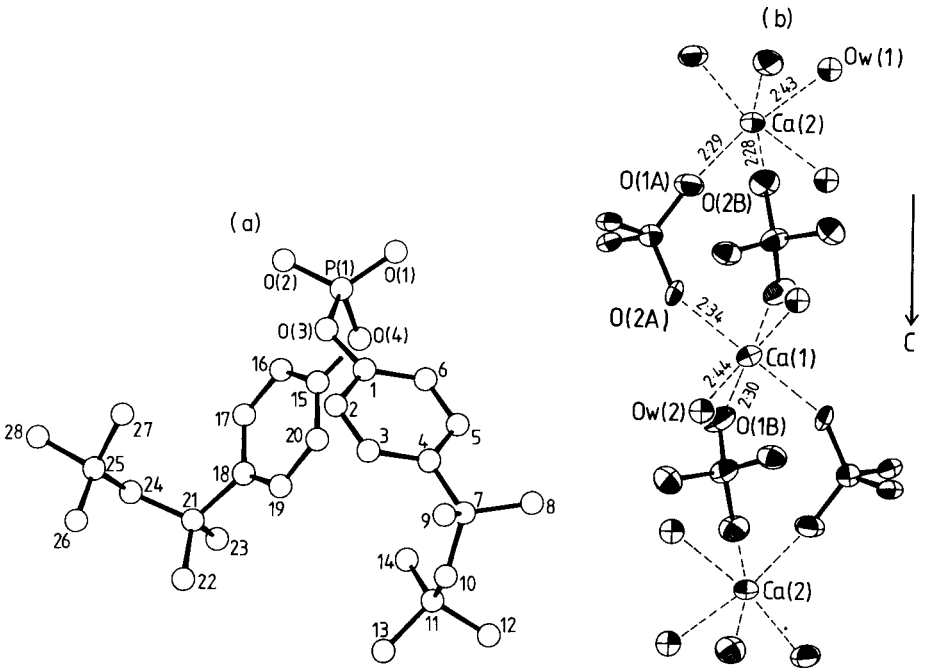

Fig. 1. (a) Calcium bis-[4-(1',1',3',3'-tetramethylbutyl)phenyl] phosphate (anion B); the carbon atoms are denoted by numbers only. (b) Calcium ion coordination.

imposed resonances of calcium bis-[4-(1',1',3',3'-tetramethylbutyl)phenyl]-phosphate and calcium 4-(1',1',3',3'-tetramethylbutyl)phenylphosphate. Hence subtraction of spectrum I from spectrum II yields the spectrum of the latter salt with resonances at 58.23, 37.53, 32.42, 31.74 and 31.33(?) ppm for the 2', 1', 3', 1'', and 3'' carbons, respectively.

It appears likely that the Mobil product is made by electrophilic addition of the most readily available octene, 2,4,4-trimethyl-1-pentene ("di-isobutylene"), to phenol [12], followed by reaction of the octylphenol with phosphorus oxychloride. Calcium bis-[4-(1',1',3',3'-tetramethylbutyl)phenyl]-phosphate is the compound which Craggs et al. [7] found to be as good a sensor for calcium as other recognized reagents, thus, there is a ready commercial source of the acid to prepare this useful sensor.

The crystallographic results are in good agreement with those from the ^{13}C-n.m.r. study. However, one unexpected but unambiguous result is of considerable interest for the understanding of calcium-selective electrodes. In the crystal structure, calcium ions make only one short contact with the phosphate oxygens of a particular anion, i.e., there is no chelation (see Fig. 1b). Each calcium ion makes a short contact with four neighbouring phosphate groups (two to both anions A and B) and with two water molecules. The six oxygens around each calcium ion form an octahedral arrangement with

TABLE 2

Bond lengths (Å) and angles (°) associated with the phosphate groups. Estimated standard deviations for the lengths are 0.02 Å and for the angles are 1°

	Anion A[a]	Anion B[a]
P(1)—O(1)	1.50	1.46
P(1)—O(2)	1.45	1.47
P(1)—O(3)	1.59	1.60
P(1)—O(4)	1.58	1.58
O(3)—C(1)	1.38	1.38
O(4)—C(15)	1.37	1.38
O(1)—P(1)—O(2)	120	121
O(1)—P(1)—O(3)	109	110
O(1)—P(1)—O(4)	109	106
O(2)—P(1)—O(3)	104	104
O(2)—P(1)—O(4)	110	110
O(3)—P(1)—O(4)	104	104
P(1)—O(3)—C(1)	129	128
P(1)—O(4)—C(15)	123	119

[a]These refer to the two independent organophosphate anions in the asymmetric unit.

TABLE 3

Observed and calculated ^{13}C-n.m.r. spectra

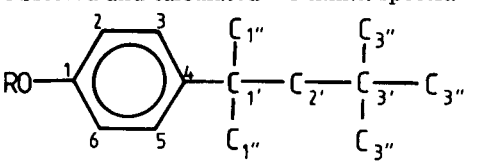

Carbon No.	^{13}C resonances and multiplicities[a]			
	Calculated	I[b]	II[b]	III[b]
1	149.0	149.0 d J^3_{C-O-P} 7.3 Hz	150.3 d J^3_{C-O-P} 7.3 Hz	148.4 s
4	146.5	145.1 s	145.1 s	146.8 s
3,5	129.0	126.6 d	126.7 d	127.2 d
2,6	122.6	120.1 d	119.9 d	119.5 d
2′	58.20	56.77 t	58.23 t 56.92 t	56.97 t
1′	44.61	38.02 s	38.07 s 37.53 s	38.24 s
3′	32.56	32.28 s 31.89 q	32.42 s 32.30 s	32.30 s
1″	30.76	31.65 q	31.87 q 31.74 q	31.79 q
3″	30.27	31.40 q	31.65 q 31.33 q	31.52 q

[a]Multiplicities, s singlet, d doublet, t triplet, q quartet in ^{1}H-coupled spectra. [b]I, calcium bis-[4-(1′,1′,3′,3′,-tetramethylbutyl)phenyl]phosphate; II, calcium salts of mixed acids; III, 4-octylphenol.

the waters in *cis* positions. The $Ca^{2+}\cdots O^{-}$ distances range from 2.28(2) to 2.34(2) Å for the phosphates and are slightly longer at 2.43(2) and 2.44(2) Å for the waters. These values compare favourably with literature data: 2.355—2.454 Å in calcium hydrogen naphthylphosphate [13], 2.299—2.964 Å in chloroapatite [14], 2.345—2.831 Å in calcium dihydrogenphosphate [15], 2.136—2.277 Å in $Ca_4(PO_4)_2O$ [16], 2.362—2.668 Å in calcium pyrophosphate dihydrate [17], 2.274—2.606 Å in ammonium calcium hydrogenpyrophosphate [18], 2.222—3.013 Å in α-calcium phosphate [19], 2.313—2.352 Å in calcium disodium pyrophosphate tetrahydrate [20], and 2.316 Å in the hydrated calcium salt of inosine 5'-phosphate [21].

It is particularly interesting that the calcium ions are not chelated by the phosphate groups in either of the organic phosphates, although the cation is equidistant from two oxygen atoms of a single phosphate tetrahedron in several of the simpler phosphate minerals. This may, in fact, facilitate ion-exchange reactions involving the organic phosphate salt.

It is well known [22] that electrodes for calcium based on the dialkylphosphates do not function if weakly or non-coordinating mediators are used. These electrodes require the presence of a second reagent with co-ordinating properties. In the case of the PVC membranes, of course, the solvent mediator must also act as a plasticizer to produce membranes with the desired characteristics. It has always been assumed that the mediator solvates the metal ions [23]. It seems likely that the solvent mediators function by displacing the two water molecules from the coordination sphere of the calcium ion making the organic phosphate salt more compatible with the membrane phase. Neutral ion-carriers also require subsidiary reagents but these are weakly coordinating (e.g., 1-nitro-2-octoxybenzene for Simon's open-chain dietherdiamides [24—26] and also for Petranek and Ryba's cyclic polyetherdiamides [27, 28]) and appear to act only to produce PVC membranes of the right characteristics.

The authors thank Mobil Chemical Co. for a gift of starting materials, Dr. J. D. R. Thomas for the authentic sample, and Drs. R. T. C. Brownlee and M. J. O'Connor for recording the ^{13}C-n.m.r. spectra.

REFERENCES

1 R. W. Cattrall, D. M. Drew and I. C. Hamilton, Anal. Chim. Acta, 76 (1975) 269.
2 R. W. Cattrall and D. M. Drew, Anal. Chim. Acta, 77 (1975) 7.
3 J. Růžička, E. H. Hansen and J. Chr. Tjell, Anal. Chim. Acta, 67 (1973) 155.
4 H. M. Brown, J. P. Pembleton and J. D. Owen, Anal. Chim. Acta, 85 (1976) 261.
5 D. Jagner and J. P. Ostergaard-Jensen, Anal. Chim. Acta, 80 (1975) 9.
6 G. H. Griffiths, G. J. Moody and J. D. R. Thomas, J. Inorg. Nucl. Chem., 34 (1972) 3043.
7 A. Craggs, P. G. Delduca, L. Keil, B. J. Key, G. J. Moody and J. D. R. Thomas, J. Inorg. Nucl. Chem., 40 (1978) 1483.

8 G. M. Sheldrick, SHELX 76. Program for crystal structure determination. Univ. Chemistry Laboratory, Cambridge University, England.
9 C. K. Johnson, ORTEP. Report ORNL-3794, Oak Ridge National Laboratory, Oak Ridge, TN.
10 L. P. Lindeman and J. Q. Adams, Anal. Chem., 43 (1971) 1245.
11 G. C. Levy, R. L. Lichter and G. L. Nelson, Carbon-13 Nuclear Magnetic Resonance Spectroscopy, 2nd edn., Wiley-Interscience, New York, 1980, pp. 50, 109.
12 B. Loev and J. T. Massengale, J. Org. Chem., 22 (1957) 988.
13 C.-T. Li and C. N. Caughlan, Acta Crystallogr., 19 (1965) 637.
14 P. E. Mackey, J. C. Elliott and R. A. Young, Acta Crystallogr., Sect. B, 28 (1972) 1840.
15 B. Dickens, E. Prince, L. W. Schroeder and W. E. Brown, Acta Crystallogr., Sect. B, 29 (1973) 2057.
16 B. Dickens, W. E. Brown, G. J. Kruger and J. M. Stewart, Acta Crystallogr., Sect. B, 29 (1973) 2046.
17 N. S. Mandel, Acta Crystallogr., Sect. B, 31 (1975) 1730.
18 M. Mathew and L. W. Schroeder, Acta Crystallogr., Sect. B, 33 (1977) 3025.
19 M. Mathew, L. W. Schroeder, B. Dickens and W. E. Brown, Acta Crystallogr., Sect. B, 33 (1977) 1325.
20 P-T Cheng, K. P. H. Pritzker and S. C. Nyburg, Acta Crystallogr., Sect. B, 36 (1980) 921.
21 E. A. Brown and C. E. Bugg, Acta Crystallogr., Sect. B, 36 (1980) 2597.
22 G. J. Moody and J. D. R. Thomas, Ion-Selective Electrode Rev., 1 (1973) 3.
23 A. Craggs, L. Keil, G. J. Moody and J. D.R. Thomas, Talanta, 22 (1975) 907.
24 D. Ammann, M. Guggi, E. Pretsch and W. Simon, Anal. Lett., 8 (1975) 709.
25 D. Ammann, R. Bissig, M. Guggi, E. Pretsch, W. Simon, I. J. Borowitz and L. Weiss, Helv. Chim. Acta, 58 (1975) 1535.
26 F. Lanter, A. Steiner, D. Ammann and W. Simon, Anal. Chim. Acta, 135 (1982) 51.
27 J. Petranek and O. Ryba, Collect. Czech. Chem. Commun., 45 (1980) 1567.
28 J. Petranek and O. Ryba, Anal. Chim. Acta, 128 (1981) 129.

Analytica Chimica Acta, 155 (1983) 243—245
Elsevier Science Publishers B.V., Amsterdam — Printed in The Netherlands

Short Communication

A RAPID METHOD FOR DETERMINATION OF 4-CARBOXYBENZALDEHYDE IN BENZENE-1,4-DICARBOXYLIC ACID BY SQUARE WAVE VOLTAMMETRY

MICHAEL SASKA

School of Chemical Engineering, Georgia Institute of Technology, Atlanta, GA 30332 (U.S.A.)

PETER E. STURROCK*

School of Chemistry, Georgia Institute of Technology, Atlanta, GA 30332 (U.S.A.)

(Received 7th July 1983)

Summary. The 4-carboxybenzaldehyde anion is readily reduced while the carboxyl group is difficult to reduce and causes no interference. Thus, square wave voltammetry at a static mercury drop electrode is suitable for determination of traces of 4-carboxybenzaldehyde in the presence of large amounts of benzene-1,4-dicarboxylic acid (terephthalic acid).

In the manufacture of terephthalic acid by oxidation of *p*-xylene, 4-carboxybenzaldehyde occurs as an impurity. Because 4-carboxybenzaldehyde acts as a chain terminator in subsequent polymerization reactions of terephthalic acid, its determination at trace levels in presence of large amounts of terephthalic acid is important. Both direct [1—3] and indirect [4] determinations have been proposed. The direct determinations make use of the increased solubility of terephthalic acid in sodium hydroxide solution [1, 2] or dimethylformamide [3]. Recently, a preliminary condensation of 4-carboxybenzaldehyde with 1,6-hexamethylenediamine was proposed to increase sensitivity over the direct determination [4]. The 4-carboxybenzaldehyde anion is reducible in alkaline solution in two steps below −1.6 V vs. Ag/AgCl [1, 5] while the carboxyl group is not reduced in this potential range. This communication describes a method for the direct determination of 4-carboxybenzaldehyde in terephthalic acid by square wave voltammetry in dimethylsulfoxide (DMSO).

Experimental

Instrumentation. Experiments were done with an IBM EC225-2a voltammetric system, a PAR 303 static mercury drop electrode stand, and an HP-7005B X-Y recorder. The instrument was operated in the differential-pulse (d.p.) mode with timer set to 0.1 s to produce a square wave. Most runs were done with a pulse magnitude of 40 mV and a sweep rate of 5 mV s^{-1}. The cable from the voltammetric unit was plugged into the J2

0003-2670/83/$03.00

connector of the electrode so that mercury drops were dislodged and dispensed only by control through the front-panel switches of the PAR 303. Thus, one electrode drop was used for the entire voltage sweep. The potential was swept from −1.3 to −1.9 V vs. Ag/AgCl. The peak potential for 4-carboxybenzaldehyde is −1.56 V.

Procedure. A 100-mg sample of terephthalic acid was weighed into the electrochemical cell (15 ml) and dissolved in 8.5—10 ml of DMSO. Then 1.5 ml of pure water and 0.5 ml of aqueous 25% (w/w) tetramethylammonium hydroxide were added to the cell. The cell was mounted on the electrode stand and purged with nitrogen for a minimum of 4 min to remove oxygen.

The mercury drop was replaced immediately before each sweep. The initial potential control was switched to the "off" position before the old drop was dislodged and "on" again after the new drop had been dispensed. Thus, the electrode was at 0 V during the drop replacement and the tendency for DMSO to penetrate up the capillary was minimized. This precaution minimized breaks in the mercury thread inside the capillary. However, continued exposure to DMSO will lead to this problem and the capillary then must be removed, cleaned, and remounted.

It has been reported [3] that traces of cobalt ion catalyst interfered with the determination of 4-carboxybenzaldehyde. Under the experimental conditions of the voltammetric measurement, no reduction peak for cobalt was observed up to the 150-μg g^{-1} cobalt level. Thus, this method is not subject to interference from cobalt.

Results and discussion

Because no sample of terephthalic acid was found to be completely free of 4-carboxybenzaldehyde, it was necessary to run the determination by standard addition of 4-carboxybenzaldehyde to the sample. For example, six successive additions of 20 μl of a 4-carboxybenzaldehyde standard solution were added to a sample of terephthalic acid (Amoco 33) that was processed as described above. A least-squares fit of the peak heights vs. concentration gave a slope of 0.106 ± 0.003 nA μg^{-1} g, y intercept of 3.1 ± 0.5 nA, a standard error (S_{yx}) of 0.70 nA, and a correlation coefficient (r) of 0.998. The x intercept indicated 29.5 μg g^{-1} 4-carboxybenzaldehyde in the terephthalic acid. This is equivalent to an initial concentration of approximately 2 μM 4-carboxybenzaldehyde in the cell. The manufacturer's literature indicates a level of 25 μg g^{-1}, while an independent determination in another laboratory indicated 60 μg g^{-1}.

In a separate experiment, comparable least-squares statistics (r = 0.999 and S_{yx} = 4.54) were obtained for 11 points extending up to 6000 μg g^{-1} 4-carboxybenzaldehyde added. The primary source of error is thought to be from successive additions of standards.

REFERENCES

1 M. Nishiyama, M. Maruyama and H. Hamaguchi, Bull. Chem. Soc. Jpn., 37 (1964) 616.
2 M. Nishiyama, M. Maruyama and H. Hamaguchi, Jpn. Analyst, 12 (1963) 150.
3 V. Jehlicka and J. Lakomy, Chem. Prumysl., 15 (1965) 163.
4 Y. S. Ignatev, M. P. Strukova and V. V. Dolbanova, Zh. Anal. Khim., 2 (1974) 1434.
5 L. Holleck and H. Marsen, Z. Elektrochem., 5 (1953) 944.

Analytica Chimica Acta, 155 (1983) 247—252
Elsevier Science Publishers B.V., Amsterdam — Printed in The Netherlands

Short Communication

THE APPLICATION OF INDUCTIVELY-COUPLED PLASMA EMISSION SPECTROMETRY TO THE DETERMINATION OF IMPURITIES IN BORON AND BORON COMPOUNDS

P. HULMSTON

Analytical Chemistry Branch, Chemistry and Explosives Division, A.W.R.E., Aldermaston (Great Britain)

(Received 28th April 1983)

Summary. Good sensitivity is achieved for 25 elements in boron, after removal of the matrix with hydrofluoric acid. The ten most common elements are studied in detail, and an overall precision of 10—15% is achieved using photographic detection. Agreement with results obtained by epithermal neutron activation analysis and flame atomic absorption spectrometry is good.

In principle, several techniques can be applied to the multielement trace analysis of boron and boron compounds. These include atomic emission spectrometry, neutron activation analysis and spark-source mass spectrometry. Each of these is influenced to various extents by the interference effects of the matrix and impurity elements present, so that the choice of method depends on the analysis required. Spark-source mass spectrometry provides high sensitivity [1] and covers a wide range of elements but has poor accuracy unless well defined analogous standards are used. The preparation of synthetic standards having a sufficiently fine dispersion of impurities for good replicate sampling, and excitation with a micro-spark is extremely difficult. Thermal neutron activation methods are limited by boron self-absorption but this can be overcome by using epithermal neutrons [2]. Optical emission spectrometry is attractive for the analysis of boron but the choice of excitation source is important. A d.c. arc has been considered for powdered samples [3] but the validity of comparing mixed powdered standards with samples is open to doubt; it is common experience that the physical form and previous history of the sample can influence the results. Furthermore, boron produces a band spectrum in the d.c. arc that extends over much of the spectrum thereby decreasing the sensitivity of the method.

The high stability and low spectral background of argon plasmas means that the use of the inductively-coupled plasma (i.c.p.) improves both sensitivity and precision compared to that obtained by arc or spark sources, and

its capability in multielement analyses is well established [4, 5]. This source was therefore examined for the analysis of boron and some of its compounds. Preliminary investigations confirmed the findings of Inlow [6] that, despite the high level of excitation in the i.c.p., which might be expected to favour atomic rather than molecular spectra, 7% (w/v) boron solutions generated strong band spectra with a consequent deterioration in the limits of detection for the trace elements. To avoid this interference, the boron was removed as the fluoride before the determination; this improved the limits of detection by one to two orders of magnitude.

Experimental

Dissolution of boron. Samples (2 g) were weighed into clean 150-ml flasks. To each, 15 ml of distilled nitric acid (Aristar) was added dropwise. When the vigorous reaction had subsided, the flasks were heated under reflux for 3 h so that all the boron was converted to boric acid. The flask contents were transferred by washing into platinum crucibles and sufficient 40% (w/v) hydrofluoric acid was added completely to react with the boric acid. After evaporation to dryness, any residue was dissolved in 2 ml of 3% perchloric acid and 2.5 ml of a cobaltous nitrate solution (1000 μg Co ml^{-1}) was added as internal standard. The solutions were diluted to 25 ml. Reagent blanks were similarly prepared, omitting the boron.

Preparation of standards. Multielement solutions containing 0.1—50 μg ml^{-1} concentrations of standards were prepared from appropriate spectrographic standards. Each solution also contained 100 μg Co ml^{-1}.

Apparatus and technique. The i.c.p. source consisted of a 27.12-MHz r.f. generator (model 120—27; International Plasma Corp.), having a maximum power output of 2.4 kW, connected coaxially to a capacitive matching unit. This incorporated a two-turn work coil within which the demountable plasma torch was located. Solutions were aspirated into the plasma using a pneumatic cross-flow nebuliser (model TN-1; PlasmaTherm). Spectra were recorded photographically on a 3.4-m Ebert spectrograph having a wavelength dispersion of 0.5 nm mm^{-1}, and measured automatically using a Joyce-Loebl double-beam microdensitometer interfaced to a PDP 11/10 computer [7]. The operating conditions for the plasma source and spectrograph are given in Table 1.

Results

Detection limits. The emission lines selected for the determination of 25 elements and the corresponding limits of detection in solution are given in Table 2. These were calculated from the expression 3 (r.s.d.)$I_b C/I_a$, where I_b and I_a are the mean background and analyte intensities relative to cobalt as internal standard, and r.s.d. is the relative standard deviation for 5 measurements of the analyte at concentration C (μg ml^{-1}). The detection limits in boron, the upper concentration limit that can be determined without dilution, and the average reagent blank are also given. Because the boron matrix

TABLE 1

Instrumental conditions for photographic determination of trace impurities

Plasma		Spectrograph	
Forward power	1.5 kW	Grating	15,000 lines $inch^{-1}$ blazed at 300 nm
Reflected power	1 W		
Coolant gas flow	15 l min^{-1}	Grating angle	5.85°
Auxiliary gas flow	NIL	Wavelength range	220—460 nm
Injector gas flow	1.1 l min^{-1} (15 psi)	Dispersion	0.5 nm mm^{-1}
Observation height	20—25 mm above work coil	Slit width	20 μm
		Slit height	2 mm
		Exposure time	120 s
Photographic plates (Eastman Kodak)			
220—340 nm	Spectrum Analysis No. 1		
340—460 nm	Spectrum Analysis No. 3		

TABLE 2

Performance of the method

Metal	λ[a] (nm)	Limit of detection[b] (μg ml^{-1})	Upper limit for calibration (μg g^{-1})[c]	Reagent blank (μg g^{-1})
Al	308.2	0.5	1000	10
Ca	315.8	0.1	500	20
Cu	327.9	0.1	500	5
Ni	305.1	0.1	1000	<5
Mo	313.3	0.5	1000	<5
Mg	383.2	0.5	500	5
Fe	259.9	0.1	500	15
Cr	283.6	0.1	500	<1
La	333.7	0.1	500	<1
Mn	294.9	0.1	500	<1
Ti	323.6	0.05	100	<0.5
V	309.3	0.05	100	<0.5
Zn	328.3	0.1	500	<1
Ga	294.4	0.5	200	<5
Sr	421.5	0.03	100	<0.3
Y	332.8	0.1	200	<1
Zr	343.8	0.1	500	<0.5
Nb	313.1	0.1	200	<0.5
Ru	267.6	0.3	500	<3
In	303.9	1	1000	<10
Cd	228.8	10	2000	<100
Gd	335.0	0.05	200	0.5
Ba	455.4	0.05	200	3.5
Dy	353.2	0.1	100	<1
Pb	283.3	1	2000	<10

[a]The line used for the cobalt internal standard was 306.182 nm. [b]Limit of detection in sample in μg g^{-1} = 10 × limit of detection in solution given. [c]In sample.

is removed, the sensitivity of the method can be adjusted as required by varying the sample size, provided that reagent blanks remain within reasonable bounds.

Precision. The standard deviations for the method are shown in Table 3. Two exposures were made on a photographic plate for each aliquot of solution tested. The precision for the i.c.p. measurement itself is good, except for aluminium, calcium, magnesium and molybdenum. For the first two elements this may be due to variations in the levels of contaminants in the reagent blank, but for molybdenum and magnesium, this argument does not apply. Comparison of the precisions obtained for separate solid sample portions and solution aliquots shows significant deterioration for iron and manganese; this may be caused by variations in the amount of these elements that can be dissolved but more likely is due to their non-uniform distribution in the matrix material.

In general, for a range of samples, the precision with which impurities in solution at concentrations an order of magnitude greater than the limit of detection can be determined was 3—8% (r.s.d.). This is typical of a method involving photographic detection. The overall r.s.d. was generally 10—15%, except for calcium, aluminium and iron, especially at low concentrations.

Accuracy. The accuracy of the method was determined by using synthetic sample solutions prepared from pure boric acid to which impurities were added at 10 and 20 $\mu g\ g^{-1}$ levels. Boron was removed as described earlier. The mean concentration and accuracy figures together with 95% confidence limits for these values are shown in Table 4. With the possible exception of manganese, little or no loss of impurity occurs. A comparison of the results

TABLE 3

Precision of i.c.p. spectrographic determination and of replicate solid and solution samples

Metal	Mean conc. ($\mu g\ ml^{-1}$)	Standard deviation ($\mu g\ ml^{-1}$)		
		I.c.p. method[a]	Sample solution aliquots[b]	Solid samples[c]
Al	280	8	28	22
Ca	270	16	40	56
Cu	29	3.1	3.7	6.0
Ni	36	3.4	1.5	5.5
Mo	165	7.7	16	33
Mg	110	9.2	10.0	19
Cr	41	3.8	5.0	2.1
La	6.0	0.6	0.5	0.2
Fe	1100	13	10	97
Mn	680	8	6	41

[a]From duplicate exposures measured on 5 aliquots of same solution. [b]5 aliquots of solution, duplicate exposures. [c]5 portions of solid sample taken through the whole procedure.

TABLE 4

Analysis of simulated samples

Metal	Metal conc. (μg ml^{-1})		Recovery[a] (%)	Metal	Metal conc. (μg ml^{-1})		Recovery[a] (%)
	Added	Found[a]			Added	Found[a]	
Al	20.0	19.0 ± 4.0	95 ± 20	Mg	20.0	18.5 ± 1.2	93 ± 6
	10.0	8.2 ± 1.5	82 ± 15		10.0	8.3 ± 1.2	83 ± 12
Ca	20.0	17.0 ± 3.3	85 ± 16	Cr	20.0	17.5 ± 2.9	88 ± 15
	10.0	8.8 ± 1.2	88 ± 12		10.0	9.0 ± 1.1	90 ± 11
Cu	20.0	21.0 ± 3.6	105 ± 20	La	20.0	22.2 ± 6.0	105 ± 30
	10.0	11.1 ± 1.5	110 ± 15		10.0	13.0 ± 3.3	110 ± 15
Ni	20.0	20.1 ± 2.0	100 ± 10	Fe	20.0	19.1 ± 1.6	95 ± 8
	10.0	10.2 ± 0.8	100 ± 8		10.0	11.0 ± 1.3	110 ± 13
Mo	20.0	20.0 ± 1.5	100 ± 8	Mn	20.0	16.5 ± 1.6	83 ± 8
	10.0	9.5 ± 2.0	95 ± 20		10.0	8.8 ± 1.2	80 ± 6

[a]Mean concentration and mean recovery ± 95% confidence limits, derived from 4 complete replicate analyses.

TABLE 5

Comparative analyses of boron control sample

Metal	Metal found[a] (μg g^{-1})			Metal	Metal found[a] (μg g^{-1})		
	I.c.p.e.s.	A.a.s.	N.a.a.		I.c.p.e.s.	A.a.s.	N.a.a.
Al	280 ± 60	310 ± 30	—	Mg	110 ± 15	130 ± 20	—
Ca	270 ± 50	230 ± 30	—	Cr	41 ± 3	38 ± 3	47 ± 7
Cu	29 ± 3	28 ± 3	—	La	6.0 ± 1.8	—	5 ± 1
Ni	36 ± 5	32 ± 5	31 ± 3	Fe	1100 ± 140	860 ± 50	1045 ± 49
Mo	165 ± 30	180 ± 30	170 ± 17	Mn	680 ± 40	650 ± 100	660 ± 20

[a]Mean concentration and 95% confidence limits of the mean derived from 3 replicate analyses.

obtained on a solid boron sample by i.c.p.e.s., epithermal neutron activation analysis (n.a.a.) and flame atomic absorption spectroscopy (a.a.s.) is shown in Table 5. The n.a.a. was done on the solid material; a.a.s. and i.c.p.e.s. were done on solutions prepared as described above. Agreement is generally good between all three methods, apart from the low iron content determined by a.a.s. The good agreement observed for manganese by all three methods indicates that at high concentrations there is no significant loss of this element.

Discussion

The limits of detection of the method, when applied to trace multielement analysis of boron, range from 0.5 to 100 μg g^{-1} for a 1-g sample. For many elements, the limit of detection is governed by the reagent blank, and high-purity reagents are necessary. The precision of the method for a single

determination is 10—15%, much of which arises from errors in chemical preparation; to optimise precision it is better to replicate sample portions rather than replicate exposures on the same portion. The accuracy of the method, evaluated from the analysis of synthetic samples, is good.

Photographic recording of emission spectra and their interpretation by computer-aided microdensitometry provides the basis of a general technique for i.c.p.e.s. Photographic detection is particularly well suited for situations requiring wide elemental coverage in matrices where spectral interferences are difficult to predict.

Although the method was developed for the analysis of boron, it is equally applicable to boron compounds provided they can be dissolved satisfactorily. Highly intractable materials such as boron carbide require digestion with 60% perchloric acid at 300°C for 72 h in sealed silica Carius tubes. Only 0.2 g of material can be dissolved by this method, which, at the concentration required, produces only 2 ml of solution. For the exposure times required, this amount is insufficient for use with commercial nebulisers, but this deficiency can be overcome by using a recirculating nebuliser [8].

REFERENCES

1 H. E. Beske, R. Gijbels, A. Hurrle and K. P. Jocum, Fresenius Z. Anal. Chem., 309 (1981) 329.
2 P. A. Hart, A.W.R.E. private communication.
3 T. S. Long, Appl. Spectrosc., 25 (1971) 1.
4 P. W. J. M. Boumans and F. J. DeBoer, Spectrochim. Acta, 33 (1978) 535.
5 V. A. Fassel and M. A. Floyd, Anal. Chem., 52 (1980) 431.
6 R. O. Inlow, Anal. Lett., 10 (1979) 1075.
7 W. A. Bettison and J. K. Bundy, A.W.R.E. Rep. No. 041/78, Feb. 1978.
8 P. Hulmston, Analyst, 108 (1983) 166.

Analytica Chimica Acta, 155 (1983) 253—257
Elsevier Science Publishers B.V., Amsterdam — Printed in The Netherlands

Short Communication

ION-EXCHANGE REMOVAL OF SOME INTERFERENCES ON THE DETERMINATION OF CALCIUM BY FLOW INJECTION ANALYSIS AND ATOMIC ABSORPTION SPECTROMETRY

O. F. KAMSON[a] and ALAN TOWNSHEND*
Chemistry Department, University of Hull, Hull HU6 7RX (Great Britain)
(Received 22nd April 1983)

Summary. The effects of phosphate and sulphate on the calcium signals are eliminated by incorporation of an anion-exchange column into the flow injection system. Silicate interference can be prevented by adding hydrofluoric acid.

Flow injection analysis (f.i.a.), when used in conjunction with atomic absorption spectrometry (a.a.s.), provides precise results and rapid sample throughput [1]. It accommodates a higher content of dissolved solids in the sample solution, because of the dilution (dispersion) inherent in the flow system, and permits single standard calibration [2]. Moreover, it provides a flexible approach to the elimination of interference effects. For example, when calcium is determined, lanthanum is readily added to the sample as a releasing agent; if a merging zone technique [3] is used for the addition, this economizes on the use of the lanthanum solution. Standard addition is also readily achieved [4].

This communication describes the application of ion-exchange resins in an f.i.a. system for removal of interferences in the determination of calcium by a.a.s. Previously, ion-exchange has been used for determination of total cation or anion concentration by f.i.a. [1], and for separation and determination of zinc and cadmium by chemiluminescence and f.i.a. [5].

Experimental

Apparatus and reagents. The f.i.a. set-up is shown schematically in Fig. 1. A peristaltic pump comprising two 10-rpm motors (Schuco Scientific Ltd., London) operating in parallel was used to give a water carrier flow of 3.0 ml min^{-1}. Sample injection was achieved by a rotary teflon valve, provided with a by-pass coil, between two perspex blocks. The sample volume was 25 μl. Tygon tubing (0.75 mm i.d.) was used throughout, and was connected to the nebulizer intake of the spectrometer. The ion-exchange resins were held in a glass tube (2 cm long, 2.5 mm i.d.).

[a]On study leave from Chemistry Department, University of Lagos, Nigeria.

0003-2670/83/$03.00

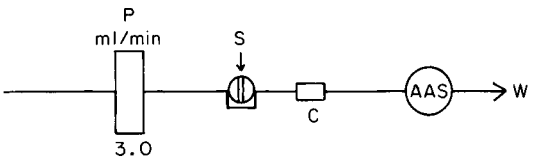

Fig. 1. Manifold for determination of calcium: (P) peristaltic pump; (S) injection valve (25-μl sample); (C) ion-exchange column; (AAS) atomic absorption spectrometer; (W) waste; line length from exit of injection valve to tip of nebulizer, 12 cm.

The detector was a Baird-Atomic A3400 atomic absorption spectrometer with a fixed nominal aspiration rate of 6.0 ml min^{-1}. The output was fed to a Tekman TE-200 chart recorder operating at 5 mV full scale deflection. The conditions for the measurement of calcium atomic absorption signals were adjusted for maximum instrumental stability rather than sensitivity, and were as follows: acetylene flow, 3.1 l min^{-1}; air flow, 7.5 l min^{-1}; hollow-cathode lamp operating current, 9 mA; slit width, 2; burner height, 3.

All reagents were analytical grade except where otherwise stated.

Results and discussion

Generally, it is desirable that the pumping rate should match the rate of uptake of solution by the nebulizer, otherwise there is a suction effect on the solution in the tubing, and air tends to be drawn through the nebulizer. In the present instance, however, greater instrumental stability and increased sensitivity were achieved at flow rates below those required by the nebulizer. For example, at 6.0 ml min^{-1}, the absorbance for an injected calcium solution was 0.15. This increased to 0.23 at 4.0 ml min^{-1} and 0.31 at 3.0 ml min^{-1}. This is believed to be at least partly due to the decreased drop size produced at the lower flow rates.

Anionic interferences. For the system used, without the resin column, a dispersion [6] of 2.1 was found, thus indicating that it was of low dispersion, as required for a simple transport system. Figure 2 shows the effect of anionic interferences on the calcium atomic absorption signal obtained by conventional aspiration and f.i.a. It confirms the dispersion of ca. 2, and that the interference effects are similar in both systems, the extent of signal depression increasing in the order of sulphate < phosphate < silicate.

Two anion-exchange resins were tested for their ability to remove interferences, Amberlite IRA-400 and De-Acidite FF (both chloride form). The injection of solutions containing calcium (10 mg l^{-1}) and 2.0×10^{-3} M interfering anions showed a complete removal of the depressive effects of phosphate and sulphate (added as the acids) as shown in Table 1, with negligible change in dispersion. Both resins were equally effective. The effect of sodium silicate, however, was unchanged. In addition, a study of the pH dependence of the removal of phosphate and sulphate interferences in the flow injection system showed that a pH between 1.8 and 3.3 gave complete recovery of the

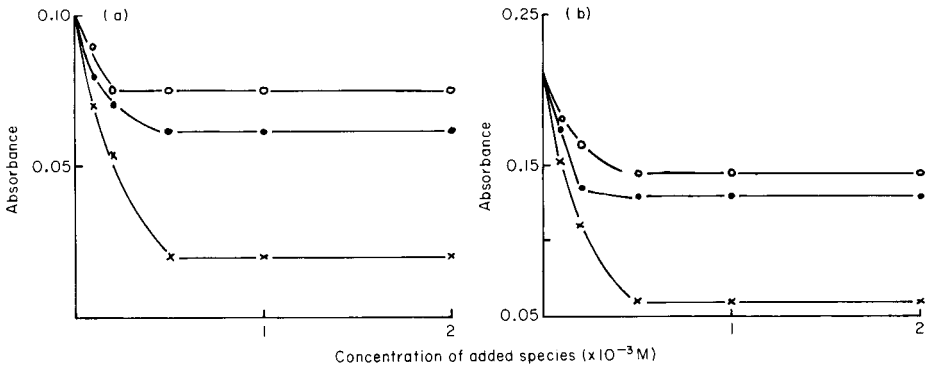

Fig. 2. Effect of anions on the absorbance of 10 mg l^{-1} calcium by: (a) f.i.a.; (b) conventional aspiration. Anion: (○) sulphate; (●) phosphate; (×) silicate.

calcium signal in the presence of either or both interfering anions. The regeneration of the column was readily accomplished in situ by the injection of 0.1 M hydrochloric acid.

In an attempt to eliminate silicate interference, silicate was converted to hexafluorosilicate by adding hydrofluoric acid to the sample to give a concentration of 0.10 M, and then subjected to anion-exchange separation. The results, included in Table 1, show that the presence of hydrofluoric acid enhances the response in the flow injection method, irrespective of the presence of the ion-exchanger, and the hydrofluoric acid also completely removes silicate interference on calcium in conventional a.a.s.

Because of the well-known leaching effect of hydrofluoric acid on borosilicate glass, investigations by f.i.a. were conducted to find the amount of acid required to restore the calcium signal completely in samples containing different amounts of silicate, in both borosilicate glass and polypropylene vessels. The results are shown in Fig. 3. In general, higher absorbances were

TABLE 1

Effect of an ion-exchange column on the absorbance of 10 mg l^{-1} calcium in the presence of 2.0×10^{-3} M interfering anion

Anion	Absorbance		
	Conventional a.a.s.	F.i.a./a.a.s.	F.i.a./a.a.s. with column[b]
None	0.21	0.10	0.10
Phosphate	0.13	0.05	0.10
Sulphate	0.15	0.07	0.10
Silicate	0.06	0.03	0.03
Silicate[a]	0.22	0.14	0.11

[a]In 0.1 M HF. [b]Both resins gave the same result.

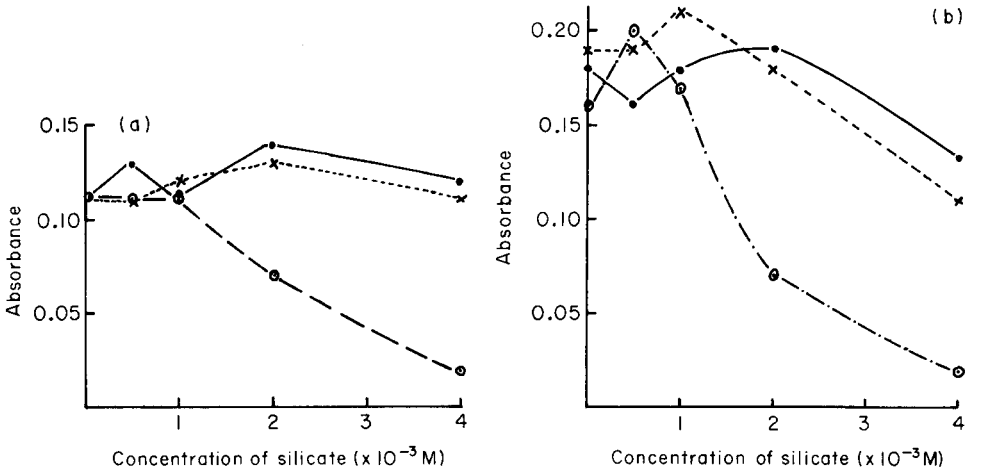

Fig. 3. Effect of silicate on the absorbance of 10 mg l^{-1} calcium in vessels of: (a) polypropylene; (b) borosilicate glass. Concentration of hydrofluoric acid present: (•) 0.10 M; (×) 0.05 M; (○) 0.02 M. Solutions were analysed immediately after preparation.

obtained in glass apparatus. The interference of $\leqslant 2 \times 10^{-3}$ M silicate (in glass vessels) or $\leqslant 4 \times 10^{-3}$ M silicate in plastic vessels, on the determination of 10 mg l^{-1} calcium was completely removed by 0.05—0.1 M hydrofluoric acid.

Because leaching from glass was a possible source of increased absorbance, the change in absorbance of calcium/hydrofluoric acid solutions on storage in glass and plastic vessels was studied. The results for borosilicate glass are summarized in Fig. 4. Absorbances increased rapidly with time for solutions $\geqslant$0.05 M in hydrofluoric acid. In contrast, such solutions stored in polypropylene vessels showed no change. Solutions in 0.02 M hydrofluoric acid gave a slightly decreased absorbance when stored in glass or plastic. Thus, calcium solutions 0.05 M in hydrofluoric acid stored in polypropylene flasks were used, although the absorbance was slightly enhanced (10%) by $\geqslant 2 \times 10^{-3}$ M silicate under these conditions. Incorporation of the anion-exchange column eliminated this enhancement.

Cationic interferences. The interferences of some cations on the calcium atomic absorption signal are well understood [7]. The effects of different concentrations (0—200 mg l^{-1}) of aluminium, iron(III), lanthanum, barium and sodium (added as their chlorides) on the absorbance of 10 mg l^{-1} calcium (as calcium chloride) in 0.1 M hydrochloric acid were measured in the flow injection system.

Some of these effects are shown in Fig. 5; barium gave a slight enhancement over this concentration range, and lanthanum was without effect. Attempts to remove the interference of aluminium by its conversion to hexafluoroaluminate and removal on the anion-exchange column were unsuccessful.

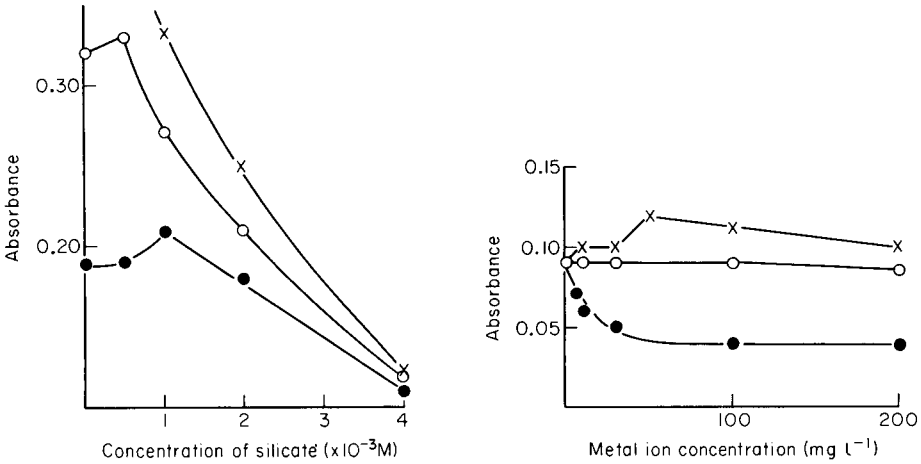

Fig. 4. Effect of storage time in borosilicate glass on the absorbance of 10 mg l^{-1} calcium in 0.05 M hydrofluoric acid in the presence of silicate: (•) immediately after preparation; (○) after 1 h; (×) after 1 day.

Fig. 5. Effect of cations on the absorbance of 10 mg l^{-1} calcium: (×) Na^{+}; (○) Fe^{3+}; (•) Al^{3+}.

REFERENCES

1 J. Růžička and E. H. Hansen, Flow Injection Analysis, Wiley, New York, 1981.
2 J. F. Tyson, J. M. H. Appleton and A. B. Idris, Anal. Chim. Acta, 145 (1983) 159.
3 E. A. G. Zagatto, F. J. Krug, H. Bergamin, S. S. Jørgensen and B. F. Reis, Anal. Chim. Acta, 104 (1979) 279.
4 E. A. G. Zagatto, A. O. Jacintho, F. J. Krug, B. F. Reis, R. E. Bruns and M. C. U. Aranjo, Anal. Chim. Acta, 145 (1983) 169.
5 J. L. Burguera, M. Burguera and A. Townshend, Anal. Chim. Acta, 127 (1981) 199.
6 J. Růžička and E. H. Hansen, Anal. Chim. Acta, 99 (1978) 37.
7 C. T. J. Alkemade, T. Hollander, W. Snelleman and P. J. T. Zeegers, Metal Vapours in Flames, Pergamon, Oxford, 1982.

Analytica Chimica Acta, 155 (1983) 259—262
Elsevier Science Publishers B.V., Amsterdam — Printed in The Netherlands

Short Communication

IMPROVED CHEMILUMINESCENCE DETERMINATION OF TRACES OF COBALT(II) BY CONTINUOUS FLOW AND FLOW INJECTION METHODS

MASAAKI YAMADA*, TAKAYUKI KOMATSU, SHINJIRO NAKAHARA[a] and SHIGETAKA SUZUKI

Department of Industrial Chemistry, Faculty of Technology, Tokyo Metropolitan University, Setagaya-ku, Tokyo 158 (Japan)

(Received 13th May 1983)

Summary. Flow injection analysis, with chemiluminescence detection based on a gallic acid/hydrogen peroxide/sodium hydroxide/methanol system, gives a sensitive and rapid determination of cobalt(II). The detection limit and sampling rate are improved to 0.6 ng l^{-1} (continuous sample flow) or 0.6 pg (10-μl sample injection) and 120 h^{-1}, respectively. The method is successfully applied to real samples.

The use of chemiluminescence produced in the gallic acid/hydrogen peroxide system for the determination of traces of cobalt(II) by continuous flow and flow injection methods was reported recently [1]. Cobalt could be determined more selectively than by any other chemiluminescent system, with a detection limit of 40 ng l^{-1} (continuous sample flow) or 40 pg (10-μl sample injection) and a logarithmic calibration linearity of 3 orders of magnitude. It was also indicated that there was room for further development of the flow injection analysis (f.i.a.)-chemiluminescence combination; better characteristics should be achieved by a faster reaction, by elevation of the reaction temperature. This communication demonstrates such improvements: increased sensitivity, more rapid sample throughput and wider pH range for sample solutions.

Experimental

A schematic diagram of the improved f.i.a.-chemiluminescence system is given in Fig. 1. It is basically as before [1], except that a second 1.6-m mixing coil (reaction coil) M_2 is placed in a heating bath controlled to ±0.5°C between J_2 and D, and that methanol is included in stream R_2 with the sodium hydroxide, the concentration of which is slightly increased for improved sensitivity. The other apparatus and reagents are as before [1].

Analysis of standard reference materials. Pepperbush or Pond Sediment (0.5 g) was boiled with 10—20 ml of concentrated nitric acid on a hot plate

[a]Present address: Mochida Pharmacy Co., Shinjuku-ku, Tokyo 160, Japan.

0003-2670/83/$03.00

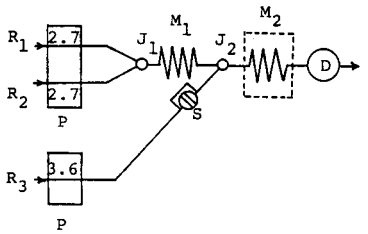

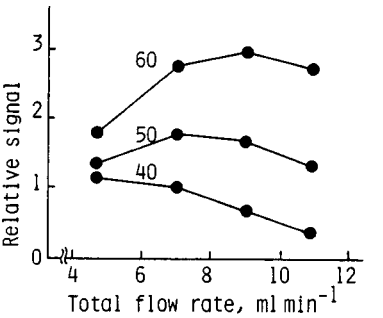

Fig. 1. Schematic diagram of the recommended system for cobalt. R_1 is 0.02 M gallic acid/0.3 M H_2O_2 solution; R_2 is 0.09 M NaOH in 3% methanol; R_3 is water. Flow rates are given as ml min^{-1}. Coil M_2 is held in a heating bath at 60°C.

Fig. 2. Effect of the bath temperature (°C, given on the curves) and total flow rate. The latter was varied so that $(R_1 + R_2)/R_3 = 1.5$ and $R_1 = R_2$; 60 pg Co(II) injected; R_3 is distilled water.

until the appearance of white fumes, and with concentrated sulphuric acid until the solution became colourless. After cooling, the solution was diluted to 100 ml. A 1-ml portion was added to each of several 100-ml volumetric flasks for standard addition of cobalt before dilution to volume, and cobalt was determined as described above.

Results and discussion

Bath temperature and total flow rate in the system. In the previous paper [1], acceleration of the slow chemiluminescent reaction by increasing the reaction temperature was proposed as a means of increasing sensitivity and sampling rate. Thus the bath temperature dependence of the signal for cobalt was explored at various total flow rates (Fig. 2); the signal profiles obtained are depicted in Fig. 3. A bath temperature of 60°C and a total flow rate of 9 ml min^{-1} (2.7 ml min^{-1} for R_1 and R_2, 3.6 ml min^{-1} for R_3) gave the highest peak. The peak became sharper with increasing bath temperature and total flow rate, and also increasing acidity of R_3 (see below). Comparison of peaks (a) and (c) in Fig. 3, shows the improved sensitivity, and indicates an improved sampling rate.

pH of R_3 and sample solution. As many sample solutions are acidic, it is desirable for the signal to be independent of the pH of the sample solution injected. Thus, the effect of the pH of the cobalt solution injected was investigated, together with that of the pH of R_3. The results are shown in Fig. 4. They indicate that the signal for cobalt is little affected by acidification of the cobalt solution with hydrochloric or nitric acid if the solution is injected into the nearly neutral stream R_3. The figure also shows that injection of a cobalt solution at pH 5.6 into R_3 at pH 2.8 gives the highest signal. This may be explained by decreased precipitation of cobalt hydroxide

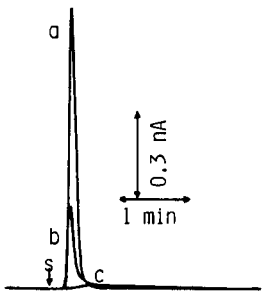

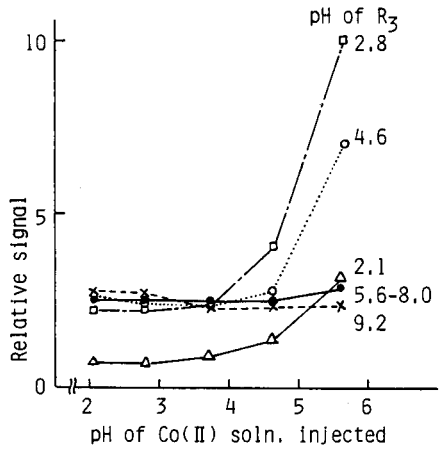

Fig. 3. Signal profiles: (a) bath temperature 60°C, total flow rate 9 ml min^{-1}, R_3 water at pH 2.8; (b) as for (a) except R_3 is distilled water; (c) conditions as in [1] (60 pg Co injected).

Fig. 4. Effect of pH of cobalt solution and R_3: 60 pg Co injected, bath temperature 60°C, total flow rate 9 ml min^{-1}.

formed between J_2 and D, the decrease being greater at elevated temperatures than at room temperature. Acidification of R_3 also prevents cobalt from adsorbing on the sample injector; this leads to decreased tailing of the peak, resulting in higher sample throughput.

Improved characteristics of the system. Under the improved experimental conditions (as specified in Fig. 1) the analytical characteristics of the system were re-investigated. The background and noise currents remained unchanged, in spite of the elevation of reaction temperature. Attempts were made to decrease the background signal, which probably arises from chemiluminescence of aldehydes in the methanol. Thus methanol was changed from R_1 to R_2, to avoid premature contact with hydrogen peroxide, which could oxidize methanol to formaldehyde. In addition, sulphite was also added to R_2 to form unreactive addition compounds with aldehydes. However, no change in background was achieved.

Logarithmic calibration graphs were linear over three decades for continuous sample flow (3.6 ml min^{-1}) and for 10-μl injections of cobalt, with slopes of unity. The detection limit (signal-to-noise ratio = 3) was lowered by a factor of 70 to 0.6 ng l^{-1} (1×10^{-11} M) for continuous sample flow and 0.6 pg for a 10-μl sample injection into stream R_3 at pH 2.8. This approaches the lowest detection limit for cobalt of 0.07 pg achieved by using luminol sonic chemiluminescence [2]. The sampling rate could be 120 h^{-1}, an increase of 6 times over the previous procedure. The relative standard deviation for ten successive 10-μl injections of a 1×10^{-7} M solution (ca. 60 pg) was also improved to 1.5%.

Only silver markedly interfered. It provided a signal 13% of that for cobalt(II) for 10-μl injections of 10^{-5} M solutions. Iron(III) and manganese(II) provided signals 0.1% that of cobalt at a similar concentration. Chromium(III), nickel(II), lead(II), copper(II) and permanganate did not cause emission. The effect of these species on the signal for cobalt when a 10^{-5} M solution of the species was injected into stream R_3, which was a 10^{-8} M cobalt solution, was that silver enhanced the cobalt signal 3.5 times, silver thus being detected three times more sensitively than in the absence of cobalt; cyanide, dichromate, carbonate or EDTA suppressed the signal by 10, 4, 2 and 98%, respectively. No interference was observed for ammonia, in contrast to the previous study.

Application to real samples. The applicability of the proposed method was evaluated by assaying NIES (National Institute for Environmental Studies) standard reference materials (Pepperbush [3] and Pond Sediment [4]) and tap water. Standard additions of cobalt to the acid-digested samples and tap water sample indicated that the results obtained for Pepperbush (22, 22, 21 $\mu g\ g^{-1}$) and Pond Sediment (24, 24, 24 $\mu g\ g^{-1}$) by injection of 10-μl samples were within the certified values (23 $\pm$ 3 and 27 $\pm$ 3 $\mu g\ g^{-1}$, respectively). The value for tap water (18, 19 $ng\ l^{-1}$) obtained by the continuous sample flow method was below the detection limits of other methods for cobalt.

REFERENCES

1 S. Nakahara, M. Yamada and S. Suzuki, Anal. Chim. Acta, 141 (1982) 255.
2 M. Yamada and S. Suzuki, Chem. Lett., (1983) 783.
3 K. Okamoto, Y. Yamamoto and K. Fuwa, Anal. Chem., 50 (1978) 1950.
4 Y. Iwata, K. Matsumoto, H. Haraguchi, K. Fuwa and K. Okamoto, Anal. Chem., 53 (1981) 1136.

Analytica Chimica Acta, 155 (1983) 263—268
Elsevier Science Publishers B.V., Amsterdam — Printed in The Netherlands

Short Communication

SPECTROPHOTOMETRIC DETERMINATION OF NITRITE IN NATURAL WATERS BY FLOW INJECTION ANALYSIS

SUSUMU NAKASHIMA* and MASAKAZU YAGI

Institute for Agricultural and Biological Sciences, Okayama University, Kurashiki-shi, Okayama 710 (Japan)

MICHIO ZENKI and AKINORI TAKAHASHI

Department of Chemistry, Okayama University of Science, Ridai-cho, Okayama-shi 700 (Japan)

KYOJI TÔEI

Department of Chemistry, Faculty of Science, Okayama University, Tsushima-naka, Okayama-shi 700 (Japan)

(Received 12th July 1983)

Summary. The method described is suitable for the determination of low $\mu g\ l^{-1}$ levels of nitrite in waters. Nitrite diazotizes *p*-aminoacetophenone and the product is coupled with *m*-phenylenediamine at 30°C. The limit of detection is 0.2 $\mu g\ l^{-1}$ for sample injections of 650 μl. The sampling rate is about 30 h^{-1} and the relative standard deviation is $\leqslant 1.3\%$.

Rapid, sensitive, and accurate methods of determining nitrite in natural waters are essential in environmental chemistry, geochemistry and limnology. Nitrite probably exists at the low parts per billion (10^9) level in uncontaminated natural waters, which makes it difficult to determine accurately. Nitrite in water has been determined successfully by flow injection analysis (f.i.a.) [1—4], a method invented by Růžička and Hansen [5]; most of the procedures have been based on the diazotization-coupling reaction with sulfanilamide and *N*-(1-naphthyl)ethylenediamine, but they are not sufficiently sensitive for direct application to uncontaminated waters. Růžička and Hansen [6] reported a manifold for the highly sensitive determination of nitrite based on *N*-(1-naphthyl)ethylenediamine, in which a special "mixing point" was inserted immediately after the confluence point; with large sample volumes and with scale expansion on the recorder, a detection limit of 0.002 mg l^{-1} nitrite-nitrogen was reached.

Okada et al. [7] reported a spectrophotometric determination of nitrite at the $\mu g\ l^{-1}$ level in river waters. Nitrite diazotized *p*-aminoacetophenone, which was then coupled with *m*-phenylenediamine at pH 1.5—3.0; the 2,4-diamino-4′-acetylazobenzene formed was measured at 460 nm. A brief description of the adaptation of this method to f.i.a. has been given [8]. The present communication describes a thorough evaluation of this flow injection

0003-2670/83/$03.00

method. This method is shown to be rapid, sensitive and accurate, and applicable to the determination of low $\mu g\ l^{-1}$ levels of nitrite in natural waters.

Experimental

Reagents. All reagents were of analytical-reagent grade. Aqueous reagents were prepared in de-ionized, distilled water.

A standard nitrite solution (1 mg ml^{-1} nitrite-nitrogen) was prepared from sodium nitrite (4.93 g), dried at 105—110°C, in 1 l of water. Nitrite standard solutions were freshly prepared by diluting the stock solution. The *p*-aminoacetophenone stock solution was prepared by dissolving 5 g of the reagent in 10 ml of concentrated hydrochloric acid and diluting to 500 ml with water; the solution was filtered through a 0.45-μm Millipore filter and stored in a brown-glass bottle in a refrigerator. The *m*-phenylenediamine stock solution was prepared by dissolving the dihydrochloride (13.8 g) in 500 ml of water and filtering through a 0.45-μm Millipore filter. It was stored in a brown-glass bottle in a refrigerator.

Apparatus. A diagram of the flow system is shown in Fig. 1. The absorbance was measured with a Shimadzu double-beam spectrophotometer UV-140-02 with a 1-cm flow cell (8 μl) and recorded by a Rikadenki R-22 recorder. A double-plunger micro pump (Kyowa Seimitsu KHU-W-52) was used; the same results were obtained by using a peristaltic pump (Tokyo Rikakikai MP-3). The sample solution (650 μl) was injected by a 6-way injection valve (Kyowa Seimitsu KMH-6V) into the reagent R_1 stream. The temperature of the water bath, in which the mixing coils were heated to accelerate the reactions, was controlled by a Taiyo Thermo Minder Jr-10. The flow lines were made from polytetrafluoroethylene (PTFE) tubing (1 mm and 0.5 mm i.d.). The mixing coils (1 mm i.d.), MC_1 and MC_2, were optimally 1.5 and 1.0 m long, respectively, and were wound around plastic rods (6 mm o.d.). The damping coils (0.5 mm i.d.) were 20 m long, to cancel the pulse from the reciprocal pump. The back-pressure tubing (0.5 mm i.d.) was 5 m long, to prevent formation of air bubbles.

Recommended procedure. The reagent solutions R_1 and R_2 were prepared by diluting 40 ml of the appropriate stock solutions to 1 l; the pH of R_1 was

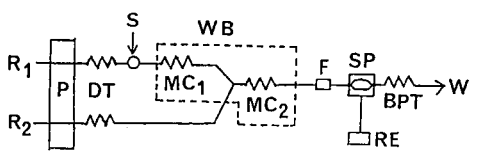

Fig. 1. Schematic flow diagram for the determination of nitrite. R_1, *p*-aminoacetophenone solution; R_2, *m*-phenylenediamine solution; P, double-plunger micro pump (1.7 ml min^{-1}); DT, damping coil (0.5 mm i.d. × 20 m); S, loop-valve sample injector (sample volume 650 μl); WB, water bath (30°C); MC_1, mixing coil (1 mm i.d. × 1.5 m); MC_2, mixing coil (1 mm i.d. × 1.0 m); F, line filter; SP, spectrophotometer with flow cell (light path 10 mm, 8 μl); RE, recorder; BPT, back-pressure coil (0.5 mm i.d. × 5 m); and W, waste.

adjusted to 1.3 and the pH of R_2 to 2.4. Both reagent solutions gave the same response for three months (maximum period tested) if kept in a refrigerator when not in use.

The flow rates of R_1 and R_2 were 1.7 ml min^{-1} each. Sample solutions were filtered through a 0.45-μm Millipore filter. From the sample loop, 650 μl of sample solution was injected into the reagent R_1 stream. Peak heights were measured at 456 nm against water as reference. The concentration of nitrite was evaluated from the peak heights by using a calibration graph prepared from freshly prepared nitrite standards.

Results and discussion

Optimum experimental conditions. The optimum lengths of the mixing coils MC_1 and MC_2 was examined over the range 50—300 cm. The length of MC_2 had little effect on the absorbance in this range, whereas the highest absorbance was obtained when MC_1 was 150—200 cm. The lengths chosen for MC_1 and MC_2 were 150 and 100 cm, respectively. Varying the flow rates of both reagent solutions R_1 and R_2 over the range 1.0—2.0 ml min^{-1} did not produce significant changes in the peak heights. Therefore, flow rates of 1.7 ml min^{-1} in each channel were used.

The volume of sample injected had a significant effect on the peak height (Fig. 2). The signal increased with increasing sample volume up to 600 μl, but decreased with larger volumes. A sample volume of 650 μl was chosen for further work.

An increase in the reaction temperature from 18°C to 50°C more than

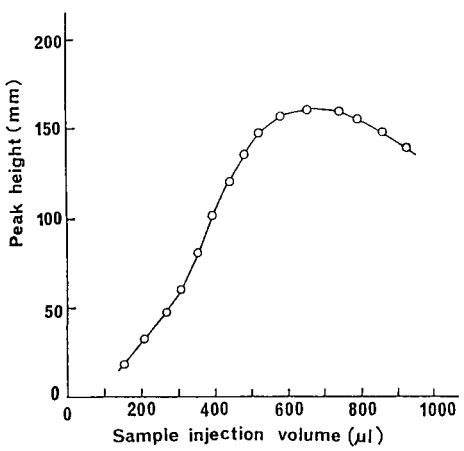

Fig. 2. Effect of sample volume on the peak heights for 30 μg l^{-1} NO_2^--N. Reaction temperature, 30°C; recorder range, 5 mV.

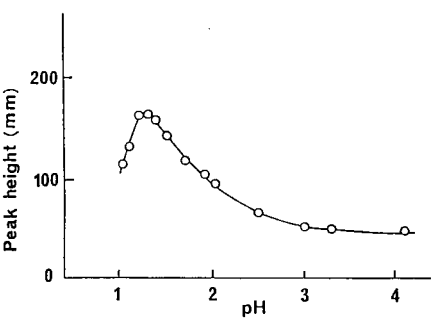

Fig. 3. Effect of pH of the *p*-aminoacetophenone solution on the signal for 30 μg l^{-1} NO_2^--N. Conditions: sample volume, 650 μl; reaction temperature, 30°C; recorder range, 5 mV; R_1, 0.04% (w/v) *p*-aminoacetophenone solution; R_2, 0.11% (w/v) *m*-phenylenediamine solution (pH 2.4).

doubled the peak height, i.e., the reaction rate; the increase with temperature followed a smooth curve and a temperature of 30°C was selected.

The effect of varying the pH of the reagent solutions over the range 1—4 was examined. The pH of the solutions was adjusted with hydrochloric acid or sodium hydroxide solution. The optimum pH range for the *p*-aminoacetophenone solution was rather critical at 1.2—1.4 (Fig. 3), whereas the pH of the *m*-phenylenediamine solution had no effect on the signals in the range 2.4—4.0. The pH values selected for these solutions were 1.3 and 2.4, respectively. The concentrations of the two reagent solutions were then varied, while these pH values were maintained. As is evident from Fig. 4, the peak height increased with increasing concentrations of the reagents up to 0.04% (w/v) and 0.11% (w/v) for *p*-aminoacetophenone and *m*-phenylenediamine, respectively. At higher concentrations, the increase in signal was less significant, so that the concentrations cited were chosen for routine work.

Calibration graph, detection limit and reproducibility. A calibration run obtained with 0—30 $\mu g\ l^{-1}$ nitrite-nitrogen standards by the proposed flow injection system is shown in Fig. 5. Calibration graphs were linear over this range. The detection limit was about 0.2 $\mu g\ l^{-1}$ nitrite-nitrogen. The proposed method is therefore one of the most sensitive flow injection procedures available for nitrite [1—4, 6]. The relative standard deviations of 10 injections each of solutions containing 10, 20 and 30 $\mu g\ l^{-1}$ nitrite-nitrogen

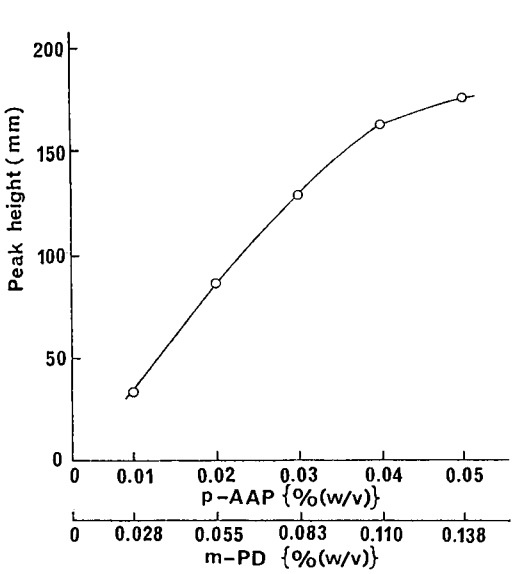

Fig. 4. Effect of concentrations of *p*-aminoacetophenone (*p*-AAP) and *m*-phenylenediamine (*m*-PD) on the signal from 30 $\mu g\ l^{-1}$ NO_2^--N. Other conditions as for Fig. 5.

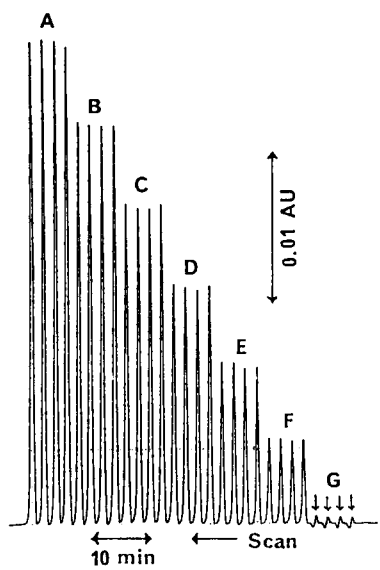

Fig. 5. A typical calibration run with the proposed flow injection system. Nitrite standards: A, 30; B, 25; C, 20; D, 15; E, 10; F, 5; G, 0 $\mu g\ l^{-1}$ NO_2^--N. Sample volume, 650 μl; reaction temperature, 30°C; recorder range, 5 mV.

were 1.3; 1.1 and 0.39%, respectively. Samples with higher concentrations of nitrite can be directly determined by decreasing the sample volume injected and the recorder sensitivity; linear calibration graphs were then obtained up to 3 mg l^{-1} nitrite-nitrogen (the maximum concentration tested). The sampling rate was about 30 samples per hour.

Effect of foreign ions. The effect of various ions on the determination of nitrite was also investigated. No interference was caused by less than 50 mg l^{-1} Ca^{2+}, Mg^{2+}, Na^{+}, K^{+}, NH_4^{+}, HCO_3^{-}, SO_4^{2-}, Cl^{-}, SiO_3^{2-}, NO_3^{-} or $H_2PO_4^{-}$ in the determination of 30 $\mu g\ l^{-1}$ nitrite-nitrogen.

Application to natural waters. To investigate the applicability of this method to natural waters, recoveries of known amounts of nitrite added to water samples were examined. Table 1 presents recovery data for nitrite.

TABLE 1

Recovery of nitrite added to natural water samples[a]

Sample	Amount of nitrite-N ($\mu g\ l^{-1}$)			Recovery (%)	Nitrite-N in sample ($\mu g\ l^{-1}$)
	Added	Found	Recovered		
River water	None	5.0			6.3
	5.0	10.3	5.3	106	
	10.0	15.2	10.2	102	
River water	None	1.4			1.8
	5.0	6.4	5.0	100	
	10.0	10.8	9.4	94	
Lake water	None	2.2			2.8
	5.0	7.2	5.0	100	
	10.0	12.5	10.3	103	
Pond water	None	3.0			3.8
	5.0	8.1	5.1	102	
	10.0	12.8	9.8	98	
Well water	None	2.4			3.0
	5.0	7.6	5.2	104	
	10.0	12.7	10.3	103	
Rain water	None	2.6			3.3
	5.0	7.8	5.2	104	
	10.0	13.2	10.6	106	
Irrigation water	None	4.9			6.1
	5.0	10.0	5.1	102	
	10.0	14.3	9.4	94	
Irrigation water	None	5.3			6.6
	5.0	10.3	5.0	100	
	10.0	14.9	9.6	96	

[a]Evaluation of recoveries of nitrite was based on the addition of nitrite to 16 ml of sample solution in a 20-ml calibrated flask.

These results indicate that the system was successful in determining nitrite at low $\mu g\ l^{-1}$ levels in natural waters.

The authors thank the Nissan Science Foundation for financial support.

REFERENCES

1 M. F. Giné, H. Bergamin F°, E. A. Zagatto and B. F. Reis, Anal. Chim. Acta, 114 (1980) 191.
2 E. A. G. Zagatto, A. O Jacintho, J. Mortatti and H. Bergamin F°, Anal. Chim. Acta, 120 (1980) 399.
3 L. Anderson, Anal. Chim. Acta, 110 (1979) 123.
4 J. F. V. Staden, Anal. Chim. Acta, 138 (1982) 403.
5 J. Růžička and E. H. Hansen, Anal. Chim. Acta, 78 (1975) 145.
6 J. Růžička and E. H. Hansen, Flow Injection Analysis, Wiley-Interscience, New York, 1981, p. 58–60.
7 M. Okada, M. Miyata and K. Tôei, Analyst, 104 (1979) 1195.
8 S. Nakashima, M. Yagi, M. Zenki, A. Takahashi and K. Tôei, Bunseki Kagaku, 31 (1982) 732.

Analytica Chimica Acta, 155 (1983) 269—272
Elsevier Science Publishers B.V., Amsterdam — Printed in The Netherlands

Short Communication

SIMULTANEOUS SPECTROPHOTOMETRIC DETERMINATION OF COPPER(II) AND IRON(III) AS THE AZIDE COMPLEXES

E. A. NEVES

Instituto de Química da USP, Caixa Postal 20780, São Paulo, SP (Brazil)

J. F. DE ANDRADE*

Departamento de Química, FFCLRP (USP), Campus de Ribeirão, Preto, 14100, SP (Brazil)

G. O. CHIERICE

Instituto de Física e Química de São Carlos, USP, Caixa Postal 369, São Carlos, SP (Brazil)

(Received 2nd June 1983)

Summary. The simultaneous spectrophotometric determination of copper and iron is based on the yellow and red azide complexes formed in 50% (v/v) water/acetone medium. Absorbances are measured at 345 and 435 nm where molar absorptitivities for the iron(III) complex are 8.77×10^3 and 8.49×10^3 l mol^{-1} cm^{-1}, respectively, and absorptivities for the copper(II) complexes are 1.47×10^3 and 5.69×10^3 l mol^{-1} cm^{-1}, respectively. The systems obey Beer's law and concentrations as low as 2.0 and 1.2 mg l^{-1} for copper and iron, respectively, can be quantified in a 1.00-cm cell. Determination of iron(III) in 23 mixtures (1.1—5.4 mg l^{-1}) yielded a relative standard deviation of 0.86%; similar data for copper(II) (2.0—8.9 mg l^{-1}) yielded a relative standard deviation of 1.6%.

Azide complexes with several metal cations have been studied [1—3]. The intense red complex developed in acidic medium by the reaction between the azide and iron(III) [4, 5] and the yellowish solution obtained with the copper(II)—azide system [6, 7] have been used spectrophotometrically to quantify the ions and the ligand, and to establish equilibrium constants. The absorption maxima at 460 and 415 nm, respectively, suggest the possibility of simultaneous determinations. This communication describes the development and evaluation of such a method for iron(III) and copper(II).

Experimental

Apparatus. Spectrophotometric measurements were made with Zeiss PMQ-II and Perkin-Elmer (Coleman 575 recording) spectrophotometers. Stoppered quartz cells of 1.00-cm optical path length were used for all measurements.

Reagents and solutions. All reagents were chemically pure or of analytical grade. Sodium azide was purified by dissolution in water, filtration, and precipitation with pure ethanol; the precipitate was dried under vacuum and

0003-2670/83/$03.00

then at 110°C. The reagent was standardized by treating samples with standardized sulfuric acid, boiling out HN_3, and titrating the excess of strong acid. A 3.0 M standard solution was then prepared.

Standard copper(II) solution (about 0.010 M) was prepared by dissolving $CuSO_4 \cdot 5H_2O$ in distilled water containing 0.001 M perchloric acid. Standard iron(III) solution (about 0.010 M) was prepared by dissolving $Fe(NH_4)(SO_4)_2 \cdot 12H_2O$ in 0.01 M perchloric acid. The solutions were standardized by EDTA titrations. Working standard solutions were prepared as needed by suitable dilutions.

Recommended procedure. Into a 25-ml volumetric flask, transfer enough of the standard perchloric acid solution to make the final concentration 0.10 M, and add a sample containing 25—135 μg of iron(III) and 50—225 μg of copper(II). Add 12.5 ml of acetone and 2.5 ml of the standardized 3.0 M sodium azide solution. Dilute to volume with distilled water and measure the absorbances of the test solutions at 345 and 435 nm against a blank (0.1 M $HClO_4$). Calculate the iron and copper concentrations with simultaneous equations.

Results and discussion

Effects of reaction variables. Of several solvents tested, acetone appeared to be the most favorable, because of the greater sensitivity and favorable spectral shifts relative to the aqueous medium. Higher acetone concentrations enhanced the intensities of the iron(III) and copper(II) colors, but the upper limit was set by the low solubility of many inorganic salts in an acetone/water medium, and by the need to keep the total volume of the reagents (including acetone) small enough to permit the use of large aliquots of the sample solution. The best compromise is a 50% (v/v) water/acetone mixture.

No improvement in molar absorptivities was gained by using free azide concentrations higher than 0.20 M. Many investigators have used nitric, hydrochloric or sulfuric acids; however, 0.1 M perchloric acid was chosen because the color was more intense and stable. The complexes were stable for 2 h. For these conditions, the copper(II) band shifted from 415 (in water) to 435 nm, and the absorption maxima of the iron(III) complexes shifted to 348 and 435 nm, respectively. Spectra for the azide/iron and copper complexes and for a mixture are shown in Fig. 1.

It was shown that the best wavelengths for the simultaneous determinations were 345 and 435 nm, the maxima for each complex. The absorbances of ten samples, each containing 0.050 mM of the respective metal ion, yielded a standard deviation of about 0.001 at 345 and 435 nm.

Beer's law and sensitivity. Spectrophotometric measurements were made on 22 iron(III) solutions (0.279—6.7 mg l^{-1}) and 24 Cu(II) solutions (0.635—17.8 mg l^{-1}). Linear plots (r^2 = 0.9999) yielded molar absorptivities (l mol^{-1} cm^{-1}) of 8.77×10^3 at 345 nm and 8.49×10^3 at 435 nm for the Fe(III) complex, and 1.47×10^3 at 345 nm and 5.69×10^3 at 435 nm for the Cu(II)

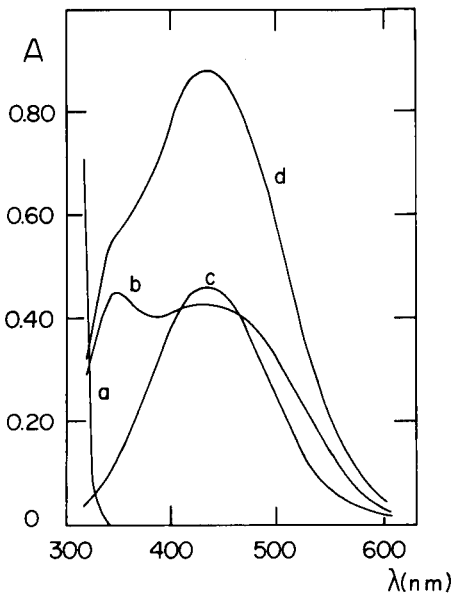

Fig. 1. Absorption spectra for complexes under the recommended conditions: (a) blank; (b) 0.050 mM Fe(III); (c) 0.080 mM Cu(II); (d) 0.080 mM Cu(II) and 0.050 mM Fe(III).

complex. As is well known, the metal ion concentrations can then be calculated from

$$C_{Fe} = (0.0896 \times A_{345} - 0.0232 \times A_{435})/0.0106$$

$$C_{Cu} = (0.157 \times A_{435} - 0.152 \times A_{345})/0.0106$$

Known mixtures. Twenty-three synthetic sample solutions containing final concentrations of 1.12—5.36 mg l^{-1} Fe(III) and 2.03—8.90 mg l^{-1} Cu(II), with Fe/Cu concentration ratios of 0.13—2.64, were treated by the recommended procedure, and the concentration of each component was then calculated. The least-squares equations of computed (y) vs. added (x) concentrations were: $y = (1.011 \pm 0.003)x - (0.032 \pm 0.008)$, with $S_{yx} = 0.016$ and $r^2 = 0.9999$ for Fe(III) and $y = (1.013 \pm 0.005)x - (0.089 \pm 0.026)$, with $S_{yx} = 0.052$ and $r^2 = 0.9998$ for Cu(II).

The relative standard deviations (disregarding the signs) were 0.86% for iron and 1.6% for copper. The better precision for iron(III) results from the fact that the wavelengths used correspond to maxima in the spectra for the Fe(III) complexes while the 345 nm value is on a descending portion of the spectrum for the Cu(II) system.

Effect of diverse ions. In the study of interfering ions, several cations (usually as nitrates) and anions as sodium salts were added separately and the effects of each were observed at selected points in the spectrum. The copper(II) and iron(III) concentrations were fixed at 3.18 mg l^{-1} and the

diverse ions were introduced at concentrations 100 times higher. If any turbidity appeared (insolubility, hydrolysis, other reactions), the solution was centrifuged before absorbance measurements. This happened, for instance, in the presence of Al^{3+}, Sr^{2+}, Ba^{2+}, S^{2-}, Ag^{+}, Bi^{3+}, $S_2O_3^{2-}$, Hg_2^{2+} and Pb^{2+}.

Of 54 ions tested, only $HAsO_4^{2-}$, CO_3^{2-}, $C_6H_5O_7^{3-}$, F^-, I^-, $HC_6H_5O_7^{2-}$, HPO_4^{2-}, $H_2PO_4^-$, PO_4^{3-}, HPO_3^{2-}, MoO_4^{2-}, S^{2-}, $C_2O_4^{2-}$, $C_4H_4O_6^{2-}$, $S_4O_6^{2-}$, $S_2O_3^{2-}$ and Hg^{2+} interfered when present at 100-fold or higher relative to Cu(II) and Fe(III). Other ions would interfere because they are colored or because they react with the reagents to give intensely colored complexes; these ions include $Cr_2O_7^{2-}$, CrO_4^{2-}, MnO_4^-, VO_3^-, Cr^{3+}, Ni^{2+}, $Fe(CN)_6^{3-}$, $Fe(CN)_6^{4-}$, UO_2^{2+}, Co^{2+}, Ce^{4+}, Pd^{2+} and SCN^-.

Because these ions generally are present at concentrations smaller than the above limits, the present method can be used to determine Cu(II) and Fe(III) in several materials without a separation.

The authors express their gratitude to the FINEP, FAPESP and CNPq foundations for financial support.

REFERENCES

1 P. Senise and E. A. Neves, J. Inorg. Nucl. Chem., 34 (1972) 1923.
2 E. A. Neves, E. Oliveira and Z. L. Santos, Talanta, 27 (1980) 609.
3 E. A. Neves, R. Tokoro and M. E. V. Suárez, J. Chem. Res. (M), 11 (1979) 4401.
4 H. K. El-Shamy and F. G. Sherif, J. Chem. U.A.R., 3 (1961) 197.
5 T. R. Musgrave and R. N. Keller, Inorg. Chem., 4 (1965) 1793.
6 E. A. Neves, E. Oliveira and L. Sant'Agostino, Anal. Chim. Acta, 87 (1976) 243.
7 M. P. Peters, Ph.D. Thesis, Instituto de Química da USP, São Paulo, Brazil, 1980.

Analytica Chimica Acta, 155 (1983) 273—277
Elsevier Science Publishers B.V., Amsterdam — Printed in The Netherlands

Short Communication

THE OPTIMUM COMPOSITION OF pH-SENSITIVE ACCEPTOR SOLUTIONS FOR MEMBRANE SEPARATION IN FLOW INJECTION ANALYSIS

W. E. VAN DER LINDEN

Department of Chemical Technology, Twente University of Technology, P.O. Box 217, 7500 AE Enschede (The Netherlands)

(Received 21st June 1983)

Summary. Gas diffusion membranes are frequently used to transfer volatile protolytes from a donor to an acceptor solution. This transfer is attended by a change in $[H^+]$ or $[OH^-]$ and an absorbance change of the acid-base indicator present. Conditions determining the linearity and the sensitivity of the calibration graphs are discussed.

The use of suitable membranes in continuous flow systems introduces the attractive possibility of selective transfer of the compound to be measured from a mostly ill-defined sample stream into a carrier stream of well-defined composition. This feature was first introduced into flow injection analysis (f.i.a.) for the determination of carbon dioxide in serum [1]. A similar approach was suggested for the determination of ammonia [2]. In both cases the compound which actually passes the membrane causes a protolytic reaction in the acceptor solution. The pH change thus obtained can be indicated photometrically if a suitable acid-base indicator is present in the solution.

With regard to selection of the optimum composition of such acceptor solutions, no general directives are available in the literature. In this contribution, such directives are developed starting from the principle that important criteria are the stability of the base-line, the sensitivity (i.e., slope of the calibration graph), and the linear range of the calibration graph. To meet the first criterion, it seems desirable to maintain a well-defined and stable pH value in the carrier stream when no sample is injected; this is achieved by using a buffer solution. It will be demonstrated that the last two criteria lead to mutually exclusive conditions for the buffer concentration. Larger buffer concentrations lead to larger linear ranges but to less sensitive response, whereas lower buffer concentrations provide higher sensitivity but narrower linear ranges.

In the case of membrane separation, the generation of a signal corresponding to the injection of a sample requires three steps: the transfer of the relevant species across the membrane, the influence of this compound on the pH of the acceptor solution by protolytic reactions, and an absorbance

0003-2670/83/$03.00

change caused by this pH change. Although a combination of non-linear relations may result in a linear calibration graph in some particular case, it will be assumed in the following discussion that each consecutive step has a linear response: i.e., the (maximum) concentration in the acceptor stream of the compound to be detected is linearly dependent on the concentration injected in the donor stream; the concentration change in H^+ or OH^- is linearly dependent on the concentration of the compound transferred across the membrane; and the absorbance measured photometrically is linearly dependent on $[H^+]$ or $[OH^-]$ in the solution.

The transfer process has been discussed [3]; it was shown that, in general, a linear dependence can be expected for this step. Hence, only the last two steps need closer consideration.

Choice of indicator

For an acid-base indicator, I, with a protonation (stability) constant β_I and present in an analytical concentration C_I, the mass balance equation yields

$$[I] = C_I\{1 + \beta_I[H^+]\}^{-1}; \qquad [HI] = \beta_I[H^+]C_I\{1 + \beta_I[H^+]\}^{-1} \tag{1}$$

(with charges omitted).

Thus, the absorbance can be expressed as

$$A = \epsilon_I bC_I\{1 + \beta_I[H^+]\}^{-1} + \epsilon_{HI}b\beta_I[H^+]C_I\{1 + \beta_I[H^+]\}^{-1} \tag{2}$$

Two extreme cases will be considered.

(i) $\beta_I[H^+] \gg 1$ *or* $\beta_I^{-1}\ K_w^{-1}\ [OH^-] \ll 1$. This condition means that the indicator is predominantly present in the acidic form HI or HI^+. Equation 2 leads then to

$$A = \epsilon_I bC_I\beta_I^{-1}[H^+]^{-1} + \epsilon_{HI}bC_I\{1 - \beta_I^{-1}[H^+]^{-1}\} \tag{3}$$

which simplifies for $\epsilon_I \to 0$ or $\epsilon_{HI} \to 0$, respectively to

$$\epsilon_I \to 0: \quad A = \epsilon_{HI}bC_I - \epsilon_{HI}bC_I\beta_I^{-1}K_w^{-1}[OH^-] \tag{3a}$$

$$\epsilon_{HI} \to 0: \quad A = \epsilon_I bC_I\beta_I^{-1}[H^+]^{-1} = \epsilon_I bC_I\beta_I^{-1}K_w^{-1}[OH^-] \tag{3b}$$

Clearly, the condition which leads to Eqns. 3a and 3b must be fulfilled to obtain an absorbance that changes linearly with $[OH^-]$. If such behaviour is required in, for example, the range $8.0 < pH < 9.0$, an indicator selected must have $\log \beta_I > 9.0$. However, an indicator with a much larger stability constant than is strictly necessary should be avoided because of the decrease in sensitivity that will occur.

(ii) $\beta_I[H^+] \ll 1$. In this case the indicator is predominantly present in the alkaline form I or I^-. Equation 2 then leads to

$$A = \epsilon_I bC_I\{1 - \beta_I[H^+]\} + \epsilon_{HI}bC_I\beta_I[H^+] \tag{4}$$

or

$$\text{for } \epsilon_I \to 0: \quad A = \epsilon_{HI}bC_I\beta_I[H^+] \tag{4a}$$

for $\epsilon_{HI} \to 0$: $A = \epsilon_I b C_I - \epsilon_I b C_I \beta_I [H^+]$ (4b)

This condition leads to a linear dependence of the absorbance on $[H^+]$ and should, therefore, be used for H^+-generating compounds like carbon dioxide and acetic acid.

From the photometric point of view, it is preferable to have situations leading to Eqn. 3b or Eqn. 4a because in these cases the signal corresponds to an increase in the absorbance starting from a relatively low absorbance level, whereas for the situations found in Eqns. 3a and 4b a decrease in absorbance from a relatively high background is observed.

Choice of buffer system

When the compound that passes the membrane is absorbed in an acceptor solution containing several different protolytes, rather complicated expressions are obtained between its concentration and $[H^+]$ or $[OH^-]$. A simpler case, first discussed here, occurs when the buffer solution consists of the same protolyte as the one that passes the membrane.

The buffer solution contains C_a M of the weak acid HA and C_b M of the base A^- (e.g. NaA). If the stability constant of this protolyte is denoted by β_A then

$$[A^-] = (C_a + C_b)\{1 + \beta_A [H^+]\}^{-1} \quad (5)$$

The charge balance leads to $[H^+] + [Na^+] = [OH^-] + [A^-]$, which for the case $[H^+] \gg [OH^-]$ (pH <6.5) yields

$$[H^+] + C_b = (C_a + C_b)\{1 + \beta_A [H^+]\}^{-1} \quad (6)$$

or

$$[H^+] = [-(1 + \beta_A C_b) + \{(1 + \beta_A C_b)^2 + 4\beta_A C_a\}^{1/2}]\ (2\beta_A)^{-1} \quad (7)$$

This equation leads to

$$d[H^+]/dC_a = \{(1 + \beta_A C_b)^2 + 4\beta_A C_a\}^{-1/2} \quad (8)$$

From Eqn. 8 it is readily seen that $[H^+]$ is linearly dependent on C_a if $4\beta_A C_a \ll (1 + \beta_A C_b)^2$. For a more quantitative condition, Eqn. 8 can better be rewritten as

$$d[H^+]/dC_a = (1 + \beta_A C_b)^{-1}[1 + 4\beta_A C_a (1 + \beta_A C_b)^{-2}]^{-1/2} \quad (8a)$$

Deviation of linearity is less than 2% as long as $4\beta_A C_a (1 + \beta_A C_b)^{-2} \leqslant 0.04$, or

$$C_a \leqslant 0.01(1 + \beta_A C_b)^2 \beta_A^{-1} \quad (9)$$

In this case

$$[H^+] = C_a (1 + \beta_A C_b)^{-1} \quad (10)$$

The same result can be obtained directly from the charge balance (Eqn. 6), provided that $\beta_A [H^+] \ll 1$. Combination of Eqns. 9 and 10 leads to the constraint $[H^+]_{lim} = 0.01\ (1 + \beta_A C_b)\beta_A^{-1}$, or

$$[H^+]_{lim} = 0.01\{\beta_A^{-1} + C_b\} \quad (11)$$

From Eqn. 10, it can be taken that the maximum sensitivity is found for $\beta_A C_b \ll 1$. In that case, $\Delta[H^+] = \Delta C_A$, i.e., each molecule passing the membrane generates one H^+ ion.

Figure 1 shows a graphical representation of Eqn. 10 as well as the constraint expressed by Eqn. 11 for the case of acetic acid ($\log \beta_A = 4.7$). It can be seen that a larger sensitivity is coupled with a narrower linear range.

For an alkaline buffer consisting of C_b M of base B and C_a M of the corresponding acid BH^+ (e.g., BHCl) and assuming pH >7.5 a similar argument as given above leads to a set of equations comparable to Eqns. 9 and 10

$$C_b \leqslant 0.01(1 + C_a K_w^{-1} \beta_A^{-1})^2 K_w \beta_A \quad (12)$$

$$[OH^-] = C_b(1 + C_a K_w^{-1} \beta_A^{-1})^{-1} \quad (13)$$

Comparison with the corresponding Eqns. 9 and 10 shows that C_a and C_b are mutually changed, while β_A is replaced by $(K_w \beta_A)^{-1}$. Thus Fig. 1 also applies for ammonia with a log β_A value of 9.3 if the coordinates C_a and C_b are interchanged and the $[H^+]$ axis is replaced by $[OH^-]$.

If it is not the compound HA that passes the membrane into an acceptor solution containing the buffer HA/A^-, but another protolyte, HP, the charge balance is given by

$$[H^+] + [Na^+] = [A^-] + [OH^-] + [P^-] \quad (14)$$

or when $[H^+] \gg [OH^-]$

$$[H^+] + C_b = (C_a + C_b)\{1 + \beta_A[H^+]\}^{-1} + \Delta C\{1 + \beta_P[H^+]\}^{-1} \quad (15)$$

where ΔC is the analytical concentration of the protolyte HP and β_P is its stability constant. Equation 15 is a cubic equation in $[H^+]$ and so no explicit expression of $[H^+]$ in dependence on ΔC can be found unless some assumptions are made. It will be assumed that again $\beta_A[H^+] \ll 1$ but also that $\beta_P[H^+] \ll 1$. If this latter condition is not fulfilled, hardly any influence of

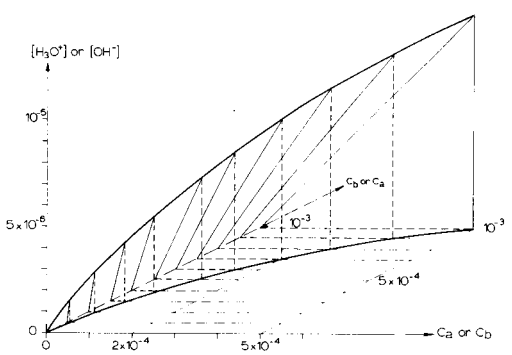

Fig. 1. Dependence of $[H^+]$ response on C_a at different values of C_b calculated for $\log \beta_A = 4.7$. The curved line corresponds to the constraint expressed by Eqn. 11. Also the dependence of the $[OH^-]$ response on C_b at different values of C_a for base with $\log \beta_A = 9.3$.

the transferred protolyte can be expected. With these assumptions, Eqn. 15 can be simplified to

$$[H^+] + C_b = (C_a + C_b)\{1 - \beta_A[H^+]\} + \Delta C\{1 - \beta_P[H^+]\}$$

or

$$[H^+] = (C_a + \Delta C)\{1 + (C_a + C_b)\beta_A + \Delta C\beta_P\}^{-1} \quad (16)$$

The slope of the calibration graph is then obtained from

$$d[H^+]/d\Delta C = \{1 + (C_a + C_b)\beta_A - C_a\beta_P\}\{1 + (C_a + C_b)\beta_A + \Delta C\beta_P\}^{-2} \quad (17)$$

This slope is independent of ΔC if

$$\Delta C\beta_P \ll \{1 + (C_a + C_b)\beta_A\} \quad (18)$$

Generally, $(C_a + C_b)\beta_A > 1$ as well as $C_a\beta_P > 1$ holds true so that Eqns. 17 and 18 can be simplified to

$$d[H^+]/d\Delta C = \{(C_a + C_b)\beta_A\}^{-1} - C_a\beta_P\{(C_a + C_b)\beta_A\}^{-2} \quad (19)$$

and $\Delta C\beta_P \ll (C_a + C_b)\beta_A$. In most cases $\Delta C < (C_a + C_b)$, thus Eqn. 20 implies that $\beta_P \leqslant \beta_A$, i.e., the protolyte HA should not be a stronger protolyte than HP. From Eqn. 20 it can be seen that greater sensitivity is obtained with a lower total buffer concentration. When the buffer concentration is decreased, the buffer action is ultimately taken over by the indicator.

To conclude this general, theoretical treatment, the use of the derived equations will be illustrated. In a previous paper [3], ammonia was determined by using an ammonia/ammonium chloride buffer as the acceptor solution. If the concentration to be determined in the donor stream is in the range 10^{-2}—10^{-4} M, and if under the prevailing circumstances about 10% of the ammonia is transferred across the membrane, then the maximum change in concentration in the acceptor stream is about 10^{-3} M. To have a linear range up to $C_b \approx 10^{-3}$ M, Eqn. 12 leads to $C_a \geqslant 10^{-2.85}$ M when the value $\log \beta_A = 9.3$ is used for ammonia. By combination of Eqns. 12 and 13, the limiting hydroxide ion concentration is obtained

$$[OH^-]_{lim} = 10^{-2}(10^{-4.7} + 10^{-1.85}) \approx 10^{-3.85}$$

or $pH_{lim} = 10.15$. In the earlier paper, a pH of 9.0 was adopted. Hence, for the indicator $\log \beta_I > 9.0$ which means that phenolphthalein is a reasonable choice.

REFERENCES

1 H. Baadenhuijsen and H. E. H. Seuren-Jacobs, Clin. Chem., 25 (1979) 443.
2 J. Růžička and E. H. Hansen, Flow Injection Analysis, Wiley, New York, 1981.
3 W. E. van der Linden, Anal. Chim. Acta, 151 (1983) 359.

Analytica Chimica Acta, 155 (1983) 279—285
Elsevier Science Publishers B.V., Amsterdam — Printed in The Netherlands

Short Communication

USE OF MULTIPLE DETECTORS AND STEPWISE ELUTION IN ION CHROMATOGRAPHY WITHOUT SUPPRESSOR COLUMNS

DENNIS R. JENKE, PRESLEY K. MITCHELL and GORDON K. PAGENKOPF*
Department of Chemistry, Montana State University, Bozeman, MT 59717 (U.S.A.)
(Received 18th May 1983)

Summary. Refractive index, spectrophotometric and conductivity detectors were coupled in tandem to an ion chromatography system without suppressor column. Quantitative sensitivity increased in the order given. The refractive index and conductivity detection limits are limited by background noise; the spectrophotometric detection limit is limited by the ability to compensate for the high eluent background absorbance. Peak distortion at high analyte concentration limits peak height linearity to about 2.5 orders of magnitude. Peak areas vary linearly with concentration over the 4-decade concentration range studied. Step-changes in eluent flow rate, pH, and total salt content were examined in order to minimize the separation time for a sample containing Cl^-, NO_3^-, Br^-, SO_4^{2-} and $S_2O_3^{2-}$. The flow change decreased separation time by 30%, but concentration changes were not of practical use. In the absence of column/eluent interactions, pH changes significantly reduced separation time.

Ion chromatography couples analyte separation by ion exchange with a variety of detection techniques. With the suppressor column, detection is accomplished by matrix modification in a second column followed by the measurement of mobile phase conductivity [1]. The presence of the second column increases the complexity of the instrumentation and increases the dead volume which extends separation time and decreases resolution.

Unsuppressed single-column separators with weak organic acids as eluents have been coupled to a variety of detectors. Eluent properties that confirm the presence of an analyte include conductivity [2], u.v. absorbance [3], and refractive index [4]. A direct comparison of the capabilities of these detection techniques has not been documented.

The most efficient utilization of unsuppressed ion chromatography requires both adequate resolution and minimization of total separation time. From a theoretical standpoint, analyte elution behavior has been related to the charge ratio of the analyte and the active species of the mobile phase [5, 6]. Practically, this charge dependence has the following importance for optimization of the technique. A low concentration eluent, although desirable in terms of producing adequate resolution of monovalent analytes, can produce unacceptably long retention times for more highly charged analytes. A more concentrated eluent, although desirable in terms of producing adequate resolution of multivalent analytes in a minimum time, can

0003-2670/83/$03.00

cause the monovalent analytes to co-elute. A potential solution to this problem is gradient elution which to date has been applied in a limited sense to the suppressed technology [7]. For weak organic acid eluents, effective eluent strength can be modified by changing eluent pH, total eluent concentration, and flow rate. In this communication, the utilization of tandem conductivity, spectrophotometric, and refractive index detectors is described and the application of gradient techniques to unsuppressed ion chromatography is discussed.

Experimental

Apparatus. The chromatographic system consisted of a Perkin-Elmer Series 3B liquid chromatograph to deliver the mobile phase and a Wescan Model 269-001 anion separator column. Detectors included a Waters R401 differential refractometer, a Vydac 6000CD conductivity detector and a Perkin-Elmer LC-85 spectrophotometric detector. The eluent proceeded from the chromatograph to the spectrophotometric detector, to the conductivity detector and finally through the refractometer. The refractometer cell was thermostated at 25.0 ± 0.1°C with a water bath and the mobile phase was used as a trapped reference. The conductivity meter, separator column, and all eluent tubing were insulated to eliminate the effect of short-term temperature fluctuations [8]. Laboratory temperature was maintained at 22.5 ± 1.0°C. Sample-loop volume was 1.00 ml and samples of 2.5 ml were introduced with a B-D Yale T312 syringe. Chromatograms were generated with three strip-chart recorders. Ultraviolet spectral scans were obtained with a Varian Series 634 dual-beam spectrophotometer using 1-cm quartz cells and a 2-nm bandpass.

Reagents. Phthalate eluents were prepared by dissolution of potassium hydrogenphthalate in 900 ml of doubly distilled water, addition of sufficient 0.1 M KOH to obtain the desired pH, and dilution to a final volume of 1.0 l with the distilled water. Eluents were degassed under suction prior to utilization. Anion stock solutions were prepared at the 1000 mg l^{-1} concentration level by dissolution of the sodium salts of Cl^-, NO_3^-, SO_4^{2-} and $S_2O_3^{2-}$ and KBr in water. Standard solutions were prepared by dilution of the appropriate stock with the eluent of interest, thus minimizing the magnitude of the solvent response in the chromatogram. All salts were reagent grade.

Results and discussion

Characterization of detector response. The use of the three tandem detectors permits characterization under nearly equivalent conditions. For the conductivity and refractive index detectors, detection limits are primarily limited by detector noise; but for the spectrophotometric detector, the detection limit is related to the ability of the instrument to compensate for the high background absorptivity of the eluent. Because the spectrophotometric technique monitors a decrease in absorbance to quantify the analyte,

the best sensitivity should occur when the difference in absorbance between the analyte and eluent is the greatest. These conditions are met for wavelengths below 220 nm; however absorbances at these wavelengths exceed 3.0, and the resulting background absorbance cannot be accurately nulled by the LC-85 detector system. As a consequence, absorbance was measured at 280 nm which represents a compromise between sensitivity and the ability to maintain background correction. Figure 1 illustrates the response of the three detectors to analyte concentrations of 10 mg l^{-1}. It is clear from the magnitude of the baseline noise that the spectrophotometric detector has the lowest detection limit. Table 1 lists the detection limit for each detector with two different eluents which had the same total concentration but different pH values, 4.6 and 6.3. For both peak area and peak height calibrations, the spectrophotometric detector is approximately twice as sensitive as the conductivity detector and 20 times more sensitive than the refractive index detector. All three detectors exhibit a linear range for peak height calibration of 2.5 orders of magnitude and a linear range for peak area of four orders of magnitude. This is not a detector-related limitation because peak shape deforms significantly as analyte concentration

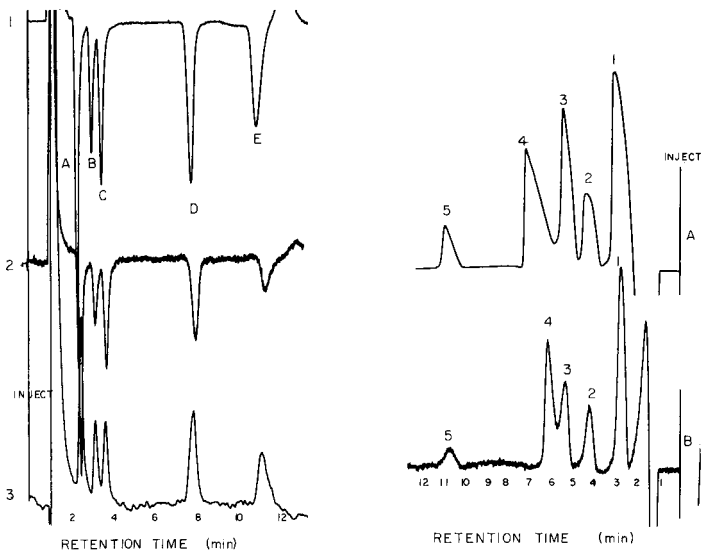

Fig. 1. Typical chromatogram obtained from the tandem detectors. Detectors 1, 2, and 3 are respectively photometric (λ = 280 nm), refractive index and conductivity. Peak identities: A, Cl^-; B, Br^-; C, NO_3^-; D, SO_4^{2-}; E, $S_2O_3^{2-}$. Conditions: 2.0 × 10^{-3} M KHP, pH 5.1, 10 mg l^{-1} analyte, flow rate 3.5 ml min^{-1}.

Fig. 2. Effect of analyte concentration on peak shape. Conditions: refractive index detector, 2.0 × 10^{-3} M KHP, pH 6.3, flow rate 3 ml min^{-1}; analyte concentration = 100 mg l^{-1} in case A, 10 mg l^{-1} in case B. Peak identity: (1) Cl^-; (2) Br^-; (3) NO_3^-; (4) SO_4^{2-}; (5) $S_2O_3^{2-}$.

TABLE 1

Detection limits for the various detectors

Analyte	Detection limit[a] (μg)					
	Spectrophotometric		Conductivity		Refractive index	
	Eluent 1	Eluent 2	Eluent 1	Eluent 2	Eluent 1	Eluent 2
Cl^-	0.02	0.04	0.02	0.06	0.2	0.5
Br^-	0.03	0.06	0.06	0.10	0.8	1.0
NO_3^-	0.03	0.04	0.06	0.10	0.8	1.0
SO_4^{2-}	0.03	0.05	0.06	0.07	0.8	0.8
$S_2O_3^{2-}$	0.04	0.08	0.08	0.20	3.0	5.0

[a]Defined as twice the peak-to-peak background noise signal, $P_T = 2.0 \times 10^{-3}$ M; eluent 1, pH 4.63; eluent 2, pH 6.3.

increases. The nature of the deformation has been attributed to column overloading [6], and has no effect on total area but produces abnormally short peak heights. The typical magnitude of the observed deformation is shown in Fig. 2. The change in pH for eluents 1 and 2 causes a speciation shift from a solution dominated by HP^- to one dominated by P^{2-}. This effectively increases the eluent concentration because P^{2-} is the more efficient eluent.

Step-change elution. Three step-changes were tested: (1) eluent flow rate, (2) eluent pH at constant total phthalate concentration, and (3) phthalate concentration at constant pH. Figure 3 documents the elution behavior of the five analytes with eluent 1 (total phthalate concentration $P_T = 2.0 \times 10^{-3}$ M, pH 4.6) at a flow rate of 3 ml min^{-1}. Resolution of the monovalent species is sufficient for accurate quantitation but the separation between NO_3^-, SO_4^{2-} and $S_2O_3^{2-}$ is excessive. Increasing the eluent flow rate after elution of nitrate will shorten the retention time although elution volume will remain essentially unchanged. As shown in the lower portion of Fig. 3, such a flow change, started at 5.7 min after sample injection, decreases separation time from 19 to 13 min. The change in flow rate (and back-pressure of the system) did not alter the refractive index response but the conductivity and spectrophotometric detectors responded to this change by producing a minor peak as designated by the arrow; the peak was sufficiently small not to affect the sulfate peak.

The pH change used was strictly a double-step process consisting of the following sequence. The pH 4.6 eluent was used for 4.5 min at which time the eluent was switched to the pH 6.3 solution; at 10.5 min, the eluent was switched back to the pH 4.6 solution. A flow rate of 3 ml min^{-1} was maintained during the entire process. The results are shown in Fig. 4. Use of a pH change will cause baseline drift for all three detectors except for spectrophotometric monitoring at an isosbestic point. The wavelength that is least sensitive to pH was found to be 262 nm. Even though the step-change is

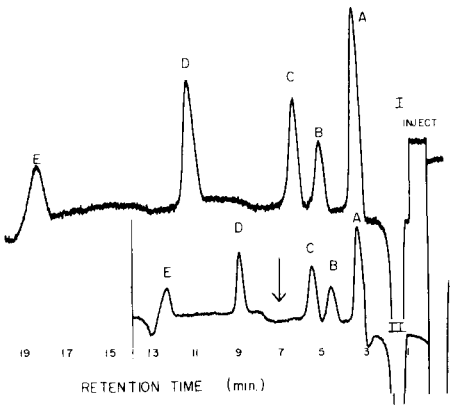

Fig. 3. Effects of change in flow-rate on chromatograms: (I) constant flow, 3 ml min^{-1}; (II) gradient 3 ml min^{-1} for 6 min then 5 ml min^{-1}. Conditions: 2.0 × 10^{-3} M KHP, pH 4.6, analytes 10 mg l^{-1}, RI detector. Scale for (I) is twice scale for (II). Peak identity: A, Cl^-; B, Br^-; C, NO_3^-; D, SO_4^{2-}; E, $S_2O_3^{2-}$.

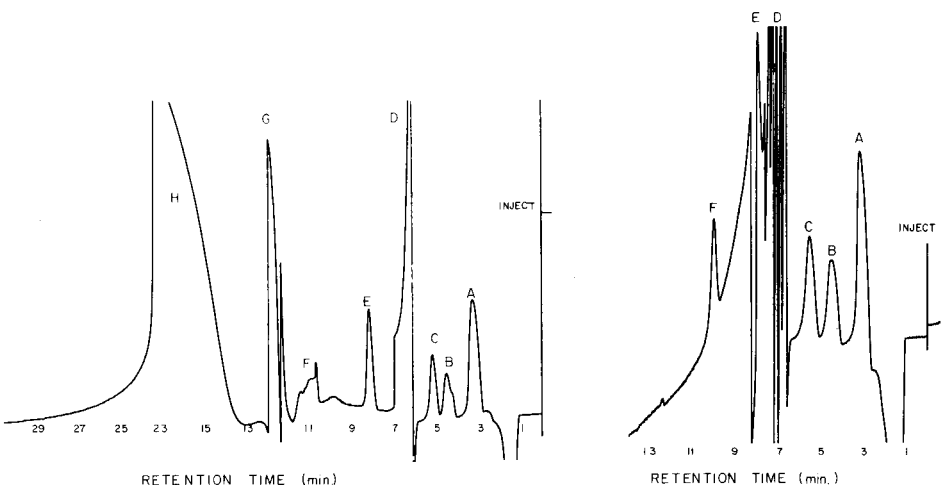

Fig. 4. Effects of pH changes on chromatograms. Conditions: spectrophotometric detector, 262 nm, flow rate 3 ml min^{-1}, 2.0 × 10^{-3} M KHP, pH 4.6 for 4.5 min, 6.3 for 7.5 min then back to 4.6, analytes 10 mg l^{-1}. Peak identity: A, Cl^-; B, Br^-; C, NO_3^-; D, gradient; E, SO_4^{2-}; F, $S_2O_3^{2-}$; G, gradient; H, P^{2-}.

Fig. 5. Effects of concentration changes on chromatograms: 1.0 × 10^{-3} M KHP for 4.5 min, then 3.0 × 10^{-3} M, pH 6.3. Analytes 10 mg l^{-1}, spectrophotometric detector, 280 nm, flow rate 3 ml min^{-1}. Peak identity: A—F, as in Fig. 4.

made in the middle of an analyte elution, the change in detector response is not manifested until 1.5 min later (peaks D and G on the chromatogram), because of the column void volume. The change in detector response corresponding to the stepwise change is shifted to an unpopulated area of the

chromatogram and does not interfere with analyte detection. Baseline stability is such that a new sample can be injected immediately after the elution of thiosulfate, and chloride will be successfully chromatographed. However, once baseline stability has been re-established, an extremely broad and large peak appears. This peak appears after each gradient sequence and neutralizes the effectiveness of the pH gradient technique for routine separations. When the pH is changed from 4.6 to 6.3, the dominant eluent species is P^{2-} which rapidly replaces HP^- from the column [6] and causes a minor change in the baseline (see peak D in Fig. 4). When the pH is changed from 6.3 to 4.6, P^{2-} is not readily eluted and the large, drawn-out peak appears. Eluent fractions collected during and after this peak confirm that total phthalate remains constant but the pH varies. The fraction collected during the peak had a pH of 5.2. Even though the changes are minimized by using the spectrophotometric detector at an isosbestic point wavelength, the magnitude of the P^{2-} peak is such that the pH change has limited utility.

The final variable studied was a step concentration change in which a less concentrated eluent was used to resolve the monovalent ions and a more concentrated eluent to increase the divalent elution rate. In order to avoid the equilibration process observed for the pH change, both eluents should have the same pH; to minimize time, the pH should be such that phthalate is present predominately as P^{2-}. In these experiments, eluent pH was maintained at 6.3 and total phthalate concentration was changed from 1.0 to 3.0×10^{-3} M. The higher concentration was introduced at 5.5 min and the concentration was returned to 1.0×10^{-3} after total time of 9.5 min. Although a change in background cannot be avoided by any of the detection methods, there should be sufficient time between the elution of NO_3^- and SO_4^{2-} to reach equilibrium. Figure 5 shows the separation achieved. Baseline resolution of the monovalent ions is observed prior to initiation of the step-change; however, no detector provided baseline stabilization prior to the elution of sulfate and thiosulfate. While thiosulfate does elute under conditions for which the baseline can be approximated with a high degree of accuracy, sulfate elutes during a period in which the baseline is still strongly responding to the stress caused by the step-changes. Again, this is not a reflection of detector instability but reflects the efficiency of flushing the separator system. The sample-to-sample difficulty in assigning an accurate baseline for the sulfate peak results in a relative standard deviation for replicate samples of ±10% which is nearly 5 times greater than the 2.1% observed for the monovalent ions at an analyte concentration 50 times the detection limit. For the phthalate concentration change, total separation time is approximately 10 min as compared to 17.5 min for 1.0×10^{-3} M phthalate.

The difficulties encountered with detector stability in both the pH and phthalate step-changes are not caused directly by changes in the eluent composition but by the manner in which the column responds to these changes. If the duration of the detector instability were directly related to the step-changes, it would be sufficiently small, as was the case with the pH

change, to be of no consequence. Additionally, such an instability could be eliminated by using dual-cell spectrophotometers and refractometers in which the eluent serves as a reference after proceeding through a length of tubing equivalent to the column void volume. This type of correction will not eliminate the column equilibration peak in the pH change, nor will it accurately model the duration of the step-change response observed for phthalate concentration.

REFERENCES

1 H. Small, T. S. Stevens and W. C. Bauman, Anal. Chem., 47 (1975) 1801.
2 D. T. Gjerde and J. S. Fritz, J. Chromatogr., 176 (1979) 199.
3 H. Small and T. E. Miller, Jr., Anal. Chem., 54 (1982) 462.
4 F. A. Baytenhuys, J. Chromatogr., 218 (1981) 57.
5 D. T. Gjerde, G. Schmuckler and J. S. Fritz, J. Chromatogr., 187 (1980) 35.
6 D. R. Jenke, Observations on the Modeling of Analyte Elution in Ion Chromatography, Ph.D. Thesis, Montana State University, 1983.
7 T. Sunden, M. Lindgren, A. Cedergren and D. D. Siemer, Anal. Chem., 55 (1983) 2.
8 D. R. Jenke and G. K. Pagenkopf, Anal. Chem., 54 (1982) 2603.

Analytica Chimica Acta, 155 (1983) 287—291
Elsevier Science Publishers B.V., Amsterdam — Printed in The Netherlands

Short Communication

RESOLUTION OF CHROMATOGRAPHIC PEAKS THROUGH VOLTAMMETRIC DETECTION FOR L-DOPA, 6-HYDROXYDOPA AND TYROSINE

THOMAS A. LAST[a]
Department of Chemistry, University of Virginia, Charlottesville, VA 22901 (U.S.A.)
(Received 3rd May 1983)

Summary. Voltammetric detection was used to resolve overlapped chromatographic peaks for L-dopa and 6-hydroxydopa. The coulostatic detector provided complete resolution (column resolution = 0.6) even though the oxidation potentials for these two species differed by less than 200 mV. The instrument can be used to resolve and accurately quantify both overlapped components from a single chromatographic injection. Further, the detector can be used to resolve three components, tyrosine, L-dopa, and 6-hydroxydopa, although the chromatographic separation provided complete resolution of tyrosine from the other components. Detection limits were 1.7 ng for tyrosine and 11 ng for L-dopa.

Most commercial grades of L-dopa [L-3-(3,4-dihydroxyphenyl)alanine] contain 6-hydroxydopa [3-(2,4,5-trihydroxyphenyl)alanine] and tyrosine as impurities. United States Pharmacopeia requirements limit the amount of 6-hydroxydopa to 0.1% of the L-dopa content Schieffer [1] has developed a rapid method for quantifying components in L-dopa preparations, based on high-performance liquid chromatography (h.p.l.c.). The method is more sensitive than the traditional thin-layer chromatography, but it is often difficult to resolve the 6-hydroxydopa and L-dopa peaks [2].

The problem described above can be solved by using voltammetric detection. Because 6-hydroxydopa and L-dopa are oxidized at different potentials ($\Delta E_{1/2} \approx 190$ mV), it is possible to resolve the components along the voltage axis (i.e., detector resolution), as well as the time axis (i.e., column resolution). Further, by using numerical peak removal, it is possible to resolve and quantify both components from a single chromatographic injection. Errors from the double-layer charging current are avoided through the use of a coulostatic technique [3].

Experimental

The chromatographic system was composed of a Milton-Roy minipump, a Laboratory Data Control (LDC) pulse-dampening system and injector, and an octadecyl (10-μm porous support particles) radial-compression column

[a]Present address: Smith-Kline/Beckman Corp., 1500 Spring Garden Street, Philadelphia, PA 19101, U.S.A.

0003-2670/83/$03.00

(Waters Associates). The detector, which is based on the coulostatic principle, has been described [3]. The instrument is capable of scanning the applied potential at rates up to 3 V s^{-1}, while simultaneously recording up to ten channels of chromatographic data, each at a different applied potential.

Samples of tyrosine, L-dopa, and 6-hydroxydopa (Sigma Chemical Company) were prepared by dissolving the appropriate amount of compound in 0.1 M phosphoric acid and diluting ten-fold with the mobile phase.

The mobile phase was 10% methanol/90% phosphate buffer. The phosphate buffer was prepared by adjusting a 0.02 M NaH_2PO_4 solution to pH 3.5 with 0.1 M phosphoric acid.

All potentials are specified as applied potential vs. Ag/AgCl (3 M KCl).

Results and discussion

The multichannel chromatogram shown in Fig. 1 demonstrates voltage and time resolution for a mixture containing 6-hydroxydopa, L-dopa, and tyrosine. The retention times are 7, 7.9 and 9.7 min, respectively. These traces (and seven others) were simultaneously recorded from a single chromatographic injection. The 6-hydroxydopa content (90 ng) of the sample corresponds to a value only ten-fold greater than the detection limit. Therefore, a significant noise level is present in the data. At the largest applied potential (1.0 V), all three components are oxidized to the corresponding quinones [4] or free radicals. At 0.6 V, tyrosine is not electroactive, and only 6-hydroxydopa and L-dopa are observed. At 0.3 V, only 6-hydroxydopa is oxidized. The slight peak in trace (c), which coincides with the tyrosine elution, is due either to reduction of the tyrosinyl radical formed by oxidation of tyrosine on the previous voltage scan, or to oxidation of the dimer formed from two such radicals. It can be seen from the figure that 6-hydroxydopa and L-dopa are well resolved by the detector, even though the column provided only partial resolution.

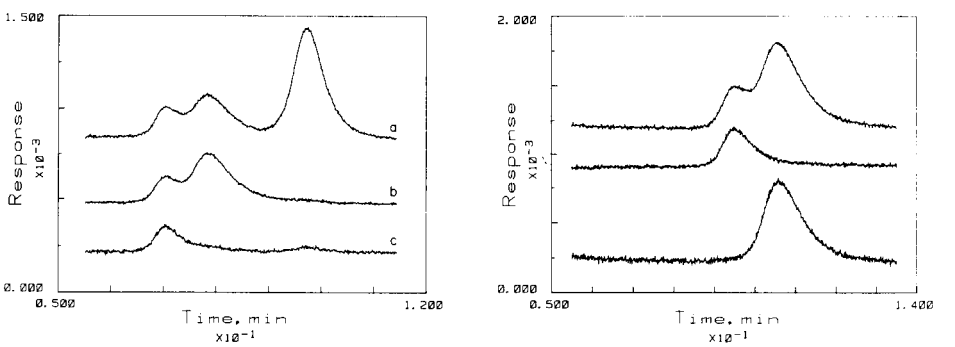

Fig. 1. Multichannel chromatogram for a mixture which contains 90 ng of 6-hydroxydopa, 87 ng of L-dopa, and 100 ng of tyrosine (given in order of elution). Applied potential: (a) 1.0 V; (b) 0.6 V; (c) 0.3 V. Flow rate 1.5 ml min^{-1}, scan rate 2 V s^{-1}.

Fig. 2. Difference chromatogram (lower trace) produced by numerical subtraction of the middle trace from the upper trace. Smaller peak is 6-hydroxydopa; larger peak is L-dopa.

Table 1 lists the peak areas as functions of applied potential for L-dopa and 6-hydroxydopa. These data were obtained from single-component injections for each analyte. The detector was operated in an identical manner (scan rate 1.3 V s^{-1}) for both samples. Each data channel was integrated over the same time interval for the L-dopa sample, and all of the channels for the 6-hydroxydopa sample were integrated over another time interval. The two integration intervals (i.e., for L-dopa and 6-hydroxydopa) overlapped (in time) by approximately 50%. It can be seen from the table that the maximum response for L-dopa corresponds to channel 7 (505 mV) or channel 8 (570 mV), and that the maximum peak area for 6-hydroxydopa occurs in channel 5 (375 mV) with significant responses in each of the adjacent channels. For potentials below the optimum value, the faradaic current is limited by the charge-transfer rate. For potentials above the optimum value, the response is decreased because of consumption (by the detector) of analyte in the former channels, leading to a reduced steady-state concentration in the detector cell. Although channel 5 would produce the largest response for 6-hydroxydopa, large L-dopa interferences would result if this channel were utilized to quantify 6-hydroxydopa in mixtures of L-dopa and 6-hydroxydopa. Therefore, channel 8 was chosen for L-dopa and channel 3 (245 mV) was chosen for 6-hydroxydopa. The response for 6-hydroxydopa at 245 mV is reduced by approximately 10% from that at 375 mV, but the detector successfully discriminates against L-dopa at the lower potential. Because the applied potential for channel 3 corresponds to a level below the diffusion-limited plateau, it is imperative that the instrument maintain tight potential control. At 245 mV, any variation in potential would surely result in a large variation in the response for 6-hydroxydopa.

Figure 2 illustrates how numerical peak removal can be used to obtain a clear L-dopa peak. The upper trace corresponds to an applied potential of 570 mV; the larger peak represents 105 ng of L-dopa and the smaller peak

TABLE 1

Peak area versus applied potential for L-dopa and 6-hydroxydopa

Channel number	Applied potential (mV)	Peak area[a]	
		L-dopa	6-Hydroxydopa
9	635	92.8	—
8	570	99.4	—
7	505	100.0	—
6	440	81.4	98.1
5	375	41.4	100.0
4	310	12.8	98.4
3	245	2.7	91.4
2	180	1.6	68.2

[a]Percent, relative to largest peak.

represents 90 ng of 6-hydroxydopa. The middle trace corresponds to 245 mV, at which potential L-dopa is not significantly oxidized. Because both traces are collected simultaneously, the middle trace can be subtracted from the upper trace to yield the difference chromatogram (L-dopa peak) shown in the lower trace. Although the column resolution for these components is only 0.6, the voltammetric detector provided complete resolution. Further, this technique allows resolution and quantitation of both components from a single chromatographic injection.

In order to test the accuracy of the peak removal technique, calibration graphs were constructed for L-dopa and 6-hydroxydopa by injecting single-component samples. Next, two different mixtures (see Fig. 3) were injected, the peaks were resolved voltammetrically, and the peak areas were compared with the values predicted by the calibration graphs. Both traces in Fig. 3 were obtained at 570 mV. The detector sensitivity for L-dopa is approximately two-fold greater than for 6-hydroxydopa, reflecting a difference in the electron-transfer rate. It should be noted that without voltammetric resolution, the peak overlap exhibited in the figure would result in a 50% error in peak area for each component in the sample represented by the lower trace.

Results for the standards and mixtures are shown in Fig. 4. The 6-hydroxydopa peak was voltammetrically isolated from the L-dopa peak by using the chromatographic channel which corresponded to 245 mV. The 6-hydroxydopa standards were likewise determined at 245 mV. The interference-free L-dopa peak was obtained by producing a difference chromatogram (see Fig. 2) for each of the mixtures by subtracting the detector response at 245 mV from that at 570 mV. The L-dopa standards were likewise determined at 570 mV. It is clear from the figure that it was possible to quantify components in the mixtures with the same degree of accuracy as for single-component solutions.

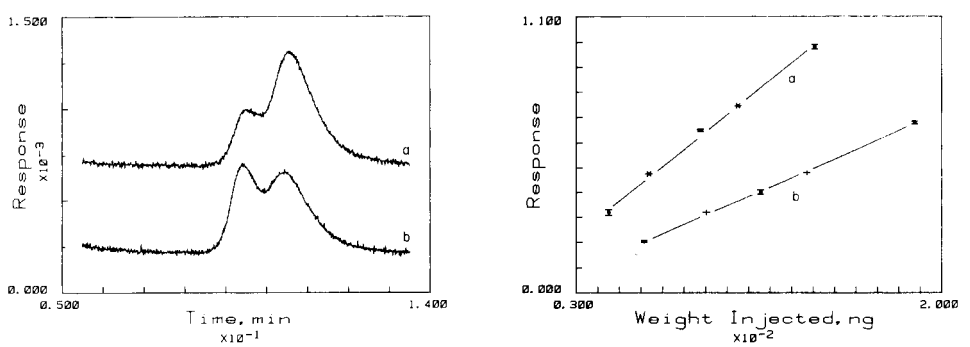

Fig. 3. Mixtures used to test the efficiency of voltammetric resolution and numerical peak removal: (a) 90 ng of 6-hydroxydopa (smaller peak) and 105 ng of L-dopa; (b) 137 ng of 6-hydroxydopa (larger peak) and 64 ng of L-dopa.

Fig. 4. Calibration graphs for (a) L-dopa and (b) 6-hydroxydopa with mixture results superimposed. Response is proportional to peak area. (•) Single component; (+) 6-hydroxydopa in mixture; (⋆) L-dopa in mixture. Lines represent least-squares fit to standards. Error bars represent the range obtained for two samples of each standard solution.

A calibration curve for tyrosine was linear over the range 16—160 ng. The detector voltage was scanned at 2 V s^{-1}, and measurements were made at an applied potential of 1.0 V. Least-squares fit yielded a slope of (1.44 ± 0.02) nC ng^{-1}, an intercept of (—3.81 ± 0.99) nC, a standard error of estimate of 0.73 nC, and a correlation coefficient of 0.9999. The relative standard deviation for the 16-ng sample was 5.5%, which leads to a tyrosine detection limit of 1.7 ng for a signal-to-noise ratio of two. The detection limit for L-dopa is approximately five-fold higher because of lower detector sensitivity.

REFERENCES

1 G. W. Schieffer, J. Pharm. Sci., 68 (1979) 1296.
2 G. W. Schieffer, Anal. Chem., 52 (1980) 1994.
3 T. A. Last, Anal. Chem., 55 (1983) 1509.
4 M. D. Hawley, S. V. Tatawawadi, S. Piekarski and R. N. Adams, J. Am. Chem. Soc., 89 (1967) 447.

Analytica Chimica Acta, 155 (1983) 293—298
Elsevier Science Publishers B.V., Amsterdam — Printed in The Netherlands

Short Communication

STRUCTURES AND RING CLOSURES OF COMPOUNDS FROM THE MOTHPROOFING AGENT EULAN WA NEU

GUNNEL WESTÖÖ, KOIDU NORÉN* and BÖRJE EGESTAD
Department of Physiological Chemistry, Karolinska Institute, Stockholm (Sweden)
LENA PALMÉR
Department of Toxicology, Karolinska Institute, Stockholm (Sweden)
GUN BLOMKVIST
Swedish National Food Administration, Uppsala (Sweden)
(Received 16th March 1983)

Summary. The main active ingredients of the mothproofing agent Eulan WA Neu are the *N*-chloromethylsulphone derivatives of 2′,3,4,4′,5-pentachloro-2-aminodiphenyl ether and 2′,3,4,4′,5,6-hexachloro-2-aminodiphenyl ether. The structures of the pentachloro-2-aminodiphenyl ether and some related compounds are discussed on the basis of n.m.r. spectroscopic data. Orientating ring closure experiments were done by heating some of the Eulan WA Neu compounds to about 390°C. The results of g.c./m.s. studies indicated the formation of polychlorinated dibenzodioxins, dibenzofurans and phenoxazines.

The contamination of fish by two polychlorinated aminodiphenyl ethers, 2′,3,4,4′,5-pentachloro-2-aminodiphenyl ether (**I**) and 2′,3,4,4′,5,6-hexachloro-2-aminodiphenyl ether (**II**), was demonstrated in 1977 [1]. These compounds emanated from the mothproofing agent Eulan WA Neu (Farbenfabriken Bayer AG), the main active constituents of which are the *N*-chloromethylsulphone derivatives (**III**, **IV**) of these amines. In 1979, Wells [2]

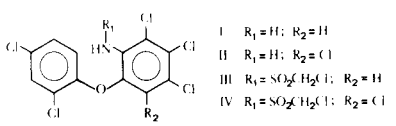

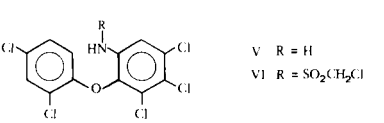

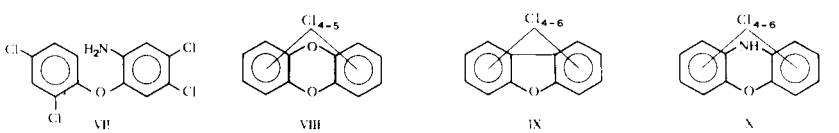

reported that fish from a water area into which Eulan WA Neu was discharged contained, in addition to two polychlorinated aminodiphenyl ethers, the *N*-chloromethylsulphone derivatives at levels up to 0.6 mg kg^{-1} in fish muscle and 5.7 mg kg^{-1} in fish liver. Using Wells' method of analysis [2], we found <0.1 mg kg^{-1} of the *N*-chloromethylsulphone compounds in fish muscle (five samples analysed).

0003-2670/83/$03.00

Based on n.m.r. and g.c./m.s. studies, Wells [2] suggested structures V and **VI**, having a hydrogen atom in the *ortho* position to the amino group for the pentachloro-2-aminodiphenyl ether and its *N*-chloromethylsulphone derivative. He also concluded that his data were in accordance with previously reported structures I and **III** [1] (having a hydrogen atom in the *meta* position to the amino group). Structures V and **VI** were also used in later reports [3—5]. However, they are incompatible with the chlorination experiments done [1] with 2′,4,4′,5-tetrachloro-2-aminodiphenyl ether (**VII**) and its *N*,*N*-diacetyl derivative. In the first case, the Eulan WA Neu compound **I** was easily formed, whereas in the second case there was no reaction. The acetylation should suppress an electrophilic substitution by chlorine in the *ortho* position to the amino group in **VII**, whereas substitution in the *meta* position should be mainly unaffected. (In the dichlorophenyl ring, Wells sometimes [2] placed the chlorine atom, that should be *para* to the oxygen, in the *meta* position, but this probably happened accidentally and is not discussed here.)

In the present investigation, nuclear magnetic resonance spectroscopy (n.m.r.) was used to confirm structures **I** and **III** for the compounds present in Eulan WA Neu. This mothproofing agent was also heated to high temperature to see if it would form potentially more toxic compounds such as polychlorinated dibenzofurans.

Discussion of structures

A pentachloro-2-aminodiphenyl ether was prepared by reducing the product obtained by coupling 1,2-dinitro-3,4,5-trichlorobenzene and 2,4-dichlorophenol. From the method of synthesis, it must have either structure **I**

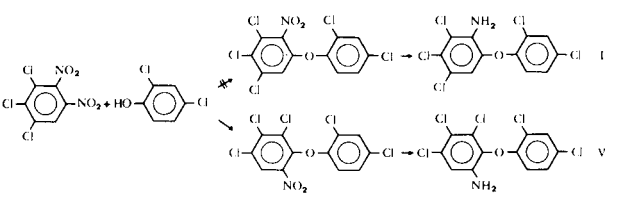

or **V**. This pentachloro-2-aminodiphenyl ether (m.p. 139.8°C) has a g.c. retention time of 1.29 relative to the pentachloro-2-aminodiphenyl ether **I** (m.p. 94.8°C) present in Eulan WA Neu and thus cannot have the structure **I**. Furthermore, in contrast to compound **I**, it reacted easily with chlorine with the formation of the previously [1] described 2′,3,4,4′,5,6-hexachloro-2-aminodiphenyl ether (**II**). The amino group strongly promotes an electrophilic substitution by chlorine in the *ortho* position, which is available in structure **V** but not in structure **I**. The synthesized compound thus must have structure **V**.

The pentachloro-2-aminodiphenyl ether, **I**, from Eulan WA Neu, its isomer **V** prepared as above, and the previously [1] synthesized compound, 2′,4,4′,5-tetrachloro-2-aminodiphenyl ether (**VII**), were studied by ^{1}H-n.m.r. The data, compiled in Table 1, can be interpreted as follows. The NH_2 resonance in

TABLE 1

^{1}H-n.m.r. data for the three polychloro-2-aminodiphenyl ethers studied (δ values)

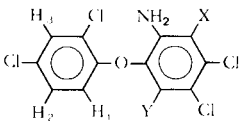

Compound I: X = Cl, Y = H
Compound V: X = H, Y = Cl
Compond VII: X = H, Y = H

Proton	Compound I[a]	Compound V	Compound VII
X (s)	—	6.89	6.89
Y (s)	6.68	—	6.75
H_1 (d)[b]	6.94	6.50	6.89
H_2 (dd)[b]	7.25	7.09	7.21
H_3 (d)[b]	7.49	7.46	7.47
NH_2 (br s)	4.42	3.95	3.94

[a]From Eulan WA Neu. [b]For the three compounds, J_{12} = 8.8 Hz, J_{23} = 2.4 Hz, and J_{13} was not observed.

compound **I** from Eulan WA Neu was shifted downfield relative to the NH_2 resonances for compounds **V** and **VII**. This shift should be caused by the chlorine substituent *ortho* to the amino group in compound **I**. In compound **V**, the resonances for H_1, and to some extent H_2, (Table 1) were shifted upfield compared to the corresponding resonances in compounds **I** and **VII**. This must be explained as an effect of the chlorine atom in position 6 (Y = Cl) in compound **V**. Thus these n.m.r. data provide conclusive evidence that the previously demonstrated [1] structure **I** is correct for the pentachloro-2-aminodiphenyl ether found in Eulan WA Neu. Accordingly, **III** (not **VI**) is the structure of its *N*-chloromethylsulphone derivative. Consequently, also in Wells' reaction sequences [2] starting from **V** and **VI**, the intermediates and reaction products have one chlorine atom in the wrong position.

Ring closures

Structures **I**—**IV** for the compounds present in Eulan WA Neu indicate that u.v. radiation or high temperature might cause ring closure (cf. [6]) with the formation of highly toxic polychlorinated dibenzofurans (**IX**). Polychlorinated phenoxazines (**X**) are also likely to be formed. Some ring closure experiments were therefore done.

Compound **II** was heated to 390°C in a glass tube, sealed without previous removal of air. Analysis of the product mixture by g.c./m.s. indicated the formation of hexachlorodibenzofuran (**IX**). When a mixture of compounds **III** and **IV** or their sodium salts was heated in the same way, various ring closures occurred. The g.c. peaks from several pyrolysis experiments (two chromatograms are shown in Fig. 1) were analyzed by m.s. The molecular ions and the typical fragments expelled are reported in Table 2. Some of the m.s. patterns are in accordance with the observations made by Nagayama et al.

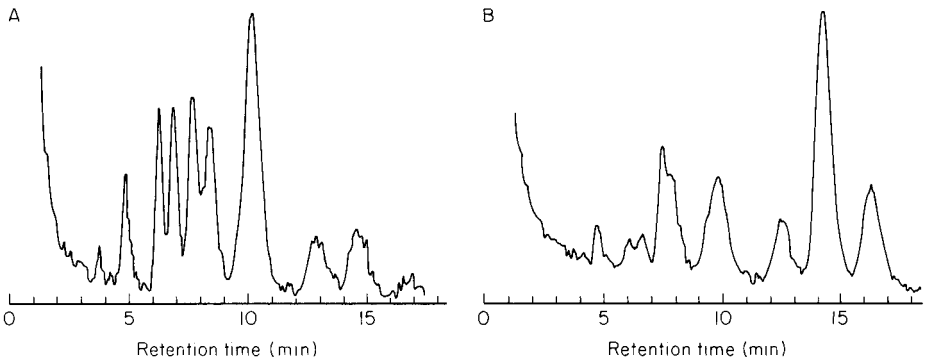

Fig. 1. Total ion current chromatograms from g.c./m.s. of compounds formed in pyrolysis experiments with III and IV (B, excess of IV) or their sodium salts (A, excess of III).

[7] and Bowes et al. [8] for tetrachlorodibenzofurans, others with observations by Nilsson et al. [6] for polychlorinated dibenzodioxins (**VIII**). Fragments probably resulting from loss of HCl + Cl and CO + Cl agree with the presence of polychlorinated phenoxazines (**X**). The g.c./m.s. data indicated the formation of two tetrachlorodibenzodioxins (**VIII**), one pentachlorodibenzodioxin (**VIII**), two pentachlorodibenzofurans (**IX**), one hexachlorodibenzofuran (**IX**), two pentachlorophenoxazines (**X**) and one hexachlorophenoxazine (**X**). Traces of a tetrachlorodibenzofuran (**IX**) and a tetrachlorophenoxazine (**X**) were also observed. The formation of the pentachloro isomers of the tricyclic compounds could be explained by ring closure to either of the *ortho* positions of the oxygen at the dichlorophenyl ring of the compounds **III** and **IV**.

TABLE 2

G.c./m.s. data for the main tricyclic compounds found in pyrolysis experiments with III and IV (B) or their sodium salts (A)

Compounds found	Retention time[a] (min)	Number of Cl atoms	Mass of molecular ion, M^+	Main fragments lost from M^+
Polychlorinated dibenzodioxins, VIII	3.3(B)	4	320	63(CO + Cl) + 63(CO + Cl)
	3.8(B), 3.8(A)			
	5.9(B)	5	354	63(CO + Cl) + 63(CO + Cl)
Polychlorinated dibenzofurans, IX	4.2(B)	5	338	63(Cl + CO) + 70(Cl + Cl)
	4.7(B), 4.8 (A)			
	7.3(B)	6	372	63(Cl + CO) + 70(Cl + Cl)
Polychlorinated phenoxazines, X	6.5(B)	5	353	71(HCl + Cl) + 63(CO + Cl)
	7.6(A)			
	12.4(B), 12.7(A)	6	387	71(HCl + Cl) + 63(CO + Cl)

[a]See Fig. 1.

Formation of compounds **I** (t_R = 6.8 min; Fig. 1A) and **II** (t_R = 9.7 min; Fig. 1B) occurred during the pyrolysis of **III** and **IV** (mass spectra have been reported [1]). Other compounds were also formed, but their structures were not established.

Experimental

A pentachloro-2-aminodiphenyl ether (m.p. 139.8°C; 49.7% Cl found, 49.6% required for $C_{12}H_6ONCl_5$) was prepared by coupling 1,2-dinitro-3,4,5-trichlorobenzene with 2,4-dichlorophenol and reducing the pentachloro-2-nitrodiphenyl ether formed according to general methods [1].

Chlorination. This pentachloro-2-aminodiphenyl ether (16.2 mg) was chlorinated by adding a solution (3.0 ml) of chlorine (3.2 mg ml^{-1}) in carbon tetrachloride. After 12 min at room temperature, the solution was diluted to 50.0 ml with heptane. After further dilution, it was analysed by g.c. which showed that 2',3,4,4',5,6-hexachloro-2-aminodiphenyl ether (**II**) had been formed (93% yield).

The same chlorination procedure was used for the pentachloro-2-aminodiphenyl ether from Eulan WA Neu. No hexachloro-2-aminodiphenyl ether (**II**) could be detected by g.c.; 89% of the starting material remained unchanged.

Pyrolysis. For the pyrolysis experiments, compound **II**, a mixture of **III** and **IV**, or a mixture of the sodium salts of **III** and **IV** (about 2 mg) in a glass tube, sealed without previous removal of the air, was gradually heated in an oven during 25 min until 390°C was reached. The heating was then switched off, and after 10 min the tubes were cooled to room temperature. The reaction mixtures were dissolved in heptane (2 ml) and subjected to g.c./m.s. (Fig. 1, Table 2).

Apparatus. For g.c., a Varian Aerograph 1200 with a tritium source electron capture detector was used. The glass column (3 mm × 1.8 m) was packed with a mixture of 3% SF-96 and 6% QF-1 [1]. N.m.r. spectra were obtained with a JEOL FX-100 instrument; the substances were dissolved in chloroform-d.

For g.c./m.s., an LKB 2091 instrument connected to an LKB 2130 data system was used. The glass column (2 mm × 2 m) was packed with a mixture of 2% OV-1 and 3% QF-1. The temperature of the column and the separator was 225°C. The ion source was kept at 220°C and the electron energy was 70 eV.

Financial support from the Swedish Products Control Board and the Swedish Council for Planning and Coordination of Research (Grant No. 81/2137) is gratefully acknowledged. We also wish to thank Dr. L. Kenne, University of Stockholm, for running the n.m.r. spectra.

REFERENCES

1 G. Westöö and K. Norén, Ambio, 6 (1977) 232.
2 D. E. Wells, Anal. Chim. Acta, 104 (1979) 253.
3 D. E. Wells, Anal. Proc., 17 (1980) 116.
4 D. E. Wells and S. J. Johnstone, J. Chromatogr. Sci., 19 (1981) 137.
5 D. E. Wells and A. A. Cowan, Analyst, 106 (1981) 862.
6 C. A. Nilsson, K. Andersson, C. Rappe and S. O. Westermark, J. Chromatogr., 96 (1974) 137.
7 J. Nagayama, M. Kuratsune and Y. Masuda, Bull. Environ. Contam. Toxicol., 15 (1976) 9.
8 G. W. Bowes, M. J. Mulvihill, B. R. T. Simoneit, A. L. Burlingame and R. W. Risebrough, Nature, 256 (1975) 305.

Analytica Chimica Acta, 155 (1983) 299—303
Elsevier Science Publishers B.V., Amsterdam — Printed in The Netherlands

Short Communication

KINETIC-CATALYTIC DETERMINATION OF MANGANESE(II) BY MEANS OF SUCCINIMIDEDIOXIME

F. GRASES*, R. FORTEZA, J. G. MARCH and V. CERDA

Department of Analytical Chemistry, Faculty of Sciences, University of Palma de Mallorca (Spain)

(Received 6th June 1983)

Summary. Kinetic methods for the determination of manganese(II) (0.2—12 and 0.5—8 $\mu g\ l^{-1}$) are described, based on catalysis of the autoxidation of succinimidedioxime to give a blue (695 nm) or yellow (310 nm) product. Palladium is the only significant interference.

Imidoximes are useful reagents in inorganic analysis; some of them provide highly selective and/or sensitive qualitative and quantitative tests, especially in acidic media [1]. The characterization and possible analytical applications of such reagents have been studied by polarography [2], potentiometry [3], spectrophotometry [4, 5] and thermometry [5—7]. Determination of metal ions by these techniques is normally based on equilibrium methods involving chelate formation. However, considerable activity in this field makes it difficult to improve on well known methods, whereas the use of kinetic techniques based on catalytic reactions does allow new methods to be established that are more selective and sensitive than the equilibrium-based methods.

Manganese(II) has well-known catalytic activity in oxidation reactions of organic compounds. Some 30 procedures have been described to determine this ion by using its catalytic action, but all except two [8, 9] require an oxidizing agent; the most sensitive allows the determination of 10—90 $\mu g\ l^{-1}$ manganese. A procedure for the determination of manganese(II), based on the catalysis of the autoxidation of succinimidedioxime (I) is developed in the present communication.

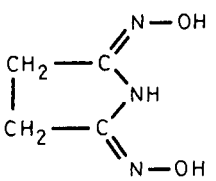

(I)

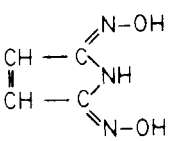

(II)

0003-2670/83/$03.00

Two products with absorption maxima at 695 nm and 310 nm are formed. They allow manganese to be determined by the tangent method in the range 0.2—12 and 0.5—8 $\mu g\ l^{-1}$, respectively.

Experimental

Reagents and solutions. Succinimidedioxime (SIDO) was synthesized as described earlier [10] in a two-step process. Succinodiamidoxime was obtained first by mixing succinodinitrile with hydroxylamine, and transformed to succinimidedioxime by reflux heating. Stock solutions included an ethanolic 1 $g\ l^{-1}$ solution of succinimidedioxime and a 1.8×10^{-2} M manganese(II) sulphate solution standardized by titration with EDTA. Analytical reagent-grade ammonium iron(II) sulphate and EDTA were dissolved in distilled water. Perchloric acid was neutralized before analysis. All solutions were thermostatted at 20°C before use.

Apparatus and measurement conditions. A Beckman Acta CIII spectrophotometer, with 1.0-cm cells was used. The absorbance-time curves were obtained by using a constant movement (50 s/in) of the chart paper.

Procedure. In a 50-ml beaker were placed 2 ml of 0.75 $g\ l^{-1}$ (695 nm) or 1 $g\ l^{-1}$ (310 nm) reagent, deionized water, so that the final volume is 4 ml, the volume of cation solution necessary for the final concentration of manganese(II) to be between 0.2 and 12 $\mu g\ l^{-1}$ (695 nm) or 0.5 and 8 $\mu g\ l^{-1}$ (310 nm) and 0.8 ml (695 nm) or 0.3 ml (310 nm) of 2 M sodium hydroxide. When 30 s had elapsed after adding alkali and mixing, recording the absorbance-time curve was started. From the curve obtained, the rate of reaction was calculated by the initial rate (tangent) method. The duration of each measurement was ca. 4 min.

Results and discussion

The colourless reagent solution in akaline media becomes blue, green and finally, very slowly, yellow and the absorption spectrum shows maxima at 695 nm and 310 nm. This reaction is accelerated by the presence of manganese(II). This transition does not occur when an inert atmosphere replaces the air. Under the same experimental conditions, the slope of the absorbance-time curves depends on the shape of the reaction vessel, owing to the different aeration efficiencies.

Effect of reaction conditions. Formation of the blue (695 nm) and yellow (310 nm) species depends on the ethanol concentration in the mixture. The influence of ethanol on the reaction rate was studied at each wavelength. The results are shown in Fig. 1. From the analytical point of view, the plateau in the curve for 695 nm is very convenient as small variations in the ethanol concentrations in this region do not influence the results. For this reason an ethanol concentration of 50% is considered optimum, at 695 nm. A concentration of 50% ethanol is also satisfactory at 310 nm even though lower concentrations would provide higher values of tan α, because at these concentrations, reaction is very rapid and the results are less reproducible.

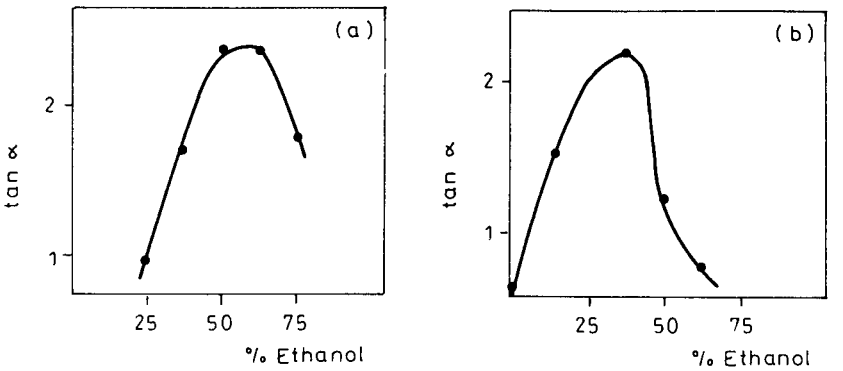

Fig. 1. Effect of ethanol concentration on the initial rate: (a) 3.8×10^{-3} M SIDO, 20 μg l^{-1} Mn^{2+}, 0.25 M NaOH, 695 nm; (b) 3.8×10^{-3} M SIDO, 1 μg l^{-1} Mn^{2+}, 0.4 M NaOH, 310 nm.

The effect of sodium hydroxide concentration is shown in Fig. 2. A final alkali concentration of 0.4 M was chosen as optimum for the determination at 695 nm; 0.15 M alkali was chosen at 310 nm even though higher concentrations provided larger values of tan α, but again these were less reproducible.

The effect of the concentration of succinimidedioxime is shown in Fig. 3. The plots show no region in which the order of reaction is zero, but around 2.9×10^{-3} M (695 nm) and 3.8×10^{-3} M (310 nm) it is a minimum. These concentrations were therefore chosen for the determination of manganese.

Characteristics of the methods. The absorbance-time curves were recorded at 695 nm and 310 nm for different amounts of manganese(II), using the optimum concentrations of ethanol, sodium hydroxide and succinimidedioxime. These curves were later treated by various established kinetic methods. The data obtained are shown in Table 1. At both wavelengths, the initial

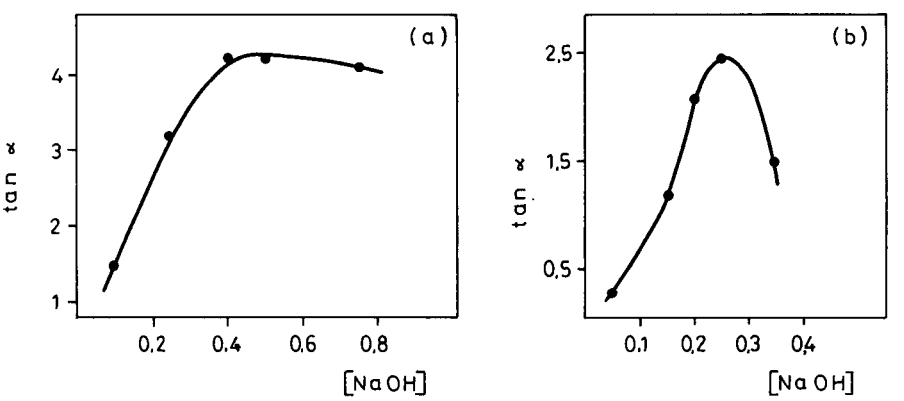

Fig. 2. Effect of sodium hydroxide concentration on the initial rate: (a) 3.8×10^{-3} M SIDO, 20 μg l^{-1} Mn^{2+}, 50% ethanol, 695 nm; (b) 3.8×10^{-3} M SIDO, 1 μg l^{-1} Mn^{2+}, 50% ethanol, 310 nm.

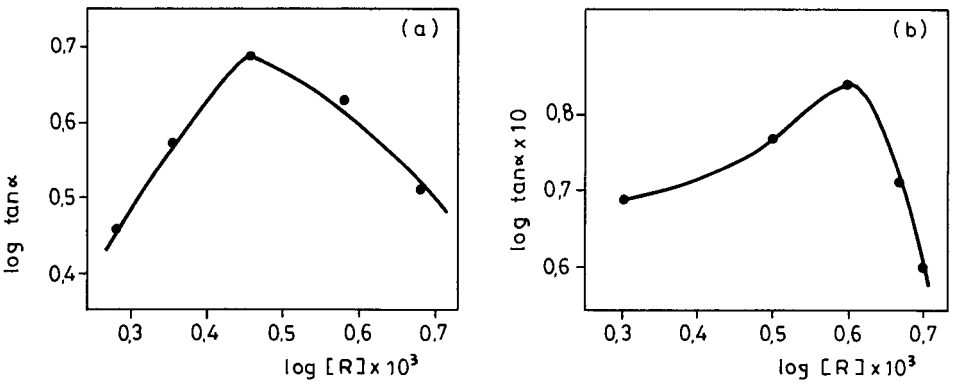

Fig. 3. Effect of succinimidedioxime concentration on the initial rate: (a) 20 $\mu g\ l^{-1}$ Mn^{2+}, 0.4 M NaOH, 50% ethanol, 695 nm; (b) 1 $\mu g\ l^{-1}$ Mn^{2+}, 0.15 M NaOH, 50% ethanol, 310 nm.

rate method gave the best analytical characteristics.

The selectivity of the methods was tested by obtaining the absorbance-time curves for 4 $\mu g\ l^{-1}$ manganese in the presence of several foreign ions under the recommended conditions. It was found that the lowest level of interferences was given by the initial rate method. At both wavelengths, 400 $\mu g\ l^{-1}$ concentrations of Ca, Sr, Ba, Zn, Cd, Ni, Co(II), Pb, Cu(II), Ag, Al, Au(III), Fe(III), Cr(III), Ce(IV), Sn(IV), Se(IV), Pt(IV), V(V), Mo(VI), CN^-, NO_3^-, SO_4^{2-} and Cl^- were without effect; and 100 $\mu g\ l^{-1}$ magnesium could be tolerated (400 $\mu g\ l^{-1}$ in presence of 0.01 M EDTA). Tolerable levels for palladium(II) were 4 $\mu g\ l^{-1}$ (695 nm) and 25 $\mu g\ l^{-1}$ (310 nm), which were raised to 400 $\mu g\ l^{-1}$ in the presence of 10 mg l^{-1} cyanide.

Of the three methods for obtaining kinetic data, the one presenting the best analytical characteristics, i.e., the smallest amount determinable, greatest precision and fewest interferences, is the initial rate method. This method is therefore recommended.

Nature of the reaction. The catalytic reaction probably involves the oxidation of manganese(II) to Mn(III), and possibly Mn(IV), by atmospheric

TABLE 1

Characteristics of the kinetic procedures for manganese(II)

Method	λ = 695 nm		λ = 310 nm	
	Useful range ($\mu g\ l^{-1}$)	R.s.d.[a] (%)	Useful range ($\mu g\ l^{-1}$)	R.s.d.[a] (%)
Initial rate	0.2—12	2.4	0.5—8	2.1
Fixed time	1—12[b]	8.0	1—6[b]	7.8
Fixed absorbance	1—10[c]	6.5	1—6[d]	4.5

[a]Relative deviation (n = 11). [b]Time = 175 s. [c]Absorbance = 0.38. [d]Absorbance = 0.70.

TABLE 2

Determination of manganese in analytical reagents

Sample	Wavelength (nm)	Reported maximum content (%)	Found (%)
Perchloric acid (Panreac GR)	310	0.00005	0.00002
Ammonium iron(II) sulphate (Merck GR)	310	0.05	0.03
EDTA (Probus GR)	695	—	0.00001

oxygen in alkaline medium. The reaction steps are probably:

$$Mn(II) + 1/2\ O_2 \rightleftharpoons Mn(III)$$

$$\text{Succinimidedioxime} + Mn(III) \rightleftharpoons \text{oxidation products} + Mn(II)$$

The spectrum of the oxidation product shows absorption bands at 310 and 695 nm. The blue species is unstable and disappears gradually, whereas the absorbance of the yellow species increases until it becomes constant. The oxidation therefore probably involves the formation of a blue nitroso compound which yields a substance readily oxidized in basic solutions to a yellow nitro compound. This is supported by the fact that when an induction period appears under certain conditions, it is shorter for the blue form. Moreover, oxidation of maleinimidedioxime(II) first gives a nitroso compound which already possesses aromatic character, so that a yellow product appears instantly, without detection of any blue form.

Applications. To test the proposed method, it was applied to the determination of traces of manganese in analytical reagents. In all instances, the standard addition method was employed. In order to detect the existence of possible interferences, the manganese recovery was calculated by comparing the results obtained before and after the addition of the manganese standard solutions. The results obtained for the different aliquots of the prepared solutions (Table 2) indicate the sensitivity of the procedures.

REFERENCES

1 F. Buscaróns, Mem. R. Acad. Cienc. Artes Barcelona, 41 (1972) 247.
2 C. Mongay and V. Cerdá, Quim. Anal., 28 (1974) 271; 29 (1975) 166.
3 M. L. Albelda, V. Cerdá, R. Pardo and P. Sánchez-Batanero, Quim. Anal., in press.
4 M. L. Albelda, V. Cerdá and C. Mongay, Bull. Soc. Chim. Fr., (1982) 19.
5 J. Rius, C. Mongay and V. Cerdá, Afinidad, 38 (1981) 357.
6 J. Lumbiarres, C. Mongay and V. Cerdá, Analusis, 8 (1980) 62; J. Thermal Anal., 22 (1981) 275.
7 M. L. Albelda, V. Cerdá and C. Mongay, J. Thermal Anal., 24 (1982) 289.
8 D. Perez-Bendito, M. Valcarcel, M. Ternero and F. Pino, Anal. Chim. Acta, 94 (1977) 405.
9 E. A. Morgen, N. A. Vlasov and L. A. Kozhemyakina, Zh. Anal. Khim., 27 (1972) 2064.
10 F. Sembritzki, Berichte, 22 (1889) 2958.

Analytica Chimica Acta, 155 (1983) 305—310
Elsevier Science Publishers B.V., Amsterdam — Printed in The Netherlands

Short Communication

DETERMINATION OF GOLD IN SILICATE ROCKS AND ORES BY COPRECIPITATION WITH TELLURIUM AND NEUTRON ACTIVATION—γ-SPECTROMETRY

C. M. ELSON*[a] and A. CHATT

Trace Analysis Research Centre, Department of Chemistry, Dalhousie University, Halifax, Nova Scotia B3H 4J1 (Canada)

(Received 24th February 1983)

Summary. The method described for determining ultra-trace levels of gold in geological materials and water samples involves the coprecipitation of gold with elemental tellurium followed by neutron activation of the precipitate. Gold-198 is measured, with detection and determination limits of 0.7 and 2.3 ng Au g^{-1}, respectively. The main interferences in the γ-spectrum are due to tellurium, iodine, and bromine, all of which were significantly reduced by evaporation without the loss of gold. The method also collects palladium and rhodium quantitatively.

The crustal abundance of gold has been estimated as 2.5 ng g^{-1} [1]; hence, irrespective of the final technique used to quantify gold in geological materials, separation and/or preconcentration steps must be used in the overall method. Because neutron activation with γ-spectrometry has a higher sensitivity for gold than other techniques [2], it is routinely applied to geological materials. The two commonest separation procedures used with neutron activation are fire-assay and either pre- or post-irradiation extractions.

Precious metals, in particular Pt and Pd, have also been separated from complex matrices by coprecipitation with tellurium [3, 4]. Gold has been reported to be quantitatively recovered from standard solutions [5] and recently tellurium collection has been combined with electrothermal atomic absorption spectrometry to determine gold and silver in rocks [6]. The present communication describes the combination of coprecipitation with tellurium and neutron activation to detect as little as 0.7 ng Au g^{-1}. One of the advantages of the present method is the elimination of the dissolution of the tellurium precipitate; instead gold is quantified by direct irradiation of the precipitate.

Experimental

Reagents. All chemicals were reagent grade unless otherwise specified. Glassware was washed with warm (1+1) nitric acid.

---

[a]On sabbatical leave from Department of Chemistry, Saint Mary's University, Halifax, Nova Scotia B3H 3C3, Canada.

0003-2670/83/$03.00

Solutions containing 1.0 mg Te ml^{-1} were prepared by dissolving 0.50 g of tellurium powder (Matheson Coleman and Bell; 99.5%) in 8 ml of aqua regia and diluting to 500 ml. Tin(II) chloride solutions were prepared by dissolving 20 g of $SnCl_2 \cdot 2H_2O$ in warm 11 M HCl and diluting to 100 ml. A 9% hydrochloric acid solution was prepared by (1 + 3) dilution of concentrated acid. Atomic absorption standard solutions (Ventron Corp.) containing the element (1 g l^{-1}) were used in the preparation of radiotracers, in the method of standard additions and as comparators, when combined with 5 mg Te, for quantification. The concentration of the gold standard solution was confirmed by comparing it to a weighed sample of ultrapure gold wire.

Tracers were prepared by 2-h irradiations of aliquots of standard gold solutions which had been dried under an infrared (i.r.) lamp in 2/5-dram polyethylene vials. Following cooling for 24 h, gold was redissolved in 2—3 ml of aqua regia and diluted to 100 ml. The addition of 1 ml of tracer solution to a sample yielded a tracer concentration comparable to that of the analyte.

Reference materials were obtained from the United States Geological Survey, Washington, D.C., the National Institute of Metallurgy, Johannesburg, South Africa (SARM 7), and the Department of Energy, Mines and Resources, Ottawa, Canada (PTC-1, PTM-1).

Irradiation and counting. Samples were irradiated in the Dalhousie University SLOWPOKE-2 reactor. The characteristics of the neutron flux and the γ-spectrometer have been described [7, 8]. Gold was quantified using the nuclide ^{198}Au ($t_{½}$ = 2.70 d, E_γ = 412 keV), after a 6-h irradiation and cooling for 50—60 h. Samples were counted for up to 30 min at a distance of 5 mm from the top of detector. The nuclide was identified from its γ-spectrum and half-life and was quantified by comparing the net photopeak area with that of standards.

Sample preparation. Weigh 0.3—1.3 g of rock into a teflon beaker and moisten with 1—2 ml of water. Add 3 ml of concentrated HNO_3, 10 ml of 40% HF and 3 ml of 60% $HClO_4$, swirl and set in a sand bath. Evaporate the sample slowly to dryness overnight. Dissolve the residue in 9% HCl with heating and transfer to a 250-ml beaker. Treat reagent blanks in a similar manner. The final volume should be approximately 100 ml.

Acidify water samples upon collection with 5 ml of hydrochloric acid (Ultrex; Baker Chemicals) per 500 ml. Filter through 0.4-μm filters (Nuclepore) and store in polyethylene bottles. Weigh 0.2—0.5 kg of water sample into a 1-l beaker and add 20—50 g of hydrochloric acid. Prepare reagent blanks by the same procedure.

Collection of tellurium. Add 5 ml of 1 mg Te ml^{-1} solution to the rock digest or acidified water samples and heat to near boiling. If the method of standard additions is to be used, spike the sample prior to the addition of tellurium. Add 5- and 2-ml volumes of the tin(II) chloride solution. Continue to heat the sample until the precipitate coagulates (15—30 min). Collect the precipitate by careful filtration through the central portion of

47-mm, 0.4-μm filter (Nuclepore). Wash the precipitate with warm 9% HCl and water. Fold the filter and dry it at 60°C for 15—30 min. Heat-seal the filter in a 5—6 mm square polyethylene bag and place it in a polyethylene vial ready for irradiation.

Prepare comparator standards by evaporating aliquots of standard solutions on filters under an i.r. lamp. Fold the filters and place them in polyethylene bags along with 5 mg of tellurium.

Volatilization of tellurium and iodine. Line a 10 ml, high-form, porcelain Coors crucible with aluminium foil. Open the polyethylene bag containing the irradiated sample prepared by normal precipitation and place it in the bottom of the crucible. Place the crucible in a cold furnace and raise the temperature to 525°C for 20—30 min. Carefully fold the foil over the residue, remove it from the crucible and count the radioactive pulses again. Alternatively, quantify the radioactivity before and after heating in an unlined crucible.

Results and discussion

All uncertainties are reported at ± one standard deviation.

Solutions of digested rocks containing tellurium trichloride were characterized by the bright yellow of iron(III). The addition of tin(II) chloride simultaneously bleached the solution and formed a dark grey-black precipitate of tellurium. The second portion of reducing agent was added to ensure that an excess was present after all the iron had been reduced. Traces of oxidizing acids were tolerated because tellurium is rapidly solubilized only by aqua regia. The tellurium precipitate coagulated with heating over the following 20 min. During filtration, care was taken to collect the precipitate only on the central portion of the filter because tellurium could not be quantitatively washed from the walls of the teflon filtering apparatus.

The coprecipitation step was assumed to involve isomorphous inclusion of elemental gold, as opposed to the formation of a telluride compound as was proposed by Sandell [5] for the collection of platinum. Moreover, not all elements that are reduced by tin(II) chloride were collected; for example, less than 12% of arsenic and antimony was collected by the above procedure, whereas these elements were quantitatively collected when selenium was substituted for tellurium [8]. Hence, the selectivity of the method is partially governed by the precipitating agent.

The efficiency of the collection procedure was determined by using radiotracers dissolved in pure solutions, rock digests, and sea-water samples; Table 1 summarizes the findings. Portions of Au(III) varying between 10 and 1000 ng were also added to a series of 100-ml solutions and the gold was coprecipitated. A plot of net counts vs. amount (ng) of gold added was linear and least-squares fitting yielded a slope of 77.2 ± 1.1 counts ng^{-1}, an intercept of −246 ± 14 counts, and a standard error of the estimate of 760 counts. Hence, the method was considered to be quantitative over the range 10—1000 ng Au (0.1 ppb—10 ppb).

TABLE 1

Recovery of gold radiotracers

Matrix	Digested SARM-7	Pure 9% HCl	Sea water
Recovery (%)	96.1 ± 2.8	98.0 ± 6.0	96.9 ± 2.5

The method was then applied to a series of rock and ore reference materials as well as sea water. The results are given in Table 2 along with published values. In general, the agreement between this work and the literature values is reasonable except for sample PTC-1. The value given for the sea water sample of less than 2.8 ng kg^{-1} is also in agreement with other work which indicated that the concentration of dissolved gold is variable in the range of 1—50 ng l^{-1} [14]. This value is also the detection limit [15] of the present method for quantifying gold in sea water. The detection and determination limits [15] for gold in geological materials were 0.7 and 2.3 ng Au g^{-1}, respectively.

Because the present values for PTC-1 and to a lesser extent for SARM-7 were less than published values, further studies appeared warranted. In the first set of experiments, two other dissolution procedures were used: aqua regia with bromine, and lithium metaborate fusion. Neither of the procedures increased the observed level of gold in the samples. Increasing the amount of tellurium also failed to increase the observed gold content. It was then suggested that copper might be interfering because both of these samples contained much more copper than typical geological materials (SARM-7 0.09% Cu, PTC-1 5.0% Cu) and because copper appeared in the γ-spectrum of the tellurium precipitates (E_γ = 1364 keV and strong annihilation peak at E_γ =

TABLE 2

Concentration of gold in geological materials and sea water

Sample	Gold concentration (ng g^{-1})	
	This work	Published work[a]
MAG-1	3.1 ± 0.4	2.43 [9], 2.58 [10]
SGR-1	9.8 ± 0.3	10.8 [9], 8.9 [10]
GSP-1	1.9 ± 0.3	1.6 [11], 1.18 [10]
SCO-1	2.0 ± 0.2	2.72 [9], 2.11 [10]
SDC-1	1.5 ± 0.4	1.1 [9], 1.89 [10]
BHVO-1	2.3 ± 0.3	1.82 [9], 1.57 [10]
QLO-1	1.1 ± 0.2	1.66 [9], 0.95 [10]
PTC-1	0.29 ± 0.01[b]	0.65 [12]
PTM-1	1.69 ± 0.02[b]	1.8 [12]
SARM-7	0.27 ± 0.02[b]	0.31 [13]
Sea water[c]	<0.0028	<0.0015 [8]

[a]With references. [b]μg Au g^{-1}. [c]Northwest Arm, Halifax Harbour.

511 keV). However, the results for the nickel-copper matte, PTM-1 with a copper content of 30.4% appeared satisfactory. Hence, the reason for the low result for PTC-1 is still unknown.

The tellurium coprecipitation procedure collects <20% of the following elements from pure solutions at the level of 1 μg per 100 ml: rhenium, mercury, copper, arsenic and antimony. The last two elements were of concern because two of USGS standards, SCO-1 and SGR-1, contained relatively large amounts of these elements and because they are readily activated by neutrons. The tellurium precipitate was also free of tin. A combination of the use of radiotracers and method of standard additions established the recoveries presented in Table 3 for four other precious metals from digested samples of SARM-7. The quantitative recoveries of palladium and rhodium and the partial recovery of iridium supported earlier work [5] but the incomplete collection of silver was contrary to earlier reports [5, 6]. Platinum was not included because Sandell had reported that its recovery was quantitative and because it could not be determined by the present method. Short irradiations (<10 min) of 5 mg Te produced a peak at 544 keV (^{131}Te) which was large enough to obscure the weak signal of ^{199}Pt at 543 keV. With longer irradiations (16 h), the Compton background arising from the long-lived Te nuclides and ^{131}I (8.06d) masked the peaks of ^{195m}Pt. Iodine-131 resulted from the β-decay of ^{131}Te ($t_{½}$ = 25 min). The β-decay product, ^{199}Au, has been used to quantify platinum but, in the present case, ^{123m}Te exhibited a peak at 159 keV which interfered strongly.

A typical γ-spectrum demonstrated sizeable peaks for ^{131}I and ^{82}Br as well as the longer-lived tellurium nuclides, ^{131m}Te, ^{129m}Te, and ^{127}Te. The observed dead-time was always less than 10%. The source of the iodine was identified and the bromine was found to originate with the Nuclepore filters. Small peaks from sodium and chloride were also present but the principal contributors to the background were tellurium, bromine and iodine. Samples of precipitates were therefore heated to 525°C in an attempt to vaporize these three elements. Experiments which involved the coprecipitation of gold-198 radiotracer proved that heating the tellurium precipitate to 525°C did not volatilize any gold; average gold recovery was 101.5 ± 5.4%. The background, however, was greatly reduced as shown by the results in Table 4 where an activated sample was counted before and after heating. The background activity was reduced by a factor of seven, which lowered the detection limit of the method to 0.3 ng Au g^{-1}.

TABLE 3

Recovery of palladium, rhodium, iridium and silver

Element	Pd	Rh[a]	Ir	Ag
Recovery (%)	102.2 ± 8.2	98.2 ± 11.3	68.9 ± 4.5	25.8 ± 16.1

[a]Method of standard additions to SARM-7.

TABLE 4

Evaporation of interfering nuclides

	Integrated counts			Gold net counts
	410—414 keV	420—424 keV	396—400 keV	
Before heating	13450	4178	4313	9204
After heating	9938	543	693	9320

The authors (C.M.E. and A.C.) acknowledge the financial support of the Natural Sciences and Engineering Research Council of Canada and the co-operation of the SLOWPOKE-2 Operations Group, Dalhousie University, in particular, Dr. J. Holzbecher.

REFERENCES

1 A. R. De Grazia and L. Haskin, Geochim. Cosmochim. Acta, 28 (1964) 559.
2 E. L. Hoffman, A. J. Naldrett, J. C. Van Loon, R. G. V. Hancock and A. Mason, Anal. Chim. Acta, 102 (1978) 157.
3 F. S. Grimaldi and M. M. Schnepfe, U.S. Geol. Surv. Prof. Pap., 575-C (1967) C141.
4 N. M. Potter and W. H. Lange, Am. Lab., (Jan. 1981) 81.
5 E. B. Sandell, Colorimetric Determination of Traces of Metals, Wiley Interscience, New York, 1959, p. 721.
6 B. J. Fryer and R. Kerrich, At. Absorpt. Newsl., 17 (1978) 4.
7 D. E. Ryan, D. C. Stuart and A. Chattopadhyay, Anal. Chim. Acta, 100 (1978) 87.
8 C. M. Elson, J. Milley and A. Chatt, Anal. Chim. Acta, 142 (1982) 269.
9 G. N. Anoshin and G. A. Perezhogin, U.S. Geol. Surv. Prof. Pap., 840 (1976) 185.
10 L. J. Schwarz and J. L. Barker, U.S. Geol. Surv. Prof. Pap., 840 (1976) 71.
11 F. J. Flanagan, Geochim. Cosmochim. Acta, 37 (1973) 1189.
12 G. H. Faye, Comp., Certified and Provisional Reference Materials available from CANMET as of 1975, Report MRP/MSL 75-25 (LS).
13 T. W. Steele, J. Levin and I. Copelowitz, Natl. Inst. Metall. Repub. S. Afr., Rep., 1696, March (1975).
14 J. P. Riley and G. Skirrow, Chemical Oceanography, Vol. III, 2nd edn., Academic Press, London, 1975, p. 358.
15 L. A. Currie, Anal. Chem., 40 (1968) 586.

Analytica Chimica Acta, 155 (1983) 311—312
Elsevier Science Publishers B.V., Amsterdam — Printed in The Netherlands

Erratum

T. Denis Rice, Gravimetric Standard Additions in Ion-Selective Electrode Potentiometry with Application to Fluoride Measurements.

Anal. Chim. Acta, 151 (1983) 383—389.

On p. 385, the sentence on lines 13—15 should read

"A calibration graph drawn from data obtained during slope determination can be used to give the approximate concentration of a sample solution after E_1 has been measured."

ANALYTICA CHIMICA ACTA, VOL. 155 (1983)

AUTHOR INDEX

Vol. 155

ACA announcements

ANNOUNCEMENTS OF MEETINGS

THE ROLE OF ANALYTICAL CHEMISTRY IN NATIONAL DEVELOPMENT, CAIRO UNIVERSITY, EGYPT, JANUARY 3–7, 1984

The symposium on the role of analytical chemistry in national development is organized by the Egyptian Chemical Society with the participation of some European Societies of Analytical Chemistry. The symposium will be held at Cairo University, Giza, Egypt. Topics covered will be: Status and Prospects of Chemical Education and Research; Implementation of National Strategies in Chemical Industries; Trends in Analytical Chemistry (product quality control, analytical data quality, trace analysis, surface analysis, information systems and computers); and Analytical Chemistry in National Development (life sciences, material sciences, food production and environmental studies).

The idea of the symposium is to discuss the possibilities of analytical chemistry for the development of countries like Egypt or other Arab nations. The symposium will include therefore lectures by Arab and European speakers on major areas of analytical chemistry and extensive discussions on matters of common interest. This joint venture can lead to establishing partnerships between Arab and European scientists.

The European plenary speakers at the symposium will be: H. Malissa, H. Kelker, W. Wegscheider, R. Kellner, E. Pungor, G. Tölg, J. Huber, W. Pfannhauser, H. Ortner, K. Varmuza, G. Verres and M. Grasserbauer.

Further information from: Professor E.M. Khairy, SCU, Cairo University, Giza, Egypt; or Professor M. Grasserbauer, Institute of Analytical Chemistry, TU-Wien, Getreidemarkt 9, A-1060 Wien, Austria.

35th PITTSBURGH CONFERENCE AND EXPOSITION ON ANALYTICAL CHEMISTRY AND APPLIED SPECTROSCOPY, ATLANTIC CITY, NJ, U.S.A., MARCH 5–10, 1984

The 1983 Conference end Exposition attracted a record 21,728 conferees and 579 exhibiting companies which used 1475 booths. The technical program consisted of 948 papers and 17 symposia. The following symposia have been organized for the 1984 Technical Program: 1. Spotlight on chromatography, 2. Analytical techniques using supercritical fluids, 3. Advanced light sources, 4. Microprobe techniques as applied to organic materials, 5. New techniques in electroanalytical chemistry, 6. New opportunities in mass spectrometry, 7. Sample introduction for plasma and flames: How can we do it better? 8. Integrating software into laboratory systems, 9. Polymer characterization, 10. Industrial hygiene monitoring, 11. New horizons in nuclear magnetic resonance, 12. The really sensitive techniques, 13. ASTM E-42 – Industrial applications of surface analysis, 14. Pittsburgh analytical chemistry award, 15. Pittsburgh spectroscopy award, 16. Dal Nogare award symposium, and 17. The Williams-Wright industrial spectroscopist award.

For further information contact: Mrs. Linda Briggs, Pittsburgh Conference, 437 Donald Road, Pittsburgh, PA 15235, U.S.A.

20th INTERNATIONAL SYMPOSIUM ON ADVANCES IN CHROMATOGRAPHY, NEW YORK, NY, APRIL 16–19, 1984

The 20th International Symposium on Advances in Chromatography will be held April 16–19, 1984, at the Sheraton Centre in New York, NY, U.S.A. The scope of the meeting will cover papers and informal discussion groups by outstanding researchers from throughout the world in all fields of

chromatography. In particular, new developments in gas, liquid and high-performance thin-layer chromatography will be included. There will also be a commercial exhibition of the latest instrumentation and books. Participation in the symposium will be on the basis of invited papers as well as unsolicited contributions. Special separate intensive two-day short courses in Capillary Chromatography, HPLC, Gas Chromatography–Mass Spectrometry and Computer Chromatography will be available on Saturday and Sunday, April 14–15, just prior to the meeting.

All correspondence pertaining to the symposium, short courses and exhibition space should be directed to: Dr. A. Zlatkis, Chemistry Department, University of Houston, Houston, TX 77004, U.S.A. Tel.: (713) 749-2623.

5th INTERNATIONAL SYMPOSIUM ON MASS SPECTROMETRY IN LIFE SCIENCES, GHENT, BELGIUM, MAY 15–18, 1984

The above symposium is being sponsored by the Faculty of Pharmaceutical Sciences of the State University of Ghent, the National Foundation of Scientific Research (N.F.W.O.–F.N.R.S.) and the Ministry of National Education of Belgium, and the Ministry of Dutch Culture. Contributed papers and posters will cover the following topics: drug metabolism, clinical chemistry, biochemistry, pharmacokinetics, toxicology, ecology and isotope labelling. All papers must be presented in English and no simultaneous translation will be provided. The deadline for receipt of abstracts is February 15, 1984.

Further information may be obtained from: Professor Dr. A. De Leenheer, Laboratoria voor Medische Biochemie en voor Klinische Analyse, Harelbekestraat 72, B-9000 Ghent, Belgium. Tel.: (091) 21 89 51, ext. 324.

2nd INTERNATIONAL CONFERENCE ON CHROMATOGRAPHY AND MASS SPECTROMETRY IN BIOMEDICAL SCIENCES, MILAN, ITALY, JUNE 18–20, 1984

The Italian Group for Mass Spectrometry in Biochemistry and Medicine is organized the above conference. The conference will illustrate and discuss all the latest aspects of chromatography, mass spectrometry (MS) and chromatography–MS, and their areas of application, including biochemistry, medicine, toxicology, drug research, nutrition science and food safety, forensic science, clinical chemistry and pollution.

A major aim of the Conference is to stimulate the exchange of information among scientists working in the above-mentioned fields. Therefore, the conference will consist of lectures by prominent invited speakers, contributed papers and discussions. Facilities will be available for participants to display poster communications. There will also be a book exhibition and displays of manufacturers' literature on chromatography and mass spectrometry and related instrumentation.

For further details, please contact: Dr. Alberto Frigerio, Italian Group for Mass Spectrometry in Biochemistry and Medicine, Via Eustachi 36, I-20129 Milan, Italy; or, Dr. Hubert Milon, P.O. Box 88, CH-1814 La Tour-de-Peilz, Switzerland. Tel.: (24) 42 11 91; Telex: 457302 LINO CH.

2nd BIENNIAL NATIONAL ATOMIC SPECTROSCOPY SYMPOSIUM, LEEDS, U.K., JULY 10–13, 1984

The Second Biennial National Atomic Spectroscopy Symposium will be held at the University of Leeds from Tuesday 10th July until Friday 13th July 1984. This is one of a series of symposia planned for the years alternate to those in which the Colloquium Spectroscopicum Internationale is held. These symposia aim to provide an opportunity for workers in the field to meet regularly for formal and informal exchange of ideas, and thus to promote and encourage developments in both fundamental and applied atomic spectroscopy in the U.K. Extensive time in the programme will be allocated to contributed papers, poster sessions and discussion. During the conference, participants will have ample time to visit manufacturers' stands where representatives will have literature on their relevant scientific equipment.

The scientific programme will cover many aspects of atomic spectroscopy, with emphasis on analytical applications of atomic emission, absorption and fluorescence and of X-ray fluorescence and emission. Reviews will be given on selected topics and accounts of recent work; these will be presented in a series of plenary and invited lectures.

Further information from: Mr. F. Buckley, Dept. of Earth Sciences, University of Leeds, Leeds, West Yorkshire LS2 9JT, U.K. Tel.: 0532-431751; Ext. 6464 or 6465.

4th SCIENTIFIC SESSION ON ION-SELECTIVE ELECTRODES, MÁTRAFÜRED, HUNGARY, OCTOBER 13–18, 1984

The Fourth Scientific Session on Ion-Selective Electrodes will be organized at Mátrafüred, Hungary, on October 13–18, 1984. The scientific program will include invited plenary and keynote lectures and contributed research papers. Considerable time will be devoted to discussions. The session will cover the following main topics: progress in the theory of ion-selective electrodes; novel developments in ion-selective electrode preparation; and application, with special emphasis on biology, clinical and environmental chemistry. The papers will be published by Akadémiai Kiadó, the Publishing House of the Hungarian Academy of Sciences. The participants will be accommodated in the Resort House of the Hungarian Academy of Sciences.

Further information may be obtained from: Organizing Committee, Fourth Scientific Session on Ion-Selective Electrodes, Institute for General and Analytical Chemistry, Technical University, 1502 Budapest, Gellért tér 4, Hungary.

30th INTERNATIONAL CONGRESS OF PURE AND APPLIED CHEMISTRY, MANCHESTER, U.K., SEPTEMBER 9–13, 1985

The 30th IUPAC Congress will be held from Monday 9 to Friday 13 September 1985 in the U.K. in Manchester. The Opening Ceremony and the Inaugural Plenary Lecture will take place on Monday morning, and the meeting will terminate at lunchtime on Friday. A full programme of evening and daytime social events is being planned. The Royal Society of Chemistry is responsible for the detailed organisation of the Congress. The scientific programme will embrace the following Divisions and topics, and prominent chemists from all over the world are being invited to present lectures. The symposia within the individual sections will take place both concurrently and sequentially. It is planned to include free-offer contributions, particularly as posters. Details regarding submission of papers will be available in March 1984.

Section 1, Analytical (Analytical Division): New Instrumental Methods, Advances in Automatic Methods to Include Microcomputers, Environmental Analyses, Biotechnology-Analytical Applications.

Section 2, Education (Education Division): Chemical Education Research, Laboratory Work: Assumptions and Realisations, Continuing Education in Chemistry, Changing Requirements for Manpower Skills (jointly with Industrial Division).

Section 3, Industrial (Industrial Division)–Chemical Industry–Year 2001: Future Basic Feedstocks, Processes for the Future–Invention and Design, The Environmental Challenge (jointly with the Environment Group), International and Regional Factors, Changing Requirements for Manpower Skills (jointly with the Education Division).

Section 4, Inorganic (Dalton Division): Electrochemistry and Electron Transfer in Inorganic and Bio-inorganic Chemistry, Chemistry of *p*-Block Elements, Applications of New Techniques in Inorganic Chemistry, Metals in Chemotherapy and Radiation Therapy.

Section 5, Organic (Perkin Division)–Organic Chemistry as a Life Science: Organic Synthesis and Biosynthesis, Chemical Regulation of Biological Mechanisms, Computer Graphics and Drug Design, Human and Animal Health Medicinals, and Agrochemicals.

Section 6, Organic (Perkin Division)/Historical: Dyestuffs – Past, Present and Future.

Section 7, Physical (Faraday Division)–Advances in Physical and Theoretical Chemistry; Dynamics of Chemical Reactions in the Gas Phase and in Solution, Surface Science, Micellar Systems.

Further information about the Congress will be available in March 1984 from: The Royal Society of Chemistry, Burlington House, London W1V 0BN, U.K.

ontinued from outside back cover)

CONTENTS

(Abstracted, Indexed in: Anal. Abstr.; Biol. Abstr.; Chem. Abstr.; Curr. Contents Phys. Chem. Earth Sci.; Life Sci.; Index Med.; Mass Spectrom. Bull.; Sci. Citation Index; Excerpta Med.)

(Continued on inside back cover)